

Doctoral thesis

Doctoral theses at NTNU, 2023:297

Agnese Babini

Hyperspectral Imaging of Stained Glass

NTNU
Norwegian University of Science and Technology
Thesis for the Degree of
Philosophiae Doctor
Faculty of Information Technology and Electrical
Engineering
Department of Computer Science



Norwegian University of
Science and Technology

Agnese Babini

Hyperspectral Imaging of Stained Glass

Thesis for the Degree of Philosophiae Doctor

Gjøvik, October 2023

Norwegian University of Science and Technology
Faculty of Information Technology and Electrical Engineering
Department of Computer Science



Norwegian University of
Science and Technology

NTNU

Norwegian University of Science and Technology

Thesis for the Degree of Philosophiae Doctor

Faculty of Information Technology and Electrical Engineering
Department of Computer Science

© Agnese Babini

ISBN 978-82-326-7294-3 (printed ver.)

ISBN 978-82-326-7293-6 (electronic ver.)

ISSN 1503-8181 (printed ver.)

ISSN 2703-8084 (online ver.)

Doctoral theses at NTNU, 2023:297

Printed by NTNU Grafisk senter

Abstract

Since its first applications in cultural heritage, hyperspectral imaging (HSI) has become a valuable tool for documenting and analyzing many kinds of artworks, thanks to the possibility of obtaining spectral information regarding relatively large areas in a non-invasive way. In the last decades, HSI has been successfully used to study paintings on panels, canvas and plaster, manuscripts, and photographic materials, and has allowed to successfully characterize the distribution of pigments and colorants in the artwork under study.

The work presented in this thesis focuses on evaluating the advantages and limitations of performing HSI on stained-glass windows. Compared to the abovementioned types of artworks, prior HSI applications on stained-glass windows are very limited due to the numerous challenges related to the optical properties of the glass and external factors that can negatively impact the quality of the image acquisition. For example, since stained-glass windows are mainly transparent, a setup for spectral transmittance measurements is necessary. If the stained-glass windows are still part of a building and cannot be removed, the intensity of sunlight (used as the light source) can vary throughout the day, and the presence of vegetation or buildings in the background can affect the actual color of the glass. In addition, accessing the stained glass with the instrument could also be an issue if no support is available (e.g., scaffolding).

One of the research project's main objectives is thus to propose new acquisition methodologies that allow carrying out HSI of stained glass in different situations, from relatively small, detached panels, to stained-glass windows in situ. The characteristics of each setup will be thoroughly discussed to highlight advantages and limitations.

The second objective is to validate the data obtained from the proposed setups to demonstrate HSI's capabilities in characterizing the materials used in stained glass. This validation process has been carried out from two perspectives; first, the correctness of the obtained spectra has been verified by comparing them with results from UV-VIS-NIR spectroscopy, which is extensively used for chromophore identification. Second, X-Ray Fluorescence spectroscopy (XRF) has been used as a complementary analytical technique to determine the elemental composition of the glass and verify the presence of the chromophore identified by HSI.

Image analysis solutions for automatically identifying and mapping stained glass components were also explored. Besides the traditional classification methodologies, unsupervised unmixing approaches were also investigated, which showed promising results.

Sammendrag

Siden de første anvendelsene innen kulturarv har hyperspektral avbildning (HSI) blitt et verdifullt verktøy for å dokumentere og analysere mange typer kunstverk, takket være muligheten for å innhente spektral informasjon om relativt store områder på en ikke-invasiv måte. I de siste tiårene har HSI blitt brukt til å studere malerier på paneler, lerret og gips, manuskripter og fotografiske materialer, noe som har muliggjort vellykket karakterisering av fordelingen av pigmenter og fargestoffer i kunstverket som studeres.

Arbeidet som er presentert i denne avhandlingen fokusere på å evaluere fordelene og begrensningene ved å utføre HSI på glassmalerier. Sammenlignet med de ovennevnte typer kunstverk, er tidligere HSI-anvendelser på glassmalerier meget begrenset i omfang, på grunn av de mange utfordringer knyttet til glassets optiske egenskaper og eksterne faktorer som kan påvirke kvaliteten på avbildningen negativt. For eksempel, siden glassmalerier hovedsakelig er gjennomsiktige, er et oppsett for spektrale transmittans-målinger nødvendig. Hvis glassmaleriene fortsatt er en del av en bygning og ikke kan fjernes, kan intensiteten av sollys (brukt som lyskilde) variere gjennom dagen, og tilstedeværelsen av vegetasjon eller bygninger kan påvirke den faktiske fargen på glasset. I tillegg kan tilgang til farget glass med instrumentet også være et problem hvis ingen støtte er tilgjengelig (som for eksempel stillas).

Et av forskningsprosjektets hovedmål er derfor å foreslå nye avbildningsmetoder som gjør det mulig å utføre hyperspektral avbildning av glassmalerier i forskjellige situasjoner, fra relativt små, enkeltstående paneler, til glassmalerier in situ. Egenskapene til hvert oppsett vil bli grundig diskutert for å fremheve fordeler og begrensninger.

Det andre målet er å validere dataene innhentet fra de foreslåtte oppsettene for å demonstrere HSI's evner til å karakterisere materialene som brukes i farget glass. Denne valideringsprosessen har blitt utført fra to perspektiver; For det første er presisjonen til de oppnådde spektrene validert ved å sammenligne dem med resultater fra UV-VIS-NIR-spektroskopi, som er mye brukt for kromoforidentifikasjon. For det andre har røntgenfluorescensspektroskopi (XRF) blitt brukt som en komplementær analytisk teknikk for

å bestemme elementsammensetningen til glasset og verifisere tilstedeværelsen av kromoforen identifisert av HSI.

Bildeanalyteløsninger for automatisk identifisering og kartlegging av glassmalerier ble også utforsket. I tillegg til de tradisjonelle klassifiseringsmetodikkene, ble også ikke-veiledete unmixing-tilnæringer undersøkt, som gav lovende resultater.

Acknowledgment

One of the first things I was told when I started my PhD is that “this is your research, you will have to decide where it goes and be responsible for it”. If I can make a comparison with my favorite sport, a PhD in a way is similar to Formula 1. It’s the driver that takes the car to the podium, but even the best ones can’t be expected to win if there isn’t a strong team behind. And I have to admit, sometimes I felt like my research strategies were as bad as Ferrari’s, and somewhere along the road Plan A became Plan E. But as a wise Sebastian Vettel once said, “There is no reason not to be motivated. You can’t always be the best, but you can do your best”. So here we are at the chequered flag, defending a PhD that could have been something completely different but in the end, is done. And it’s time to thank everyone who kept my motivation high and contributed to this success.

So first of all, let me thank my “team principals”, my supervisor Dr. Sony George, and my co-supervisors, Dr. Jon Yngve Hardeberg at NTNU and Dr. Tiziana Lombardo at the Swiss National Museum. Thank you for choosing me for this project and trusting in my capacities. Working with you was like dealing with a very wise three-headed dragon, everyone with their own background and ideas. Finding common ground wasn’t always easy, but I am truly grateful for the advice and knowledge you shared with me. Your feedback made me a better researcher, and now “working in a multidisciplinary context” is not just an overused sentence I can write in my curriculum.

I would like to thank all the people that provided me with the case studies, the fuel of my research: Tine Grette Poulsson and Mari Sjørgulen Evensen from the National Museum in Oslo, for giving me access to the Vigeland stained glass; Elizabeth Sinnerud from the Nidaros Domkirke Restoration Workshop for sending me the colored glass pieces, you saved my work during the pandemic; Dr. Lindsay MacDonald for lending me his mock-up stained-glass panels; Dr. Katharina Schmidt-Ott and the staff of the Swiss National Museum and the Collection Center, who gave me access to the museum’s fantastic collection and helped me before, after, and during the analysis. Without all of you, this thesis wouldn’t have existed, so I want to thank you from the bottom of my heart.

Of course, I wouldn’t be here without my CHANGE “teammates”. I am extremely grateful for the friends I made in this project, it is super rare to find 14 people getting along so well, and I feel so lucky I can say that this is exactly the case. The support we have for each other is

something that I will never forget. So, thank you, Dipendra, Evi, Sunita, Sia, Jizhen, Yoko, Ram, David, Jan, Silvia, Deepshikha, Ale, and Amalia, for the hours spent on the phone laughing out loud at banter and jokes in the group chat and the unforgettable memories from the Training Schools and other events. I love you all my fellow Kalamatchis. Let's keep that chat alive, I am also sure our paths will cross again one day.

Within the CHANGE group, a special thanks goes to my fellow "musketeers" Jan, Silvia, and "mama" Amalia. Thanks for all the support (I lost count of the virtual hugs we sent each other in the last few months), the restorer/conservator/conservation scientist's ranting time, the advice for life and work, the laughs, the wine, the good food, the good times around Europe and Switzerland (#mymountains), the memes. I am so grateful I shared this important chapter of my life with you.

And a huge, huge, huge thank you goes to the "crew" at NTNU, IDI, and Colorlab. NTNU has been one of the few places where I felt welcomed as the person I am, and I am happy to call this place one of my "home away from home". I am amazed at how many kind, generous, and helpful people are here at NTNU, everyone makes it feel like it's the best working place in the world (if anyone asks, yes, you can recycle this sentence on your flyers, you are very welcome).

So, I would like to thank Irina, Greg, Davit, Aland, Mekides, Vlado, Ahmed, Zeeshan, Mohib, and Cong Cong for welcoming me when I first arrived in Gjøvik and for introducing me to the group and the city.

My wonderful office mates and "siblings from another project" (hello APPEARS!) Tanzima, Majid, Tom, and his family (Zoe and little Ada). A little thank you also to Nauhel who shared the office with us for a short time during my first year and became part of the crazy gang for a while.

The colleagues and friends I met along the way in these three and a half years, Ali (my fellow cat person), Aida, Anuja, Fereshteh, Luvin (thank you for trying to keep me in good shape when I wanted to be a couch potato), Markus and Mathieu ("grazzie ragazzzi"), Olga, "grandpa" Raed, Siamak (ikke sant?), Simon, Zuzanna and their baby girl Freja.

I want to dedicate a special thanks to Federico for bearing with me in my "Panic at the room A010" moments. "I write sins not codes" so thank you for your patience, your invaluable help when my brain decided to forget the basics of imaging science, and "for being ~~not~~ so Italian" (necessary quote).

Mobina, Bitu, Mitra, Zo, and Ilaria, I wish we met at a happier and less busy time, but I am very thankful for the good times we spent together, even if for a short period.

Another round of thanks goes to Hilda, for your inspiring view of the researcher's life and your empathy; Giorgio for all the tips you shared with me and all the good moments spent with you and your family, Raquel, and Olivia; Peter Nussbaum for all the random hallway chats, it was always a pleasure to stop and talk with you.

Outside NTNU, I would like to thank Cosima, whom I was lucky to meet in Oslo thanks to Jan. Thanks a lot for the adventure we had together. You are a wonderful person and the best cross-country ski teacher I could have asked for. A little thanks goes also to Arianna, for the time spent together in Neuchatel, bonding over tales from our experiences in Ravenna. You are a very caring person and I'm glad I met you during these years.

The biggest and most heartfelt thanks go of course to my family, my mum, my dad, and my sisters Caterina and Valentina for supporting me through all the steps that led to this moment. Most of all, thank you for believing in my choice of becoming a researcher in the field of Cultural Heritage despite the ghost of precariousness looming over my shoulders. I'm also very glad that this opportunity allowed us to get some holidays together around Europe (thank you CHANGE).

Another special thanks goes to my best friend Gemma. I think one of the best things about carrying out the PhD in Norway is that it got us closer, like, literally closer. I am so glad that I could visit you so often and I am very grateful for all the time I spent with you and Jessy. It was always refreshing staying a couple of days with you just cooking, cuddling "little" Poe, and watching random episodes of "Murder, She Wrote".

Last but not least, I would like to thank all my friends from the good old times in Sirolo and Ravenna, who kept wondering all the time why I chose a country with four hours of light in the winter (if you are lucky), too many days with temperatures below 0°, and weird alcohol selling policies (the 12 euros Tavernello cooking wine at the Vinmonopolet will always haunt me) to do my PhD. Just so you know, I think that auroras on winter nights and neverending light on summer days make up for it a lot. But jokes aside, thank you for all the support and care. I know it was hard to keep in touch, but I appreciated every message and every little moment that we could share in the past years. It was comforting to know that despite the distance and busy lives I could always count on you, and for this, I will be forever grateful.

Table of Contents

Abstract.....	I
Sammendrag.....	III
Acknowledgment.....	V
Part I	1
Introduction.....	2
1.1 Motivations	2
1.2 Aims and research questions.....	4
1.3 List of publications.....	6
1.4 Thesis Organization	8
Background	9
2.1 Stained-glass windows	9
2.1.1 The colors of stained glass.....	11
2.1.2 Photographic documentation of stained glass	15
2.1.3 Scientific analysis of stained glass.....	16
2.2 Hyperspectral imaging of stained glass.....	20
2.2.1 Transmittance vs. Reflectance imaging geometries.....	22
2.2.2 Hyperspectral image processing and analysis.....	26
Summary of included papers	30
3.1 Paper 1: Potential and challenges of spectral imaging for documentation and analysis of stained-glass windows.....	30
3.2 Paper 2: Comparison of hyperspectral imaging and fiber optic reflectance spectroscopy for reflectance and transmittance measurements of colored glass	30
3.3 Paper 3: Hyperspectral imaging workflow for the acquisition and analysis of stained-glass panels.....	31
3.4 Paper 4: A portable setup for hyperspectral imaging of stained-glass panels ..	32
3.5 Paper 5: Acquisition strategies for <i>in-situ</i> hyperspectral imaging of stained-glass windows: case studies from the Swiss National Museum.....	33
3.6 Paper 6: Blind unmixing of hyperspectral images of stained glass: adapting the LUMoS algorithm for chromophore mapping.....	34
Discussion.....	35
4.1 Research outcomes	35

4.1.1 Hyperspectral imaging.....	35
4.1.2 Data validation	54
4.1.3 Hyperspectral image analysis: a work in progress.	58
4.2 Research contributions	62
Conclusion and perspectives	63
5.1 Conclusion.....	63
5.2 Perspectives.....	64
Bibliography	67
Part II.....	77
Paper 1	78
Paper 2	84
Paper 3	103
Paper 4	115
Paper 5	130
Paper 6	154

Part I

Chapter 1

Introduction

1.1 Motivations

The work presented in this thesis has been carried out in the frame of the European project CHANGE-ITN, which focuses on researching new applications of imaging techniques for the documentation, analysis, and monitoring of various typologies of works of art. Among these techniques, hyperspectral imaging (HSI) is one of the most widely used in cultural heritage. HSI is based on acquiring many finely sampled images across a portion of the electromagnetic spectrum. As a result, a full spectrum can be obtained in each pixel of the image. These spectra can be compared with reference spectral libraries to identify the materials present in the scene, and by means of specific algorithms, it is possible to display their distribution. In cultural heritage, the materials of interest can be pigments and colorants used by a particular artist or in a specific period. The way these artistic materials are applied across the artwork under study can provide precious insights into the painting technique or the chronology of the artwork (Delaney, Dooley, van Loon, & Vandivere, 2020; Floréal & Mounier, 2015). This aspect is one of the reasons behind the popularity of this technique in the field of cultural heritage. Another reason is that HSI is a non-invasive technique, as the camera does not come in contact with the artifacts, and taking a sample from the object is not required. This represents a significant advantage, especially when the works of art are vulnerable, and sampling is not permitted (Radpour, Delaney, & Kakoulli, 2022).

Since its first applications in cultural heritage, HSI setups have evolved to account for the specific needs of the artworks under study, becoming more and more versatile (Picollo, Cucci, Casini, & Stefani, 2020). HSI applications now range from small objects, such as photographic materials (Picollo et al., 2020) and manuscripts (Ciortan, Deborah, George, & Hardeberg, 2015; Cucci et al., 2017; Cucci, Delaney, & Picollo, 2016), to large and monumental paintings (Balas, Epitropou, Tsapras, & Hadjinicolaou, 2018; Cutajar et al., 2022; Floréal et al., 2016; Gabrieli et al., 2021; Radpour et al., 2022). From the image processing point of view, many algorithms from the field of remote sensing have been adapted and used to automatically identify and map artistic materials (Picollo et al., 2020). In addition, the possibility of creating

spectral libraries of known painting materials has allowed experimenting with machine learning-based classification and unmixing algorithms, which provide more accurate results (Balas et al., 2018; Deborah, George, & Hardeberg, 2019; Grabowski, Masarczyk, Głomb, & Mendys, 2018; Polak et al., 2017; Pouyet, Miteva, Rohani, & de Viguerie, 2021; Rohani, Pouyet, Walton, Cossairt, & Katsaggelos, 2018).

With regards to stained-glass windows, however, HSI applications are still minimal. The reasons for its limited use can be drawn from the literature available regarding photographic documentation of stained glass, which already stresses the challenging aspects of imaging these particular artworks (MacDonald, Findlater, Song, Giani, & Suganthan, 2006; MacDonald & Oldfield, 1996; Suganthan & MacDonald, 2010). Stained glass windows, in fact, are complex works of art that also fulfill the functional role of filling gaps in architecture to protect from atmospheric agents and heat, allowing at the same time the light to enter and illuminate the interiors of the building (Parker & Martlew, 2021; Raguin, 2013).

From a technical point of view, stained-glass windows consist of colored and transparent glass pieces held together by lead strips called *comes* that form the basic shapes of the figures represented. The color of the glass can be obtained in several ways: exploiting impurities (naturally colored glass) or adding oxides of transitional elements (chromophores) in the glass batch (pot-colored glass) and controlling temperature and atmosphere (oxidizing or reducing) in the furnace to get the desired color; fusing a thin layer of metallic nanoparticles to the surface of transparent glass (flashed glass); painting the glass surface with enamels or vitreous paint (Meulebroeck, Wouters, Nys, & Thienpont, 2016; Raguin, 1988). A particular form of vitreous paint is *grisaille*, which has a reddish to brown/black color and is usually applied to depict finer details, outlines, or shadows (Machado, Vilarigues, & Palomar, 2021; Raguin, 1988).

Since stained-glass windows are primarily transparent, the most efficient way to photograph stained glass is by using transmitted light, either natural or artificial. However, the different optical properties of the components described above can represent an issue during the imaging phase. For instance, the contrast between the darker areas (such as lead comes, grisaille, and deep-colored glass) and lighter glass can result in over-exposure or under-exposure of certain portions of the stained glass (MacDonald et al., 2006; Suganthan & MacDonald, 2010). In addition, stained glass's appearance can be affected by weathering layers, dirt deposition, and other forms of alteration if exposed to polluted environments or temperature and humidity variations for a long time (Frenzel, 1985; Suganthan & MacDonald, 2010).

If stained-glass windows are photographed *in situ*, the variation of sunlight throughout the day and the background behind the windows must also be taken into account to obtain good-quality images (MacDonald & Oldfield, 1996).

These challenges also apply to HSI; however, in this case, the abovementioned factors affect both the image quality and the spectral information obtained, which may lead to erroneous identifications of the chromophores responsible for the glass color.

Nonetheless, HSI can be a valuable technique for investigating stained glass. From a certain point of view, HSI can be considered a combination of conventional imaging and UV-VIS-IR spectroscopy. In recent years, UV-VIS-NIR spectroscopy has become an established technique for identifying chromophores in archaeological and historic glass objects (Bracci, Bartolozzi, Burnam, & Corallini, 2020; Hunault et al., 2021; Hunault, Lelong, et al., 2016; Meulebroeck et al., 2012; Meulebroeck, Baert, et al., 2010; Meulebroeck et al., 2016). However, it can only collect spectral data from one point at a time. Considering this aspect, having simultaneous spatial and spectral information can represent a great advantage of HSI, especially when analyzing large surfaces such as stained-glass windows.

In light of these considerations, this thesis aims to demonstrate the capabilities of HSI in characterizing the materials used in stained glass and the possible benefits of this imaging technique to the conservation scientists, conservators, and restorers involved in the study of colored glass and glass paints in stained-glass windows. The limitations will also be discussed, suggesting possible solutions for future implementations.

1.2 Aims and research questions

One of the main objectives of this research project is to develop acquisition methodologies for the HSI of stained glass that could work in different conditions and environments. As explained previously, the best way to deal with the transparency of these artworks is to work in transmittance mode. Most of the existing systems are designed to work in reflectance mode. An HSI transmittance setup has been recently developed for imaging photographic materials (Cucci, Casini, Stefani, Cattaneo, & Picollo, 2023; Picollo et al., 2020); however, the different constituting materials, sizes, thicknesses, and weights of stained-glass windows require other specifications. It is thus necessary to adapt existing reflectance setups or build new systems that can work in transmittance mode with such big objects.

Another aspect to consider is the size and location of stained glass. Depending on their function (decoration or architecture) as well as their conservation conditions (e.g. fragments from broken windows), the size of the stained-glass may vary from a few centimeters to tens of meters. Many stained-glass windows and panels are still part of the buildings they were meant for. In other cases, the windows could have been removed from their original place for various reasons (change of aesthetic taste, wars, building renovations) and dismembered, becoming, with time, part of museums or private collections. Depending on the choice of display, the illumination source could be natural or artificial (e.g., lightboxes) (Eatman, 2008; Raguin, 2013). If stained-glass windows are disassembled for restoration interventions and are too fragile to be reinstalled, the constituting panels may be separated and permanently stored in museums' deposits.

All these scenarios require different specifications, especially concerning the available illumination source (natural vs. artificial light). The main challenge is thus to design imaging setups that can be used in any illumination condition and environment, for example, in conservation centers or even *in situ* if the stained glass is in its original location or exhibited in a permanent collection. In the latter cases, ideally, it should be possible to implement the setup on stained glass panels and windows of any size without dismantling them.

The research presented in this thesis has been focused on three distinct situations: in the laboratory (controlled illumination), using a portable system (suboptimally controlled illumination), and *in-situ* (variable illumination). However, due to the project's time constraints, the portable and *in-situ* setups have been tested only on a few real-case scenarios.

The second objective is to validate the data obtained from the setups described above to encourage more extensive use of hyperspectral imaging as a tool for stained-glass windows' characterization. This validation process should be carried out from two perspectives; first of all, the accuracy of the spectra obtained should be ensured by comparing them with results from UV-VIS-NIR spectroscopy, which is extensively used for chromophore identification. The second validation step regards material identification. It is a known concept in the cultural heritage field that a single technique can rarely answer all the research questions regarding an artwork. Thus, complementary analysis is necessary to confirm the results obtained with HSI. For the scope of this research, X-Ray Fluorescence spectroscopy (XRF) has been employed to determine the elemental composition of the glass and verify the presence of the chromophore identified by HSI.

In light of these observations, five specific objectives (*SO*) have been defined:

SO1: Implement a laboratory setup for the HSI of stained-glass panels (standard geometry condition and stable light source).

SO2: Develop a portable setup for the HSI of stained-glass panels using commercially available and low-cost materials (partially standard geometry condition and stable light source).

SO3: Develop a portable setup for the *in-situ* HSI of stained-glass windows, exploiting natural (solar radiation) or artificial light sources (uncontrolled environment).

SO4: Validation of the spectral data: comparison with UV-VIS-NIR spectroscopy of stained-glass samples and available literature.

SO5: Validation of identified chromophores: use of complementary analysis such as X-Ray Fluorescence spectroscopy (XRF) to characterize the elemental composition of the glass.

From these five specific objectives, the following set of research questions (*RQ*) can be formulated:

RQ1: What are the best setups and acquisition parameters for good-quality stained glass HSI? Can HSI be used to successfully analyze and document stained glass in different scenarios (e.g., laboratory, museum depots/conservation laboratories, *in-situ*...)? What are the advantages and limitations of each case?

RQ2: From the spectral point of view, does the HSI technique allow obtaining comparable results to the available techniques (UV-VIS-NIR spectroscopy)?

RQ3: What kind of information can HSI provide? Can it be recommended for accurate material characterization? Can it help to select the correct areas for additional point analysis or sampling?

The connection between objectives, research questions, and the published papers is schematized in Fig. 1.1 at the end of the last section.

1.3 List of publications

The content of the thesis is built on a collection of five papers; **Papers 1, 3, and 4** are conference proceedings, while **Papers 2 and 5** are journal papers. **Paper 6** is a draft paper. The six papers do not follow a chronological order but are listed according to their contribution to the thesis structure shown in Fig.1.1:

- **Paper 1:** Agnese Babini, Sony George, Tiziana Lombardo, & Jon Y. Hardeberg. (2020). Potential and Challenges of Spectral Imaging for Documentation and Analysis of Stained-Glass Windows. London Imaging Meeting, 2020(1), 109-113.
- **Paper 2:** Agnese Babini, Phil Green, Sony George, & Jon Y. Hardeberg. (2022). Comparison of Hyperspectral Imaging and Fiber-Optic Reflectance Spectroscopy for Reflectance and Transmittance Measurements of Colored Glass. *Heritage*, 5(3), 1401-1418.
- **Paper 3:** Agnese Babini, Sony George, & Jon Y. Hardeberg. (2021). Hyperspectral imaging workflow for the acquisition and analysis of stained-glass panels. In Proc. SPIE Optics for Arts, Architecture, and Archaeology VIII (Vol. 11784).
- **Paper 4:** Agnese Babini, Sony George, Tiziana Lombardo, & Jon Y. Hardeberg. (2022). A Portable Set up for Hyperspectral Imaging of Stained-Glass Panels. In Rocco Furferi, Lapo Governi, Yary Volpe, Kate Seymour, Anna Pelagotti, & Francesco Gherardini (Eds.), *The Future of Heritage Science and Technologies: ICT and Digital Heritage* (Vol. 1645, pp. 57-70). Cham: Springer International Publishing.
- **Paper 5:** Agnese Babini, Tiziana Lombardo, Katharina Schmidt-Ott, Sony George, & Jon Y. Hardeberg. (2023). Acquisition strategies for *in-situ* hyperspectral imaging of stained-glass windows: case studies from the Swiss National Museum. *Heritage Science*, 11(1), 74.
- **Paper 6:** Agnese Babini, Tiziana Lombardo, Sony George, Jon Y. Hardeberg. (2023). Blind unmixing of hyperspectral images of stained glass: adapting the LUMoS algorithm for chromophores mapping. Draft paper.

Paper 1 is a literature review and sets the aims and the research questions described in the previous section. **Papers 2** and **3** present the results obtained using the laboratory setup but considering different aspects. **Paper 2** compares laboratory HSI and UV-VIS-IR-spectroscopy performances, while **Paper 3** describes the setup design and the image pre-processing steps in detail and presents preliminary results on a real case study. **Papers 4** and **5** focus on the implementation of the portable and the *in-situ* setups, respectively. **Paper 6** integrates the contents of **Paper 4**, presenting preliminary results of chromophore mapping on the case studies analyzed with the portable setup and the XRF measurements for data validation.

1.4 Thesis Organization

The work presented in this thesis results from the integration of knowledge from various disciplines, such as imaging science, color science, conservation-restoration, and conservation science. Due to this multidisciplinary nature, it is expected that readers with different backgrounds and professional training may not be familiar with all the concepts mentioned in the published papers. The first part of the thesis thus aims to provide the necessary background knowledge to understand the research context, both from the object and the imaging side.

Chapter 2 is divided into two parts; the first part provides the background on stained-glass windows, describing their characteristics and the principle of color formation in glass. A review of photographic documentation and scientific analysis is also provided. The second part describes the fundamentals of HSI and its applications on stained glass.

Chapter 3 contains the summaries of the published paper contributing to the thesis, highlighting the aims and the main findings. The full-text publications are provided in the second part of the thesis.

Chapter 4 presents the main contributions and the limitations of the research project.

Chapter 5 discusses the conclusions of the research and its future perspectives.

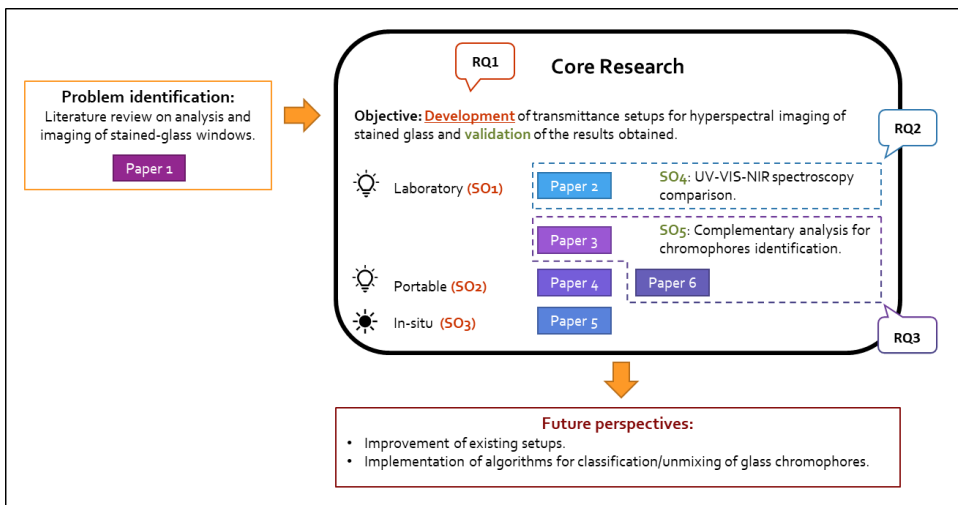


Figure 1.1: Scheme of the thesis structure showing the connection between objectives, research questions, and the published papers. Paper 1 is a literature review that illustrates the state-of-the-art and explains the motivations of the research. The core research includes five specific objectives (SO). Three out of these five objectives regard the three different setups (laboratory, portable, and in situ) and aim to answer the first research question (RQ1). The symbols associated with the setups indicate the type of light sources employed. The other two specific objectives regard the data validation part of the research. Paper 2 deals with the comparison between HSI and UV-VIS-NIR spectroscopy, providing the answer to research question RQ2. Papers 3 and 6 aim to answer the third research question (RQ3) from two different points of view, which will be explained in the discussion section of the thesis.

Chapter 2

Background

This chapter aims to provide an extensive literature review to help the readers understand the research context. The chapter is divided into two parts:

The first part (Section 2.1) focuses on the object studied, the stained glass. This section is introduced by a brief discussion regarding the function and meaning of stained glass. Then the main parts constituting the stained glass are shortly described, highlighting the challenges they can represent during the acquisition process. Section 2.1.1 provides a short overview of the color formation mechanism in glass and a literature review on the topic. The last sections extend the literature review on photographic documentation (Section 2.1.2) and scientific analysis of stained glass (2.1.3 and 2.1.4) presented in **Paper 1**.

The second part of the chapter (Section 2.2) focuses on HSI and its applications on stained-glass windows. This section also briefly discusses the differences between reflectance and transmittance imaging modes (Section 2.2.1) and gives a short overview of hyperspectral image processing and analysis (Section 2.2.2).

2.1 Stained-glass windows

Stained glass windows are complex works of art from many points of view. From the architectural side, stained-glass windows fulfill the functional role of filling gaps in religious and secular buildings to protect from atmospheric agents and heat, allowing at the same time the light to enter and illuminate the rooms. The iconographic themes, the color palette, and the materials used to secure the stained glass to the window compartments are strictly connected to the building for which they were designed. The study of these materials can provide a wealth of information on the social status of the patrons, the aesthetic tastes, as well as resources and knowledge available in a specific historical period or geographical region (Adlington et al., 2019; Hunault et al., 2017; Parker & Martlew, 2021; Patin, Nys, Thienpont, & Meulebroeck, 2022; Raguin, 2013; Rodrigues et al., 2021; Simmons & Mysak, 2010).

From the material point of view, stained-glass windows consist of many parts with distinct physical, chemical, and optical characteristics. The glass pieces composing the stained-glass

figures can be transparent or translucent, depending on their color and thickness, but the lead comes that hold those pieces are opaque and reflect the light. The grisaille, a reddish or brownish vitreous paint applied on the surface to define details and shadows, can be fairly opaque, thus also limiting the light passing through the glass, depending on the thickness of the painted layer (Machado et al., 2021; Meulebroeck et al., 2016; Raguin, 1988).

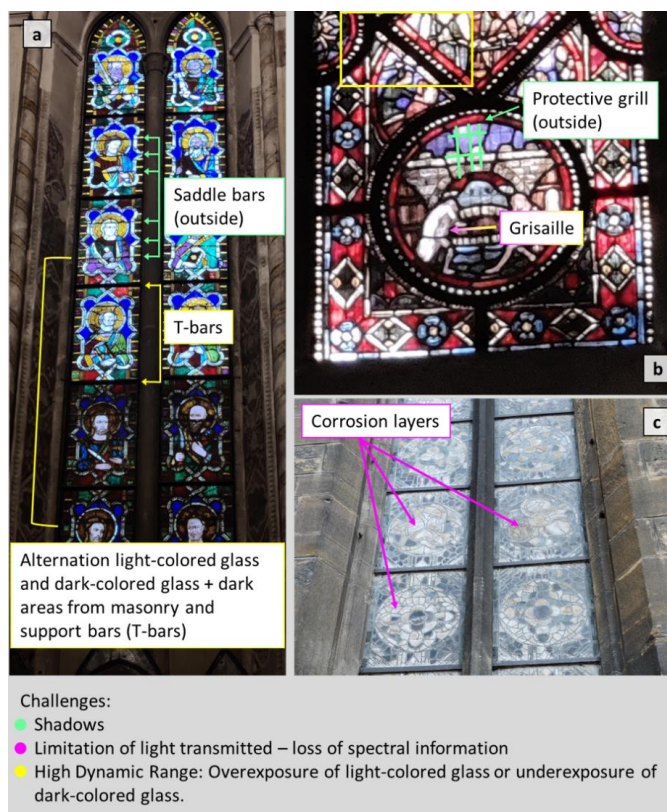


Figure 2.1: Images showing stained-glass parts that mostly affect the quality of the acquisition. Picture taken by the candidate at a) Basilica di Santa Croce (Firenze, Italy). b) Nidaros Domkirke (Trondheim, Norway), c) Église des Dominicains (Colmar, France).

Because of their different composition, these materials are also subjected to diverse types of degradation that may affect the stained glass’ integrity and appearance. Degradation can occur both on the internal and external surfaces, and it can become an issue when applying imaging techniques, especially if the transparency of the glass is compromised (Suganthan & MacDonald, 2010).

The loss of transparency can be caused by several factors: from simple dry deposition of soot, dust, and dirt to the development of inorganic and organic corrosion crusts, pitting (i.e., small

craters on the glass surface), and browning phenomena¹ caused by the interaction between the stained glass surface, atmospheric agents (primarily water, in the form of rain or condensation), pollutants and often also microorganisms (Aulinas et al., 2009; Gentaz, Lombardo, Chabas, Loisel, & Verney-Carron, 2012; Lombardo et al., 2010; Pinar et al., 2013; Valbi, Perez, Verney-Carron, & Rossano, 2023). Some types of degradation can be firmly attached to the glass surface and penetrate deep into the glass body; thus, any cleaning process should be carefully evaluated by expert conservators. A thorough discussion on degradation processes and glass conservation-restoration practices is beyond the scope of this introductory chapter since it is not the primary focus of the research presented in this thesis. For more general information, the readers can refer to online resources from dedicated research groups and institutions (e.g., the Corpus Vitrearum² and the Stained Glass Museum³), as well as stained-glass windows experts⁴.

2.1.1 The colors of stained glass.

The mechanism of color formation in glass is a complex topic and requires a deep knowledge of chemistry concepts such as ligand field theory, redox reactions, and charge-transfer mechanisms (Calas, Galoisy, & Cormier, 2021; Cartechini, Miliani, Nodari, Rosi, & Tomasin, 2021; Möncke, Papageorgiou, Winterstein-Beckmann, & Zacharias, 2014). The detailed explanation of such concepts is beyond the scope of the thesis. However, providing a basic description of the origin of colors in glass has been deemed beneficial to help the readers understand what information regarding the chromophores can be retrieved from HSI spectra.

From the spectral point of view, HSI follows the same working principle as UV-VIS-NIR spectroscopy. Both techniques, in fact, help understand the interaction between light and matter; the information observed in the spectra is related to chemical species (ions or molecules) that selectively absorb the light at specific wavelengths. In the extended visible range (including a portion of UV and NIR), the chemical species detected are those responsible

¹ In manganese-containing glass.

² Corpus Vitrearum Medii Aevii (CVMA), "Conservation of Stained Glass", <https://www.cvma.ac.uk/conserv/index.html> ; Corpus Vitrearum USA, "Conservation Organizations & Guidelines", <https://corpusvitrearum.us/conservation-organizations/> ; Corpus Vitrearum Italia (ICVMA), "Guidelines of ancient monumental stained and painted glass", <http://www.icvbc.cnr.it/bivi/eng/preservation/guidelines.htm>

³ The Stained Glass Museum, "Resources", <https://stainedglassmuseum.com/resources.php>

⁴ Julie L. Sloan "Owners Manual of Stained Glass Conservation", <https://www.jlsloan.com/stained-glass-conservation-manual> ; Leonie Selinger, "Cleaning Historic Stained Glass Windows.", <https://www.buildingconservation.com/articles/cleaning-stained-glass/cleaning-stained-glass.htm>

for the color of the object investigated (Meulebroeck et al., 2016; Möncke et al., 2014; Palomar et al., 2019).

The color in glass materials is mainly due to the presence of ionic species of transitional elements (iron, manganese, copper, cobalt, and chromium), which could be present as impurities in the raw materials (e.g., iron) or intentionally added to the glass batch. In the first case, they are defined as naturally colored glass, while in the second case as pot-colored glass (Meulebroeck et al., 2016). The desired color is obtained by controlling the temperature and atmosphere in the furnace to favor the elements' reduction or oxidation. For example, when only iron is present, a range of colors from yellow to green and light blue can be obtained depending on the equilibrium between the yellow ferric ion Fe^{3+} and the blue ferrous ion Fe^{2+} (Cartechini et al., 2021). When iron is present as impurities, manganese (as Mn^{2+}) can be used as a decoloring agent to oxidize the iron and obtain a colorless glass. Alternatively, a range of colors between yellow and purple can be achieved. Manganese alone, as Mn^{3+} , gives the glass shades from pink to reddish-purple (Cartechini et al., 2021; Rossano et al., 2022). Cobalt (as Co^{2+}) is used to achieve an intense blue color, Cu^{2+} a turquoise blue or a deep green (in combination with Fe^{3+}), while Cr^{3+} has been used since the 19th century to obtain a bright emerald green (Cartechini et al., 2021; Hunault & Loisel, 2020; Meulebroeck et al., 2016).

The use of copper (Cu^0) and silver (Ag^0) nanoparticles is also well documented. Cu^0 nanoparticles give the glass a deep red color, too dark to be used for windows. Thus, the flashing technique was invented in medieval times to overcome this problem. This technique consists in applying a thin layer of red-colored glass over a transparent one (plaqués) or alternating multiple thin layers of red and transparent glass (feuilletés) (Colomban, Tournie, & Ricciardi, 2009; Farges, Etcheverry, Scheidegger, & Grolimund, 2006).

Ag^0 nanoparticles, on the other hand, can be found in yellow decorative paint layers, applied through a technique called silver staining. It consists in coating the glass surface with a silver compound dispersed in a clay medium and firing at a temperature just below the softening range of the glass. During the firing, the silver ions are exchanged with the glass matrix's potassium (K^+) or sodium (Na^+) ions, diffusing inside the glass. Lastly, the ions are reduced to the metallic state, leading to the growth of silver nanoparticles. The final color depends on the nanoparticles' size, shape, and concentration and could range from pale yellow to orange; in the latter case, the warmer hue is given by the additional presence of copper (Jembrih-Simbürger et al., 2002; Meulebroeck et al., 2016).

These elements, as well as clusters, microcrystalline phases, or structural defects, modify the transmittance efficiency of the glass by absorbing the light at specific wavelengths (Calas et al., 2021). When the internal scattering is negligible, the light absorption depends on the thickness of the glass d (expressed in cm), the concentration of the coloring agents c , and the molar extinction coefficient ε , which describes the intensity of the absorption bands of the specific ions (i.e., their coloring potential). According to the Beer-Lambert law, the relationship between transmittance and absorbance can thus be expressed as follows (Calas et al., 2021; Möncke et al., 2014):

$$T = \frac{I_t}{I_0} \quad (\text{Eq. 1})$$

$$A_\lambda = \log\left(\frac{I_0}{I_t}\right)_\lambda = \log\left(\frac{1}{T}\right)_\lambda = \varepsilon_\lambda cd \quad (\text{Eq. 2})$$

Where A is the absorbance, I_0 is the incident light, I_t is the transmitted light, and T is the transmittance, calculated at a wavelength λ . The absorbance expressed as $\log\left(\frac{1}{T}\right)_\lambda$ in Eq. 2 is defined as optical density.

From Eq. 2 and the spectral curves, it is possible to retrieve valuable information on the color formation in the glass investigated. First, the conversion of HSI transmittance data into absorbance allows better identification of the absorbance bands (Calas et al., 2021) and facilitates the comparison with the available literature, in which spectra are often presented in absorbance.

Once converted in absorbance, the spectral data can be normalized by the thickness according to the ratio A/d so that the intrinsic color of the glass can be measured without the influence of the thickness (Calas et al., 2021; Meulebroeck, Nys, Patin, & Thienpont, 2021).

The concentration c of chromophores and the molar extinction coefficient ε can also be calculated from Eq.1 if the thickness and either one or the other parameter (c or ε) are known. This methodology is often applied when working with model glass samples, which are studied to investigate particular glass-making and coloration techniques (Ceglia et al., 2015; Hunault & Loisel, 2020; Möncke et al., 2014).

The information inferred from the Beer-Lambert law regarding the chromophores can be complemented by colorimetric measurement, which provides a quantitative measure of the color of the glass investigated (Capobianco et al., 2019). For example, the colorimetric

coordinates x and y of a group of colored glass can be calculated from the spectral data and plotted in the CIE 1931 chromaticity diagram. Depending on the position of each glass within the diagram, it is possible to identify patterns related to the presence of specific chromophores, glass production technology, and chronology (Capobianco et al., 2019; Meulebroeck et al., 2016). Alternatively, the CIELAB $L^*a^*b^*$ values can also be calculated from the spectra and used for the colorimetric characterization and to determine the color difference ΔE (Hunault et al., 2021; Hunault, Lelong, et al., 2016; Meulebroeck et al., 2021).

For more in-depth studies on the topic, the readers can refer to the papers listed in Table 2.1, which thoroughly investigate the color formation in historical and archaeological glass and provide detailed explanations of the chemical processes that allow reaching a specific color. Publications regarding grisailles have not been included in this list since they cannot be characterized in HSI acquisitions performed in transmittance; thus, they were not studied in depth during the PhD project. An extensive literature review on grisaille compositions through the ages can be found in (Machado et al., 2021). Additional papers regarding relevant case studies are listed in Table 2.2 in Section 2.1.3.

Table 2.1: List of useful references regarding glass coloration technologies.

Chromophores	Colors	References
Iron (Fe^{2+}, Fe^{3+}, Fe^{3+-S})	Blue, yellow, green, amber	(Bidegaray et al., 2019; Capobianco et al., 2021; Ceglia et al., 2015; Gimeno et al., 2008; Hunault & Loisel, 2020; Micheletti et al., 2020; Möncke et al., 2014; Rossano et al., 2022; Schreurs & Brill, 1984; Thiemsorn, Keowkamnerd, Phanichphant, Suwannathada, & Hessenkemper, 2008)
Manganese (Mn^{2+}, Mn^{3+})	Pink, purple	
Manganese and iron	Uncolored; yellow to purple	
Copper (Cu^{2+})	Blue turquoise; green (with Fe^{3+})	
Cobalt (Co^{2+})	Blue	(Ceglia et al., 2012; Fornacelli, Ceglia, Bracci, & Vilarigues, 2018; Hunault, Bauchau, et al., 2016; Micheletti et al., 2020; Möncke et al., 2014)
Copper Nanoparticles (Cu^0)	Red	(Bring, Jonson, Kloo, & Rosdahl, 2007; Delgado et al., 2011; Kunicki-Goldfinger et al., 2014; Meulebroeck, Patin, Nys, & Thienpont, 2023; Molina et al., 2013; Pérez-Villar, Rubio, & Oteo, 2008)
Silver nanoparticles (Ag^0)	Pale yellow to orange	
Other chromophores (chromium, nickel, cadmium sulfide and selenide)	Green (Cr^{3+}); purple, brown, yellow, green (Ni^{2+}); red to yellow ($\text{CdS}_x\text{Se}_{1-x}$)	(Calas et al., 2021; Fornacelli, Colombari, & Memmi, 2015; Meulebroeck et al., 2016; Vilarigues et al., 2022)

2.1.2 Photographic documentation of stained glass

Photographic documentation is a fundamental step in every conservation and restoration campaign. As good practice, it must be performed before, during, and after any treatment to record changes that happened or are happening to the artwork.

Documentation of stained glass is carried out both in transmittance and reflectance mode. Photography in transmittance is carried out on light tables, with the light shining through the object, to assess the general appearance of the colored glass, to understand the nature of the color (i.e., whether the glass is body-colored or flashed), and to document the presence of inhomogeneities in the glass body (e.g., air bubbles and streaks) (Davison, 2003).

Reflectance photography is performed to document the conservation condition of the glass surface, as well as the opaque elements of the stained glass such as grisaille and the lead comes. It is useful to assess the types of patinas or degradation layers, which would not be visible in transmittance, as they reduce the transparency of the glass. The use of raking light (i.e., directed at the glass surface at an angle almost parallel to the surface plane) is also recommended to highlight surface irregularities and textures (Davison, 2003), as well as painted areas marking a replacement from modern restorations (Raguin, 2013).

Concerning the photography of stained glass *in situ*, common issues in photographing stained glass depend on both the light source available (sunlight) and the stained glass' materials, as well as their conservation condition (see Fig. 2.1 in the previous section).

For example, the intensity of sunlight illumination may vary throughout the day due to sudden weather changes. In addition, the stained-glass windows may not be adequately exposed to sunlight due to the orientations of the walls; thus, the light reaching the glass may not be sufficient for a good exposure. In general, obtaining optimal exposure during the imaging of stained glass can be very challenging due to the strong contrast between the light areas of the transparent glass panes and the dark ones of the metal bars of the supporting ironwork (ferramenta) and the deep-colored glass (Fig. 2.1a). Thus, setting the proper exposure time might be complicated, as some areas might be unavoidably overexposed or underexposed. High dynamic range (HDR) photography, which consists in fusing multiple images taken at different exposure levels is a solution used very often by professional photographers to improve the quality of stained-glass images.

Lastly, the background behind the windows must be taken into consideration. The landscape outside the windows might be visible from the more transparent glass and influence the color

of the light-colored glass. Metal structures such as saddle bars and protective grills can cause shadows on stained-glass windows, resulting in a dark area covering part of the image.

The works of (MacDonald, 1997; MacDonald et al., 2006) address many of these challenges, suggesting good practices to improve the quality of the images captured. For example, a solution to remove the influence of external light was proposed based on the use of an illuminated panel placed outside the window to be scanned. The panel is based on a commercial photographic 'soft box' with a tungsten-halogen flood light as the illumination source.

Other works have been done to improve the quality of acquisition and archival procedures. The research of the European project VITRA (Veridical Imaging of Transmissive and Reflective Artefacts), carried out from 2002 to 2004 (MacDonald, 2006), was focused on “developing a practical method for the acquisition, storage, and visualization of high-quality images of architectural details in historic buildings”, including stained-glass windows. The acquisitions were carried out through a remote-controlled robotic arm, which allowed reaching higher zones (up to 15 m). In this way, it was possible to obtain high-resolution images of those areas that are usually difficult to capture from the ground, avoiding loss of details and image distortions. The imaging of stained-glass windows was performed in transmittance using natural light, and many images were collected in different exposures to deal with the high dynamic range of the stained glass (MacDonald, 2006).

On the image processing side, research has been conducted on many aspects: to highlight relevant features (Giani, MacDonald, Machy, & Suganthan, 2003); to correct defects (Suganthan & MacDonald, 2008); to remove unwanted effects (e.g., shadows from the supporting bars) (Suganthan & MacDonald, 2010) and to perform rendering, relighting and virtual restoration (MacDonald & Oldfield, 1996; Thanikachalam et al., 2016).

Worthy of mention is also the work of (Simmons & Mysak, 2010) which does not focus on scientific photography *per se* but on the use of HDR images to estimate luminance data from stained-glass windows and determine the change of the windows' transmissivity through the centuries.

2.1.3 Scientific analysis of stained glass

In cultural heritage, scientific analyses are performed to answer various research questions. In the specific case of stained glass, scientific investigations are conducted to study the provenance of constituting materials and the technology used for glass production, which can shed light on the historical and cultural context in which the glass was created. Scientific

analyses are also applied to understand the causes of degradation and alteration processes occurring on stained glass windows so that solutions can be developed to slow down or stop these processes. (Trümpler, Wolf, Kessler, & Goll, 2012).

Depending on the accuracy required to answer the research question, these analyses can be performed by means of non-invasive or invasive techniques. Invasive techniques are called in such a way because they require collecting small samples from the artifact. In the case of stained glass, the samples are often collected during restoration treatments that involve the removal of the old lead comes for cleaning or substitutions (Adlington et al., 2020). Those samples can be fragments that cannot be reintegrated during the reassembling (Palomar et al., 2019) or removed from corners of the glass panes that the lead comes will cover once put back in place (Adlington et al., 2020; Schalm, Caen, & Janssens, 2010). Depending on the technique employed, the collected samples may be kept for further analysis or destroyed in the process. Most of these analyses are performed in a laboratory, and sometimes they require specific facilities (e.g., XANES, which requires access to a synchrotron) (Hunault, Bauchau, et al., 2016).

Other techniques, like Laser Ablation-Inductively Coupled Plasma–Mass Spectrometry (LA-ICP-MS) and Laser-Induced Breakdown Spectroscopy (LIBS), do not require mechanical sampling but exploit a laser to remove a minimal portion of the glass. These techniques are considered micro-invasive since the part removed is barely perceivable to the naked eye.

Non-invasive techniques, on the other hand, do not require samples or material removal. This aspect is advantageous when sampling is not possible or not permitted. In addition, non-invasive methods are often portable, allowing performing the analysis in situ. This is convenient when the stained-glass windows cannot be detached and moved to the laboratory. For these reasons, non-invasive techniques have become increasingly popular throughout the years, especially for preliminary investigation of stained-glass composition and conservation conditions. In many cases, these techniques are sufficient to get the necessary information without requiring further invasive procedures (Vandenabeele & Donais, 2016).

Scientific analysis can be further divided depending on the type of information provided (e.g., elemental or molecular). Elemental techniques exploit high-energy radiations (X-rays, particles, or laser beams) to excite the materials and obtain qualitative or quantitative information (depending on the instruments' specifics or setup) on the elemental composition

of the object under study. An example of an elemental technique is XRF, which has been used multiple times during this PhD as a complementary analysis to HSI.

On the other hand, molecular techniques, such as Fourier Transform Infrared Spectroscopy (FTIR) or Raman Spectroscopy, can provide information on groups of molecules (functional groups) associated with the alteration of the glass matrix, degradation products or chromophores (if present as nanoparticles).

Table 2.2 (modified from **Paper 1**) lists the most used scientific techniques for analyzing stained glass. Note that some references are mentioned multiple times for different instruments, as it is often necessary to combine various methods to characterize the glass completely.

Table 2.2: Summary table of the most used analytical techniques for the analysis of stained glass. A brief description of the information obtainable and an estimation of the invasiveness of the method are provided.

Analytical technique	Invasive	Information	References
Fourier Transform IR spectroscopy (FTIR)	Yes/No (depending on the analysis mode)	Molecular; degradation products.	(Aulinas et al., 2009; Rodrigues et al., 2014)
Laser ablation-Inductively Coupled Plasma–Mass Spectrometry LA-ICP-MS	Yes	Elemental; quantitative information on trace elements; isotopes identification for provenance purposes	(Kunicki-Goldfinger et al., 2014; Pradell et al., 2016; Van Ham-Meert et al., 2021; Wilk, Kamińska, Walczak, & Bulska, 2017)
Laser-induced Breakdown Spectroscopy (LIBS)	Yes	Elemental; stratigraphic information on corrosion layers for cleaning monitoring; identification of chromophores.	(Carmona, Oujja, Rebollar, Romich, & Castillejo, 2005; Klein, Hildenhagen, Dickmann, Stratoudaki, & Zafirooulos, 2000; Palomar et al., 2022; Szelagowska et al., 2008)
Particle-induced X-ray Emission (PIXE)	No	Elemental; quantitative information of major, minor, and trace elements	(Calligaro, 2008; Hunault et al., 2017; Jembrih-Simbürger et al., 2002)
RAMAN spectroscopy	Yes/No (depending on the size of the object). It can be portable	Molecular; colorants and glass components; degradation products (results may vary from lab instruments to portable ones).	(Baert et al., 2012; Colomban, Etcheverry, Asquier, Bounichou, & Tournie, 2006; Colomban & Tournie, 2007; Colomban et al., 2009; Fernandes, Vilarigues, Alves, & da Silva, 2008; Fornacelli et al., 2015; Rodrigues et al., 2014; Walczak, Kamińska, Karaszkiwicz, Szczerbinski, & Szymonski, 2013)
Scanning Electron Microscope (SEM), sometimes coupled with	Yes	Elemental; quantitative information on major, minor, and trace	(Falcone et al., 2010; Jembrih-Simbürger et al., 2002; Kunicki-Goldfinger et al.,

an electron microprobe (EPMA)		elements; microscopic observation of the topography of the surface and degradation layers; semi-quantitative information on the distribution of elements on the surface.	2014; Lombardo et al., 2010; Pradell et al., 2016; Rodrigues et al., 2014; Verita, Bracci, & Porcinai, 2019; Walczak et al., 2013; Wilk et al., 2017)
UV-VIS-NIR spectroscopy (absorption/reflectance); Fiber Optic Reflectance Spectroscopy (FORS)*	Yes/No* (depending on the size of the object). It can be portable	Elemental (ionic species); information on oxidation states, coordination of colorants (UV-VIS-NIR), and degradation mechanisms (NIR).	(Bacci, Corallini, Orlando, Picollo, & Radicati, 2007; Bracci et al., 2020; Ceglia et al., 2015; Fernandes et al., 2008; Fornacelli et al., 2015; Hunault, Lelong, et al., 2016; Hunault et al., 2017; Meulebroeck et al., 2012; Meulebroeck et al., 2023; Meulebroeck et al., 2016; Rodrigues et al., 2021; Zaleski et al., 2019)
X-ray Absorption Spectroscopy (XAS/XANES)	Yes	Elemental (ionic species); oxidation states of chromophore elements in glass.	(Ceglia et al., 2015; Farges et al., 2006; Ferrand et al., 2015; Hunault, Bauchau, et al., 2016)
X-Ray Diffraction (XRD)	Yes	Molecular (crystalline phases); identification of corrosion product; characterization of chromophore nanoparticles and grisaille composition.	(Aulinas et al., 2009; Gentaz et al., 2012; Pradell et al., 2016)
X-Ray Fluorescence spectroscopy (XRF)	No. It can be portable	Elemental; qualitative information on major, minor, and sometimes trace elements (results may vary from the lab instrument to the portable one).	(Adlington & Freestone, 2017; Adlington et al., 2020; Bracci et al., 2020; Carmona, Ortega-Feliu, Gomez-Tubio, & Villegas, 2010; Fernandes et al., 2008; Jembrih-Simbürger et al., 2002; Rodrigues et al., 2021; Walczak et al., 2013)

Most techniques described in Table 2.1 are considered point analysis, as the information is collected from a point, usually of a few microns. Sometimes, methodologies such as FTIR and Raman offer the option of mapping small areas to verify the distribution of a particular component in a limited region of interest, depending on the model of the instrument used. On the other hand, the term "chemical (or spectral) imaging" is used to define techniques that can analyze large areas, from several centimeters to a few meters.

Apart from HSI, which will be discussed separately in section 2.2, it is worth mentioning another chemical imaging technique used to investigate stained glass. Macro X-Ray Fluorescence (MA-XRF) spectroscopy consists of scanning the surface of a work of art at a given step size with an X-ray fluorescence spectrometer connected to a moving stage. The image is formed from the acquired points, resulting in a datacube, like the hyperspectral one, where every pixel contains information regarding the elemental composition of the material under study. The datacube can be treated with suitable software, which allows the creation of maps of elements (or combination of elements) to estimate which kind of material (i.e., pigments or colorants) was employed by the artist. With regards to stained glass and historical windows, MA-XRF has been used for various aims: to discriminate between body-colored glass, flashed glass, and other paint layers (e.g., the grisaille); to distinguish ancient glass pieces from modern ones; and to detect glass alterations (Bernady, Goryl, & Walczak, 2021; Cagno et al., 2021; Gestels et al., 2022; Legrand, Van der Snickt, Cagno, Caen, & Janssens, 2019; Van der Snickt et al., 2016).

2.2 Hyperspectral imaging of stained glass

As briefly explained in the introduction, HSI consists in acquiring hundreds of images across the electromagnetic spectrum. The output of HSI is a datacube (Fig.2.2), a three-dimensional image with two spatial (x and y) and one spectral dimension (λ) (Radpour et al., 2022).

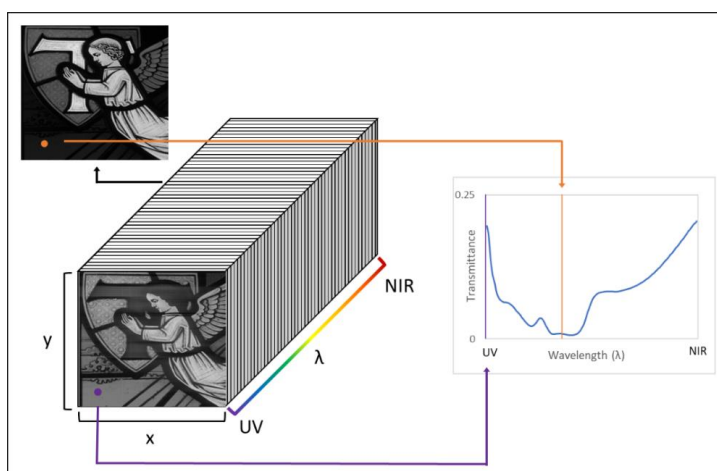


Figure 2.2: Example of a hyperspectral datacube. Each image in the datacube shows grayscale values representing how the materials absorb and reflect (in case of glass, transmit) the light at a given wavelength. The spectrum collected in a pixel (x, y) shows the reflectance/transmittance of a certain material across all the sampled wavelengths.

Hyperspectral cameras can be classified into different categories depending on the spectral range covered and the acquisition mode. The following paragraphs will describe examples of hyperspectral camera systems, focusing more specifically on those employed to analyze stained glass. In-depth reviews of HSI systems and their applications in cultural heritage are available in (Alfeld & de Viguerie, 2017; Cucci & Casini, 2019; Fischer & Kakoulli, 2006; Funatomi et al., 2022; Striova, Dal Fovo, & Fontana, 2020).

Concerning the spectral range, hyperspectral cameras can be divided into three groups:

- Visible-near-infrared (VNIR) cameras, with a spectral range usually around 400-1000 nm. Cameras working in this spectral range are the most used in cultural heritage, allowing the characterization of pigments and colorants and faithful color reproduction of artworks.
- Short-wavelength infrared (SWIR) cameras, with a spectral range usually around 900/1000 - 2500 nm. In cultural heritage, these cameras are employed to get complementary information on organic and inorganic pigments and to investigate other organic materials (e.g., paint binders). There is no documented use of SWIR cameras for imaging stained-glass windows.
- Mid-wave infrared (MWIR) cameras, with a spectral range from 2700-5500 nm. Those cameras are rarely used in cultural heritage.

Regarding the classification based on the acquisition mode, most of the HSI cameras used in cultural heritage are based on pushbroom (line scanning) systems (Fig. 2.3), which record the datacube collecting one spatial line of pixels at a time by means of a 2-dimensional detector (focal plane array) and a light dispersive element (prism or grating). The acquisition is performed by keeping the camera fixed and moving the object or vice versa, depending on the imaging setup. Datacubes built this way generally have one fixed dimension (across-track, perpendicular to the camera movement), while the other (along-track) depends on the size of the object to be scanned. Other pushbroom cameras are built with an internal scanning device and do not need external scanning equipment to be moved or move the object. In this case, the datacube has fixed dimensions, depending on the camera specifics (Picollo et al., 2020). The HySpex VNIR-1800 and the SpecimIQ cameras used during this project are push-broom systems; their setup and specifics will be discussed in Chapter 4. A push-broom camera was also used for the HSI of the two Art Nouveau stained-glass windows from the Casa-Museu Dr. Anastácio Gonçalves (Lisbon, Portugal), which results are presented in the work of (Palomar et al., 2019).

On the other hand, whiskbroom (point-scanning) systems are based on a linear array detector and collect a point at a time while the sensor is moved across the two dimensions (x and y), often following a raster scanning pattern (Fig. 2.3). Whiskbroom cameras are slower than pushbroom systems but have the advantage of a higher spectral resolution and more flexibility in terms of spatial scanning (Funatomi et al., 2022; Picollo et al., 2020). A hyperspectral camera based on this system was used by (Funatomi et al., 2022) to propose a methodology to mitigate the temporal illumination variations during the imaging of stained glass.

A recently developed HSI camera based on a Fourier Transform (FT) spectrometer, described by (Perri et al., 2019), was also used to study a stained-glass window from the Santo Spirito Church in Milan (Italy). These types of cameras, however, are not yet very popular in cultural heritage applications.

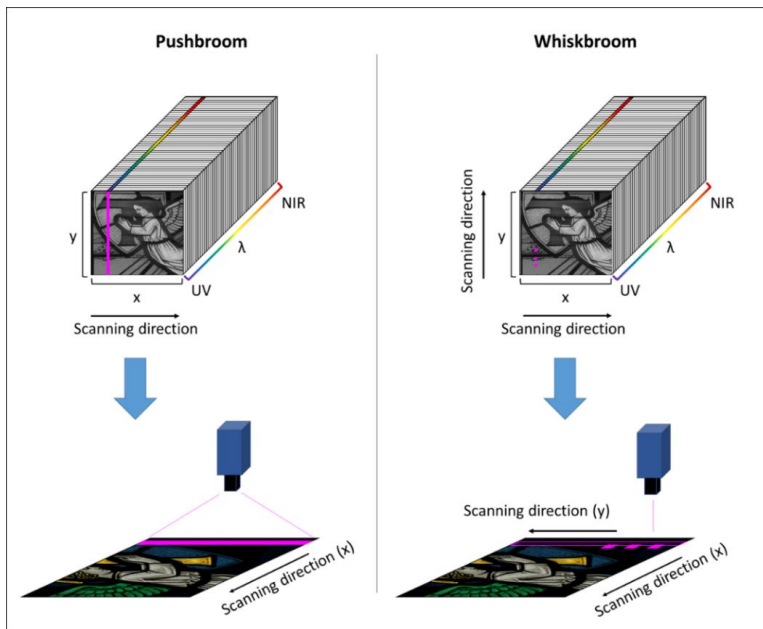


Figure 2.3: Image capture schematics for pushbroom (left) and whiskbroom (right) HSI systems.

2.2.1 Transmittance vs. Reflectance imaging geometries

One of the fundamental components of an HSI setup is the light source, which is necessary to illuminate the object and record the datacube. Broadband light sources (such as halogen lamps) are usually adopted because of their continuous spectrum, which allows avoiding gaps in the recorded spectrum that may affect the interpretation of the data (Mandal, George, Pedersen, & Boust, 2021).

Depending on the position of the light source in relation to the object investigated, it is possible to perform the acquisition in transmittance or reflectance mode (Fig.2.4).

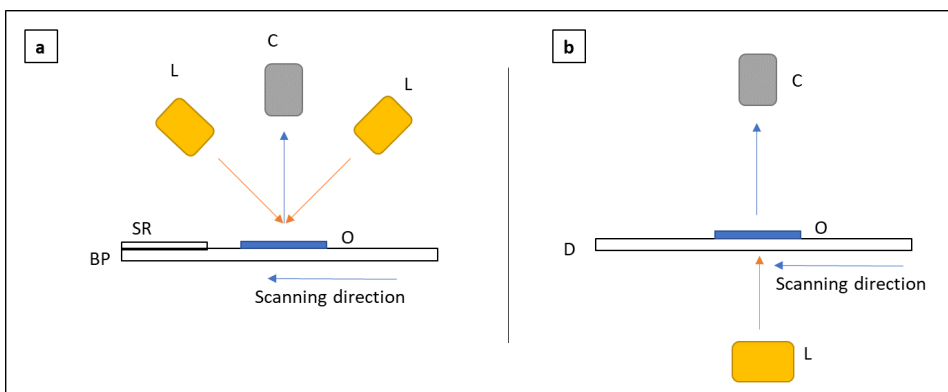


Figure 2.4: Schematic of a) reflectance and b) transmittance HSI setups for acquisition of stained glass. BP = backing paper; C = camera; D = diffuser; L = light source(s); O = object; SR = Spectralon® reference.

Most of the imaging setups are designed for acquisition in reflectance geometry. In this configuration, two light sources are positioned at the two sides of the camera with an angle of 45°-0-45°⁵ (Fig. 2.4a). This setup works for most of the artworks since they are opaque. On the other hand, as explained in the first section, stained glass windows are mostly transparent, and their colors can be observed and appreciated as the light passes through the glass sections. For this reason, a transmittance setup is necessary for the acquisition so that the light can shine through the object before reaching the camera.

Transmittance measurements can be distinguished into directional or diffused^{5, 6}. In diffused modality, standard geometry requires using opal glass (a material made of tiny colorless particles embedded in a clear glass matrix⁶) to obtain a diffuse light distribution. According to the opal glass position with respect to the light source or the receiver, the modalities can be distinguished in “diffuse influx mode”, where the geometry of the light source is diffused and that of the receiver is directional, and “diffuse efflux mode”, where the geometry of the light source is directional and that of the receiver is diffused⁶. Generally, in transmittance hyperspectral imaging performed in laboratory conditions, the light source is diffused; thus, the acquisition is carried out in diffuse influx mode. When the stained glass cannot be moved from its original place, using sunlight as the light source is a very convenient and often the only

⁵ (CIE 15: Technical Report: Colorimetry 3rd edition, 2004)

⁶ (“ISO 5-2:2009 Photography and graphic technology - density measurements: part 2: geometric conditions for transmittance density,")

possible solution. The main disadvantage, as stressed in the literature, is that the sunlight intensity changes throughout the day; it may be influenced by the weather or partially blocked by other objects in the background, casting shadows on the stained glass. Nonetheless, since solar radiation also has a continuous spectrum, the spectra obtained with this approach are relatively comparable to those obtained under standard conditions with UV-VIS-NIR spectroscopy (Palomar et al., 2019) if the interferences from external factors are limited.

Almost all the works about HSI of stained glass adopted this approach, except for the one published by (Rebollo, Ratti, Cortelazzo, Poletto, & Bertinello, 2011). In this case, the stained-glass windows were detached, and the single panels could be analyzed separately by means of a transmittance setup developed for the purpose. The setup proposed by the authors was compliant with standard geometries for diffuse transmittance measurement; tungsten-halogen lamps were used as light sources and positioned between a diffuser and the stained-glass panel, while the camera was placed on the other side. The stability of the light source and the homogeneity of the background represent a considerable advantage, especially during the radiometric correction process, which is necessary to convert the raw data into radiance data and, consequently, transmittance or reflectance (Grillini, Thomas, & George, 2021; Pillay, Hardeberg, & George, 2019; Rebollo et al., 2011).

It is essential at this point to explain the main difference between the radiometric correction for reflectance and transmittance. Regardless of the geometry, in principle, the procedure to convert radiance data to transmittance or reflectance is very similar. The signal at each pixel of the object image, acquired under a homogeneous illumination, must be corrected by the signal of a material with perfect transmittance or reflectance properties (the so-called reference) acquired under the same condition, according to the following formulas:

$$T = \frac{S_{x,\lambda} - D_{x,\lambda}}{W_{x,\lambda} - D_{x,\lambda}} \quad (\text{Eq. 3})$$

$$R = \frac{S_{x,\lambda} - D_{x,\lambda}}{W_{x,\lambda} - D_{x,\lambda}} P_{x,\lambda} \quad (\text{Eq. 4})$$

In Eq. 3, T is the transmittance, $S_{x,\lambda}$ is the signal relative to the light transmitted by the object, and $W_{x,\lambda}$ is the signal relative to the reference diffusing material, which is assumed to have a perfect transmittance. $D_{x,\lambda}$ is the signal of the dark current. Indices x and λ indicate the spatial and spectral dimensions, respectively. Depending on the camera model or brand, the dark current can be automatically subtracted by the camera while recording the raw datacube.

Otherwise, a datacube is recorded while the objective is covered and used to subtract the dark current manually (Foster & Amano, 2019).

The formula to calculate reflectance R is very similar (Eq.4). In this case, $S_{x,\lambda}$ is the signal relative to the light reflected by the object. $W_{x,\lambda}$ is the signal relative to the reference material, which is assumed to have Lambertian properties (i.e., reflects the incident light uniformly in all directions). When a standard reference is used (e.g., Spectralon[®] tiles), a quantitative measure of the reflectance can be obtained by multiplying for the additional parameter $P_{x,\lambda}$. This factor refers to the certified reflectance spectrum of the standard reference measured by the manufacturer under specific conditions. In this case, R is referred to as the reflectance factor. To the best of the candidate's knowledge, the diffusing materials used for transmittance acquisitions do not have certified transmittance values, and it is only possible to assume that the diffuser employed has a homogeneous response across the considered spectral range. For this reason, the results obtained in transmittance may not always be accurate and quantifiable. This issue is even more pronounced during in situ acquisition; besides the illumination variations, the chemical composition of the selected transmittance reference also has an essential role in the quality of the corrected data. The presence of impurities, in fact, may impart a pale coloration to the glass. This coloration is often barely visible to the naked eye. Still, the specific absorption bands of the impurities can be detected by the camera and alter the shapes of the spectra of other colored glass. This aspect will be discussed in more detail in Chapter 4, Section 4.1.1.3, dedicated to the *in-situ* application of HSI.

Reflectance imaging, while relatively uncommon for stained glass, can also be a valid option for the analysis of stained glass. For example, as stated by (Rebollo et al., 2011), this approach can be helpful when the panels are too fragile to be held in a vertical position and a transmittance setup is unavailable. In this case, the camera and the light source are positioned following the reflectance geometry recommendations. A white backing material free of optical brighteners⁷ is placed beneath the stained glass to enhance the reflectance signal; since the light has to travel twice inside the glass, this solution has also been called "double transmittance". The results are usually of lower quality compared to transmittance, especially for very dark glass; however, it seems to yield better results for light-colored glass pieces, enhancing the intensity of weak bands such as iron (Fe^{3+}) and chromium (Cr^{3+}).

⁷ See recommendations in ("ISO 13655:2017 Graphic technology - Spectral measurement and colorimetric computation for graphic arts images,")

2.2.2 Hyperspectral image processing and analysis.

Hyperspectral images have high spectral dimensionality, and dedicated software (such as ENVI⁸ or ImageJ⁹) or programming environments (such as MATLAB[®] or Python) are required to handle the processing of such large datasets. These tools can be used for simple datacube manipulations; for example, to visualize specific bands or to get a quick overview of the materials present by manually extracting a spectrum and comparing it with references. In addition, specific algorithms can be implemented for more sophisticated operations; for example, to automatically find the spectral signature of the pure materials composing the object (the so-called “endmembers”) and display their distribution across the scene. (Cucci & Casini, 2019; Radpour et al., 2022).

Since there is little literature regarding hyperspectral image analysis of stained-glass windows, this topic has been briefly addressed in this thesis. The challenges of chromophore mapping in stained glass and possible approaches for chromophore mapping will be discussed in depth in Chapter 4, Section 4.1.3. Thus, the following section aims to provide a brief overview of the most common methodologies for processing and analyzing the datacubes in cultural heritage, providing the general background necessary for the later discussion.

Most of the algorithms, like the image-processing software mentioned previously, are often adapted from remote sensing. In this sense, one of the most popular examples is the ENVI Spectral Hourglass wizard, a user-friendly pipeline for classification or unmixing on the datacube under study. The advantage of this pipeline is that the user is guided through every step, so there is no need to have a deep knowledge of image processing. This approach, for example, was used to map the colored glass of the two Art Nouveau stained-glass windows studied by (Palomar et al., 2019). Nonetheless, the same workflow can also be implemented in other platforms, such as Matlab or Python.

After image pre-processing, described in the previous section, the first step of this workflow is dimensionality reduction, which aims to select the datacube's most meaningful bands to reduce the computational load. This step can be performed through Minimum Noise Fraction (MNF) (Harris, 2006), but Principal Component Analysis (PCA) can be also used for the same purpose. The second step is endmember extraction, which aims to identify the “pure” spectra (i.e., the

⁸ The standard image processing and analysis software in remote sensing and industrial applications. Available under license. See <https://www.l3harrisgeospatial.com/Software-Technology/ENVI>

⁹ Free and open-source software for processing and analyzing scientific images, with many derivatives and variants (e.g., ImageJ2, Fiji, and others). See <https://imagej.net/software/imagej/>

signal related to a single material) from within the datacube, defined as the “endmember”. One of the most common methods to perform this step is the Pixel Purity Index (PPI) algorithm (Boardman, Kruse, & Green, 1995), which projects every spectral vector onto a large set of random vectors (skewers). The points corresponding to extremes, for each skewer direction, are stored. A cumulative account records the number of times each pixel (i.e., a given spectral vector) is found to be extreme. The pixels with the highest scores are identified as endmembers (Bioucas-Dias et al., 2012).

Another popular endmember extracting algorithm is N-FINDR (Winter, 1999). This algorithm is based on the assumption that in spectral dimensions, the volume defined by a simplex formed by the purest pixels is larger than any other volume defined by any other combination of pixels. This algorithm finds the set of pixels defining the largest volume by inflating a simplex inside the data, starting from a random set of pixels. For each pixel and each endmember, the endmember is replaced with the spectrum of the pixel, and the volume is recalculated. If it increases, the spectrum of the new pixel replaces that endmember. This procedure is repeated until there are no more replacements (Bioucas-Dias et al., 2012; Winter, 1999).

Alternatively, a library of reference spectra prepared by the user can be used if available. The spectral library obtained is used to perform the last step, classification or unmixing. Classification algorithms assume that the signal observed in a pixel represents a single material and assign each pixel to a class by comparing the similarity of the reference spectra with the spectra in each pixel of the datacube (target). One of the most popular classification algorithms is Spectral Angle Mapper (SAM) (Kruse et al., 1993). It treats the spectra as vectors with dimensionality equal to the number of bands and performs the comparison by measuring the angle between the reference spectra (r_λ) and the target (t_λ), according to Eq. 5.

$$\alpha = \cos^{-1} \frac{(\sum_{\lambda} t_{\lambda} r_{\lambda})}{(\sum_{\lambda} t_{\lambda}^2)^{1/2} (\sum_{\lambda} r_{\lambda}^2)^{1/2}} \quad (\text{Eq. 5})$$

Smaller values of α (expressed in radians) indicate higher similarity. An important parameter to set for a correct classification is the maximum angle (in radians) which determines the angular threshold for classifying the distance between the spectral data and the endmembers (Cucci & Casini, 2019; Deborah, George, & Hardeberg, 2014).

A similar but more accurate algorithm is Spectral Correlation Mapper (SCM) which calculates the similarity through Pearson’s correlation coefficient R (Eq.6). The algorithm centralizes the

data in its mean so that R has a value between 1 (total correlation) and -1 (negative correlation) (Deborah et al., 2014).

$$R = \frac{(\sum_{\lambda}(t_{\lambda} - \bar{t})(r_{\lambda} - \bar{r}))}{(\sum_{\lambda}(t_{\lambda} - \bar{t})^2)^{1/2} (\sum_{\lambda}(r_{\lambda} - \bar{r})^2)^{1/2}} \quad (\text{Eq. 6})$$

On the other hand, spectral unmixing aims to decompose the signal of a mixed pixel into a collection of endmembers, and a set of fractional abundances that indicate the proportion of each endmember (Dobigeon, Altmann, Brun, & Moussaoui, 2016; Keshava, 2002). Compared to classification, unmixing algorithms are usually more reliable since they are based on physically meaningful mixture models that describe the interaction between light, material, and the sensor of the hyperspectral camera during the acquisition.

These mixture models are divided into linear and non-linear. The choice of one or another model to solve the unmixing problem is extremely important in data processing since they are based on different assumptions that can be crucial for obtaining meaningful results (Dobigeon et al., 2016; Keshava, 2002).

The linear mixture model is based on three fundamental assumptions: 1) the unmixing process occurs on a macroscopic scale; 2) the pixel components appear in spatially segregated patterns (like a checkerboard); 3) each incident photon interacts with a single pixel component.

If the three assumptions are satisfied, a mixed pixel can be described as a linear combination of pure spectral signatures of its constituent components (Eq. 7):

$$\mathbf{x} = \sum_{i=1}^M a_i s_i + \mathbf{w} = \mathbf{S}\mathbf{a} + \mathbf{w} \quad (\text{Eq. 7})$$

Where \mathbf{x} is the vector of the spectrum observed in a pixel with dimension $L^{10} \times 1$, \mathbf{S} is the $L \times M$ matrix whose columns are the $L \times 1$ endmembers s_i , $i = 1, \dots, M^{11}$, \mathbf{a} is the fractional abundance vector with dimension $M \times 1$ whose entries are a_i , $i = 1, \dots, M$. \mathbf{w} is the vector related to the noise, with dimension $L \times 1$ (Keshava, 2002).

The most basic algorithm to perform linear unmixing is Least Squares, which can be implemented in its unconstrained, constrained, and fully constrained variants. Linear unmixing, in fact, is subjected to two physically-based constraints: the abundance non-negativity (ANC),

¹⁰ Number of spectral bands

¹¹ Number of endmembers

which requires that the abundances' values must be positive, and the abundance sum-to-one (ASC), which requires that the abundances in the mixed pixel must not go above 1. When both constraints are applied, Least Squares is defined as fully-constrained. Depending on the acquisition conditions, however, the sum-to-one constraint may be discarded, since the combined abundances' values may be less or more than 1. In this case, Least Squares is defined as constrained or non-negative Least Squares.

The non-linear mixture model, on the other hand, considers the components in an intimate association or multilayered; thus, the light interacts with more than one component as it is multiply scattered. While the non-linear model has been proven to be more accurate and more representative of a real case scenario, linear mixture models still represent a good approximation, due to their relative computational simplicity with respect to non-linear algorithms (Bioucas-Dias et al., 2012; Dobigeon et al., 2016).

When the endmembers are unknown or spectral libraries are not available, unsupervised (or blind source separation) methods can be implemented. In this case, the endmembers and their fractional abundances are simultaneously estimated. Algorithms based on Non-negative Matrix Factorization (NMF) are very popular for these kinds of applications (Dobigeon et al., 2016). The LUMoS algorithm (McRae, Oleksyn, Miller, & Gao, 2019), proposed in this thesis for chromophore mapping (see Chapter 4 for further details) is also part of unsupervised methods.

Through the years, more sophisticated algorithms have been adapted from other fields and optimized for cultural heritage needs. Unsupervised classification methods, such as t-Distributed Stochastic Neighbor Embedding (t-SNE) (Pouyet, Rohani, Katsaggelos, Cossairt, & Walton, 2018) and Uniform Manifold Approximation and Projection for Dimension Reduction (UMAP) (Vermeulen, Smith, Eremin, Rayner, & Walton, 2021) have been proposed for data reduction and visualization of hyperspectral images of artwork (Picollo et al., 2020). The wealth of information available from art treatises and scientific investigations has also allowed researchers to create spectral libraries of painting materials that can be used to investigate the work of a particular author or a defined historical period. The ground truth provided by those spectral libraries has allowed experimenting with machine learning-based classification and unmixing algorithms, which seem to output more accurate distribution maps (Balas et al., 2018; Deborah, Ulfarsson, & Sigurdsson, 2021; Grabowski et al., 2018; Polak et al., 2017; Pouyet et al., 2021; Rohani et al., 2018).

Chapter 3

Summary of included papers

In this chapter, the papers contributing to the thesis are summarized. The summary briefly reports the objectives, the motivations, and the main findings. As mentioned in the first chapter, the papers are not organized chronologically but according to the thesis's narrative, which will be discussed in detail in the next chapter. The full versions of the publications are available in Part II of the thesis.

3.1 Paper 1: Potential and challenges of spectral imaging for documentation and analysis of stained-glass windows

Paper 1 starts with a literature review of the main techniques for documenting and analyzing stained glass, from traditional photography to chemical imaging, to non-invasive and invasive scientific techniques. After the literature review, a more systematic application of spectral imaging to stained glass is proposed, discussing the advantages of HSI compared to the other analytical techniques described in the paper and the challenges to be addressed. The outlined methodology represents the foundation of the research project presented in this work.

The candidate conducted the literature review and wrote and edited the original draft.

3.2 Paper 2: Comparison of hyperspectral imaging and fiber optic reflectance spectroscopy for reflectance and transmittance measurements of colored glass

Chronologically, this work was published in the last year of the PhD. However, according to the PhD structure outlined in Chapter 1, this paper should be considered the first concerning HSI applications. This paper, in fact, aims to compare the performance of UV-VIS spectroscopy and HSI to validate the results obtained from the latter. Instead of stained-glass panels, fourteen glass pieces of five different colors (green, red, blue, yellow/amber, purple), with various thicknesses and transparency, were used to facilitate the application of the two instruments. The measurements were carried out in transmittance and reflectance modes to investigate the differences and similarities between the two modalities. In the reflectance modality, a white sheet of paper without optical brighteners was used as a backing material to

enhance the reflectance signal of the glass pieces. The differences between the two geometries and the characteristics of the glass pieces are discussed in-depth to show how these factors influence the quality of the two modalities' results.

The degree of agreement between the two instruments in the two modalities was evaluated by comparing the spectra obtained and validated by calculating $L^*a^*b^*$ values and the color difference ΔE_{00} .

The results demonstrated that under standard transmittance mode conditions (ISO 5-2:2009), HSI could provide results of similar quality as UV-VIS spectroscopy in terms of spectral shape and intensity, showing the lowest ΔE_{00} . In reflectance modality, on the other hand, the spectra obtained by the FORS showed higher intensity than the hyperspectral ones, especially in the case of the darkest samples.

In general, compared to the transmittance mode, the reflectance mode did not perform very well, especially with dark-colored glass, as most of the light was absorbed while traveling twice through the glass. From the spectral point of view, this resulted in the loss of the chromophores' characteristic bands. However, the reflectance modality could enhance the intensity of small peaks in light-colored glass, allowing, for example, better identification of chromium and iron bands in green glass pieces. In this sense, the results were consistent with the observations expressed in (Rebollo et al., 2011).

The candidate was responsible for conceptualizing the work, developing the methodology, acquiring, interpreting, validating the data, and writing and editing the original draft.

3.3 Paper 3: Hyperspectral imaging workflow for the acquisition and analysis of stained-glass panels

Paper 3 presents a workflow for the imaging and analysis of stained-glass windows in laboratory conditions. Chronologically, this is the second paper published, describing for the first time the laboratory setup and the image processing steps for radiometric correction of datacubes acquired in transmittance.

The paper proposes various applications of HSI for the investigation of stained glass and focuses on two main aspects: visualization and chromophore identification. A mock-up stained-glass panel consisting of 100 colored and transparent glass tiles was used as a case study.

Regarding visualization, the paper compares the color accuracy of RGB images obtained from bands selected from the datacube and images rendered from spectral data through color matching functions and the D65 standard illuminant spectrum. Compared to band-selected images, the rendered ones show more realistic colors and allow a better appreciation of dark-colored glass. The spectral rendering methodology was also used to simulate the change in color of the glass under the D series illuminants representing different moments on the days. Lastly, the use of IR-false color images as a fast visualization tool was proposed for the first time. The results shown in the paper demonstrated that this methodology works particularly well for preliminary discrimination of green and blue glass colored by different chromophores.

Concerning chromophore identification, the paper proved the capability of HSI to distinguish glass with similar colors but different compositions by showing examples of green glass. The spectra of two groups of green glass, containing copper, iron, and chromium in diverse concentrations, were compared to validate the correctness of the IR-false color image results. Elemental analysis (XRF) results were also provided to support the HSI data interpretation.

The candidate was responsible for conceptualizing the work, developing the methodology, acquiring and interpreting the data, and writing and editing the original draft.

3.4 Paper 4: A portable setup for hyperspectral imaging of stained-glass panels

Paper 4 presents a portable HSI setup able to acquire relatively small-sized panels (max 45×45 cm). The setup consists of a system of two diffusers and two light sources fixed on an easel and placed behind the stained glass. The stained-glass panels are kept vertical on an easel and secured through ethafoam pieces and strings to prevent the artwork from falling. The hyperspectral camera is mounted on a rotational stage and is placed in front of the stained glass.

The setup was designed at the Colorlab and subsequently developed and tested at the Swiss National Museum (SNM) facilities. Ten stained glass panels, representative of different historical periods and glass-making techniques, were analyzed to evaluate the capability of the setup for acquiring stained glass panels of various sizes and shapes. The system's characteristics are thoroughly described in the paper, and relevant examples are shown to highlight the advantages and limitations of the system. One of the main drawbacks of the setup, for example, is the geometric (radial) distortions visible in the images due to the movement of the rotational stage. On the other hand, the spectral data are well comparable with the results obtained with the laboratory setup and consistent with the available literature. Following the same workflow

proposed in **Paper 3**, rendered images were provided for data visualization. False color images were used as a fast tool to identify glass of similar color but containing different chromophores. Spectra from green and red areas were compared to prove the results from the false color images.

The candidate was responsible for conceptualizing the work, developing the methodology, acquiring, interpreting, validating the data, and writing and editing the original draft.

3.5 Paper 5: Acquisition strategies for *in-situ* hyperspectral imaging of stained-glass windows: case studies from the Swiss National Museum

Paper 5 presents the results of an *in-situ* campaign at the Swiss National Museum. The scope of this work was to propose strategies to tackle the challenges that can affect the quality of HSI of stained-glass windows when they cannot be removed from their original location. Two different scenarios were considered during the imaging campaign. In the first case, the stained-glass windows are exposed to sunlight, which can be exploited as a light source. The main challenges in this situation are represented by inhomogeneous illumination and the presence of buildings and vegetation in the background. In the second case, the stained-glass panels are located in the windows of an internal wall, and they are not directly exposed to sunlight or other sources of stable illumination.

The proposed methodology was tested on eight stained-glass panels displayed in windows at the Swiss National Museum, chosen after discussion with the museum conservators considering various factors related to the environment and the artwork characteristics. All the case studies were captured multiple times, selecting different transmittance references for the pre-processing to evaluate the quality of the HSI datacubes in various conditions. Some panels exposed to sunlight were imaged before and after placing a diffusing sheet behind the windows and, in a few cases, acquired at different moments of the day. Regarding the stained glass in the windows of the internal wall, a lighting setup consisting of a photography light diffuser and a halogen lamp was developed and tested to perform the acquisitions.

Results from five representative case studies, four exposed to sunlight and one from the internal wall, are discussed in the paper to compare the different acquisition scenarios (natural vs. artificial illumination) and provide general recommendations to consider during imaging campaigns.

The candidate was responsible for conceptualizing the work, developing the methodology, acquiring, interpreting, validating the data, and writing and editing the original draft.

3.6 Paper 6: Blind unmixing of hyperspectral images of stained glass: adapting the LUMoS algorithm for chromophore mapping.

This paper focuses on the image analysis of stained-glass panels acquired with the portable setup at the SNM Collection Center. The paper proposes a blind unmixing methodology to map glass pieces colored in a similar way (same group and concentration of chromophores) as an alternative to traditional approaches (endmember extraction + classification/unmixing). The advantage of blind unmixing is that it is not required to have a ground truth regarding the object under investigation, as the endmembers and their fractional abundances are estimated simultaneously. For this reason, this approach is particularly feasible for stained glass, especially when the color palette is broad and the information on the glass-making technique is scarce. The LUMoS algorithm was chosen among others because it allows searching for potentially an unlimited number of endmembers. Moreover, its implementation is relatively straightforward, as the input from the user is minimal.

Two 20th-century stained-glass panels characterized by a complex palette were used as case studies to test the algorithm's performance. Preliminary results on the most recurring colors (green and blue; red glass only in the first case study) were discussed to highlight the advantages and limitations of the proposed methodology. XRF analyses were carried out to validate the algorithm's results.

The results demonstrated that the LUMoS algorithm could provide sufficiently correct abundance maps of those chromophore combinations defined enough to be considered a specific endmember. The accuracy of the maps was confirmed by spectra comparison of the glass classified in the same groups. The classification errors could be easily identified and associated with the too-similar spectral shape of those glass pieces erroneously mapped together. The complementary elemental information from XRF analyses also confirmed the correctness of the generated maps and provided additional information on the production technology of the colored glass. In addition, XRF measurements on both sides of the stained glass helped identify overlaid (layered) glass that could not be characterized by HSI.

The candidate was responsible for conceptualizing the work, developing the methodology, acquiring, interpreting, validating the data, and writing and editing the original draft.

Chapter 4

Discussion

In this chapter, the research outcomes from the papers summarized in the previous chapter will be discussed, highlighting how successful they were in fulfilling the objectives and answering the research questions stated in the first chapter. The full details regarding the camera parameters and setups' specifics can be found in the published papers. However, general information will be provided when necessary to compare the performance of the three systems. The research's contribution to the imaging and cultural heritage fields will also be discussed at the end of the chapter.

4.1 Research outcomes

4.1.1 Hyperspectral imaging

Regarding HSI, most of the research focused more on developing the imaging setups (SO1-3) than image processing. This choice is related to the fact that, as explained in the introductory chapter, stained glass can be found both in buildings and as detached panels. The two situations require different specifications, especially concerning the source of illumination available (natural vs. artificial light). Thus, it was deemed necessary to develop systems that could be employed in both conditions. The following sub-sections will describe the characteristics and main advantages, while Table 1 at the end of this section summarizes and compares some of the most relevant technical aspects of the three setups.

4.1.1.1 *Laboratory setup*

Chronologically, the laboratory setup was the first to be used. The system has been designed by the HySpex branch of Norsk Elektro Optikk (NEO)¹² to work in connection with the VNIR and SWIR HySpex push-broom cameras. During the research, the HySpex VNIR-1800 model was employed; the camera acquires 186 images in the visible and near-infrared (VNIR) range (400–1000nm) and has a spatial resolution of 1800 pixels across the track. The camera can be equipped with three different objectives with fixed focusing distances at 30 cm, 1 m, and 3 m;

¹² <https://www.hyspex.com/hyspex-turnkey-solutions/laboratory-systems/>

if the 30 cm lens is employed, the linear field of view will correspond to around 8 cm across track.

The laboratory setup consists of a translational stage, fixed light sources, and a support to hold the camera. The latter can be moved along a pole to adjust the height required by the working distance (30 cm or 1 m) of the camera objective in use during the measurement. Since the camera and the light sources are fixed, the image is recorded line by line while the translational stage moves; the HSI acquisition parameters control the movement of the stage and, consequently, the speed of the acquisition. In this configuration, the light distribution and intensity are approximately the same for each recorded line, representing an advantage during the image pre-processing stage. This way, it can be assumed that the signal collected and averaged from a few lines can represent the light distribution across the whole field of view. Thus, instead of collecting the reference over the entire field of view before the acquisition, it is necessary to include only a portion of the reference material (Spectralon® for reflectance measurements or a transparent area for transmittance ones) covering the camera’s field of view to capture the light information on the object. This portion can be used to obtain the reference spectrum and perform the radiometric correction, according to the workflow shown in Fig.4.1.

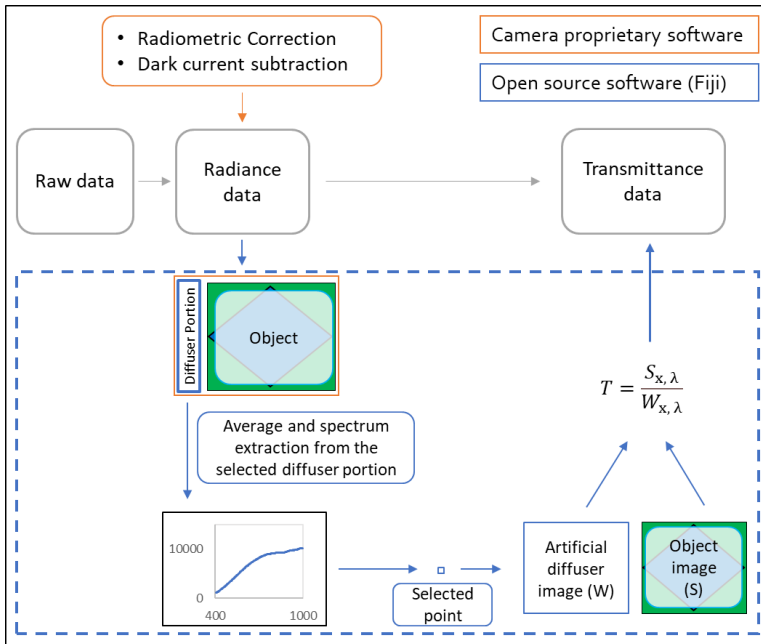


Figure 4.1: Acquisition and preprocessing workflow for HSI performed with the laboratory setup. T = transmittance, $S_{x,\lambda}$ = signal relative to the light transmitted by the object on top of the diffuser. $W_{x,\lambda}$ = signal relative to the artificial reference image created from the averaged spectra of a portion of the diffuser. In this case, all the pixels at location x , have the same intensity value. Indices x and λ indicate respectively the spatial and the spectral dimension.

During this step, all 1800 across-track pixels must be included when averaging the lines from the reference to consider the possible light variation along the lines.

The system was initially meant for reflectance measurements and was subsequently modified to allow imaging in transmittance (Fig. 4.2).

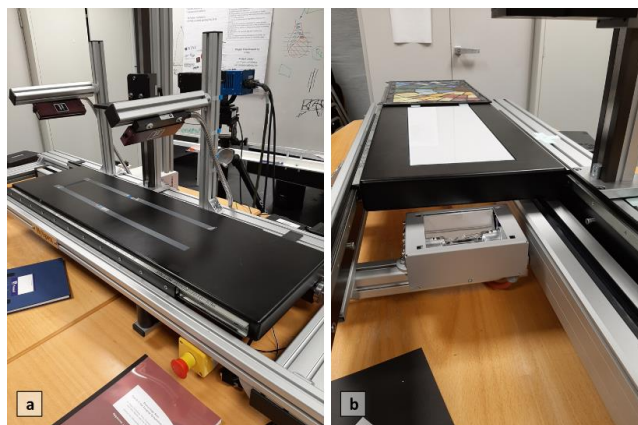


Figure 4.2: The laboratory HSI setup for a) reflectance measurements and b) transmittance measurements (notice the white diffusing panel at the center of the stage).

The stage was replaced with a new one equipped with a diffuser panel, large enough to cover the camera's field of view, under which a halogen lamp was positioned as the light source. Before these modifications, some experiments were performed in reflectance mode. This constraint represented the motivation to study the performance differences between reflectance and transmittance imaging geometries, which resulted in the publication of **Paper 2**. The paper confirmed the observations stated in the work of (Rebollo et al., 2011); the reflectance modality does not work well with dark-colored glass, as most of the light is absorbed while traveling twice through the glass. From the spectral point of view, this results in the loss of the characteristic absorbance band associated with the chromophores in intensely colored glass. On the other hand, the reflectance modality helps enhance the intensity of weak bands in light-colored glass, such as iron (Fe^{3+}) and chromium (Cr^{3+}), in green glass.

Regarding applications on real stained glass, with this setup, it is possible to safely acquire panels with a maximum size of 50 x 50 cm. The system's feasibility for such relatively large objects was tested on two occasions. The first time, the setup was disassembled and rebuilt at the old National Museum of Oslo premises to scan four of Emmanuel Vigeland's stained-glass panels (Fig 4.3). These panels were made in 1923 and were originally part of a larger stained-glass window called "God's spirit and scenes of earthly life with comforting angels", installed

in one of the staircases of the museum. The panels were removed during an extensive restoration campaign in 2019 and stored separately (Nidaros Domkirkes Restaureringsarbeider, 2019). This imaging campaign was a valuable occasion to evaluate the advantages and limitations of the technique from many points of view.



Figure 4.3: a, b) the two Vigeland's stained-glass panels analyzed at the old building of the National Museum of Oslo. Notice the darkness of the glass pieces and the presence of a thick patina applied over all the glass pieces. c, d) RGB images rendered from the datacube through color matching function and a standard illuminant (D65). Note that the brightness has been slightly increased to improve the visualization of darker colors (e.g., green, blue, and purple).

Concerning the setup, its size, weight, and design were not optimal for transportation. The disassembling, packing, and rebuilding were highly time-consuming and required the presence of at least three or four people. In addition, the stage was too narrow to fit the entire panels; a makeshift support made of cardboard was attached to the stage to solve the issue (Fig.4.4). This solution was allowed by the museum's object conservator, thanks to the fact that the stage moves slowly enough to ensure the safety of the object during the scanning.

The type of light source employed was also an issue: the halogen lamp supplied with the system is very powerful and emits a considerable amount of heat. This can be harmful to stained glass since the high temperature could cause the expansion of the different materials at different rates. Therefore, depending on the state of conservation of the object, alteration, and detachment of painted surfaces can be generated (Palomar, Agua, & Gomez-Heras, 2018).



Figure 4.4: Configuration of the setup during the acquisition of Vigeland's stained-glass panels. An extended support was used to handle large-sized objects.

An attempt to reduce the temperature was made by positioning the lamp as far as possible from the stage and turning off the light between every acquisition.

Other complications regarded the objects themselves. Vigeland's glass-making technique is characterized by the use of thick and uneven glass pieces and the application of a dark patina all over the surface of the stained glass (Fig 4.3a and b). These artistic choices have two main consequences: first, most of the incident light is absorbed, resulting in very underexposed and noisy images, even after setting a long integration time (43000 μs). Second, the signature peaks of the glass chromophores are altered by the signal of the patina, hindering the data interpretation process.

For the reasons explained above, very few results could be obtained from these stained-glass panels in terms of material identification and mapping, also due to the availability of very little ground truth information on the glass-making technique of Vigeland. Nonetheless, it was a valuable opportunity to test the limits of the HSI not only from the acquisition point of view but also from the image processing one.

With regard to the second experiment, the laboratory setup was used to analyze a mock-up stained glass panel, kindly lent by Dr. Lindsay MacDonald. The panel was created initially for camera calibration within the Fairford project (MacDonald & Oldfield, 1996). The dimension of the panel is 51.5 x 40.5 cm, and it consists of 80 colored and 20 clear glass arranged in a 10 x 10 grid of rectangular glass tiles (Fig. 4.5a). The glass tiles are painted with grisaille and silver stained yellow in various textures. Thanks to these characteristics, the panel represented an excellent case study to better understand the potential of HIS.

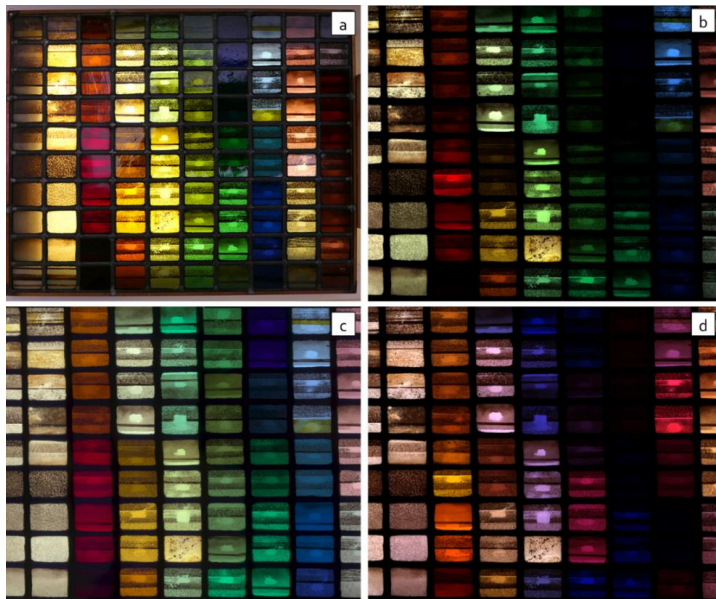


Figure 4.5: a) High-quality picture of the mock-up panel used for the second experiment with the laboratory setup, photographed at a light table (©Lindsay MacDonald). b) RGB image obtained by selecting three bands (related to red, green, and blue) from the datacube. Note that the last column and last row of the panel are missing as they were not included in the final stitching. c) Color image obtained by using color matching function and standard illuminant D65. d) IR-false color image (for more details see section 4.1.2.2).

Fig. 4.6 shows the acquisition conditions of the panel in the laboratory. Also in this case, a piece of cardboard was used to support the panel portion exceeding the stage. A total of twelve datacubes were collected to cover the entire panel, but only eight of them were stitched together (Fig. 4.5b, c, d) for the image analysis.

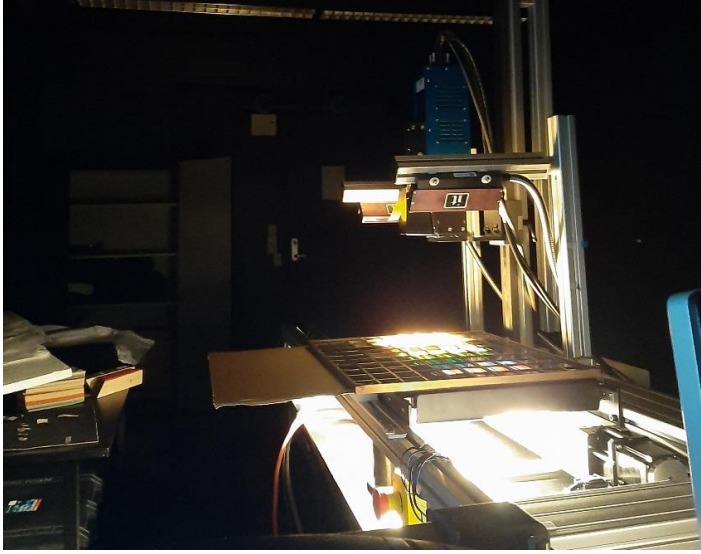


Figure 4.6: Acquisition of the mock-up stained-glass panel in the laboratory.

The first results on this panel were presented at the SPIE Optics for Arts, Architecture, and Archaeology VIII conference in 2021 and published in **Paper 3**. The paper proposed a workflow for image acquisition and preprocessing using the laboratory setup. In addition, it provided an overview of the results that can be obtained with HSI in terms of data visualization and material identification. Concerning visualization, the paper highlights the advantages of exploiting the spectral information from HSI to obtain color images that are more accurate than those generated through simple band selection from the datacube (Fig. 4.5b). The rendered image of the test panel (Fig. 4.5c) was obtained by calculating the CIE XYZ values from the spectrum in each pixel (u, v) of the image (Eq. 9-11):

$$X(u, v) = k \int L(u, v; \lambda), \bar{x}(\lambda) d\lambda \quad (\text{Eq. 9})$$

$$Y(u, v) = k \int L(u, v; \lambda), \bar{y}(\lambda) d\lambda \quad (\text{Eq. 10})$$

$$Z(u, v) = k \int L(u, v; \lambda), \bar{z}(\lambda) d\lambda \quad (\text{Eq. 11})$$

where k is a constant so that $Y = 100$ for a perfectly white surface under full illumination, $L(u, v; \lambda)$ is the radiance image obtained by multiplying the reflectance image and the chosen standard illuminant (in this case D65) and \bar{x} , \bar{y} , \bar{z} are the CIE 1931 2° standard observer color

matching functions. The XYZ values were then converted to the sRGB tristimulus values by applying the following linear transformation (Eq. 12) to obtain the RGB image:

$$\begin{bmatrix} R \\ G \\ B \end{bmatrix} = \begin{bmatrix} 3.2406 & -1.572 & -4986 \\ -0.9689 & 1.8758 & 0.4986 \\ 0.0557 & -0.2040 & 1.0570 \end{bmatrix} \begin{bmatrix} X \\ Y \\ Z \end{bmatrix} \quad (\text{Eq. 12})$$

The entire procedure was performed in MATLAB following the workflow described in (Foster & Amano, 2019) and the related tutorial.

The article also proposes for the first time the use of false color imaging as a fast tool for preliminary discrimination of glass with similar color but containing different chromophores or varying concentrations of the same ones (Fig 4.5d).

Regarding material identification, this paper addresses the benefits of complementary analysis for thoroughly characterizing stained-glass materials. XRF spectra were used to validate the grouping of some green glass characterized by a similar appearance in IR-false color images and similar spectral shapes (Fig 4.7). This topic will be discussed more in-depth in Section 4.1.2 regarding data validation.

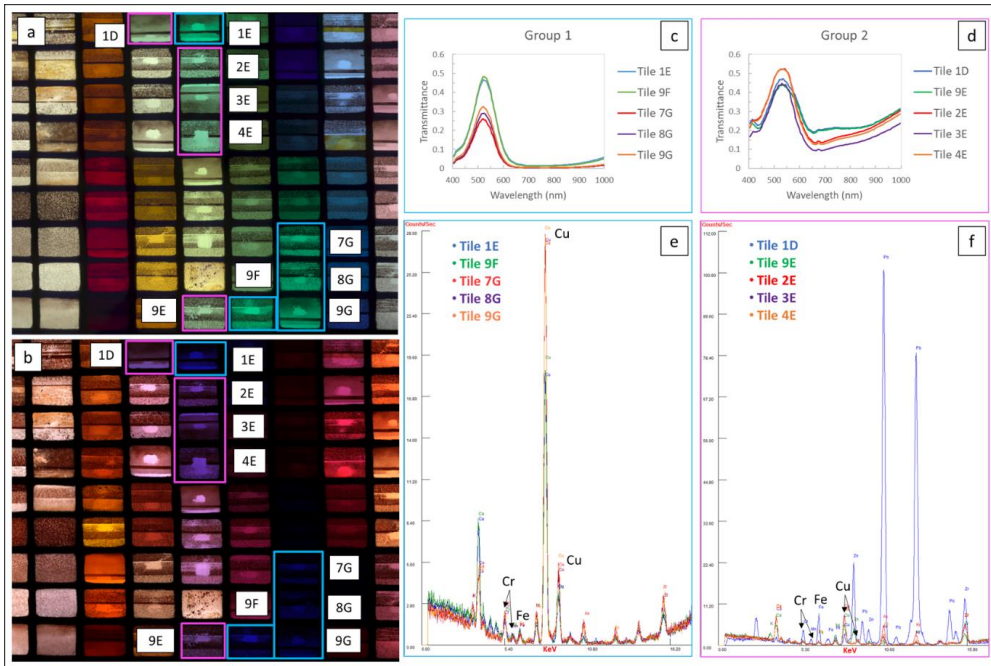


Figure 4.7: a) Rendered color image and b) IR false-color image of the mock-up panel. Two groups of green glass are highlighted. c and d) HSI spectra of the two identified groups of green glass. Notice that the spectra of tiles 1D and 9E are slightly different from the others. e and f) XRF spectra of the two identified groups of green glass. The two groups are characterized by different amounts of Copper (Cu), Chromium (Cr) and Iron (Fe). The presence of lead (Pb) in sample 1D could be related to the proximity of the lead came to the spot where the XRF point was taken (clear area on the bottom).

4.1.1.2 Portable setup

The development of a more portable system arose from the necessity of carrying out an acquisition campaign on stained-glass panels that cannot be moved from their storage location. In this case, the most significant challenge was to design a more flexible setup that could either be transported or built easily at the location where the imaging campaign should have been performed. To test the feasibility of the methodology, a few stained-glass panels stored at the Collection Center of the Swiss National Museum (SNM) were chosen as case studies.

The first step to improve the portability was to substitute the translating stage with a lighter system consisting of a tripod equipped with a rotational stage. In this configuration, however, the camera is the part that moves; thus, it was necessary to create a stable supporting structure for both the light source and the object. The initial idea, discussed with the museum's conservators, was to create a sort of light table that could allow the acquisition of the stained glass in a horizontal position to ensure the panels' safety during the measurements. In this case, as shown in Fig.4.8a, the camera should have been rotated 90° facing down. Unfortunately, the rotational stage was not designed to work extensively in this configuration due to the camera weight and the stage motor's limited power. This limitation led to a malfunctioning of the rotating stage, which had to be substituted during the imaging campaign. Thus, to carry on with the analysis in the little time available the first design (Fig. 4.8a) was modified so the stained-glass panels could be safely kept in a vertical position (Fig. 4.8b).

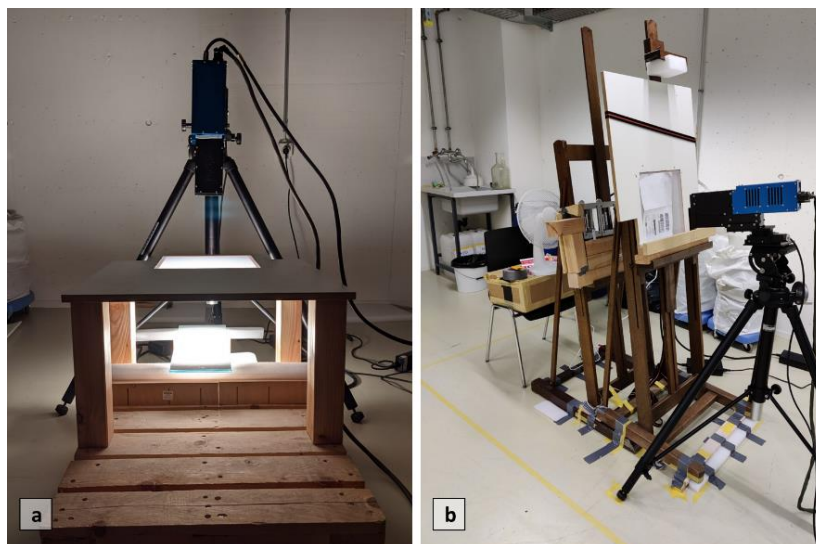


Figure 4.8: First and second prototype of the portable HSI setup a) before and b) after the modifications to allow the acquisition of the panels in a vertical position.

The light-object support was built entirely using materials available at the conservation workshop of the Collection Center or bought at common hardware shops. The mounting required the collaboration of three people. The characteristics of the portable setup and the camera parameters are thoroughly described in **Paper 4**; nonetheless, it is worth discussing some aspects to highlight the main differences with the previous setup.

The first difference regards the stage connected to the camera. As stated in the previous section, push-broom cameras build the image by acquiring one line at a time. When using a translating stage, the camera is fixed, and the datacube is recorded as the stage supporting the object moves. This approach allows collecting a potentially unlimited number of lines and, consequently, a large portion of an object in a single acquisition.

On the other hand, when a rotational stage is used, the datacube is recorded while the camera moves from one side to another (left to right or vice versa). This way, it is possible to acquire only around a thousand lines (corresponding to a few centimeters) for a single acquisition before significant geometric distortions occur. These geometric distortions consist of a combination of vertical distortion (due to the camera optics) and horizontal distortion (caused by the camera movement), which affects the aspect ratio of the datacubes. While vertical distortion requires specific calculations to be corrected, horizontal distortion can be avoided by taking note of the maximum number of lines that it is possible to acquire before the start of the acquisition. This task can be performed by acquiring a printed grid of known dimensions to observe at which point the horizontal distortions start to appear (Fig. 4.9a). In addition, a loss of focus can be noticed at the edge of the image going toward the scanning direction (Fig. 4.9b), which appears blurred.

Thus, compared to the results obtained from the laboratory setup, the images obtained from the portable one can be only considered individually and for the sole purpose of material identification. The geometrical distortions, in fact, can become an issue when attempting to stitch two images together (see for comparison the stitched images of the mock-up panel in Fig. 4.10b and the two single datacubes from one of the SNM case studies in Fig 4.10e). If the stained-glass panel has been scanned in two different directions, the overlapping parts will not match, as the points taken as references are shifted. The loss of focus at one side of the image represents an additional issue during the stitching process, as the blurring reduces the quality of the final image (Fig. 4.9b).

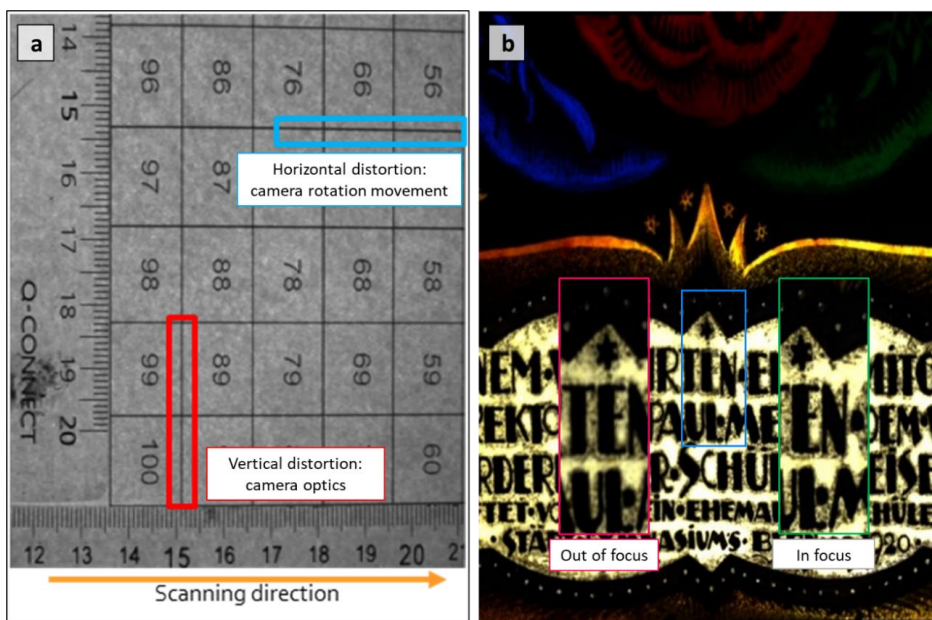


Figure 4.9: a) Printed grid used to visualize the horizontal (blue rectangle) and vertical (red rectangle) distortions. b) RGB image of the lower part of case study LM-167914 (see Paper 4) obtained by stitching two datacubes. The red and green rectangles show details of the overlapping areas (blue rectangles) of the two datacubes used for the stitching. The loss of focus visible in the image on the left (red rectangle) is due to the rotation movement of the camera.

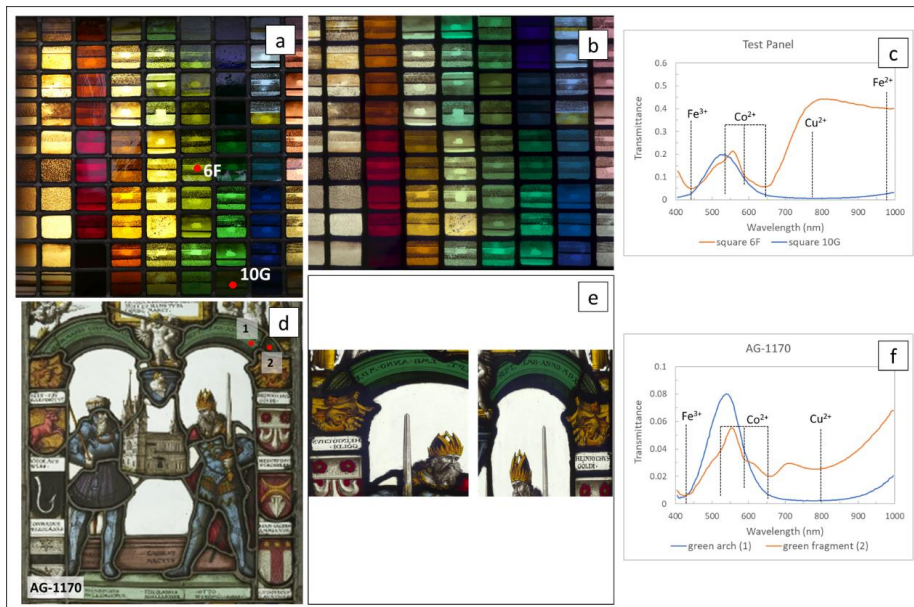


Figure 4.10: a) High-quality picture of the mock-up panel. b) Rendered color image. Note that the distortions in the stitched image are minimal and the image proportion is overall respected. d) High-quality picture of case study AG-1170 (© Swiss National Museum). e) Examples of two datacubes recorded putting the panel in a different orientation during the acquisition. Notice the different aspect ratio of the two images; in this case, the stitching is impossible, unless the geometric distortions are corrected. c, f) spectra of four green glass (two for each case study in a and d respectively) with similar composition. In both cases, the spectra are smooth and the bands of the chromophores well identifiable.

The rotational movement of the camera also influences the radiometric correction process. Differently from the laboratory setup, in this case, the camera moves while the lights are fixed. For this reason, it cannot be assumed that the light intensity is the same in all the collected lines. Thus, the transmittance reference (i.e., the diffusing plate) was recorded across the whole field of view to account for this issue. This process was repeated four times (in the morning, midday, early afternoon, and late afternoon) to consider the intensity fluctuation of the light source during the day. The radiometric correction was performed following the workflow shown in Fig. 4.11.

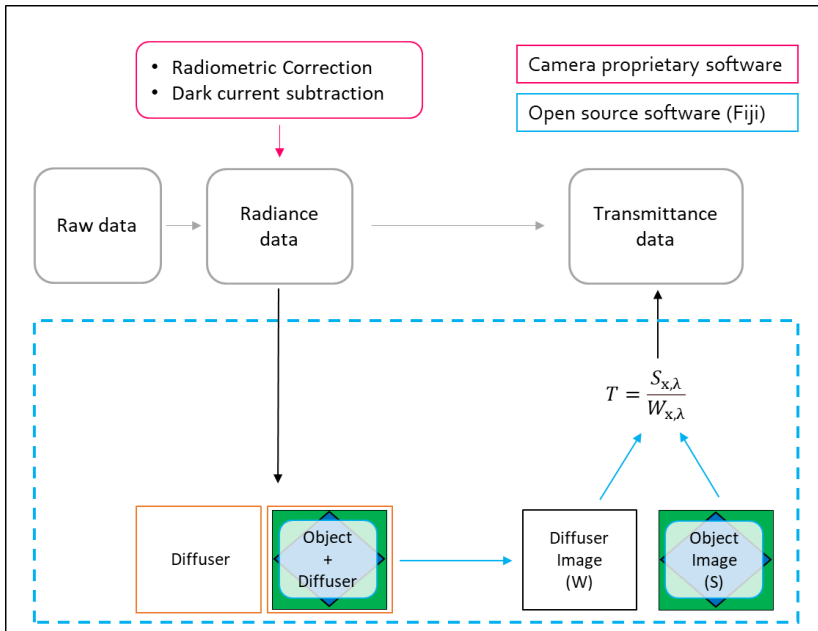


Figure 4.11: Acquisition and preprocessing workflow for HSI performed with the portable setup. T = transmittance, $S_{x,\lambda}$ = signal relative to the light transmitted by the object on top of the diffuser. $W_{x,\lambda}$ = signal relative to the light transmitted by the diffuser alone, at pixel location x , λ . Indices x and λ indicate respectively the spatial and the spectral dimension.

Concerning the lighting arrangement of the portable setup, the main difference with the laboratory system lies in the implementation of two light sources and two diffusers (Fig 4.8 and 4.12a). The reason behind this complicated system is related to the shape and power of the halogen lamp employed. These lamps are relatively big (16 x 11,5 cm) and have a line-shaped light bulb (Fig. 4.12a); this results in a light distribution characterized by a strongly illuminated area in correspondence with the light bulb and a gradual loss of intensity at the edge of the lamp (Fig 4.12b). It was decided thus to use two halogen lamps to maximize the light distribution across the field of view. However, as explained in the previous section, halogen lamps generate a high amount of heat that can be harmful to stained glass. During the designing

stage, it was suggested by the museum conservators that the temperature on the surface of the artwork should have not exceeded 25-30 °C during the acquisitions. For this reason, the double system of diffusers was developed; this method not only helped reduce the artwork's exposure to thermal radiation but also partially improved the light distribution (Fig 4.12b).

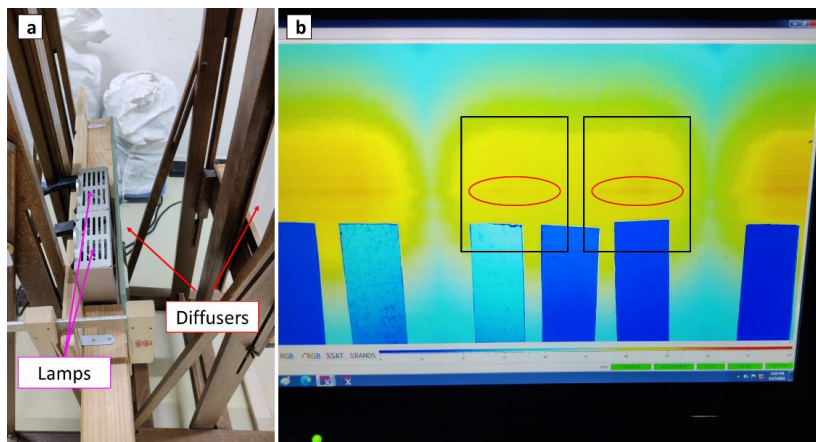


Figure 4.12: Real-time saturation map showing the light distribution during the acquisition. The two red/orange lines (red circles) in the center of the yellow area indicate the position of the bulbs. The saturation map demonstrates how the use of two lamps (black squares, approximately) improved the light distribution in the horizontal axis, while the vertical axis is affected by the rectangular shape of the lamps.

The results obtained from the imaging campaign have been presented in two papers (**Paper 4** and **Paper 6**), which separately address two aspects of the research. **Paper 4** thoroughly describes the setup and the image preprocessing workflow for the datacubes recorded with the portable setup. Spectral data from selected colored glass are also shown to demonstrate the setup's capability to identify glass chromophores as correctly as the laboratory setup (see examples in Fig. 4.10c, f). The abovementioned limitations are addressed as well.

Paper 6, on the other hand, focuses more on identifying and mapping chromophores in two case studies analyzed with this setup. The paper also briefly addresses the issue of stitching two datacubes with different aspect ratios and proposes a simple solution to obtain a single image from separate areas of the object for mapping purposes.

4.1.1.3 *In-situ measurements*

The last set of experiments was focused on testing the feasibility of performing HSI on stained glass in *in-situ* conditions. It is essential at this point to stress the main difference between using a portable setup *in situ* and simply transporting the instrument in another controlled environment. The definition “*in-situ* analysis”, in fact, implies that the object under study is not moved from where it is exhibited.

In the case of the imaging campaign described in the previous section, for example, the panels were stored at the SNM Collection Center deposit. The instrumentation was transported to the facility, and the selected case studies were taken out and moved to the chosen room for acquisition. As shown in the previous section, apart from the differences related to the stage movements (translational vs. rotational), the acquisition condition of the portable setup can be considered overall standard, and the results obtained, from the spectral point of view (see Fig. 4.10c, f in the previous section), are well comparable with those obtained with the laboratory setup.

On the other end, the second acquisition campaign was planned to be carried out in the rooms of the Swiss National Museum itself, where the stained-glass panels are part of the museum’s windows. Many factors had to be considered during the planning phase; first, the presence of other works of art displayed in the room limits the space to place or move the equipment around. For this reason, the lightness and compactness of the instrument were the first characteristics to be evaluated. The second aspect was the source of illumination available; in most cases, solar radiation was used, as the majority of the stained-glass panels were exposed to sunlight (Fig. 4.13a, c). However, two stained-glass panels were also chosen from a window in an internal wall, which required the development of an artificial illumination system to perform the acquisition (Fig. 4.13b, d).

In light of these considerations, it was decided to use a Specim IQ hyperspectral camera instead of the HySpex VNIR-1800. Similar to the HySpex VNIR-1800, the Specim IQ is a push-broom camera, but the scanning process is performed through internal mechanisms (Picollo et al., 2018). For this reason, this camera is more compact and easier to transport, as it does not require any particular stage and can be fixed to any tripod used in a photography studio. In addition, the camera does not need to be connected to any computer or power supply since it is battery-charged.

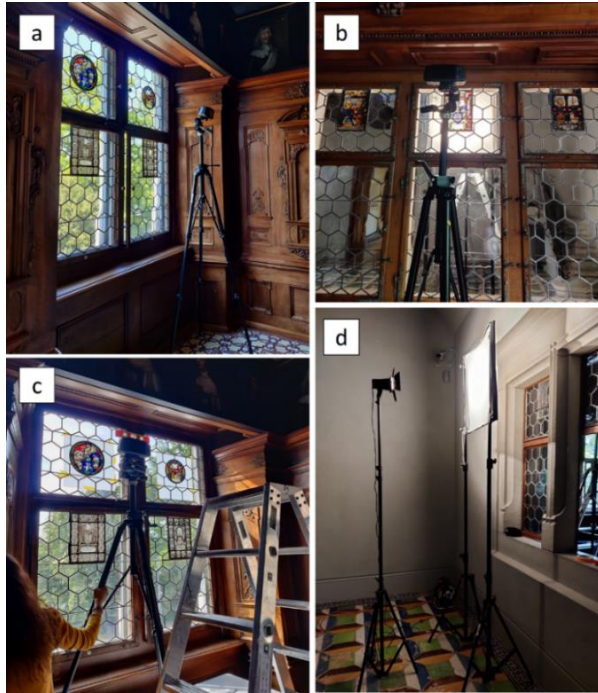


Figure 4.13: a, c) HSI of stained-glass panels exposed to sunlight. b, d) HSI of stained-glass panels in windows of an internal wall. Notice the lighting system made of a studio light and a diffusing fabric.

However, the counterpart of this portability is the quality of the datacubes obtained. Compared to the Hyspex VNIR-1800, the image size is very limited. Since the objective of this camera has no focus limit, the image's resolution depends on the distance from the object. Most of the time, the camera was positioned at a distance of around 50 cm to capture the entire stained-glass panel, which meant the loss of the finest details of the stained glass (usually in the order of half a millimeter). The Specim camera is thus not ideal for high-quality documentation purposes; nonetheless, its resolution is still good enough to distinguish different colored areas that can be selected for the identification of chromophores, which was successful in most cases.

The limitations, in this case, depended on the presence of vegetation in the background, the illumination variation, and the transmittance reference selection during the image processing step. Regarding the first two points, the issues were easily solved by applying a diffusing sheet of baking paper behind the stained glass. This solution allowed minimizing the vegetation's signal covering the characteristic peaks of the chromophores and reduced the effects of inhomogeneous light.

Concerning the latter point, it is necessary first to explain how the SpecimIQ processes the data. Unlike the Hypspec VNIR-1800, which outputs raw or radiance data (depending on the camera settings), the SpecimIQ immediately converts the data in reflectance (in this case, transmittance) before saving the image. This step is performed by selecting an area considered the reference within the imaged scene. As explained in Chapter 2, in reflectance measurements, this reference can be a white Spectralon[®] tile which is known to have a perfect reflectance at each wavelength. In transmittance, on the other hand, it is only possible to assume that the chosen transparent area has a perfect transmittance. Transparent glass produced in antiquity was less pure than contemporary ones and could still contain traces of impurities (e.g., iron and cobalt) from the raw material (Meulebroeck et al., 2021; Meulebroeck, Wouters, et al., 2010). As demonstrated in **Paper 5**, these impurities can absorb light at specific wavelengths causing errors during the radiometric correction process. It was thus decided to acquire multiple images of the same stained-glass panels using different transparent areas as reference (Fig. 4.14) to solve the issue. The results obtained are discussed more in-depth in **Paper 5**.

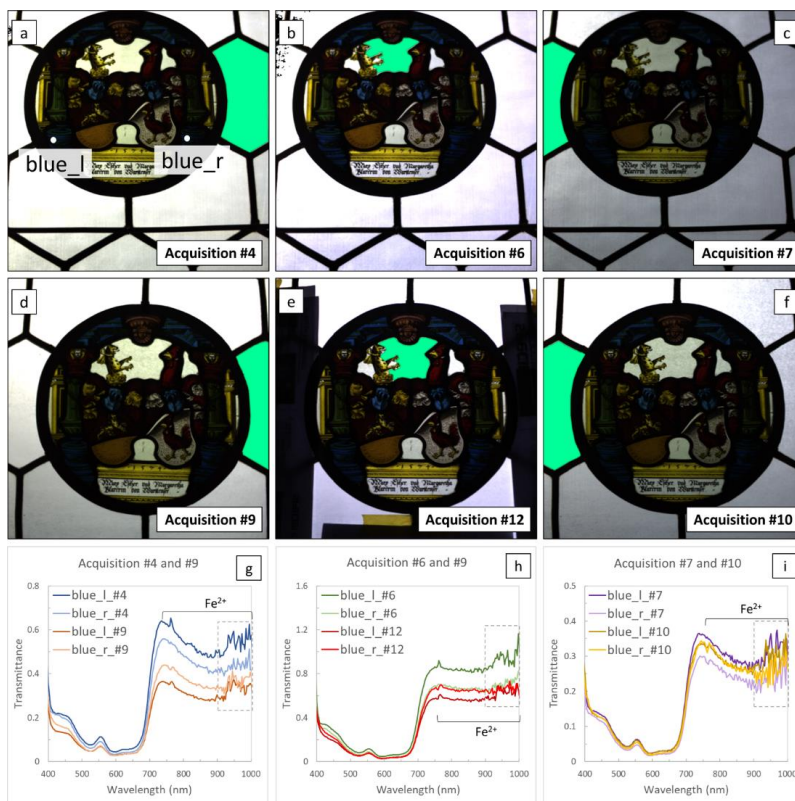


Figure 4.14: a-b) Pictures showing the areas chosen as transmittance reference (in green) for acquisitions #4 to #12 of the case study AG-1177. Acquisition #4 and #9 (a, d), #6 and #12 (b, e), and #7 and #10 (c, f) were processed using the same glass pane. g-i) Comparison of blue glass spectra obtained from the pair of datacubes processed using the same glass pane as reference. The noisy area in the NIR range (dotted line rectangle) is correlated to atmospheric oxygen. Notice how the band of Fe²⁺ tends to disappear when the radiometric correction is performed using a transparent area inside the stained-glass panel as the reference. Fig. 14a shows the points where the spectra were taken.

Concerning the two stained-glass panels exhibited in the windows of an internal wall, the most significant advantage was the possibility of using a stable light source instead of solar radiation. This way, the issues related to light variation and noise from the atmosphere signal could be eliminated. Nonetheless, the necessity of developing a proper setup to diffuse the light represented a challenging task.

As shown in Fig. 4.13b, d, the lighting setup used in this work consisted of a single halogen studio light positioned facing the center of the object under study. The light is diffused by a diffusing fabric commonly used in photography studios, held by a makeshift stretcher and two poles. The studio light and the diffusing fabric were placed at a long distance from each other (70 cm) and from the object (60 cm) to improve the light distribution across the field of view. However, this was not sufficient to obtain a perfectly diffused illumination. It can be noticed

in Fig. 4.15b, c that the light distribution was characterized by an intensely illuminated area gradually losing intensity at the edges. Moreover, the difficulties in keeping the diffusing textile well stretched also contributed to the sub-optimal lighting conditions, as the folds generated by the fabric's lack of rigidity contributed to causing shadows within the field of view.

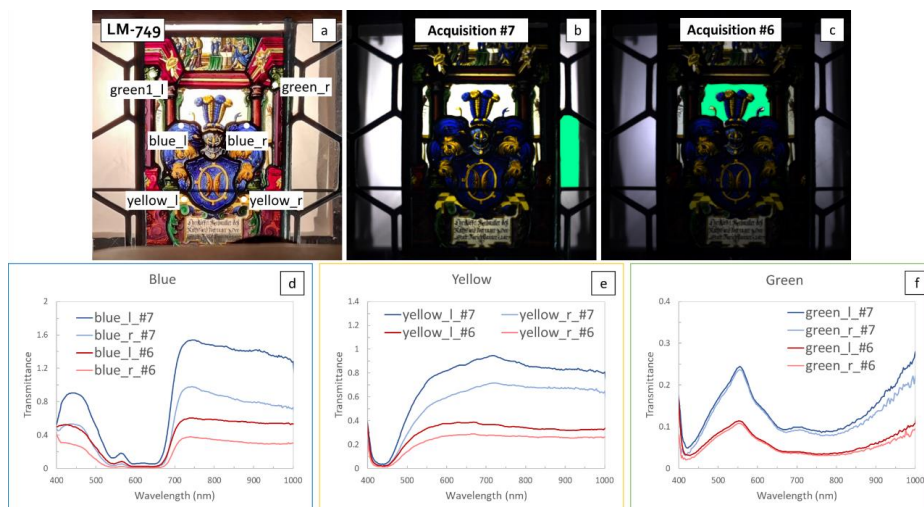


Figure 4.15: a) Close-up picture of case study LM-749, showing the points selected for the spectra comparison. b, c) Pictures showing the areas chosen as transmittance reference (in green). d, e, f) Comparison of spectra obtained on the left and right side from acquisitions #7 and #6 for three selected colors (blue, yellow, and green).

Fig. 4.15d, e, f show examples of spectra from three selected colored glass panes. In this case, the spectra are smoother, and the red-infrared region is unaffected by atmospheric oxygen noise. On the other hand, the abovementioned phenomenon related to the choice of the reference glass pane is still occurring, causing a loss of intensity of the cobalt and ferric iron characteristic bands.

4.1.1.4 Answering RQ1

What are the best setups and acquisition parameters for good-quality HSI of stained glass? Can HSI be used to successfully analyze and document stained glass in different scenarios (e.g., laboratory, museum depots/conservation laboratories, in-situ...)? What are the advantages and limitations of each case?

As discussed in the previous section, three imaging setups with different characteristics have been used during the project to deal with specific acquisition conditions. In order to answer the first research question, the main differences between the three setups are reported in Table 1 for a straightforward comparison.

Table 4.1: Summary table of the most relevant technical information of each setup used during the PhD project.

	Laboratory	Portable	In-situ
Max object dimension	50 x 50 cm	50 x 50 cm	Potentially unlimited.
Camera model	HySpex VNIR-1800	HySpex VNIR-1800	Specim IQ
Max datacube spatial dimension (in px)	1800 (across-track) x ∞ px (potentially)	1800 (across-track) x 1600 px (along-track)	512 x 512 px
Max area imaged (in cm)	~ 8 cm (across-track)	~ 8 (across-track) x 7 cm (along-track)	Depends on the distance from the object. 15 cm is the closest distance between the camera and the object.
Spectral range	400-1000 nm	400-1000 nm	400-1000 nm
Spectral Resolution	186 channels	186 channels	204 channels
Light source	Halogen light	Halogen light	- Sunlight - Halogen studio lights (stained glass on inner walls)
Diffusing system	Diffusing glass panel (8 mm thickness)	Diffusing glass panel (8 mm thickness) + Diffusing acrylic plate (3 mm thickness)	- Diffusing sheet - Diffusing fabric (stained glass on inner walls)
Standard geometry compliant	Yes	Approximately	- No - Approximately (stained glass on inner walls)
Reference collection	Collection of a few representative lines from the reference.	Collection of the reference image for the entire field of view.	Collection of a transparent area as the reference.
Radiometric correction	Manual	Manual	Automatically performed by the camera before saving the image.
Distortions	No	Yes	No.

From this comparison, it can be concluded that every setup has advantages and limitations, and it would not be correct to try to establish which one should be considered the best. In most cases, the choice is constrained by the size and location of the stained glass, and often it is necessary to compromise between data quality and portability. Concerning the documentation aspect, the main advantage of HSI over traditional RGB photography is the high spectral resolution. As shown in Section 4.1.1.1, the hundreds of spectral bands finely sampled across the electromagnetic spectrum allow obtaining a continuous spectrum from which it is possible

to create an image that is colorimetrically more faithful and able to discriminate between metameric colors (i.e., colors that are perceived the same, but have different spectral responses).

However, it is worthy of mention that the rendered images are solely based on the transmittance values of the stained glass, without taking into account other phenomena such as specular reflection occurring on the glass surface (see for example the dark blue and green glass tiles in Fig. 4.5a, c). Thus, these images are not representative of the global appearance of stained glass.

On the other hand, hyperspectral cameras are known to have a limited spatial resolution, related to an intrinsic trade-off between the spectral and spatial sensitivities of the sensor (Dobigeon et al., 2016). RGB cameras generally provide images of higher spatial resolution and are more flexible in adjusting the optics to capture images at long distances from the object.

To better visualize the finer details in hyperspectral images a solution could be to record and stitch together multiple datacubes taken at a closer distance. However, this procedure must be performed carefully to avoid stitching distortions. Otherwise, superresolution techniques could be considered to improve the spatial resolution of HSI. It consists in fusing an RGB image with an HSI datacube to obtain an image with both high spatial and spectral resolution (Lanaras, Baltsavias, & Schindler, 2017). The methodology is quite popular in the remote sensing domain, and it could be worth exploring in the field of cultural heritage in the future.

4.1.2 Data validation

The data validation aspect was addressed from two points of view: validation of the spectral data (SO4) and validation of the materials identified using complementary analysis (SO5). The related research questions (RQ2 and RQ3, respectively) are answered briefly below.

4.1.2.1 Answering RQ2

From the spectral point of view, does HSI allow obtaining comparable results to the available technologies (UV-VIS-NIR spectroscopy)?

In light of the results obtained and published during the PhD, it is possible to demonstrate that the spectral data produced by HSI are consistent with those shown in the literature regarding UV-VIS-NIR spectroscopy. This statement is also concretely proved by the experiments presented in **Paper 2**, where the performance of HSI and UV-VIS-NIR spectroscopy are compared. Besides being comparable, the two techniques can also be complementary. A limitation of HSI compared to spectroscopy is the shorter spectral range in the UV region. In

this sense, the spatial dimension of HSI can be exploited for mapping the distribution of glass colored with different chromophores, while the extended range in the UV (and also in the NIR, depending on the instrument models) can be exploited to confirm the presence of those chromophores whose spectral band are located at the extremes of the HSI's spectral range.

4.1.2.2 Answering RQ3

What kind of information can HSI provide? Can it be recommended for accurate material characterization? Can it help to select the correct areas for additional point analysis or sampling?

Before answering this question, it is essential to stress that, in general, a single analysis is not sufficient to obtain a complete characterization of the artwork under study. A multi-analytical approach should be implemented when possible. During the PhD project, the results obtained by HSI were often supported by XRF analysis to get additional information on the glass composition and confirm the metal oxides used as colorants detected by HSI. From this point of view, the two techniques can be defined as complementary in the true sense of the word. Thanks to HSI, for example, it was possible to easily identify chromophores such as cobalt or chromium, whose detection by XRF is often difficult. Indeed, since they are usually present in little or trace amounts, their concentrations can be below the instrument's detection limit. In addition, in the case of cobalt, its characteristic peaks partially overlap with the signal of iron, which is present in higher amounts in most glass (Meulebroeck et al., 2021; Rebollo et al., 2011). However, since these two chromophores have a high molar extinction coefficient (Meulebroeck et al., 2021), their characteristic absorbance band are usually well visible in HSI spectra.

On the other hand, XRF can provide valuable information on the composition of the whole glass (matrix and colorants). It can be used, for example, to confirm the presence of chromophores whose absorbance bands overlap with others, such as Cr^{3+} , Fe^{3+} , and Cu^{2+} (Rebollo et al., 2011). The glass' global composition can help characterize the raw materials; consequently, it is possible to estimate the provenance and age of the glass if the glass surface is not too corroded and statistically relevant data are available for reference. In addition, the elements forming the glass matrix can also have a role in the glass's final color by influencing the chromophore elements' reduction or oxidation (Hunault & Loisel, 2020; Meulebroeck et al., 2016; Thiemsorn et al., 2008). Practically, this can result in a shift in the position of the signature absorbance bands in the HSI spectra (Ceglia et al., 2012; Fornacelli et al., 2018). From the qualitative point of view, the shifts of the peaks are generally minimal and do not

hinder the identification of chromophores. However, observing these subtle shifts can be used to formulate hypotheses about the composition of the glass, which can be confirmed by means of XRF or other analytical techniques.

HSI can also be used to rapidly assess the areas to choose for XRF measurements, exploiting the possibility of selecting a combination of spectral bands to create false color images. The most common example is the IR-false color method (described in detail in **Papers 3 and 4**), which consists in substituting an image's red, green, and blue channels with the infrared, red, and green ones, respectively. The image obtained in such ways shows “false” colors related to the material's response in the IR region.

The technique works particularly well for green and blue glass since they are the ones that show the most variation in composition, especially in the NIR range, as demonstrated by the results obtained with the mock-up stained glass panel (see Fig. 4.7 Section 4.1.1.1). However, it may fail to distinguish between colored glass with a similar spectral shape, despite its different compositions and hues (see examples in Fig. 4.16). If subtle differences can be noticed in the spectra, other bands in the NIR, red, and green range can be selected by looking at the wavelengths where these differences are visible, which could help distinguish the glass pieces with similar colors and improve the visualization.

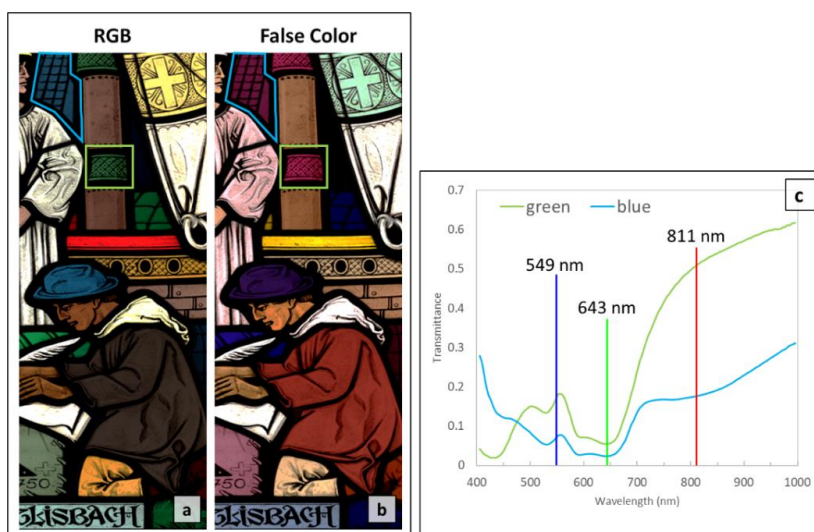


Figure 4.16: a) RGB and b) IR-false color image from case study LM-167924 (SNM Collection Center). Notice how the blue sky on the left of the mast show a very similar color to the green decoration of the mast, despite the different color in the RGB image and chemical composition. c) comparison of spectra from the two areas. The three lines indicate the wavelengths associated with the band chosen to create the false color image.

Concerning real case studies, false-color images were exploited during the XRF analyses of the stained-glass panels stored at the SNM Collection Center to visualize areas with possible similar compositions quickly. Thanks to this approach, it was possible to make a first selection of the areas to investigate and avoid the collection of too many XRF spectra of glass with the same composition. Additional points were collected when it was necessary to double-check the hypothesis on the relative concentration of the chromophores present in a glass.

In this sense, XRF was beneficial in revealing particular combinations of chromophores or artistic choices in stained glass making. The case of the two Luis Halter's stained-glass panels presented in **Paper 6** is an excellent example. For instance, by acquiring XRF on the back and the front of one of Halter's stained-glass panels, it was possible to discover that two green glass pieces with identical spectra were actually "overlay" glass pieces, made of multiple distinctive layers (at least two) with different compositions. As shown in Fig. 4.17d (adapted from **Paper 6**), two of the four XRF spectra (the front side of Green2, red line, and the back side of Green3, orange line) overlap perfectly, hinting at a very similar, if not identical, elemental composition. On the other hand, the other two XRF spectra are entirely different. In particular, the front side of Green3 (blue line) shows a considerable amount of cobalt compared to the back side of Green2 (pink line). It is not easy to explain why the two glass pieces show an almost identical spectral shape despite the apparent different chemical compositions. While XRF was crucial to discovering the existence of double layers in the glass used by Halter, additional and possibly invasive techniques are required to better understand the glassmaker's artistic preferences.

In light of these observations and the results published in **Papers 3, 4, and 6**, it is possible to conclude that the HSI can be a valuable instrument for the non-invasive characterization of stained-glass windows. When used as a stand-alone technique, HSI can provide an overview of the combination of chromophores used to color the glass and the distribution of specific colored glass pieces across the stained-glass panel. The results obtained can be integrated with other non-invasive or invasive techniques. In this sense, the spectral information from HSI can help the conservators select areas that require further investigation.

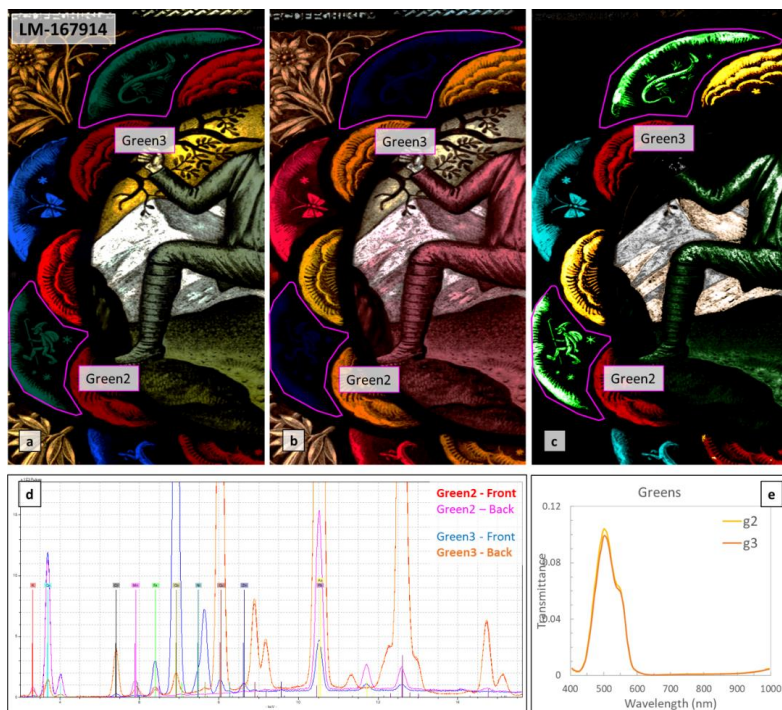


Figure 4.17: a) RGB image of case study LM-167914 (SNM Collection Center) created from the datacube through band selection. b) IR false color image c) LUMoS maps of red, green, and blue glass sections combined in a single image. d) XRF spectra of two green glass e) HSI spectra of the green glass.

4.1.3 Hyperspectral image analysis: a work in progress.

Apart from the technical limitations of the setups described in the previous sections, the most significant challenges are not as related to the acquisition phase as to the image processing one.

Chromophore identification and mapping, for example, are complex tasks for several reasons. Since stained-glass windows consist of many parts with distinct optical properties, the interaction of these parts with light can cause considerable spectral variability. This phenomenon occurs as a variation of the spectral signature of an endmember due to illumination variations or intrinsic properties of the materials (Borsoi et al., 2021). For example, lead came and grisaille, which are opaque, are characterized by multiple spectra due to the scattering of light on the surface; thus, their distribution is usually separated into several distinct maps. If the grisaille is thin and the color is still visible below the layer, the combination “colored glass + grisaille” will also be classified as a different component. This spectral variability represents a significant obstacle when defining and extracting the effective number of components (endmembers) in the stained glass.

The first step in dealing with the challenge of mapping stained-glass components was exploiting the IR-false color method described in the previous section. This method works well for a quick overview of the stained-glass palette. However, proper image processing algorithms are necessary to correctly visualize the distribution of glass colored with the same types and amount of chromophores.

For stained glass, choosing between a classification or an unmixing approach is not a straightforward task. Unlike paintings, stained glass windows are mostly made of separated pieces of glass of a single color given by a defined combination of chromophores. For this reason, no mixing between different components occurs unless a light grisaille, stained yellow, or enamel paint is applied on the surface of the colored glass to depict details. Thus, classification methods seem to be the most reasonable choice for chromophore mapping. A few classification attempts were made following the approach described in Section 2.2.2 (endmember extraction + classification): NFINDR (Winter, 1999) was chosen as the algorithm for the endmember extraction step, but Pixel Purity Index (PPI) (Boardman et al., 1995) was also tested. Spectral Angle Mapper (SAM) (Kruse et al., 1993) was used for the classification. The implementation of these algorithms was performed by using the MATLAB[®] Hyperspectral imaging toolbox¹³.

The endmember extraction step was carried out in two ways. In the first one, without specifying the number of endmembers, the algorithm output a vast number of endmembers' spectra. Most were just redundant spectra of the same endmember or not physically meaningful. The resulting maps were often complicated to interpret due to the presence of too many endmembers, which often belonged to the same component but were mapped separately. In the second case, the number of endmembers to extract was estimated by visual inspection of the panel under study, followed by a spectra comparison to ensure all the endmembers were considered. In this case, the endmember extracting algorithms failed to detect a few components identified by the previous visual inspection while others were repeated; thus, the obtained maps showed misclassified areas due to missing endmembers.

Unsupervised unmixing (or blind source separation) algorithms were considered to evaluate whether these methods could yield better results. As explained in Chapter 2, the advantage of unmixing compared to classification is the assumption that the signal in a pixel is the result of a linear combination of a few pure components and their fractional abundances. The

¹³ <https://se.mathworks.com/help/images/hyperspectral-image-processing.html>

unsupervised unmixing approach was chosen as the preferred methodology because it simultaneously estimates the endmembers and their abundances without going through the endmember extraction process and without the need for a ground truth regarding materials used in the object studied. As stated in the previous paragraph, it is not really possible to talk about unmixing in stained glass since each color is well-defined and separated by the lead comes (apart from the few abovementioned exceptions). However, it has been noticed that unsupervised unmixing seems to perform exceptionally well, even with stained glass. While some classification errors are still evident, the unmixing approach seems to be more flexible in identifying the subtle color variation within the same glass piece due to inhomogeneous chromophores concentration, allowing to partially overcome the issue of spectral variability.

In this sense, the LUMoS algorithm (McRae et al., 2019), described in **Paper 6**, represented a successful choice, also considering the complex palette of the stained-glass panels chosen as case studies. The algorithm could provide sufficiently corrected abundance maps of those chromophores' combinations defined enough to be considered a specific endmember (see Fig. 4.18).

The classification errors could be easily identified and associated with an underestimation of the endmembers effectively present or the too-similar spectral shape of those glass pieces erroneously mapped together. Nonetheless, the results shown in **Paper 6** are promising. Its use could be encouraged in future applications of HSI on stained glass, both as a stand-alone algorithm or even to prepare a spectral library for supervised methods.

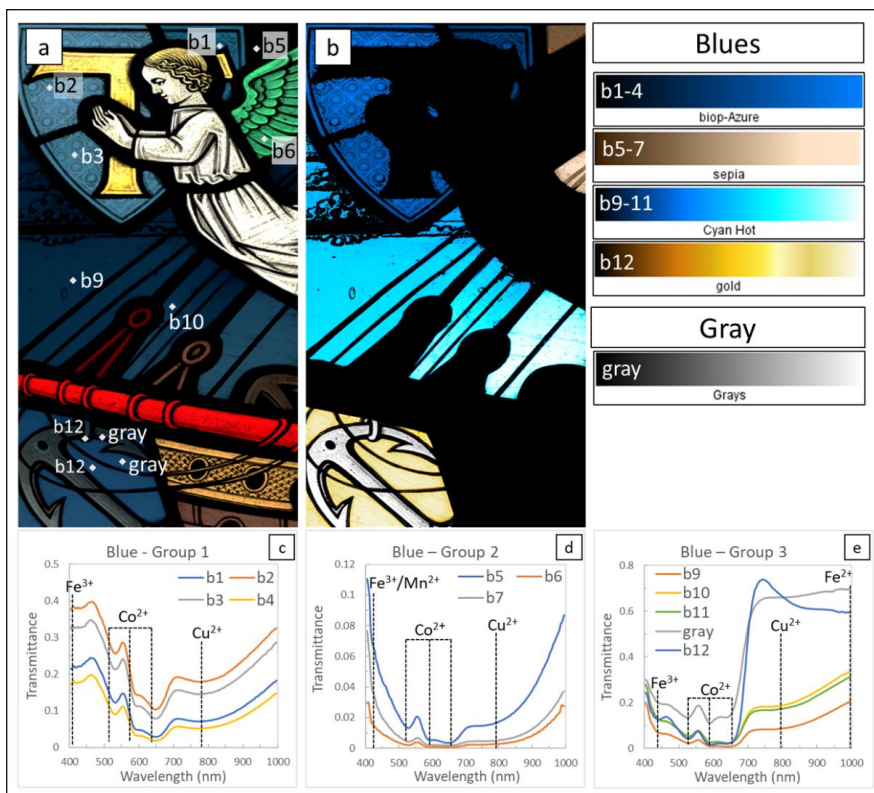


Figure 4.18: a) RGB image of case study LM-167924 created from the datacube through band selection. b) LUMoS maps of blue glass sections combined in a single image. The lookup tables and the associated endmembers are provided on the left. c, d, e) spectra of the identified endmembers.

The use of spectral libraries of known materials was also considered. However, this approach is not very feasible for stained glass. Since the color in the glass is not given by pigments or colorants with fixed recipes but by a combination of chromophores, creating a spectral library would require considering all the combinations of oxides, furnace temperature, and atmosphere for all the existing colors. It is worth mentioning that creating such a library was planned at some point during the PhD. During the first visit to the SNM Collection Center, 811 glass pieces with an extensive range of colors were acquired with HSI, in addition to the ten stained glass panels. These 811 glass pieces were donated to the Swiss National Museum by the Atelier Halter, a stained-glass restoration workshop based in Bern. The spectra obtained from these 811 pieces should have been used to build a spectral library for supervised classification, possibly taking advantage of machine-learning approaches. Unfortunately, the manual processing of these data was too time-consuming, and it was decided to put this part of the research aside.

4.2 Research contributions

As stated in the first chapter of the thesis, the research on hyperspectral imaging of stained glass is minimal compared to other categories of artworks. The work carried out during the PhD had two main contributions: expanding the existing literature on the topic and sparking the interest of other researchers working in imaging and cultural heritage. Concerning the first point, the published papers present examples of successful hyperspectral imaging applications in different environments, even in suboptimal lighting conditions, providing valuable background material to researchers interested in working on this topic in the future. The second point was proven by the many positive and encouraging comments received during dissemination activities and presentations at international conferences. In addition, **Paper 1** has been cited in two other works related to HSI of stained-glass windows (Caron, Kessy, Mukaigawa, & Funatomi, 2022; Funatomi et al., 2022). This positive outcome indeed encourages further work on the topic, which will be discussed in the following chapter about conclusions and future perspectives.

Chapter 5

Conclusion and perspectives

5.1 Conclusion

The work presented in this thesis aimed to explore the potentialities of HSI for analyzing stained-glass windows. Since the research so far on the topic is scarce, the main contribution of this project has been to demonstrate the feasibility of HSI in analyzing stained glass under different conditions. The laboratory and the portable setup were respectively adapted and developed for the purpose, allowing to obtain spectral results comparable to UV-VIS-NIR spectroscopy, a technique extensively used to identify chromophores in glass. However, compared to spectroscopy, HSI offers the additional advantage of getting spatial and spectral information that can be exploited to understand the distribution of the colored glass without the need to take a point at a time.

Concerning *in-situ* measurement, the work carried out at the Swiss National Museum was a valuable opportunity to study the challenges related to the illumination conditions of the stained glass (exposed or not exposed to sunlight), as well as the influence of the background and the purity of the glass chosen as reference. This part of the research represents the first time that the *in-situ* analysis of stained glass is performed in such a systematic way.

Image analysis solutions for automatically identifying and mapping stained glass components were also roughly explored. Besides the traditional classification methodologies, unsupervised unmixing approaches were also investigated, which showed promising results.

In light of the results obtained, it is possible to state that this thesis represented a pioneer work regarding the use of HSI for the analysis and characterization of colored glass. The advantages of the technique demonstrated in this work could encourage more extensive use of this technique on stained-glass windows, as it happens for paintings and manuscripts. The following section suggests some research prompts that would be worth exploring in the future.

5.2 Perspectives

- *Improving acquisition setups for high-quality documentation and change monitoring.*

Documentation and change monitoring are two important research topics that should be investigated further. Currently, the laboratory setup is the most reliable in producing high-quality data in terms of image proportions and spectral information. Thus, the use of this setup can be encouraged for documentation purposes. As demonstrated by **Paper 2**, the color rendering from spectral data provides more accurate color images than traditional RGB cameras, especially in the visualization of dark-colored glass. In addition, IR-false color images could be integrated into conservation reports as a fast tool for discriminating colored glass obtained with similar chromophores. Cameras working in the SWIR range should also be explored, both in transmittance, to support the chromophore identification, and in reflectance mode, to investigate degradation products.

However, only stained-glass panels that can be safely moved to the laboratory and are small enough to fit in the translational stage can be analyzed with this setup. For this reason, it would not be possible to perform routine analyses for the change monitoring.

For this purpose, the portable setup was developed, as it could be moved, for example, to conservation laboratories or museum depots. The setup proposed in this thesis allowed for obtaining satisfying results during the acquisition campaign at the Collection Center of the Swiss National Museum. However, at the current stage, the geometric distortions in the images limit the use of this technique as a documentation tool since the images' proportions are not realistic. Further work should thus focus on either solving the issue of distortions through suitable algorithms or developing a setup based on a translational stage to avoid the problem altogether. Of course, the setup should have a sturdy design and be easy to disassemble and transport to the desired location.

Concerning the *in-situ* analysis of stained-glass windows, the imaging campaign at the Swiss National Museum was a valuable learning opportunity. From this experience, it was possible to learn how to tackle issues that can affect the quality of the results, such as illumination variation, the influence of the background, and the purity of the transparent glass chosen as a reference. On this specific occasion, many factors contributed to easing the acquisition campaign. First of all, the case studies analyzed were relatively easy to access. The tripod used could reach most stained-glass panels, and a small table was enough to get the optimal height

when necessary. Second, plenty of transparent glass panes could be chosen inside and outside the stained glass panel as a reference to perform the radiometric correction, so that it was possible to take multiple acquisitions and select the best result. In addition, the possibility of opening the window and applying a diffusing sheet behind the panels represented a great advantage in improving the quality of the spectra.

From this description, it is clear that these favorable conditions are rare and may not truly represent scenarios of other case studies. For this reason, to evaluate the feasibility of HSI in more challenging situations, the technique should be tested on stained-glass panels of huge windows, such as those in churches or other secular buildings, where, for example, perfectly transparent areas may not be available. Developing a system to mitigate the variation of sunlight in these conditions should also be considered. For example, a methodology similar to that described in (MacDonald & Oldfield, 1996) could be implemented.

Concerning *in-situ* imaging, it is also worth considering situations where stained-glass windows are not exposed to natural sunlight. The two stained-glass panels integrated into the internal windows of the Swiss National Museum, for example, required the development of an alternative lighting system. The solution proposed in **Paper 5** allowed recording datacubes of moderate quality, but a more efficient lighting system is necessary. Particular attention should be given to the light diffuser, which should be rigid and flat, preferably. Lastly, it would be worth exploring the analysis of stained-glass windows displayed in museums by means of light boxes to evaluate how the light chosen as illumination would influence the acquisitions.

- *Image analysis: exploring new classification/unmixing approaches.*

As discussed in the previous chapters, a few attempts were made to achieve a successful chromophores mapping. The lack of earlier studies on the topic represented a considerable limit in selecting the best algorithm to perform this task. In the case of stained glass, one of the main issues is the lack of ground truth regarding the combination of chromophores used to reach the desired color. While the number of chromophore elements is limited, the combination of the same elements can give different hues depending on the concentration, the furnace temperature, and the atmosphere. Visual inspection can not always be sufficient to clearly understand the palette, especially if the panels have been restored using modern pieces of similar color. In addition, the presence of many components of different materials (glass and metal), the color inhomogeneity within the same glass piece, and the superimposition of grisaille layers of

various thicknesses favor the phenomenon of spectral variability due to the way they interact with the incident light.

Unsupervised unmixing approaches, such as the LUMoS algorithm presented in **Paper 6**, represented a successful solution to deal with the abovementioned challenges. In addition, its implementation as a Fiji plugin is a great advantage since no programming skill is required to run the algorithm, which could facilitate its diffusion within the cultural heritage community. The results demonstrated that the LUMoS algorithm could be considered a useful tool for preliminary chromophore mapping in stained glass. However, a better understanding of the relationship between each glass component (glass, metal, and “paint layers”) could help develop a more robust solution for image analysis of these artworks.

Another aspect worth exploring is the possibility of exploiting spectral libraries, an option more and more popular for pigment mapping in paintings and manuscripts. The 811 pieces of colored glass analyzed with HSI at the Swiss National Museum have also been characterized with XRF, making a rough ground truth available for each sample. These glass pieces could thus represent a starting point to evaluate the use of supervised approaches to perform the classification task. In addition, the vast palette of these colored glass pieces could become a valuable set of references for the researchers working in the field since spectral data are relatively scarce and representative of a few historical periods.

Bibliography

- Adlington Laura W., & Freestone Ian C. (2017). Using handheld pXRF to study medieval stained glass: A methodology using trace elements. *Mrs Advances*, 2(33-34), 1785-1800. doi:10.1557/adv.2017.233
- Adlington Laura W., Freestone Ian C., Kunicki-Goldfinger Jerzy J., Ayers Tim, Scott Heather G., & Eavis Anna. (2019). Regional patterns in medieval European glass composition as a provenancing tool. *Journal of Archaeological Science*, 110. doi:10.1016/j.jas.2019.104991
- Adlington Laura W., Freestone Ian C., Seliger Leonie, Marcos Martinon-Torres, Brock Fiona, & Shortland Andrew J. (2020). In Situ Methodology for Compositional Grouping of Medieval Stained Glass Windows: Introducing the "Windolyzer" for Handheld X-Ray Fluorescence Spectrometry. In Mary Virginia Orna & Seth C. Rasmussen (Eds.), *Archaeological Chemistry: A Multidisciplinary Analysis of the Past*: Cambridge Scholars Publishing.
- Alfeld Matthias, & de Viguier Laurence. (2017). Recent developments in spectroscopic imaging techniques for historical paintings - A review. *Spectrochimica Acta Part B: Atomic Spectroscopy*, 136, 81-105. doi:10.1016/j.sab.2017.08.003
- Aulinas Meritxell, Garcia-Valles Maite, Gimeno Domingo, Fernandez-Turiel José Luis, Ruggieri Flavia, & Puges Montserrat. (2009). Weathering patinas on the medieval (S. XIV) stained glass windows of the Pedralbes Monastery (Barcelona, Spain). *Environmental Science and Pollution Research*, 16(4), 443-452. doi:10.1007/s11356-008-0078-0
- Bacci Mauro, Corallini Americo, Orlando Andrea, Picollo Marcello, & Radicati Bruno. (2007). The ancient stained windows by Nicolo di Pietro Gerini in Florence. A novel diagnostic tool for non-invasive in situ diagnosis. *Journal of Cultural Heritage*, 8(3), 235-241. doi:10.1016/j.culher.2007.02.001
- Baert Kitty, Meulebroeck Wendy, Ceglia Andrea, Wouters Hilde, Cosyns Peter, Nys Karin, Thienpont Hugo, & Terryn Herman. (2012). The potential of Raman spectroscopy in glass studies. In *Proc. SPIE Integrated Approaches to the Study of Historical Glass* (Vol. 8422, pp. 842207).
- Balas Costas, Epitropou George, Tsapras Athanasios, & Hadjinicolaou Nicos. (2018). Hyperspectral imaging and spectral classification for pigment identification and mapping in paintings by El Greco and his workshop. *Multimedia Tools and Applications*, 77(8), 9737-9751. doi:10.1007/s11042-017-5564-2
- Bernady Edyta, Goryl Maria, & Walczak Małgorzata. (2021). XRF Imaging (MA-XRF) as a Valuable Method in the Analysis of Nonhomogeneous Structures of Grisaille Paint Layers. *Heritage*, 4(4), 3193-3207. doi:10.3390/heritage4040179
- Bidegaray Anne-Isabelle, Godet Stéphane, Bogaerts Michel, Cosyns Peter, Nys Karin, Terryn Herman, & Ceglia Andrea. (2019). To be purple or not to be purple? How different production parameters influence colour and redox in manganese containing glass. *Journal of Archaeological Science: Reports*, 27, 101975. doi:10.1016/j.jasrep.2019.101975
- Bioucas-Dias José M., Plaza Antonio, Dobigeon Nicholas, Parente Mario, Du Quian, Gader Paul, & Chanussot Jocelyne. (2012). Hyperspectral Unmixing Overview: Geometrical, Statistical, and Sparse Regression-Based Approaches. *IEEE Journal of Selected Topics in Applied Earth Observations and Remote Sensing*, 5(2), 354-379. doi:10.1109/JSTARS.2012.2194696
- Boardman Joseph W., Kruse Fred A., & Green Robert O. (1995). Mapping target signatures via partial unmixing of AVIRIS data. In *Fifth Annual JLP Airborne Earth Science Workshop* (Vol. Volume 1: Aviris Workshop).
- Borsoi Ricardo A., Imbiriba Tales, Bermudez José Carlos M., Richard Cédric, Chanussot Jocelyne, Drumetz Lucas, Tournet Jean Yves, Zare Alina, & Jutten Christian. (2021). Spectral

- Variability in Hyperspectral Data Unmixing: A comprehensive review. *IEEE Geoscience and Remote Sensing Magazine*, 9(4), 223-270. doi:10.1109/MGRS.2021.3071158
- Bracci Susanna, Bartolozzi Giovanni, Burnam Renée K., & Corallini Americo. (2020). Integration of both non-invasive and micro-invasive techniques for the archaeometric study of the stained-glass window Apparizione degli Angeli in the basilica of Santa Croce in Florence, Italy. *Journal of Cultural Heritage*, 44, 307-316. doi:10.1016/j.culher.2020.02.006
- Bring Torun, Jonson Bo, Kloo Lars, & Rosdahl Jan. (2007). Colour development in copper ruby alkali silicate glasses. : Part 2. The effect of tin (II) oxide and antimony (III) oxide. *Glass Technology-european Journal of Glass Science and Technology Part A*, 48, 142-148.
- Cagno Simone, Van der Snickt Geert, Legrand Stijn, Caen Joost, Patin Mathilde, Meulebroeck Wendy, Dirx Yarince, Hillen Michaël, Steenackers Gunther, Rousaki Anastasia, Vandenabeele Peter, & Janssens Koen. (2021). Comparison of four mobile, non-invasive diagnostic techniques for differentiating glass types in historical leaded windows: MA-XRF, UV-Vis-NIR, Raman spectroscopy and IRT. *X-Ray Spectrometry*, 50(4), 293-309. doi:10.1002/xrs.3185
- Calas Georges, Galois Laurence, & Cormier Laurent. (2021). The color of glass. In Pascal Richet (Ed.), *Encyclopedia of Glass Science, Technology, History and Culture* (Vol. 1, pp. 667-691). Hoboken, New Jersey: Wiley-American Ceramic Society.
- Calligaro Thomas. (2008). PIXE in the study of archaeological and historical glass. *X-Ray Spectrometry*, 37(2), 169-177. doi:10.1002/xrs.1063
- Capobianco Natan, Hunault Myrtille O. J. Y., Balcon-Berry Sylvie, Galois Laurence, Sandron Dany, & Calas Georges. (2019). The Grande Rose of the Reims Cathedral: an eight-century perspective on the colour management of medieval stained glass. *Scientific Reports*, 9, 3287. doi:10.1038/s41598-019-39740-y
- Capobianco Natan, Hunault Myrtille O. J. Y., Loisel Claudine, Trichereau Barbara, Bauchau Fanny, Trcera Nicolas, Galois Laurence, & Calas Georges. (2021). The representation of skin colour in medieval stained glasses: The role of manganese. *Journal of Archaeological Science: Reports*, 38, 103082. doi:10.1016/j.jasrep.2021.103082
- Carmona Noemi, Ortega-Feliu Ines, Gomez-Tubio Blanca, & Villegas Maria-Angeles. (2010). Advantages and disadvantages of PIXE/PIGE, XRF and EDX spectrometries applied to archaeometric characterisation of glasses. *Materials Characterization*, 61(2), 257-267. doi:10.1016/j.matchar.2009.12.006
- Carmona Noemi, Oujja Mohamed, Rebollar Esther, Romich Hannelore, & Castillejo Marta. (2005). Analysis of corroded glasses by laser induced breakdown spectroscopy. *Spectrochimica Acta Part B-Atomic Spectroscopy*, 60(7-8), 1155-1162. doi:10.1016/j.sab.2005.05.016
- Caron Guillaume, Kessy Suzan J., Mukaigawa Yasuhiro, & Funatomi Takuya. (2022). Direct Alignment Of Narrow Field-Of-View Hyperspectral Data And Full-View Rgb Image. In *2022 IEEE International Conference on Image Processing (ICIP)* (pp. 3201-3205).
- Cartechini Laura, Miliani Costanza, Nodari Luca, Rosi Francesca, & Tomasin Patrizia. (2021). The chemistry of making color in art. *Journal of Cultural Heritage*, 50, 188-210. doi:10.1016/j.culher.2021.05.002
- Ceglia Andrea, Meulebroeck Wendy, Baert Kitty, Wouters Hilde, Nys Karin, Thienpont Hugo, & Terryn Herman. (2012). Cobalt absorption bands for the differentiation of historical Na and Ca/K rich glass. *Surface and Interface Analysis*, 44(2), 219-226. doi:10.1002/sia.3810
- Ceglia Andrea, Nuyts Gert, Meulebroeck Wendy, Cagno Simone, Silvestri Alberta, Zoleo Alfonso, Nys Karin, Janssens Koen, Thienpont Hugo, & Terryn Herman. (2015). Iron speciation in soda-lime-silica glass: a comparison of XANES and UV-vis-NIR spectroscopy. *Journal of Analytical Atomic Spectrometry*, 30(7), 1552-1561. doi:10.1039/C5JA00046G
- CIE 15: Technical Report: Colorimetry 3rd edition. (2004). Retrieved from
- Ciortan Irina, Deborah Hilda, George Sony, & Hardeberg Jon Yngve. (2015). Color and hyperspectral image segmentation for historical documents. In *2015 Digital Heritage* (Vol. 1, pp. 199-206).

- Colomban Philippe, Etcheverry Marie-Pierre, Asquier Magali, Bounichou Mathieu, & Tournie Aurélie. (2006). Raman identification of ancient stained glasses and their degree of deterioration. *Journal of Raman Spectroscopy*, 37(5), 614-626. doi:10.1002/jrs.1495
- Colomban Philippe, & Tournie Aurélie. (2007). On-site Raman identification and dating of ancient/modern stained glasses at the Sainte-Chapelle, Paris. *Journal of Cultural Heritage*, 8(3), 242-256. doi:10.1016/j.culher.2007.04.002
- Colomban Philippe, Tournie Aurélie, & Ricciardi Paola. (2009). Raman spectroscopy of copper nanoparticle-containing glass matrices: ancient red stained-glass windows. *Journal of Raman Spectroscopy*, 40(12), 1949-1955. doi:10.1002/jrs.2345
- Cucci Costanza, Bracci Susanna, Casini Andrea, Innocenti Silvia, Marcello Picollo, Stefani Lorenzo, Rao Ida, & Scudieri Magnolia. (2017). The illuminated manuscript Corale 43 and its attribution to Beato Angelico: Non-invasive analysis by FORS, XRF and hyperspectral imaging techniques. *Microchemical Journal*, 138, 45-57. doi:10.1016/j.microc.2017.12.021
- Cucci Costanza, & Casini Andrea. (2019). Chapter 3.8 - Hyperspectral imaging for artworks investigation. In José Manuel Amigo (Ed.), *Data Handling in Science and Technology* (Vol. 32, pp. 583-604): Elsevier.
- Cucci Costanza, Casini Andrea, Stefani Lorenzo, Cattaneo Barbara, & Picollo Marcello. (2023). A Novel Transmittance Vis–NIR Hyper-Spectral Imaging Scanner for Analysis of Photographic Negatives: A Potential Tool for Photography Conservation. *Sensors*, 23(7), 3562.
- Cucci Costanza, Delaney John K., & Picollo Marcello. (2016). Reflectance Hyperspectral Imaging for Investigation of Works of Art: Old Master Paintings and Illuminated Manuscripts. *Accounts of Chemical Research*, 49(10), 2070-2079. doi:10.1021/acs.accounts.6b00048
- Cutajar Jan Dariusz, Babini Agnese, Deborah Hilda, Hardeberg Jon Yngve, Joseph Edith, & Frøysaker Tine. (2022). Hyperspectral Imaging Analyses of Cleaning Tests on Edvard Munch's Monumental Aula Paintings. *Studies in Conservation*, 67(sup1), 59-68. doi:10.1080/00393630.2022.2054617
- Davison Sandra (2003). Examination of glass, recording and documentation. In *Conservation and Restoration of Glass*. Oxford: Butterworth Heinemann.
- Deborah Hilda, George Sony, & Hardeberg Jon Yngve. (2014). Pigment Mapping of the Scream (1893) Based on Hyperspectral Imaging. In Abderrahim Elmoataz, Olivier Lezoray, Fathallah Nouboud, & Driss Mammass (Eds.), *Image and Signal Processing* (pp. 247-256). Cham: Springer International Publishing.
- Deborah Hilda, George Sony, & Hardeberg Jon Yngve. (2019). Spectral-divergence based pigment discrimination and mapping: A case study on The Scream (1893) by Edvard Munch. *Journal of the American Institute for Conservation*, 58(1-2), 90-107. doi:10.1080/01971360.2018.1560756
- Deborah Hilda, Ulfarsson Magnus O., & Sigurdsson Jakob. (2021). Fully Constrained Least Squares Linear Spectral Unmixing of The Scream (Verso, 1893). In *2021 11th Workshop on Hyperspectral Imaging and Signal Processing: Evolution in Remote Sensing (WHISPERS)* (pp. 1-5).
- Delaney John K., Dooley Kathryn A., van Loon Annelies, & Vandivere Abbie. (2020). Mapping the pigment distribution of Vermeer's Girl with a Pearl Earring. *Heritage Science*, 8(1), 4. doi:10.1186/s40494-019-0348-9
- Delgado Joana, Vilarigues Marcia, Ruivo Andreia, Corregidor Victoria, da Silva Rui C., & Alves Luís C. (2011). Characterisation of medieval yellow silver stained glass from Convento de Cristo in Tomar, Portugal. *Nuclear Instruments and Methods in Physics Research Section B: Beam Interactions with Materials and Atoms*, 269(20), 2383-2388. doi:10.1016/j.nimb.2011.02.059
- Dobigeon Nicholas, Altmann Yoann, Brun Nathalie, & Moussaoui Saïd. (2016). Chapter 6 - Linear and Nonlinear Unmixing in Hyperspectral Imaging. In Cyril Ruckebusch (Ed.), *Data Handling in Science and Technology* (Vol. 30, pp. 185-224): Elsevier.

- Eatman Sherrie. (2008). Displaying stained glass in a museum. *Autumn 2008*(56).
<http://www.vam.ac.uk/content/journals/conservation-journal/issue-56/displaying-stained-glass-in-a-museum/>
- Falcone Roberto, Nardone Michele, Sodo Armida, Sommariva Giuseppe, Vallotto Marta, & Verità Marco. (2010). SEM-EDS, EPMA and MRS analysis of neo-crystallisations on weathered glasses. *IOP Conference Series: Materials Science and Engineering*, 7(1), 012009.
 doi:10.1088/1757-899X/7/1/012009
- Farges François, Etcheverry Marie-Pierre, Scheidegger André, & Grolimund Daniel. (2006). Speciation and weathering of copper in "copper red ruby" medieval flashed glasses from the Tours cathedral (XIII century). *Applied Geochemistry*, 21(10), 1715-1731.
 doi:10.1016/j.apgeochem.2006.07.008
- Fernandes Paula, Vilarigues Márcia, Alves Luís C., & da Silva Rui C. (2008). Stained glasses from Monastery of Batalha: Non-destructive characterisation of glasses and glass paintings. *Journal of Cultural Heritage*, 9, e5-e9. doi:10.1016/j.culher.2008.07.005
- Ferrand Jessica, Rossano Stephanie, Loisel Claudine, Trcera Nicolas, van Hullebusch Erik D., Bousta Faisal, & Pallot-Frossard Isabelle. (2015). Browning Phenomenon of Medieval Stained Glass Windows. *Analytical Chemistry*, 87(7), 3662-3669. doi:10.1021/ac504193z
- Fischer Christian, & Kakoulli Ioanna. (2006). Multispectral and hyperspectral imaging technologies in conservation: current research and potential applications. *Studies in Conservation*, 51(sup1), 3-16. doi:10.1179/sic.2006.51.Supplement-1.3
- Floréal Daniel, & Mounier Aurélie. (2015). Mobile hyperspectral imaging for the non-invasive study of a mural painting in the Belves Castle (France, 15th C). *STAR: Science & Technology of Archaeological Research*, 1(2), 81-88. doi:10.1080/20548923.2016.1183942
- Floréal Daniel, Mounier Aurélie, Pérez-Arantegui Josefina, Pardos Carlos, Prieto-Taboada Nagore, Fdez-Ortiz de Vallejuelo Silvia, & Castro Kepa. (2016). Hyperspectral imaging applied to the analysis of Goya paintings in the Museum of Zaragoza (Spain). *Microchemical Journal*, 126, 113-120. doi:10.1016/j.microc.2015.11.044
- Fornacelli Cristina, Ceglia Andrea, Bracci Susanna, & Vilarigues Marcia. (2018). The role of different network modifying cations on the speciation of the Co²⁺ complex in silicates and implication in the investigation of historical glasses. *Spectrochimica Acta Part A: Molecular and Biomolecular Spectroscopy*, 188, 507-515. doi:<https://doi.org/10.1016/j.saa.2017.07.031>
- Fornacelli Cristina, Colomban Philippe, & Memmi Isabella T. (2015). Toward a Raman/FORS discrimination between Art Nouveau and contemporary stained glasses from CdSxSe1-x nanoparticles signatures. *Journal of Raman Spectroscopy*, 46(11), 1129-1139.
 doi:10.1002/jrs.4758
- Foster David. H., & Amano Kinjiro. (2019). Hyperspectral imaging in color vision research: tutorial. *Journal of the Optical Society of America A*, 36(4), 606-627. doi:10.1364/JOSAA.36.000606
- Frenzel Gottfried. (1985). The Restoration of Medieval Stained Glass. *Scientific American*, 252(5), 126-137.
- Funatomi Takuya, Ogawa Takehiro, Tanaka Kenichiro, Kubo Hiroyuki, Caron Guillaume, Mouaddib El Mustapha, Matsushita Yasuyuki, & Mukaigawa Yasuhiro. (2022). Eliminating Temporal Illumination Variations in Whisk-broom Hyperspectral Imaging. *International Journal of Computer Vision*, 130, 1310-1324. doi:10.1007/s11263-022-01587-8
- Gabrieli Francesca, Delaney John K., Erdmann Robert G., Gonzalez Victor, van Loon Annelies, Smulders Patrick, Berkeveld Roy, van Langh Robert, & Keune Katrien. (2021). Reflectance Imaging Spectroscopy (RIS) for Operation Night Watch: Challenges and Achievements of Imaging Rembrandt's Masterpiece in the Glass Chamber at the Rijksmuseum. *Sensors*, 21(20), 6855. doi:10.3390/s21206855
- Gentaz Lucile, Lombardo Tiziana, Chabas Anne, Loisel Claudine, & Verney-Carron Aurélie. (2012). Impact of neocrystallisations on the SiO₂-K₂O-CaO glass degradation due to atmospheric dry depositions. *Atmospheric Environment*, 55, 459-466. doi:10.1016/j.atmosenv.2012.03.008

- Gestels Arthur, Van der Snickt Geert, Caen Joost, Nuyts Gert, Legrand Stijn, Vanmeert Frederik, Detry Flore, Janssens Koen, & Steenackers Gunther. (2022). Combined MA-XRF, MA-XRPD and SEM-EDX analysis of a medieval stained-glass panel formerly from Notre Dame, Paris reveals its material history. *Microchemical Journal*, *177*, 107304. doi:10.1016/j.microc.2022.107304
- Giani Alfredo, MacDonald Lindsay W., Machy Caroline, & Suganthan Shanmugalingam. (2003). Image segmentation of stained glass. *Color Imaging VIII: Processing, Hardcopy, and Applications*, *5008*, 150-158. doi:10.1117/12.474880
- Gimeno Domingo, Garcia-Valles Maite, Fernandez-Turiel José Luis, Bazzocchi Flavia, Aulinas Meritxell, Puges Montserrat, Tarozzi Camillo, Riccardi Maria Pia, Basso Elena, Fortina Consuelo, Mendera Marja, & Messiga Bruno. (2008). From Siena to Barcelona: Deciphering colour recipes of Na-rich Mediterranean stained glass windows at the XIII-XIV century transition. *Journal of Cultural Heritage*, *9*, E10-E15. doi:10.1016/j.culher.2008.08.001
- Grabowski Bartosz, Masarczyk Wojciech, Głomb Przemysław, & Mendys Agata. (2018). Automatic pigment identification from hyperspectral data. *Journal of Cultural Heritage*, *31*, 1-12. doi:10.1016/j.culher.2018.01.003
- Grillini Federico, Thomas Jean-Baptiste, & George Sony. (2021). Radiometric spectral fusion of VNIR and SWIR hyperspectral cameras. In *Color and Imaging Conference* (Vol. 2021, pp. 276-281): Society for Imaging Science and Technology.
- Harris A. Thomas. (2006). Spectral mapping tools from the earth sciences applied to spectral microscopy data. *Cytometry Part A*, *69A*(8), 872-879. doi:10.1002/cyto.a.20309
- Hunault Myrtille O. J. Y., Bauchau Fanny, Boulanger Karine, Hérold Michel, Calas Georges, Lemasson Quentin, Pichon Laurent, Pacheco Claire, & Loisel Claudine. (2021). Thirteenth-century stained glass windows of the Sainte-Chapelle in Paris: An insight into medieval glazing work practices. *Journal of Archaeological Science: Reports*, *35*, 102753. doi:10.1016/j.jasrep.2020.102753
- Hunault Myrtille O. J. Y., Bauchau Fanny, Loisel Claudine, Hérold Michel, Galois Laurence, Newville Matthew, & Calas Georges. (2016). Spectroscopic Investigation of the Coloration and Fabrication Conditions of Medieval Blue Glasses. *Journal of the American Ceramic Society*, *99*(1), 89-97. doi:10.1111/jace.13783
- Hunault Myrtille O. J. Y., Lelong Gerald, Gauthier Michel, Gelebart Frédéric, Ismael Saindou, Galois Laurence, Bauchau Fanny, Loisel Claudine, & Calas Georges. (2016). Assessment of Transition Element Speciation in Glasses Using a Portable Transmission Ultraviolet-Visible-Near-Infrared (UV-Vis-NIR) Spectrometer. *Applied Spectroscopy*, *70*(5), 778-784. doi:10.1177/0003702816638236
- Hunault Myrtille O. J. Y., & Loisel Claudine. (2020). Looking through model medieval green glasses: From color to recipe. *International Journal of Applied Glass Science*, *11*(3), 463-470. doi:10.1111/ijag.15134
- Hunault Myrtille O. J. Y., Loisel Claudine, Bauchau Fanny, Lemasson Quentin, Pacheco Claire, Pichon Laurent, Moignard Brice, Boulanger Karine, Hérold Michel, Calas Georges, & Pallot-Frossard Isabelle. (2017). Nondestructive Redox Quantification Reveals Glassmaking of Rare French Gothic Stained Glasses. *Analytical Chemistry*, *89*(11), 6278-6649. doi:10.1021/acs.analchem.7b01452
- ISO 5-2:2009 Photography and graphic technology - density measurements: part 2: geometric conditions for transmittance density. In Geneva: ISO.
- ISO 13655:2017 Graphic technology - Spectral measurement and colorimetric computation for graphic arts images. In Geneva: ISO.
- Jembrih-Simbürger Dubravka, Neelmeijer Christian, Schalm Olivier, Fredrickx Peggy, Schreiner Manfred, De Vis Kristel, Mäder Michael, Schryvers Dominique, & Caen Joost. (2002). The colour of silver stained glass—analytical investigations carried out with XRF, SEM/EDX, TEM, and IBA. *Journal of Analytical Atomic Spectrometry*, *17*(4), 321-328. doi:10.1039/B111024C

- Keshava Nirmal, Mustard, John F. (2002). Spectral unmixing. *IEEE Signal Processing Magazine*, 19(1), 44-57. doi:10.1109/79.974727
- Klein Stefan, Hildenhagen Jens, Dickmann Klaus, Stratoudaki T., & Zafiropulos Vassilis. (2000). LIBS-spectroscopy for monitoring and control of the laser cleaning process of stone and medieval glass. *Journal of Cultural Heritage*, 1, S287-S292. doi:10.1016/S1296-2074(00)00173-4
- Kruse Fred A., Lefkoff Adam B., Boardman Joseph W., Heidebrecht Kathleen B., Shapiro A. T., Barloon P. J., & Goetz Alexander F. H. (1993). The spectral image processing system (SIPS)—interactive visualization and analysis of imaging spectrometer data. *Remote Sensing of Environment*, 44(2), 145-163. doi:10.1016/0034-4257(93)90013-N
- Kunicki-Goldfinger Jerzy J., Freestone Ian C., McDonald Iain, Hobot Jan A., Gilderdale-Scott Heather, & Ayers Tim. (2014). Technology, production and chronology of red window glass in the medieval period - rediscovery of a lost technology. *Journal of Archaeological Science*, 41, 89-105. doi:10.1016/j.jas.2013.07.029
- Lanaras Charis, Baltasavias Emmanuel, & Schindler Konrad. (2017). Hyperspectral Super-Resolution with Spectral Unmixing Constraints. *Remote Sensing*, 9(11). doi:10.3390/rs9111196
- Legrand Stijn, Van der Snickt Geert, Cagno Simone, Caen Joost, & Janssens Koen. (2019). MA-XRF imaging as a tool to characterize the 16th century heraldic stained-glass panels in Ghent Saint Bavo Cathedral. *Journal of Cultural Heritage*, 40, 163-168. doi:10.1016/j.culher.2019.06.003
- Lombardo Tiziana, Loisel Claudine, Gentaz Lucile, Chabas Anne, Verita Marco, & Pallot-Frossard Isabelle. (2010). Long term assessment of atmospheric decay of stained glass windows. *Corrosion Engineering, Science and Technology*, 45(5), 420-424. doi:10.1179/147842210X12710800383800
- MacDonald Lindsay W. (1997). Digitization of stained glass. In *Proc. SPIE 3025, Very High Resolution and Quality Imaging II* (Vol. 3025, pp. 40-48).
- MacDonald Lindsay W. (2006). A robotic system for digital photography In *Proc. SPIE 6069, Digital Photography II* (Vol. 6069, pp. 60690I).
- MacDonald Lindsay W., Findlater Keith, Song Richard Tao, Giani Alfredo, & Suganthan Shanmugalingam. (2006). Imaging of Stained Glass Windows. In L. MacDonald (Ed.), *Digital Heritage. Applying Digital Imaging to Cultural Heritage* (pp. 411- 444). Oxford: Elsevier Butterworth-Heinemann.
- MacDonald Lindsay W., & Oldfield John. (1996). Image capture and restoration of medieval stained glass. In *Fourth Color Imaging Conference: Color Science, Systems and Applications* (pp. 44-49).
- Machado Carla, Vilarigues Márcia, & Palomar Teresa. (2021). Historical grisailles characterisation: A literature review. *Journal of Cultural Heritage*, 49, 239-249. doi:10.1016/j.culher.2021.03.010
- Mandal Dipendra J., George Sony, Pedersen Marius, & Boust Clotilde. (2021). Influence of Acquisition Parameters on Pigment Classification using Hyperspectral Imaging. *Color and Imaging Conference, 2021*(29), 334-346. doi:10.2352/J.ImagingSci.Technol.2021.65.5.050406
- McRae Tristan D., Oleksyn David, Miller Jim, & Gao Yu-Rong. (2019). Robust blind spectral unmixing for fluorescence microscopy using unsupervised learning. *PLOS ONE*, 14(12), e0225410. doi:10.1371/journal.pone.0225410
- Meulebroeck Wendy, Baert Kitty, Ceglia Andrea, Cosyns Peter, Wouters Hilde, Nys Karin, Terryn Herman, & Thienpont Hugo. (2012). The potential of UV-VIS-NIR absorption spectroscopy in glass studies. In *Proc. SPIE Integrated Approaches to the Study of Historical Glass* (Vol. 8422, pp. 842208).
- Meulebroeck Wendy, Baert Kitty, Wouters Hilde, Cosyns Peter, Ceglia Andrea, Cagno Simone, Janssens Koen, Nys Karin, Terryn Herman, & Thienpont Hugo. (2010). The identification of chromophores in ancient glass by the use of UV-VIS-NIR spectroscopy. In *Proc. SPIE Optical Sensing and Detection* (Vol. 7726, pp. 77260D): SPIE.

- Meulebroeck Wendy, Nys Karin, Patin Mathilde, & Thienpont Hugo. (2021). The interaction between daylight and fifteenth and sixteenth century glass windows from the Low Countries. *Scientific Reports*, 11(1), 21338. doi:10.1038/s41598-021-00359-7
- Meulebroeck Wendy, Patin Mathilde, Nys Karin, & Thienpont Hugo. (2023). Using absorption spectroscopy as a non-destructive tool for the study of silver-staining in glass: An operational flowchart to assign the technology parameters. *Journal of Non-Crystalline Solids*, 602, 122066. doi:10.1016/j.jnoncrysol.2022.122066
- Meulebroeck Wendy, Wouters Hilde, Baert Kitty, Ceglia Andrea, Terryn Herman, Nys Karin, & Thienpont Hugo. (2010). Optical spectroscopy applied to the analysis of medieval and post-medieval plain flat glass fragments excavated in Belgium. In *Proc. SPIE Optical Sensing and Detection* (Vol. 7726, pp. 77261E): SPIE.
- Meulebroeck Wendy, Wouters Hilde, Nys Karin, & Thienpont Hugo. (2016). Authenticity screening of stained glass windows using optical spectroscopy. *Scientific Reports*, 6, 37726. doi:10.1038/srep37726
- Micheletti Francesca, Orsilli Jacopo, Melada Jacopo, Gargano Marco, Ludwig Nicola, & Bonizzoni Letizia. (2020). The role of IRT in the archaeometric study of ancient glass through XRF and FORS. *Microchemical Journal*, 153, 104388. doi:10.1016/j.microc.2019.104388
- Molina Gloria, Murcia Sonia, Molera Judit, Roldan Clodoaldo, Crespo Daniel, & Pradell Trinitat. (2013). Color and dichroism of silver-stained glasses. *Journal of Nanoparticle Research*, 15(9), 1932 doi:10.1007/s11051-013-1932-7
- Möncke D., Papageorgiou M., Winterstein-Beckmann A., & Zacharias N. (2014). Roman glasses coloured by dissolved transition metal ions: redox-reactions, optical spectroscopy and ligand field theory. *Journal of Archaeological Science*, 46, 23-36. doi:10.1016/j.jas.2014.03.007
- Nidaros Domkirkes Restaureringsarbeider. (2019). Emanuel Vigelands glassmalerier, Nasjonalmuseet for kunst, arkitektur og design.
- Palomar Teresa, Agua Fernando, & Gomez-Heras Miguel. (2018). Comparative assessment of stained-glass windows materials by infrared thermography. *International Journal of Applied Glass Science*, 9(4), 530-539. doi:10.1111/ijag.12352
- Palomar Teresa, Grazia Chiara, Cardoso Isabel P., Vilarigues Marcia, Miliani Costanza, & Romani Aldo. (2019). Analysis of chromophores in stained-glass windows using Visible Hyperspectral Imaging in-situ. *Spectrochimica Acta Part a-Molecular and Biomolecular Spectroscopy*, 223, 117378. doi:10.1016/j.saa.2019.117378
- Palomar Teresa, Martínez-Weinbaum Marina, Aparicio Mario, Maestro-Guijarro Laura, Castillejo Marta, & Oujja Mohamed. (2022). Spectroscopic and Microscopic Characterization of Flashed Glasses from Stained Glass Windows. *Applied Sciences*, 12(11). doi:10.3390/app12115760
- Parker John M., & Martlew David. (2021). Stained Glass Windows. In Pascal Richet (Ed.), *Encyclopedia of Glass Science, Technology, History and Culture* (Vol. II, pp. 1341-1359). Hoboken, New Jersey: Wiley-American Ceramic Society.
- Patin Mathilde, Nys Karin, Thienpont Hugo, & Meulebroeck Wendy. (2022). Prestige markers in art: subtle stratagems in material selection for fifteenth-century stained-glass windows. *Heritage Science*, 10(1), 106. doi:10.1186/s40494-022-00698-2
- Pérez-Villar Sofía, Rubio Juan, & Oteo Jose Luis. (2008). Study of color and structural changes in silver painted medieval glasses. *Journal of Non-Crystalline Solids*, 354(17), 1833-1844. doi:10.1016/j.jnoncrysol.2007.10.008
- Perri Antonio, Nogueira de Faria Barbara E., Ferreira Danielle C. Teles, Comelli Daniela, Valentini Gianluca, Preda Fabrizio, Polli Dario, de Paula Ana Maria, Cerullo Giulio, & Manzoni Cristian. (2019). Hyperspectral imaging with a TWINS birefringent interferometer. *Optics Express*, 27(11), 15956-15967. doi:10.1364/OE.27.015956

- Piccolo Marcello, Casini Andrea, Cucci Costanza, Jussila Jouni, Poggesi Marco, & Stefani Lorenzo. (2018). A New Compact VNIR Hyperspectral Imaging System for Non-Invasive Analysis in the Fine Art and Architecture Fields. In *Proceedings e report* (pp. 69-74): Firenze University Press.
- Piccolo Marcello, Cucci Costanza, Casini Andrea, & Stefani Lorenzo. (2020). Hyper-Spectral Imaging Technique in the Cultural Heritage Field: New Possible Scenarios. *Sensors (Basel, Switzerland)*, 20(10), 2843. doi:10.3390/s20102843
- Pillay Ruven, Hardeberg Jon Y., & George Sony. (2019). Hyperspectral imaging of art: Acquisition and calibration workflows. *Journal of the American Institute for Conservation*, 58(1-2), 3-15. doi:10.1080/01971360.2018.1549919
- Pinar Guadalupe, Garcia-Valles Maite, Gimeno-Torrente Domingo, Fernandez-Turiel Jose L., Ettenauer Jorg, & Sterflinger Katja. (2013). Microscopic, chemical, and molecular-biological investigation of the decayed medieval stained window glasses of two Catalonian churches. *International Biodeterioration & Biodegradation*, 84, 388-400. doi:10.1016/j.ibiod.2012.02.008
- Polak Adam, Kelman Timothy, Murray Paul, Marshall Stephen, Stothard David J. M., Eastaugh Nicholas, & Eastaugh Francis. (2017). Hyperspectral imaging combined with data classification techniques as an aid for artwork authentication. *Journal of Cultural Heritage*, 26, 1-11. doi:10.1016/j.culher.2017.01.013
- Pouyet Emeline, Miteva Tsveta, Rohani Neda, & de Viguerie Laurence. (2021). Artificial Intelligence for Pigment Classification Task in the Short-Wave Infrared Range. *Sensors*, 21(18), 6150. doi:10.3390/s21186150
- Pouyet Emeline, Rohani Neda, Katsaggelos Aggelos K., Cossairt Oliver, & Walton Marc. (2018). Innovative data reduction and visualization strategy for hyperspectral imaging datasets using t-SNE approach. *Pure and Applied Chemistry*, 90(3), 493-506. doi:doi:10.1515/pac-2017-0907
- Pradell Trinitat, Molina Gloria, Murcia Sonia, Ibáñez Rafael, Liu Chaoren, Molera Judit, & Shortland Andrew J. (2016). Materials, Techniques, and Conservation of Historic Stained Glass "Grisailles". *International Journal of Applied Glass Science*, 7(1), 41-58. doi:10.1111/ijag.12125
- Radpour Roxanne, Delaney John K., & Kakoulli Ioanna. (2022). Acquisition of High Spectral Resolution Diffuse Reflectance Image Cubes (350-2500 nm) from Archaeological Wall Paintings and Other Immovable Heritage Using a Field-Deployable Spatial Scanning Reflectance Spectrometry Hyperspectral System. *Sensors*, 22(5), 1915. doi:10.3390/s22051915
- Raguin Virginia C. (1988). Conservation and Restoration of Stained Glass - An Owner's Guide. <https://www.icomos.org/publications/93stain13.pdf>
- Raguin Virginia C. (2013). *Stained Glass: Radiant Art*. Los Angeles, California: J. Paul Getty Museum.
- Rebollo E, Ratti F., Cortelazzo G. M., Poletto L., & Bertoncello R. (2011). New trends in imaging spectroscopy: the non-invasive study of the Scrovegni Chapel stained glass windows. In *Proc. SPIE, O3A: Optics for Arts, Architecture, and Archaeology III* (Vol. 8084, pp. 808407).
- Rodrigues Alexandra, Coutinho Mathilda, Machado Andreia, Martinho Bruno A., Cerqueira Alves Luís, Macedo Maria Filomena, & Vilarigues Márcia. (2021). A transparent dialogue between iconography and chemical characterisation: a set of foreign stained glasses in Portugal. *Heritage Science*, 9(1), 22. doi:10.1186/s40494-021-00480-w
- Rodrigues Alexandra, Gutierrez-Patricio Sara, Miller Ana Zelia, Saiz-Jimenez Cesareo, Wiley Robert, Nunes Daniela, Vilarigues Marcia, & Macedo Maria Filomena. (2014). Fungal biodeterioration of stained-glass windows. *International Biodeterioration & Biodegradation*, 90, 152-160. doi:10.1016/j.ibiod.2014.03.007
- Rohani Neda, Pouyet Emeline, Walton Marc, Cossairt Oliver, & Katsaggelos Aggelos K. (2018). Nonlinear Unmixing of Hyperspectral Datasets for the Study of Painted Works of Art. *Angew Chem Int Ed Engl*, 57(34), 10910-10914. doi:10.1002/anie.201805135

- Rossano Stephanie, Khomenko V., Bedidi Ali, Muller C., Loisel Claudine, Ferrand Jessica, Sarrasin Lola, & Bertin A. (2022). Glass colourations caused by Mn-Fe redox pair : Application to ancient glass technology. *Journal of Non-Crystalline Solids*, 594, 121710. doi:10.1016/j.jnoncrysol.2022.121710
- Schalm Olivier, Caen Joost, & Janssens Koen. (2010). Homogeneity, Composition and Deterioration of Window Glass Fragments and Paint Layers from Two Seventeenth-Century Stained Glass Windows Created by Jan de Caumont (similar to 1580-1659). *Studies in Conservation*, 55(3), 216-226. doi:DOI 10.1179/sic.2010.55.3.216
- Schreurs J. W. H., & Brill Robert H. (1984). Iron and sulfur related colors in ancient glasses. *Archaeometry*, 26(2), 199-209. doi:10.1111/j.1475-4754.1984.tb00334.x
- Simmons Christopher T., & Mysak Lawrence A. (2010). Transmissive properties of Medieval and Renaissance stained glass in European churches. *Architectural Science Review*, 53(2), 251-274. doi:10.3763/asre.2009.0073
- Striova Jana, Dal Fovo Alice, & Fontana Raffaella. (2020). Reflectance imaging spectroscopy in heritage science. *La Rivista del Nuovo Cimento*, 43(10), 515-566. doi:10.1007/s40766-020-00011-6
- Suganthan Shanmugalingam, & MacDonald Lindsay W. (2008). Correcting Image Defects of Stained Glass Windows. *International Journal of Imaging Systems and Technology*, 18(5-6), 296-306. doi:10.1002/ima.20160
- Suganthan Shanmugalingam, & MacDonald Lindsay W. (2010). Shadow Removal from Image of Stained Glass Windows. *International Journal of Imaging Systems and Technology*, 20(3), 223-236. doi:10.1002/ima.20241
- Szelagowska K., Szymonski M., Krok F., Walczak M., Karaszkiwicz R., & Prauzner-Bechcicki J. S. (2008). Comparative study of historic stained glass by LIBS and SEM/EDX. *Lasers in the Conservation of Artworks*, 141-+.
- Thanikachalam Niranjan, Baboulaz Loic, Prandoni Paolo, Trumpler Stefan, Wolf Sophie, & Vetterli Martin. (2016). VITRIL: Acquisition, Modeling, and Rendering of Stained Glass. *Ieee Transactions on Image Processing*, 25(10), 4475-4488. doi:10.1109/Tip.2016.2585041
- Thiemsorn Worapong, Keowkamnerd K., Phanichphant Sukon, Suwannathada Pongthorn, & Hessenkemper Heiko. (2008). Influence of glass basicity on redox interactions of iron-manganese-copper ion pairs in soda-lime-silica glass. *Glass Physics and Chemistry*, 34(1), 19-29. doi:10.1134/S1087659608010033
- Trümpler Stefan, Wolf Sophie, Kessler Cordula, & Goll Jürg. (2012). Potential and challenges of interdisciplinary research on historical window glass, stained glass and reverse glass paintings. *Proc. SPIE Integrated Approaches to the Study of Historical Glass*, 8422, 84220B. doi:10.1117/12.978231
- Valbi Valentina, Perez Anne, Verney-Carron Aurélie, & Rossano Stéphanie. (2023). Impact of a Mn-oxidizing bacterial strain on the dissolution and browning of a Mn-bearing potash-lime silicate glass. *npj Materials Degradation*, 7(1), 20. doi:10.1038/s41529-023-00338-5
- Van der Snickt Geert, Legrand Stijn, Caen Joost, Vanmeert Frederik, Alfeld Matthias, & Janssens Koen. (2016). Chemical imaging of stained-glass windows by means of macro X-ray fluorescence (MA-XRF) scanning. *Microchemical Journal*, 124, 615-622. doi:10.1016/j.microc.2015.10.010
- Van Ham-Meert Alicia, Bolea-Fernandez Eduardo, Belza Joke, Bevan Dan, Jochum Klaus Peter, Neuray Brigitte, Stoll Brigitte, Vanhaecke Frank, & Van Wersch Line. (2021). Comparison of Minimally Invasive Inductively Coupled Plasma–Mass Spectrometry Approaches for Strontium Isotopic Analysis of Medieval Stained Glass with Elevated Rubidium and Rare-Earth Element Concentrations. *ACS Omega*, 6(28), 18110-18122. doi:10.1021/acsomega.1c01939
- Vandenabeele Peter, & Donais Mary Kate. (2016). Mobile Spectroscopic Instrumentation in Archaeometry Research. *Appl Spectrosc*, 70(1), 27-41. doi:10.1177/0003702815611063

- Verita Marco, Bracci Susanna, & Porcinai Simone. (2019). Analytical investigation of 14th century stained glass windows from Santa Croce Basilica in Florence. *International Journal of Applied Glass Science*, 10(4), 546-557. doi:10.1111/ijag.13446
- Vermeulen Marc, Smith Kate, Eremin Katherine, Rayner Georgina, & Walton Marc. (2021). Application of Uniform Manifold Approximation and Projection (UMAP) in spectral imaging of artworks. *Spectrochimica Acta Part A: Molecular and Biomolecular Spectroscopy*, 252, 119547. doi:10.1016/j.saa.2021.119547
- Vilarigues Márcia, Ruivo Andreia, Hagendijk Thijs, Bandiera Mario, Coutinho Mathilda, Alves Luis C., & Dupré Sven. (2022). Red glass in Kunckel's *Ars Vitraria Experimentalis*: The importance of temperature. *International Journal of Applied Glass Science*, n/a(n/a). doi:10.1111/ijag.16605
- Walczak Małgorzata, Kaminska Marta, Karaszkiwicz P., Szczerbinski Jacek, & Szymonski Marek. (2013). The preliminary results on the investigation of historic stained glass panels from Grodziec collection, Poland. In *Proc. SPIE Optics for Arts, Architecture, and Archaeology IV* (Vol. 8790, pp. 87901F).
- Wilk Dariusz, Kamińska Marta, Walczak Małgorzata, & Bulska Ewa. (2017). Archaeometric investigations of medieval stained glass panels from Grodziec in Poland. In Piotr Targowski, Małgorzata Walczak, & Paraskevi Pouli (Eds.), *Lasers in the Conservation of Artworks XI, Proceedings of the International Conference LACONA XI, Kraków, Poland, 20–23 September 2016* (pp. 263-277): Nicolaus Copernicus University Press.
- Winter Michael E. (1999). N-FINDR: an algorithm for fast autonomous spectral end-member determination in hyperspectral data. In *Proc. SPIE Imaging Spectrometry V* (Vol. 3753, pp. 266-275).
- Zaleski Stephanie, Montagnino Elizabeth, Brostoff Lynn, Muller Isabelle, Buechele Andrew, Lynn Ward-Bamford Carol, France Fenella, & Loew Murray. (2019). Application of fiber optic reflectance spectroscopy for the detection of historical glass deterioration. *Journal of the American Ceramic Society*, 103(1), 158-166. doi:10.1111/jace.16703

Part II
Original Papers

Paper 1

Reprint of:

Agnese Babini, Sony George, Tiziana Lombardo, & Jon Y. Hardeberg. (2020). Potential and Challenges of Spectral Imaging for Documentation and Analysis of Stained-Glass Windows. London Imaging Meeting, 2020(1), 109-113

Potential and Challenges of Spectral Imaging for Documentation and Analysis of Stained-Glass Windows

Agnese Babini*, Sony George*, Tiziana Lombardo**, Jon Yngve Hardeberg*

*Norwegian University of Science and Technology, Gjøvik, Norway; **Swiss National Museum, Affoltern am Albis, Switzerland

Abstract

Stained-glass windows are very particular artifacts; they not only have an intrinsic artistic and historical meanings, but also a functional role, strictly connected to the buildings where they were originally placed. The investigation of these artifacts is a challenging research opportunity, due to their optical, chemical and physical characteristics. However, these properties could change with time, depending on the raw materials used, or due to exposure in a very aggressive environment. For this reason, developing imaging techniques that could both digitize and document the morphological/chemical changes of these objects, would solve two important issues: first, it would be possible to obtain a digital model of the object, ensuring the preservation of the objects for the future; second, it would be possible to get information on the materials employed, the ways they change with time, and how these changes modify the final appearance of the artwork. In this paper a proposal for a more systematic application of spectral imaging to stained glass is presented, discussing challenges and potential of the technique.

Introduction

Stained-glass windows are very particular artifacts; they not only have an intrinsic artistic and historical meanings, but also a functional role. They were built to close gaps in the architecture and at the same time the images, as well the chosen color palette, were designed to communicate stories or represent themes closely connected to the buildings where they were originally placed. The context in which stained glass are found is extremely important: the mounting technique, the materials and technologies employed to produce and color the glass can give many information on the resources and knowledge available in a certain historical period or geographical region [1-4].

From the material point of view, the investigation of these artifacts is a challenging research opportunity, due to their optical, chemical and physical characteristics. Stained-glass windows are made of many components, which together influence their general appearance: their integration in the building structure is guaranteed by a wooden or metallic frame; supporting bars (ferramenta) are added on the external side to give stability to the panels; the lead comes form the constructive framework that connects the glass pieces together in a firm but elastic way, and constitute the outlines of the depicted images; the colored glass, lastly, allows the light to enter the building and creates fascinating effects depending on the color palette and the external and internal illumination conditions. The coloration of glass pieces could be obtained in many ways, to create a variety of artistic effects: exploiting impurities (naturally-colored glass) or adding oxides (pot-colored glass), and then controlling temperature and atmosphere in the furnace to change the oxidation state of the chromophores, and get the desired color; using metallic nanoparticles; fusing thin layer of colored glass

on the surface of a transparent glass (flushed glass); painting the surface with vitreous paint or enamels. Grisaille, a brown/black vitreous paint, was often applied on the glass surface to add fine details in the scene represented [1, 5-8].

Stained glass, however, can be very fragile, and their appearance could change with time, depending on the raw material used and/or due to exposure in a very aggressive environment. The presence of pollutants and strong variation in temperature and humidity, favors the development of weathering crusts on the surface, which modifies the transparency of the glass. Consequently, the optical properties are affected, and it becomes difficult to understand the image represented, if the weathering layer is highly developed [7, 8]. For this reason, developing imaging techniques that could both digitize and document the morphological/chemical changes of these objects, would solve two important issues: first, it would be possible to obtain a digital model of the object, ensuring the preservation of the objects for the future; second, it would be possible to get information on the materials employed, the ways they change with time, and how these changes modify the final appearance of the artwork.

In this sense, spectral imaging could be a valuable tool: this technique allows obtaining spatial and spectral information simultaneously. The spectral data, by means of suitable algorithms, allows the visualization of the distribution of the materials in the object [9]. However, the reported use of this technique for stained-glass windows is quite limited, probably due to difficulties in finding proper acquisition methodologies to deal with the transparency of these artifacts. Here, a proposal for a more systematic application of spectral imaging to stained glass is presented, discussing its challenges and potentials.

The paper is organized as follows: first, a review of past works made in the field of imaging and image processing is presented. Then a brief overview of the most common analytical techniques employed in the field of Cultural Heritage for analysis of stained-glass windows is showed. The objectives of the project are stated, comparing the possible outcomes from spectral imaging vs. traditional analysis and discussing potential and challenges of the research presented. Lastly, a small section is dedicated to the presentation of preliminary works carried out on commercial and historical case studies.

Imaging techniques: a review

In this section, image acquisition and processing methodologies applied to stained-glass windows are presented, including both traditional RGB photography and spectral imaging.

RGB photography acquisition and processing

Documentation of stained-glass windows has traditionally been performed with analog cameras and, more recently, with digital cameras. Photographic documentation is a fundamental step in every conservation campaign and must be done before

and after any treatment, to document any change happened or happening on the artifact. Suggestions for accurate technical documentation were proposed in [10]. The paper describes the most common issues in photographing stained glass, and presents a methodology developed specifically to deal with these issues and obtain high quality pictures. For example, the paper proposed an innovative way to control the external light, by using an illuminated panel based on a commercial photographic 'soft box' placed outside the window to be scanned. The selected illumination source was a 500-watt tungsten-halogen flood light. A methodology for camera characterization specific for photography of stained-glass window has been proposed in the same paper and more details are provided in [11]. A pair of custom glass color checkers (a test and a training set) were built and employed for the purpose; the checkers are built including a large number of colored glass used in medieval times, with colors ranging from very dark to very light, to mimic the high dynamic range of a real stained glass. A way to control the illumination during the acquisition was proposed within the digitization campaign at Fairford Church. Other works have been done to improve the quality of acquisition and archival procedures; the research of the European project VITRA (Veridical Imaging of Transmissive and Reflective Artefacts), carried out from 2002 to 2004, was focused on "developing a practical method for the acquisition, storage and visualization of high-quality images of architectural details in historic buildings", including stained-glass windows. The acquisitions were carried out by means of a robotic arm remotely controlled, which allowed to reach higher areas (up to 15 m). In this way, it was possible to obtain high resolution images of those areas usually difficult to capture from the ground, avoiding loss of details and image distortions. The imaging of stained-glass windows was performed in transmittance using natural light, and many pictures were collected in different exposures to deal with the high dynamic range of the stained glass [12]. On the image processing side, investigations have been conducted to highlight relevant features [13], to correct defects [14] and to remove unwanted features such as shadows coming from the background or from the supporting bars [6], as well as to perform rendering, relighting and virtual restoration [15, 16].

Spectral imaging applications

Compared to RGB photography, application of spectral imaging on stained-glass windows is very limited. At the best of the authors' knowledge, only two papers exist in literature on this specific topic. The first one involved the analysis of the stained-glass windows of the Scrovegni Chapel (Padua); the panels were removed from their original place and acquired in laboratory under controlled illumination, namely transmission and double transmission mode [17]. In the transmission mode, the light sources were simply placed at the opposite side of the camera, while in double transmittance the camera and the lights were placed at the same side, and a scattering white support was placed below the stained glass to be scanned. The latter solution was proposed for stained-glass panels which could not be acquired vertically, and actually yielded better results for light-colored glass pieces. While spectral images are not available in the paper, they showed that results from the two methodologies were complementary and they were able to identify most of the chromophores [17]. The second paper, published in 2019, presented the first hyperspectral acquisition of stained-glass windows in situ [18]. In this case, the window was kept in its place and the analysis was performed in passive mode, using the

solar radiation coming through the window as light source. The mapping of the colorants used for the glass pieces in the windows was then performed using Spectral Angle Mapper, a classification algorithm widely used for hyperspectral applications in the field of Cultural Heritage. Despite some limitation due to changing in the light conditions during the day and effect of external background (i.e. trees) on the lighter colored glass, the analysis showed promising results, especially when comparing and mapping the spectral results of glass with same color and composition but with different transparency [18].

Another imaging technique worthy of mention is Macro X-Ray Fluorescence (MA-XRF); it is also called "chemical imaging", as the image obtained is made of many points collected with an X-ray fluorescence spectrometer which is connected to a moving stage and scanned over the surface of the painting at a given step size. The result is a datacube, like the hyperspectral one, where every pixel contains information regarding the elemental composition of the material under study. The datacube can then be treated with a suitable software which allows to create maps of elements (or combination of elements) to estimate which kind of material (i.e. pigments or colorants) was employed by the artist. While MA-XRF is very popular for the study of paintings, it is still quite limited for the study of stained glass. Only two papers have been published so far, in 2016 and 2019 [19, 20]. In both cases the analysis was carried out in laboratory. Despite the few applications on stained-glass windows, the results obtained are very interesting, especially to distinguish ancient glass pieces from modern ones, to understand how the color in glass was reached, and to detect glass alteration. An interesting result highlighted in the first paper is worthy of mention: the possibility of understanding how the color was obtained in the glass, by scanning both surfaces and comparing them. If a specific chromophore element appears on only one side, then it is possible to guess that the colorant was painted on the back of the glass panels, instead of being added during the glass production.

Scientific analysis of stained-glass windows: a brief review

Regarding the determination of the conservation state of stained-glass windows, scientific analysis usually involves a combination of invasive and non-invasive techniques. Invasive techniques are called as such because they require the collection of small samples from the surface of the artifact, which may be kept for further analysis or destroyed in the process, depending on the kind of technique employed. Most of these analyses must be performed in laboratory, and sometimes they require very specific facilities (i.e. XANES, which requires the access to a synchrotron) [3].

Non-invasive techniques, on the other hand, do not require samples and are sometimes portable, which allow to perform analysis in situ. They have become very popular in the last years, especially for preliminary investigation of composition and conservation state of the stained glass and are often enough to get the necessary information without requiring further invasive techniques [21].

In the table below the most used scientific techniques employed for the analysis of stained-glass windows are listed; for each technique, a brief description is given regarding the kind of information obtainable and the level of invasiveness is specified.

Table 1: List of scientific techniques

Analytical technique	Invasive	Information given
Fourier Transform IR spectroscopy (FTIR)	Yes/no (depending on the analysis mode)	Molecular; degradation products. [22, 23]
Particle induced X-ray emission (PIXE)	No	Elements; quantitative information of major, minor and trace elements. [22-25]
RAMAN spectroscopy	Yes/no (depending on size of the object); can be portable	Molecular; colorants and glass components; degradation products (results may vary from lab instrument to portable ones). [26, 27]
Scanning Electron Microscope (SEM); sometimes coupled with electron microprobe (EPMA)	Yes	Elemental; quantitative information on major, minor and trace elements; microscopic observation of the topography of the surface; semi-quantitative information on the distribution of elements on the surface. [28, 29]
UV-VIS-NIR spectroscopy (absorption/reflectance) ; Fiber Optic Reflectance Spectroscopy (FORS) *	No; can be portable	Molecular; information on oxidation states and coordination of colorants (UV-VIS-NIR) and degradation mechanisms (NIR). [3, 25, 30-32]
X-ray Absorption Spectroscopy (XAS/XANES)	Yes	Elemental; oxidation state of chromophore elements in glass. [3, 30, 33, 34]
X-Ray Fluorescence spectroscopy (XRF)	No; can be portable	Elemental; qualitative information on major, minor and sometimes trace elements (results may vary from the lab instrument to the portable one) [35, 36]; possibility of element mapping in MA-XRF configuration.
X-Ray Diffraction (XRD)	Yes	Molecular; identification of corrosion products [37, 38].

The proposed methodology

The methodology presented here will aim at extending the use of hyperspectral (and multispectral) imaging for the documentation of stained-glass window. Since hyperspectral imaging can be considered a combination of spectroscopy (see

table 1*) and imaging, the purpose of the research will be to investigate advantages and disadvantages of employing these techniques to acquire simultaneously spectral and spatial information. At the moment, the project has two main objectives: firstly, improve the acquisition and image processing methodology; applying spectral unmixing techniques to obtain maps of the different glass components, validated using other non-invasive techniques (i.e. XRF). In a later stage, integration of the data obtained, and virtual restoration will be also considered. These objectives will aim to answer different research questions, discussed in detail in the following paragraphs, and developed from this literature review.

Acquisition methodology

As discussed in the previous section on imaging techniques, many works have been done in studying the correct acquisition conditions for RGB cameras, but little has been done for hyperspectral imaging; one of the purpose of this research, within the framework of the CHANGE-ITN project, will be then to study the different situations in which the stained glass are either exhibited, in a museum, in situ (either in high or low places) or in laboratories and restoration workshops. Depending on the location of the stained glass, it is expected that the lighting condition will be more or less controlled; this aspect will be taken into consideration to understand how much it will be possible to control the illumination directly in situ, like in [10], and how much it will be necessary to correct afterwards during the image processing stage. Once the methodology has been defined, then it could be possible to apply it to similar objects, such as reverse glass painting.

Image processing and validation with scientific analysis

One of the main purposes of the project is also to determine the materials and the techniques employed to produce the stained-glass windows.

To fulfill this objective, employing spectral imaging has a great advantage; with hyperspectral imaging, the possibility of getting a spectrum in each pixel of the image will allow the detection and mapping of colorants and alteration products distribution. This information can be extremely useful to highlights the use of different colorants to obtain certain shades of the same color, or to identify areas where original pieces have been substituted during restoration with modern glass. Also, it will be possible to detect areas more prone to degradation or more exposed to pollutants or strong variation of atmospheric conditions. While multispectral imaging does not always allow to obtain a complete spectrum (depending on the spectral bands available in the camera), this technique has the advantage of being easier to carry and cheaper than a hyperspectral system. For this reason, it could be a valuable instrument for a preliminary investigation, especially in situ. In order to extract information from the databse several algorithms will be investigated to understand which one could be more suitable for the purpose. For example, one of the tasks of the project will be to compare the performance between classification methods (such as Spectral Angle Mapper) and the less known, at least in the field of Cultural Heritage, unmixing algorithms. Hopefully, using unmixing algorithms will allow, not only to understand an eventual superimposition of colored glass and vitreous paint, but also it will help to deal with unwanted features in the image such as shadows from ferramenta or background.

Potential and limitations of spectral imaging

As already mentioned, one of the main advantages of using spectral imaging is the possibility to obtain at the same time, spatial and spectral information. Also, the technique is totally non-invasive and the possibility to be carried in situ is surely an added value.

The possibility to map the different typologies of glass and the presence of degradation products, could be certainly useful to conservators, especially for windows still in situ that cannot be removed, or that are difficult to reach. For example, with spectral imaging it could be possible to highlight areas restored with new glass, filled fractures, as well as to determine the areas more sensitive to weathering, distinguish between different alterations, and understand how those degradation products are distributed on the surface. The maps obtained then could be used to help the establishment of a condition report before carrying out a new restoration campaign.

However, some limitations are to be taken into consideration; first, with respect to RGB images, spectral datacubes (especially the hyperspectral ones) are way more complex to analyze, due to their high dimensionality (both spatial and spectral). For this reason, it is expected that pre-processing and processing of data will not be as straightforward as for RGB images[39].

Regarding chemical information, it is clear that the use of spectral imaging alone will not be able to answer all the research questions posed by conservators. For this reason, the use of other non-invasive techniques is already considered to validate the spectral imaging results. However, employing only non-invasive techniques may be another limitation itself; while it has been demonstrated that UV-VIS-NIR spectroscopy is able to substitute destructive techniques like XANES to identify chromophores by their oxidation state [30], some other information are obtainable only by taking samples, as most of the portable instruments proposed for validation can give only surface information. This may be a limitation, for instance, when trying to understand the colorant distribution within the glass or to determine glass composition, which very often vary between the surface and the deeper part of the glass, depending on the presence of weathering layer and its thickness.

Nonetheless, spectral imaging represents a valid non-invasive solution to have a general understanding of the work of art. In addition, the spectral maps themselves could be useful for a correct identification of sampling areas, by showing the points where the collection of samples could be more significant.

Preliminary works

Preliminary studies have been performed both on commercial (modern) and historical stained-glass panels. The panels were scanned with a HySpex VNIR-1600 pushbroom hyperspectral camera. The camera works in the visible and infrared region, in the range between 400 and 1000 nm. The image is built line by line keeping the camera and the light source fixed, while a translational stage moves beneath. The acquisitions were performed in transmittance as well as in reflectance, in order to understand whether it was possible to obtain complementary information (i.e glass composition and deposition of degradation products on both surfaces). In reflectance mode, the glass panels were acquired placing a white diffuser sheet under the stained glass and keeping the traditional lighting system for reflectance (two light sources at 0-45), similarly to [17]. On the other hand, in transmittance mode the stained-glass panels were positioned above a white diffuser panel

large enough to cover the field of view of the camera, and located in the middle of the translational stage; in this set-up, a halogen lamp was positioned under the stage, in correspondence with the diffuser panel, so that the light could shine through it and the stained glass. Despite some difficulties, these preliminary tests showed promising results and were extremely useful to understand some of the challenges that need to be addressed in the future. For example, modification of the lighting set-up for the transmission mode is planned, in order to improve the spatial distribution of the light over the diffuser panel and decrease the heat coming from the halogen lamp, while trying to improve the obtainable spectral signal even for very dark stained-glass windows.

Publication of complete results on the historical stained glass is planned in the near future.

Conclusion

The aim of this paper was to present a proposal of a research project with the aim of exploring the use of spectral imaging for the documentation of stained-glass windows. To clarify the purpose of the project, a review of existing literature regarding application of imaging techniques (RGB and spectral) on stained-glass windows has been shown. In addition, scientific techniques used for the analysis of stained glass have been described to show which kind of information can be retrieved with invasive and non-invasive techniques. Lastly, potential and limitation of these techniques have been presented, explaining in which way spectral imaging could add information or substitute destructive analysis for some specific tasks.

Acknowledgment

The research presented here is being carried out as part of a PhD program within the CHANGE Innovative Training Network. The CHANGE-ITN project has received funding from the European Union's Horizon 2020 research and innovation programme under the Marie Skłodowska-Curie grant agreement No. 813789.

References

- [1] V. Raguin. Conservation and Restoration of Stained Glass - An Owner's Guide. Available from: <https://www.icomos.org/publications/93stain13.pdf>.
- [2] S. Trumpler, S. Wolf, C. Kessler, J. Goll, Potential and challenges of interdisciplinary research on historical window glass, stained glass and reverse glass paintings, Proc. SPIE 8422. (2012).
- [3] M. Hunault, F. Bauchau, C. Loisel, M. Herold, L. Galoisy, M. Newville, G. Calas, Spectroscopic Investigation of the Coloration and Fabrication Conditions of Medieval Blue Glasses, J. Am. Ceram. Soc., 99, p. 89-97 (2016).
- [4] J. Taralon. Problématique de la Conservation et de la Restauration des Vitreaux. Available from: <https://www.icomos.org/publications/93stain2.pdf>.
- [5] W. Meulebroeck, H. Wouters, K. Nys, H. Thienpont, Authenticity screening of stained-glass windows using optical spectroscopy. Sci Rep, 6, 37726 (2016).
- [6] S. Suganthan and L. MacDonald, Shadow Removal from Image of Stained-Glass Windows, Int J Imaging Syst Technol, 20 (2010).
- [7] E. Bacher. Introduction - Conservation of Ancient Monumental Stained and Painted Glass. Available from: <https://www.icomos.org/publications/93stainintro1.pdf>.
- [8] G. Frenzel. The Restoration of Medieval Stained Glass. Available from: <https://www.icomos.org/publications/93stain5.pdf>.
- [9] H. Deborah, S. George, and J.Y. Hardeberg, Spectral-divergence based pigment discrimination and mapping: A case study on The Scream (1893) by Edvard Munch, J Am Inst Conserv (2019).

- [10] L.W. MacDonald, Digitization of stained glass, *Proc. SPIE* 3025, p. 40-48. (1997).
- [11] L. MacDonald, K. Findlater, R. T. Song, A. Giani, S. Suganthan, *Imaging of Stained-Glass Windows*, in *Digital Heritage. Applying Digital Imaging to Cultural Heritage* (Elsevier Butterworth-Heinemann, Oxford, 2006) p. 411-444.
- [12] L.W. MacDonald, A robotic system for digital photography, *Proc. SPIE* 6069. (2006).
- [13] A. Giani, L. MacDonald, C. Machy, S. Suganthan, Image segmentation of stained glass, *Proc. SPIE* 5008, p. 150-158. (2003).
- [14] S. Suganthan and L.W. MacDonald, Correcting Image Defects of Stained-Glass Windows. *Int J Imaging Syst Technol*, 18 (2008).
- [15] L.W. MacDonald and J. Oldfield, Image capture and restoration of medieval stained glass, *Proc. IS & T/SID*, p. 44-49. (1996).
- [16] N. Thanikachalam, L. Baboulaz, P. Prandoni, S. Trumpler, S. Wolf, M. Vetterli, VITRAIL: Acquisition, Modeling, and Rendering of Stained Glass, *IEEE Trans. Image Process*, 25 (2016).
- [17] E. Rebollo, F. Ratti, G.M. Cortelazzo, L. Poletto, R. Bertonecello, New trends in imaging spectroscopy: the non-invasive study of the Scrovegni Chapel stained glass windows, *Proc. SPIE* 8084, (2011).
- [18] T. Palomar, C. Grazia, I.P. Cardoso, M. Vilarigues, C. Miliani, A. Romani, Analysis of chromophores in stained-glass windows using Visible Hyperspectral Imaging in-situ, *Spectrochim Acta A Mol Biomol Spectrosc*, 223, (2019).
- [19] G. Van der Snickt, S. Legrand, J. Caen, F. Vanmeert, M. Alfeld, K. Janssens, Chemical imaging of stained-glass windows by means of macro X-ray fluorescence (MA-XRF) scanning, *Microchem J*, 124 (2016).
- [20] S. Legrand, G. Van der Snickt, S. Cagno, J. Caen, K. Janssens, MA-XRF imaging as a tool to characterize the 16th century heraldic stained-glass panels in Ghent Saint Bavo Cathedral, *J. Cult. Herit.*, 40 (2019).
- [21] P. Vandenaebelle and M.K. Donais, Mobile Spectroscopic Instrumentation in Archaeometry Research, *Appl Spectrosc*, 70 (2016).
- [22] M. Vilarigues, P. Fernandes, L.C. Alves, R.C. da Silva, Stained glasses under the nuclear microprobe: A window into history, *Nucl. Instrum. Methods Phys. Res. B*, 267 (2009).
- [23] M. Vilarigues, P. Redol, A. Machado, P.A. Rodrigues, L.C. Alves, R.C. da Silva, Corrosion of 15th and early 16th century stained glass from the monastery of Batalha studied with external ion beam, *Mater. Charact.*, 62 (2011).
- [24] T. Calligaro, PIXE in the study of archaeological and historical glass, *X-Ray Spectrom.*, 37 (2008).
- [25] M.O.J.Y. Hunault, C. Loisel, F. Bauchau, Q. Lemasson, C. Pacheco, L. Pichon, B. Moignard, K. Boulanger, M. Herold, G. Calas, I. Pallot-Frossard, Nondestructive Redox Quantification Reveals Glassmaking of Rare French Gothic Stained Glasses, *Anal. Chem.*, 89 (2017).
- [26] K. Baert, W. Meulebroeck, A. Ceglie, H. Wouters, P. Cosyns, K. Nys, H. Thienpont, H. Terryn, The potential of Raman spectroscopy in glass studies. Integrated Approaches to the Study of Historical Glass, *Proc. SPIE* 8422. (2012).
- [27] P. Colombari and A. Toumie, On-site Raman identification and dating of ancient/modern stained glasses at the Sainte-Chapelle, Paris, *J. Cult. Herit.*, 8 (2007).
- [28] M. Verità, S. Bracci, and S. Porcinai, Analytical investigation of 14th century stained glass windows from Santa Croce Basilica in Florence, *Int. J. Appl. Glass Sci*, 10 (2019).
- [29] R. Falcone, M. Nardone, A. Sodo, G. Sommariva, M. Vallotto, M. Verità, SEM-EDS, EPMA and MRS analysis of neo-crystallisations on weathered glasses, *IOP Conf. Ser.: Mater. Sci. Eng.*, 7. (2010).
- [30] A. Ceglie, G. Nuyts, W. Meulebroeck, S. Cagno, A. Silvestri, A. Zoleo, K. Nys, K. Janssens, H. Thienpont, H. Terryn, Iron speciation in soda-lime-silica glass: a comparison of XANES and UV-vis-NIR spectroscopy, *J. Anal. At. Spectrom.*, 30 (2015).
- [31] S. Zaleski, E. Montagnino, L. Brostoff, I. Muller, A. Buechele, C. L. Ward-Bamford, F. France, M. Loew, Application of fiber optic reflectance spectroscopy for the detection of historical glass deterioration, *J. Am. Ceram. Soc.*, (2019).
- [32] M.O.J. Y. Hunault, G. Lelong, M. Gauthier, F. Gelebart, S. Ismael, L. Galois, F. Bauchau, C. Loisel, G. Calas, Assessment of Transition Element Speciation in Glasses Using a Portable Transmission Ultraviolet-Visible-Near-Infrared (UV-Vis-NIR) Spectrometer, *Appl Spectrosc*, 70 (2016).
- [33] F. Farges, M.P. Etcheverry, A. Scheidegger, D. Grolimund, Speciation and weathering of copper in "copper red ruby" medieval flashed glasses from the Tours cathedral (XIII century), *Appl Geochem*, 21 (2006).
- [34] J. Ferrand, S. Rossano, C. Loisel, N. Trcera, E.D. van Hullebusch, F. Bousta, I. Pallot-Frossard, Browning Phenomenon of Medieval Stained-Glass Windows, *Anal. Chem.*, 87 (2015).
- [35] L.W. Adlington and I.C. Freestone, Using handheld pXRF to study medieval stained glass: A methodology using trace elements, *MRS Advances*, 2, 33-34, (2017).
- [36] N. Carmona, I. Ortega-Feliu, B. Gomez-Tubio, M.A. Villegas, Advantages and disadvantages of PIXE/PIGE, XRF and EDX spectrometries applied to archaeometric characterization of glasses, *Mater. Charact.*, 61 (2010).
- [37] L. Gentaz, T. Lombardo, A. Chabas, C. Loisel, A. Verney-Carron, Impact of neocrystallisations on the SiO₂-K₂O-CaO glass degradation due to atmospheric dry depositions. *Atmos. Environ*, 55 (2012).
- [38] M. Aulinas, M. Garcia-Valles, D. Gimeno, J.L. Fernandez-Turiel, F. Ruggieri, M. Puges, Weathering patinas on the medieval (S. XIV) stained glass windows of the Pedralbes Monastery (Barcelona, Spain), *Environ Sci Pollut Res*, 16 (2009).
- [39] R. Pillay, J.Y. Hardeberg, and S. George, Hyperspectral imaging of art: Acquisition and calibration workflows, *J Am Inst Conserv* (2019).

Author Biography

Agnese Babini received her master's degree in Science for Conservation of Cultural Heritage at the University of Bologna, with a thesis on applications of hyperspectral imaging and image processing on cultural heritage. She is currently carrying out her PhD at the Norwegian University of Science and Technology (NTNU) within the European project CHANGE-ITN. Her research is focused on applications of spectral imaging techniques on historical stained-glass windows for the characterization of materials and degradation products.

Sony George is currently Associate Professor at The Norwegian Colour and Visual Computing Laboratory, Norwegian University of Science and Technology (NTNU) since 2017. Sony obtained a PhD in Photonics from the Cochin University of Science and Technology, India in 2012. He has been involved in several national and EU projects: EU MSCA-ITN project HiPerNav (project manager), EU MSCA-ITN project CHANGE (deputy coordinator). He has been active member in the EU COST Actions TD1201 and CA16101 MULTIFORESEE.

Tiziana Lombardo received a PhD in chemistry from the university Paris Est Créteil (UPEC), France in 2002. From 2004 to 2013 she worked as assistant professor at the UPEC and carried out research on atmospheric corrosion of medieval stain glass. Currently she works as conservation scientist at the collection center of the Swiss National Museum.

Jon Y. Hardeberg received his PhD from Ecole Nationale Supérieure des Télécommunications in Paris, France in 1999. He is currently Professor of Colour Imaging at NTNU and member of the Norwegian Colour and Visual Computing Laboratory. He has led several projects funded by the Research Council of Norway, been NTNU's representative in two Erasmus Mundus Joint Master Degrees (CIMET and COSI), and the coordinator of three Marie Curie ITN projects (CP7.0, ApPEARS, CHANGE)

Paper 2

Reprint of:

Agnese Babini, Phil Green, Sony George, & Jon Y. Hardeberg. (2022). Comparison of Hyperspectral Imaging and Fiber-Optic Reflectance Spectroscopy for Reflectance and Transmittance Measurements of Colored Glass. *Heritage*, 5(3), 1401-1418.

Article

Comparison of Hyperspectral Imaging and Fiber-Optic Reflectance Spectroscopy for Reflectance and Transmittance Measurements of Colored Glass

Agnese Babini , Phil Green, Sony George  and Jon Yngve Hardeberg 

Department of Computer Science, Norwegian University of Science and Technology, 2815 Gjøvik, Norway; philip.green@ntnu.no (P.G.); sony.george@ntnu.no (S.G.); jon.hardeberg@ntnu.no (J.Y.H.)

* Correspondence: agnese.babini@ntnu.no

Abstract: The work presented in this paper is part of a wider research project, which aims at documenting and analyzing stained glass windows by means of hyperspectral imaging. This technique shares some similarities with UV-VIS-IR spectroscopy, as they both provide spectral information; however, spectral imaging has the additional advantage of providing spatial information, since a spectrum can be collected in each pixel of the image. Compared to UV-VIS-IR spectroscopy, spectral imaging has rarely been used for the investigation of stained glass windows. One of the objectives of this paper is, thus, to compare the performance of these two instruments to validate the results of hyperspectral imaging. The second objective is to evaluate the potential of analyzing colored-glass pieces in reflectance modality and compare the results with those obtained in transmittance, in order to highlight the differences and similarities between the two approaches. The geometry of the systems and the backing material for the glass, as well as the characteristics of the glass pieces, are discussed. $L^*a^*b^*$ values obtained from the spectra, as well as the calculated color difference ΔE_{00} , are provided, to show the degree of agreement between the instruments and the two measurement modalities.

Keywords: stained glass; UV-VIS spectroscopy; hyperspectral imaging; colorimetry; transmittance measurements; reflectance measurements



check for updates

Citation: Babini, A.; Green, P.; George, S.; Hardeberg, J.Y. Comparison of Hyperspectral Imaging and Fiber-Optic Reflectance Spectroscopy for Reflectance and Transmittance Measurements of Colored Glass. *Heritage* **2022**, *5*, 1401–1418. <https://doi.org/10.3390/heritage5030073>

Academic Editors: Marcia Vilarigues, Sophie Wolf and Teresa Palomar

Received: 11 May 2022

Accepted: 21 June 2022

Published: 23 June 2022

Publisher's Note: MDPI stays neutral with regard to jurisdictional claims in published maps and institutional affiliations.



Copyright: © 2022 by the authors. Licensee MDPI, Basel, Switzerland. This article is an open access article distributed under the terms and conditions of the Creative Commons Attribution (CC BY) license (<https://creativecommons.org/licenses/by/4.0/>).

1. Introduction

The work presented in this paper has been carried out within a wider research project [1], which aims at documenting and analyzing stained-glass windows by means of hyperspectral imaging. Hyperspectral imaging (HSI) can be considered as a combination of conventional imaging and UV-VIS-NIR spectroscopy. The technique is based on the acquisition of many images finely sampled across a portion of the electromagnetic spectrum, and, as a result, a full spectrum can be obtained in each pixel of the image, providing information on the materials used as well as their distribution across the artwork under study.

UV-VIS-IR spectroscopy is a well-established technique for the identification of the coloring agents (chromophores) in stained glass windows, whereby the specific absorbance peaks in the spectra can be analyzed and interpreted [2–23]. This information allows for understanding the mechanisms responsible for the color of the glass, which can provide important insights into the technological development in glass production during a particular historical period or geographical region. The use of hyperspectral imaging, on the other hand, is quite limited, and very few works have been published so far on the topic, especially in comparison to the literature available for other typologies of artworks, such as painting and manuscripts [24–27]. Since stained glass is transparent, one of the main practical challenges is to have access to setups that can measure in transmittance. In addition, the setup should be easily, as stained glass windows are usually located in buildings and can be difficult to access without scaffoldings or other supports. The easiest solution, and the most widely used [25–27], is to perform the acquisition by exploiting

solar radiation as light source. However, variations of light distribution throughout the day, as well as the presence of external structures (vegetation, buildings, etc.) might affect the spectra.

Nonetheless, the possibility of having simultaneous spatial and spectral information in HSI can represent a great advantage when analyzing large surfaces such as stained glass windows, compared to spot measurement. In light of these considerations, we recently presented a laboratory setup to perform transmittance hyperspectral imaging of stained glass panels [28].

It is important to highlight that while the detector technologies of HSI and UV-VIS spectroscopy are essentially the same, the two instruments have different optical configuration (array vs. spot measurement) and measurement geometry. One of the objectives of this study is, thus, to evaluate the use of HSI for the analysis of stained glass windows by comparing the results obtained with this technique to those from UV-VIS spectroscopy, following standard geometric recommendations for measurement in transmittance [29–31]. Note that the results from the HSI will be considered only from the spectral point of view, while the spatial dimension will not be taken into account.

Another aim of the paper is to compare the results of two different acquisition modalities: transmittance and reflectance. Traditionally, color measurements of glass are carried out in transmittance mode [30]. Measurements in reflectance are less common; nonetheless, they can be helpful in revealing some properties of the glass under study. In this case, a non-spectrally selective, diffusing surface with high reflectance can be used as a backing material to enhance the reflectance signal of the glass pieces [24,31].

Depending on the transparency of the glass and the surface characteristics, the differences between the results in the two modalities could be interpreted as effects of the surface condition of the colored glass, as can their optical properties.

In this paper, 14 pieces of colored glass have been used as a case study. To compare the results, the geometry of the systems, the characteristics of the glass pieces, and the effects of the backing material for the reflectance measurements will be discussed. The spectra obtained in reflectance and transmittance will be shown together, to visualize the differences in shape and intensity between the two modalities.

CIELAB $L^*a^*b^*$ values and the color difference ΔE_{00} , between the two modalities and the two instruments will be provided for the selected glasses, to show the degree of agreement.

2. Materials and Methods

2.1. Glass Samples

For the experiment, 14 pieces of colored glass, provided by the restoration workshop of the Nidaros Cathedral (Trondheim, Norway), were used (Figure 1). Glass pieces were preferred to real case studies, to facilitate the measurement of transmittance and reflectance as well as the comparison of the instrument configurations.

The glass pieces are modern glass used for restoration purposes, characterized by different thicknesses and surface roughnesses, which strongly influence the intensity and quality of the signals obtained. All the glass pieces are colored in body, except for the red ones; these latter samples consist of two layers, a thinner red layer over a thicker transparent one, consistent with the recipes to create red-colored glass in antiquity.

2.2. Instrumentation

2.2.1. Metrology

The measurements were made using two instruments, a spectrometer and a hyperspectral camera. The Ocean Optic USB2000+ spectrometer (denoted FORS below), is equipped with a fiber-optic connector between the measurement probe and the spectrometer entrance port, with a diffuser mounted over the probe. The hyperspectral camera used for the study was a HySpex VNIR-1800, developed by Norsk Elektro Optikk AS. Figure 2 shows the

respective geometries of the two instruments and the measurement modalities employed, while Table 1 reports the specifications of the instruments.

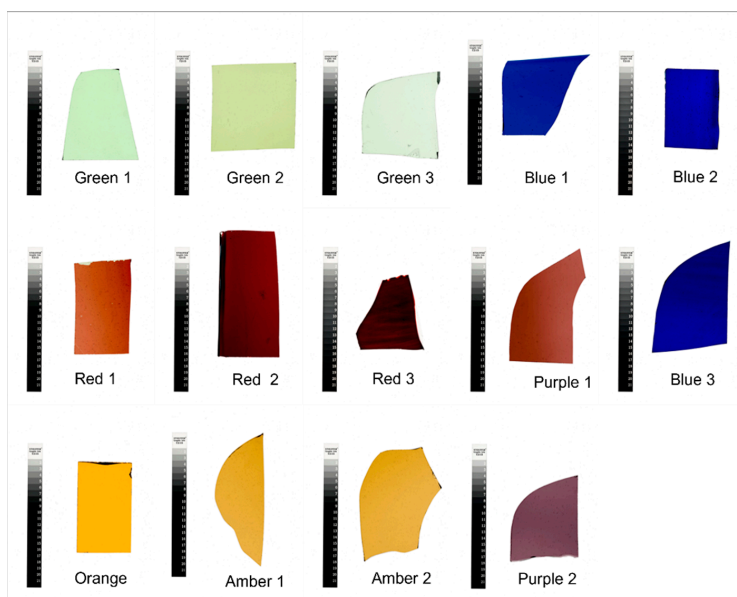


Figure 1. Glass samples photographed on a light table (credits to Ottar A.B. Anderson at SEDAK).

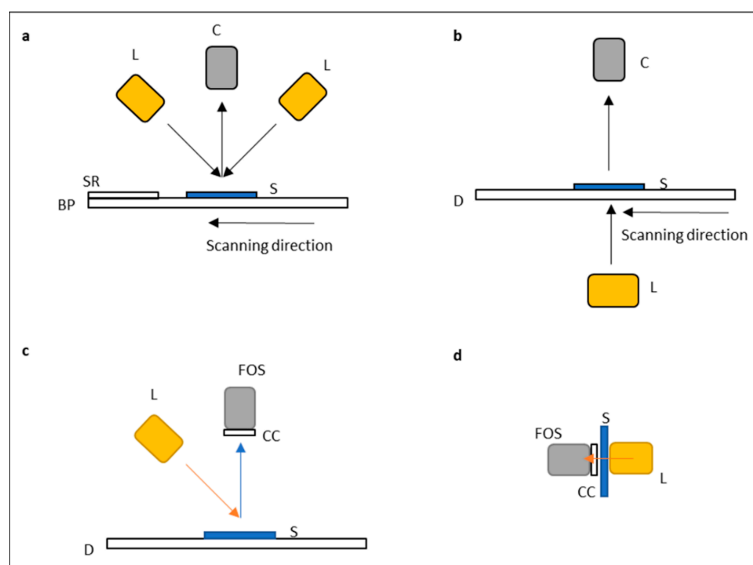


Figure 2. Schematic of the geometry for each instrument and measurement mode: (a) hyperspectral camera (reflectance), with the lights positioned at 45° (L) and the camera objective normal to the sample (S), which lays on the backing paper (BP). The standard reference (SR) is acquired together with the sample. In transmittance mode, (b) the light source is positioned below a diffuser panel (D), on top of which lies the glass sample in direct contact. The transmitted light is collected by the camera (C). (c) OceanOptics USB2000+ in reflectance mode and (d) in transmittance mode; the fiber-optic spectrometer (FOS) is equipped with a cosine corrector (CC) to diffuse the light.

Table 1. Instrument specifics.

	OceanOptics USB2000+	HySpex VNIR-1800
Type of instrument	Spectrometer	Hyperspectral camera
Type of measurement	Point analysis	Line scanning
Spectral range	180–890 nm	400–1000 nm
Spectral sampling	0.38–0.39 nm (2048 channels)	3.26 nm (186 bands)
Geometry	Reflectance:directional, 45:x:0	Reflectance:directional, 45:a:0
Distance from sample	Transmittance: Diffuse efflux Around 0.5 cm	Transmittance: Diffuse influx 30 cm
Spot size	A few μm	Arbitrary selection of an area in the image
Light source	Tungsten-Halogen (Thorlabs)	Tungsten-Halogen

Two Spectralon references, one with 99% diffuse reflectance and one with 50% diffuse reflectance, were used to perform radiometric calibration for the OceanOptic USB2000+ and the hyperspectral camera, respectively.

The HySpex VNIR-1800 is a push-broom system, which means that the image is built line by line as the translation stage moves, while the camera and the light source stay fixed (Figure 2). This aspect is fundamental when performing the radiometric calibration; since the camera acquires one line at a time, it can be assumed that the signal collected and averaged from a few lines is representative of the light distribution across the whole field of view [32]. For this reason, only a small portion of the Spectralon reference was included in the image and used to calculate the reference spectrum. The radiometric-calibration step was carried out through the open-source software Fiji [33], following a procedure similar to that described in [28].

The reflectance was calculated as follows:

$$R_S = \frac{V_S}{V_{\text{Ref}}} * P_{\text{Ref}} \quad (1)$$

where R_S is the sample reflectance, V_S and V_{Ref} are the samples and the Spectralon radiance, respectively, and P_{Ref} is the certified-reflectance spectrum of the Spectralon reference, provided by the manufacturer. The dark current is automatically collected by the instrument in the beginning of the image acquisition.

In the case of HSI, radiometric calibration from radiance to transmittance was performed by simply dividing the radiance spectra of the sample by the radiance spectra of the diffusing panel (considered as reference), following the procedure described in [28]. With regards to the OceanOptic USB2000+, the reference was obtained by taking a measurement without the sample, collecting all the light coming from the light source, which was diffused by the cosine corrector. The radiometric calibration for the transmittance measurements was then calculated by dividing the spectra of each sample by the reference.

Since the calibration methods are different, some variation between the measured reflectance and transmittance spectra is expected, considering also that no calibration treatment was performed to improve the data. In all cases, the spectra were collected at the center of the glass pieces, where the glass was as homogeneous as possible.

2.2.2. Reflectance: Backing-Material Selection

For transmissive or translucent materials, the reflectance signal is strongly affected by light from the obverse. An alternative approach is to measure with only air as background, but in the proposed setup the sample is laid on a surface, and then the reflectance of this surface through the glass inevitably affects the signal. To overcome this issue, a non-spectrally selective backing substrate (perfect white diffuser) can be used to calibrate the reflectance. In the field of cultural heritage, a similar approach has been used in the work of Rebollo et al. [24] to analyze the stained glass windows of the Scrovegni Chapel (Padua, Italy). The influence of backing material on the result of reflectance measurements is

an important aspect that must be considered when working with transparent materials. According to the ISO 13655:2017 standard recommendations [31], the backing material should be free of optical brighteners, in order to avoid unwanted artifacts in the spectra, especially in the UV region. The backing material for reflectance measurements was, thus, carefully selected to be as compliant as possible with the recommendation proposed in the ISO 13655:2017 standard. Two paper sheets were compared for the purpose: the first one is a commercially available inkjet paper, while the second one is a IGT Reference paper C2846 [34].

The two sheets were analyzed with the OceanOptic USB2000+ spectrometer before the beginning of the experiment. Note that in this case the intensity range is between 0–100 because the data were collected directly in reflectance using the spectrometer software. For the rest of the experiment, on the other hand, the reflectance was calculated manually from radiance data. The measurements were repeated placing one of the green-glass pieces (Green 1) over each sheet. Green 1 was selected for this part of the experiment due to its specific peak in the UV region, which is the most influenced by the effects of composition and treatment of the paper. It can be noticed that the reflectance of the inkjet paper sheet (Figure 3, gray dotted line) drops at around 350 nm which may be related to the presence of optical brightener, consequently leading to artifacts in the reflectance spectrum of the green glass.

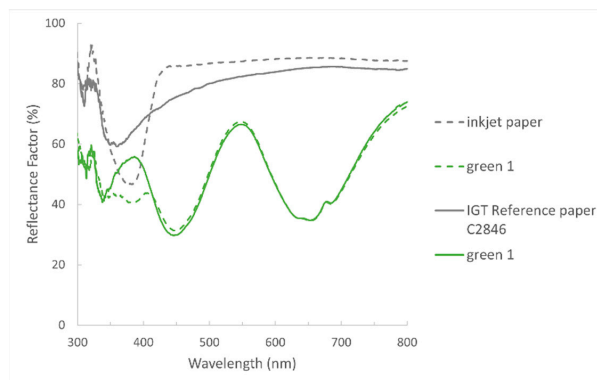


Figure 3. Effects of the backing material are clearly visible in the spectral shape of the sample Green 1, especially in the UV region. The peak at around 380 nm is visibly distorted when the first type of paper is used as background.

2.2.3. Complementary Analysis

XRF analysis was performed by means of a Thermo Scientific Niton XL3t handheld XRF spectrometer, equipped with a silver anode and a GOLDD detector. The acquisition time was set at 120 s and the voltage at 40 kV for each measurement. Note that the instrument is not equipped with a program for glass analysis, and the measurements were performed in Cu/Zn mining mode. Moreover, the measurements could not be calibrated against glass standards as they were unavailable. For this reason, the results obtained must be considered only from a qualitative point of view. The Niton NDT software was used for the spectra interpretation. Three points were collected across the surface of each glass piece, to verify the homogeneity of the glass. The exact positions of the points are shown in Figure S15, available in the Supplemental Material.

2.3. FORS and HSI Performance Evaluation

To evaluate the performance of the two instruments, the CIELAB $L^*a^*b^*$ values and the color difference ΔE were calculated as suggested in ISO/TS 23031 for the inter-model agreement [35]. To calculate the $L^*a^*b^*$ values, the spectral data were first converted to XYZ, using the CIE 1931-2° Standard Observer Color Matching Function and CIE standard

illuminant D65 [36]. $L^*a^*b^*$ values were obtained using the formula in CIE 15:2004 [30], using the D65 reference white values for X, Y, and Z. The formula was implemented in MATLAB through the Color Engineering Toolbox [37].

The color difference ΔE_{00} was calculated using the CIEDE2000 formula [30,38,39] through the same toolbox [37], setting the USB2000+ as reference, both for transmittance and for reflectance. The reproducibility of the measurements was not evaluated.

It is worth mentioning that there is no ground truth for these glass samples; their optical properties and composition have not been measured quantitatively yet, and the interpretation of the spectra could be only made by comparing the results with the existing literature and qualitative pXRF analysis. For these reasons, the color differences have only been reported, and no statistical treatment has been performed on them.

3. Results

The result section is divided into two parts. In the first part, the chromophores responsible for the color of each glass piece are discussed, to show how these elements influence the color of the samples. Results from qualitative XRF analysis are used as supporting information; the chromophore elements identified are summarized in Table 2 for each glass piece, listed in reverse order of their contribution to the color formation. XRF spectra of each sample are provided as Supplementary Material (S1–S14). Some results for the darkest samples were omitted (two of the blue glass) because they were considered too noisy and not significant. The results of the two amber samples were included in the same plot, since they have the same composition.

Table 2. List of elements contributing to the color of the glass samples ordered from the most to the least abundant.

	Chromophores
Green 1	Cr, Cu, Fe
Green 2	Fe, Cr, Mn (decoloring), Cu
Green 3	Mn (decoloring), Fe
Blue 1	Cu, Fe, Co, Mn (decoloring)
Blue 2	Fe, Mn (decoloring?), Cu, Co
Blue 3	Cu, Fe, Mn (decoloring?), Co
Red 1	Red layer: Cu. Uncolored layer: Fe, Mn (decoloring)
Red 2	Red layer: Cu, Sn, Sb. Uncolored layer (?): Fe, Mn (decoloring)
Red 3	Red layer: Cu, Sn, Sb. Uncolored layer (?): Fe, Mn (decoloring)
Orange	Fe
Amber 1 and 2	Mn (decoloring), Fe
Purple 1	Mn (colorant), Fe
Purple 2	Mn (colorant), Fe, Co

In the second part, the glasses L^*a^*b values from each instrument and modality, together with the color difference ΔE_{00} , are reported.

3.1. Chromophore Identification

3.1.1. Green Glass

All the spectra of the green samples show a good agreement and are very easy to identify. The reason behind this good agreement may be that, compared to the other samples, the green glasses are relatively thin and present a very flat surface with almost no defects. The presence of bubbles inside the glass does not seem to create interference as it was possible to find areas without them for measurements.

Sample Green 1 and Green 2 (Figure 4a,b) show a similar spectrum, with an absorption band centered at 450 nm and two bands at around 658 and 686 nm, which are characteristic of chromium (Cr^{3+}) [17,20,22,24,40]. A third band is barely visible at around 638 nm, especially in the reflectance modality.

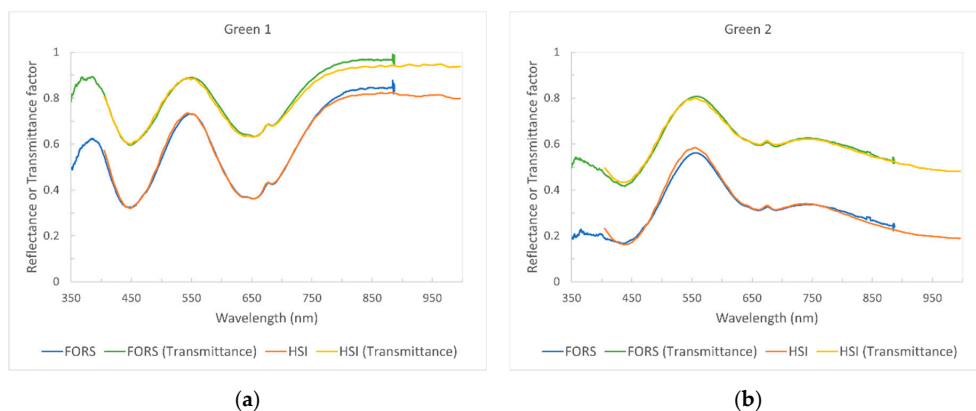


Figure 4. (a) Spectra comparison for sample Green 1; (b) spectra comparison for sample Green 2.

Sample Green 2 appears to contain a higher amount of iron, suggested by the more pronounced absorption band at the end of the NIR region [22], which is confirmed by XRF analysis. The band in the NIR region usually has a maximum at around 1100 nm (out of the range of the instruments) and is associated with iron as Fe^{2+} , which gives a yellow color to glass [12,16,18,22,41,42]; this explains the more yellowish appearance of the sample Green 2, and, consequently, the highest values of b^* among the three green samples.

The spectra of the Green 3 (Figure 5) sample on the other end are very different from the others. In this case, the color is given only by iron.

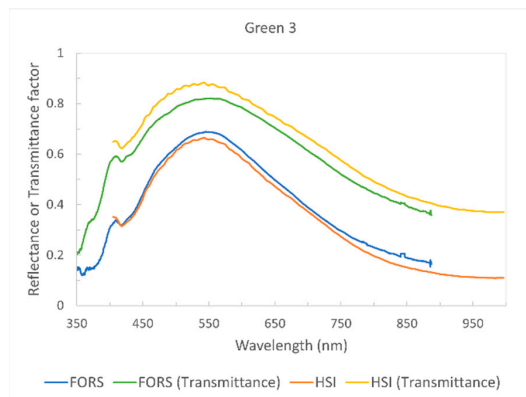


Figure 5. Spectra comparison for sample Green 3.

Here, iron is present both as Fe^{2+} and Fe^{3+} , as suggested by the three small absorption bands at 380, 420, and 435–440 nm, associated with Fe^{3+} , and the broad band of Fe^{2+} in the NIR region [12,16,18,22,41,42]. Fe^{3+} gives a blue color to glass. Thus, the pale-green color of the glass is due to the redox equilibrium between Fe^{3+} and Fe^{2+} species. Manganese, in its oxidation state Mn^{2+} , also has an absorption band at 420 nm, which in some papers is referred to as the Fe/Mn complex band [11,12,16,18,22,41,42]. Since Mn^{2+} is uncolored, it could have been used as a decoloring agent.

3.1.2. Blue Glass

The three blue-glass pieces are characterized by a very dark color, and, consequently, the magnitudes of the spectra obtained are very low, especially in the case of samples Blue 2 and 3. These two glass pieces are among the thickest samples in the group and also have

a very rough surface. In reflectance mode, it is difficult to distinguish the signature peaks of the coloring agents used; in this case, transmittance measurements are more helpful as the characteristic bands become more visible. Note that the FORS' reflectance results for sample Blue 2 and HSI's reflectance results for samples Blue 2 and 3 were discarded, as they did not provide satisfying results. For this reason, the color difference was calculated only for the Blue 1 sample, as it was the only one that gave sufficiently good spectra for all the instruments.

The shape of the spectra suggests that the three samples were colored using a distinct combination of chromophores. This is confirmed by the XRF analysis, which identified cobalt, copper, and iron in different concentrations. The three signature bands of cobalt (Co^{2+}) at around 530–540, 590–600, and 650–670 nm can be observed in Blue 1, while in Blue 2 and 3, the last two bands are barely visible [3,12,16,20,24,40,43] (Figure 6).

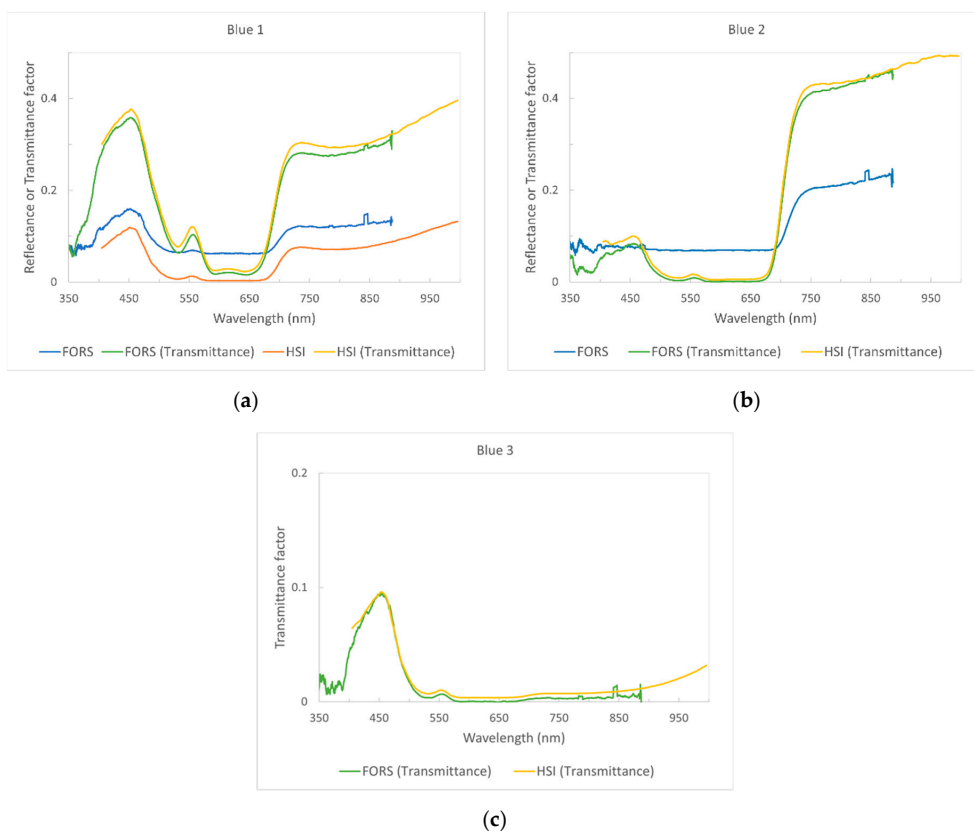


Figure 6. (a) Spectra comparison for sample Blue 1; (b) spectra comparison for sample Blue 2; (c) spectra comparison for sample Blue 3.

The absorption band centered at around 780–790 nm in samples Blue 1 and 3 suggests that copper could have been used as an additional coloring agent as Cu^{2+} [3,15,16,20] and probably in higher concentrations in sample Blue 1, as confirmed by XRF analysis.

3.1.3. Red Glass

The production of red glass is very different from the other type of colored glass. Obtaining a red glass in the past was challenging, as even a small amount of colorant in the glass body was enough to produce a deeply colored glass, too dark to be employed in a

window [2]. To overcome this problem, the red color was achieved by adding a thin red layer made of copper nanoparticles over a transparent one. This could have been made in two ways, by alternating multiple thin red layers and transparent ones (feuillettes) or by applying a single red layer over a thicker colorless glass (plaques) [44–46]. The glass pieces studied in this paper belong to the second category. The red layers of these samples are characterized by different hues and thickness, going from a thin, pale red layer (Red 1) to a thicker and darker one (Red 3).

Sample Red 1 (Figure 7a) is the only one among the three red glass that clearly shows the characteristic absorbance bands related to the surface plasmonic resonance (SPR) of the copper nanoparticles (at around 565 nm) [3–6,10,19,20,24,45] and the one at 430 nm, which could be related to isolated Cu^0 atoms [3,5,24]. This is especially visible in transmittance mode. In Red 2 (Figure 7b), only the band at 565 nm is visible, while the one at 430 nm is completely absent. The reason behind this is not clear yet; the available literature suggests that it could be related to variation in the roughness of the red layer [4], the size of the copper particles, the annealing temperature during the formation of the colored layer, or its chemical composition [14,47].

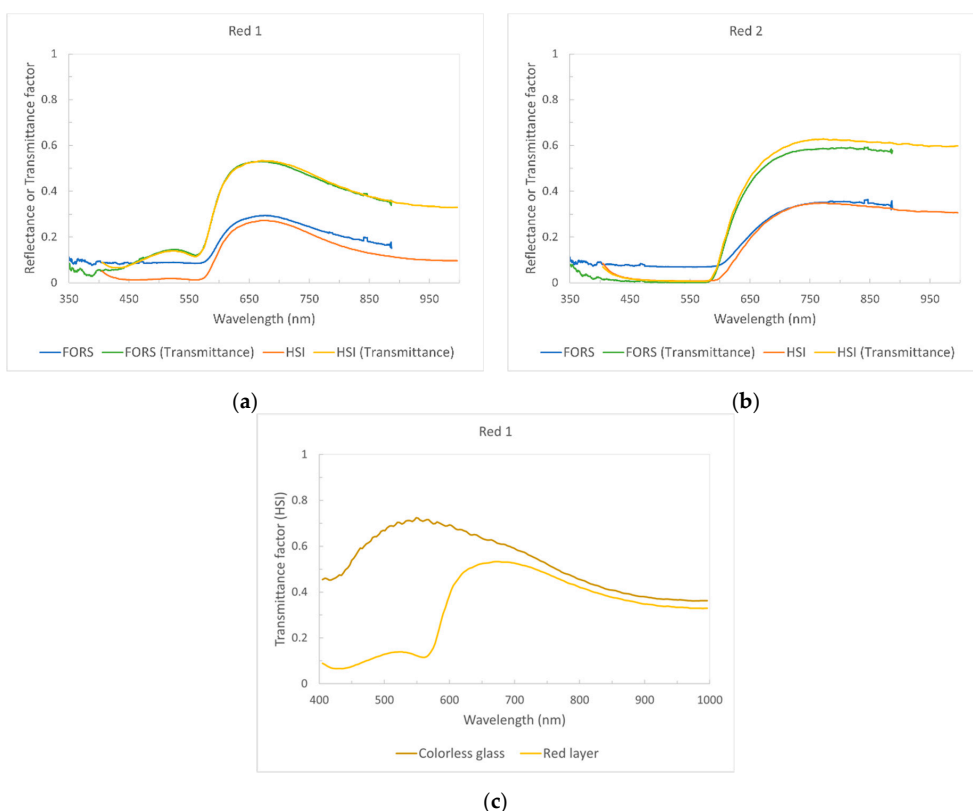


Figure 7. (a) Spectra comparison for sample Red 1; (b) spectra comparison for sample Red 2; (c) spectra comparison between the two layers of Red 1.

In addition to copper, the presence of Fe^{2+} in both samples can be inferred by the presence of its absorption band at 1000 nm, which is more intense in sample Red 1 [10,19,20], even if XRF analysis detected a higher amount of iron in sample Red 2. Most probably, Fe^{2+} does not contribute to the red color of the thin layer but could be present in the colorless layer (which appears slightly yellowish) as an intentional addition or impurity. In the case

of Red 1, this conjecture seems to be confirmed by comparing spectra taken from the red layer and the transparent layer (Figure 7c). Unfortunately, a similar comparison could not be made with sample Red 2, as there are no areas where the transparent layer is accessible.

The Red 3 sample (Figure 8) is quite different from the other two glass pieces: it shows a more significant difference between the reflectance and the transmittance spectra, not only in intensity but also in shape.

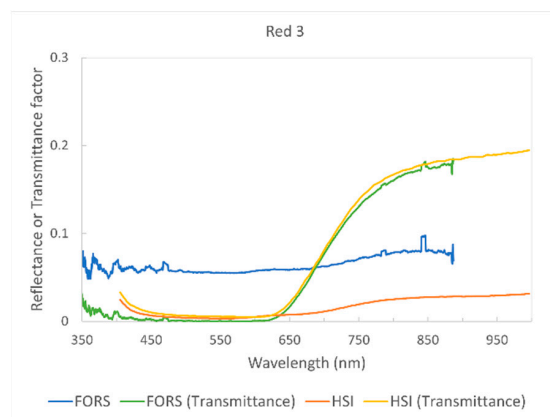


Figure 8. Spectra comparison for sample Red 3.

In reflectance modality, for example, an additional band appears at around 680–700 nm, while in transmittance, the absorption band of the copper nanoparticles is shifted toward longer wavelengths, at about 630 nm.

Red 3 has very low and sometimes negative values of CIELAB b^* , hinting at a more bluish hue compared to the other two red-glass pieces. Bring and Jonson [14] suggest that the presence of antimony (as Sb^{3+}) and tin (as Sn^{2+}) can play an important role in the coloring process of the red layer. A significant amount of antimony and tin has been found in Red 2 and 3 by XRF, with Red 3 having a lower quantity of antimony than Red 2; according to Bring and Jonson a smaller concentration of Sb^{3+} can give a deep red color with a bluish tint to the glass [14]. This observation seems to be consistent with the combined results from the FORS, HSI, and XRF for Red 3. Nonetheless, additional quantitative or semi-quantitative analyses are necessary to confirm this hypothesis.

It is also interesting to notice how the L^* value from the fiber spectrometer in transmittance is extremely low (see Colorimetry subsection). This is probably caused by the great thickness and dark color of the red layer, which may have prevented the light from being transmitted through the sample, generating a very low signal. On the other hand, the L^* values obtained in reflectance are relatively high, indicating that the first surface reflectance of sample Red 3 has a higher contribution. However, the data obtained with the HSI show an opposite trend, with the two values of L^* (reflectance and transmittance) being almost comparable. This likely arises from the different optical designs of the instruments.

3.1.4. Orange and Amber Glass

The spectra of both orange and amber samples show differences in intensity and shape when comparing the results obtained in the two modalities (Figure 9).

For the three glass pieces, more than in other samples, the absorption bands of the spectra collected in transmittance shift to shorter wavelengths with respect to those acquired in reflectance, hinting at a more yellowish color. This phenomenon is also confirmed by visual inspection and from the CIELAB $L^* a^* b^*$ values (see Colorimetry subsection); in both cases, the a^* values calculated in transmittance are lower than that in reflectance, while the b^* values remain quite similar.

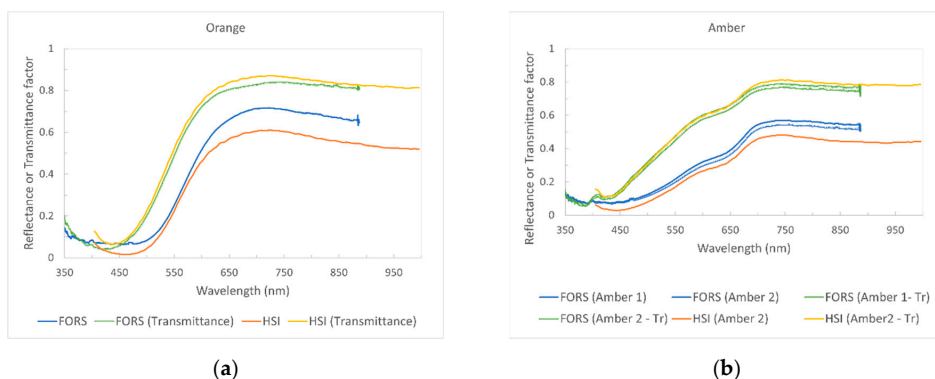


Figure 9. (a) Spectra comparison for sample Orange; (b) spectra comparison for sample Amber.

Since the two amber pieces come from the same batch and, thus, have the same composition, their results were grouped in the same plot. The results obtained with the FORS show a difference in magnitude between the two samples, both in transmittance and in reflectance. Interestingly, in transmittance mode, the spectra taken from Amber 1 with the fiber optic agrees more with the spectra taken from Amber 2 with the HSI, as opposed to the Amber 2 spectra taken with the fiber at almost the same location. This could mean that, in this case, the characteristic of the surface greatly influences the result, and particular care must be taken when selecting the areas from which to collect the spectra.

From the chemical point of view, according to the available literature, the orange/amber color in the glass is given by the ferric iron-sulfide ($\text{Fe}^{3+}\text{-S}$) complex. This chromophore can be recognized by a broad absorption band at around 410 nm [4,10,12,13,16,20,42,48]. The shallow, broad band at around 1000 nm suggests that iron could be present also as Fe^{2+} . Iron was detected by XRF analysis in both samples, confirming the involvement of this element in the glass coloration; sulfur was found as well, but the amount is too small, especially compared to other glass, to make any solid conclusion on the presence of the iron-sulfide ($\text{Fe}^{3+}\text{-S}$) complex. Further analyses are necessary to have a clear understanding of the coloring process of this glass, as well as the reason behind the color shifting between transmittance and reflectance.

Compared to the orange sample, the amber fragments also seem to contain a consistent amount of manganese, probably as uncolored Mn^{2+} [13]; the presence of this oxide could be suggested by a small band at 420 nm, which is visible only in the spectra obtained by the FORS in transmittance mode [16]. Despite some shifting in the position of the absorbance band, the shape of the spectra obtained for the orange pieces in this experiment is consistent with the results found in previous works. Regarding the amber glass, however, the extra band at around 630–650 nm is difficult to interpret; no other example exists in the available literature, except for the work of Bacon and Billian [48], which unfortunately does not explain the nature of this band.

3.1.5. Purple Glass

The two glass pieces clearly show a difference in composition, which also explains the difference in color (Figure 10).

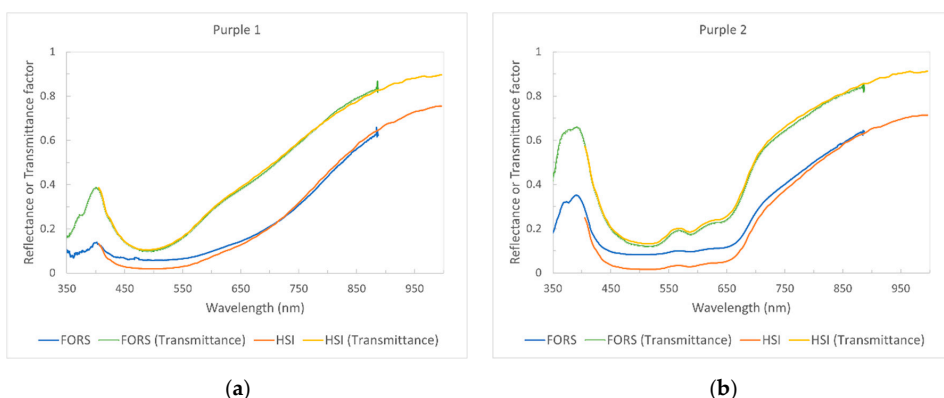


Figure 10. (a) Spectra comparison for sample Purple 1; (b) spectra comparison for Purple 2.

The first sample (Purple 1) has a warm-purple, almost brownish color, while the second one (Purple 2) appears more bluish. This observation is confirmed by the calculated values of b^* , which are positive for the first sample and negative for the other (see Colorimetry subsection). From a chemical point of view, the different color is due to the fact that for sample Purple 1 the main chromophore is manganese (Mn^{3+}), characterized by a broad band at around 500–490 nm and a shoulder at about 670 nm, with a small contribution of iron (as Fe^{3+}) [4,9,11,16,20,22,24,42,49], while in Purple 2 the three absorption bands at around 525, 590, and 650 nm suggest that cobalt (Co^{2+}) has been added to give a more bluish hue [4,50].

3.2. Colorimetry

3.2.1. CIELAB $L^*a^*b^*$ Values

Tables 3–14 report the CIELAB $L^*a^*b^*$ values of each colored glass, calculated from the spectra obtained with FORS and HSI in transmittance and reflectance mode.

Table 3. $L^*a^*b^*$ values for sample Green 1.

Green 1	L^*	a^*	b^*
USB2000+ (Tr)	92.26	−13.63	13.83
HySpex VNIR-1800 (Tr)	92.04	−14.50	13.83
USB2000+	82.33	−24.98	25.03
HySpex VNIR-1800	82.54	−26.21	25.24

Table 4. $L^*a^*b^*$ values for sample Green 2.

Green 2	L^*	a^*	b^*
USB2000+ (Tr)	88.76	−13.36	24.44
HySpex VNIR-1800 (Tr)	88.54	−13.51	23.22
USB2000+	74.36	−19.89	35.95
HySpex VNIR-1800	75.49	−22.13	38.62

Table 5. $L^*a^*b^*$ values for sample Green 3.

Green 3	L^*	a^*	b^*
USB2000+ (Tr)	91.51	−7.53	9.70
HySpex VNIR-1800 (Tr)	93.87	−8.44	8.91
USB2000+	84.19	−14.25	17.64
HySpex VNIR-1800	82.83	−14.87	17.28

Table 6. L*a*b* values for sample Blue 1.

Blue 1	L*	a*	b*
USB2000+ (Tr)	33.43	15.35	−50.88
HySpex VNIR-1800 (Tr)	35.87	12.68	−48.66
USB2000+	31.62	9.64	−45.49
HySpex VNIR-1800	10.47	29.18	−21.52

Table 7. L*a*b* values for sample Red 1.

Red 1	L*	a*	b*
USB2000+ (Tr)	52.65	29.77	30.28
HySpex VNIR-1800 (Tr)	52.13	30.76	29.59
USB2000+	40.70	22.13	9.30
HySpex VNIR-1800	28.04	41.83	26.11

Table 8. L*a*b* values for sample Red 2.

Red 2	L*	a*	b*
USB2000+ (Tr)	25.62	58.38	33.33
HySpex VNIR-1800 (Tr)	27.96	56.97	22.65
USB2000+	33.87	13.25	1.137
HySpex VNIR-1800	16.25	37.07	0.90

Table 9. L*a*b* values for sample Red 3.

Red 3	L*	a*	b*
USB2000+ (Tr)	0.99	6.15	−1.30
HySpex VNIR-1800 (Tr)	5.71	7.90	−6.54
USB2000+	28.44	1.37	−1.45
HySpex VNIR-1800	3.74	5.12	−4.45

Table 10. L*a*b* values for the Amber samples.

Amber	L*	a*	b*
USB2000+ (Tr)			
Amber 1	75.00	3.92	43.77
Amber 2	73.47	4.41	44.70
HySpex VNIR-1800 (Tr)	74.75	3.88	44.92
USB2000+			
Amber 1	55.41	11.91	33.89
Amber 2	53.51	12.19	32.27
HySpex VNIR-1800	49.98	12.18	44.92

Table 11. L*a*b* values for sample Orange.

Orange	L*	a*	b*
USB2000+ (Tr)	76.31	13.31	72.35
HySpex VNIR-1800 (Tr)	78.05	12.26	69.34
USB2000+	62.20	28.91	52.36
HySpex VNIR-1800	58.65	27.20	70.37

Table 12. L*a*b* values for sample Purple 1.

Purple 1	L*	a*	b*
USB2000+ (Tr)	50.68	24.66	9.01
HySpex VNIR-1800 (Tr)	51.42	23.94	9.59
USB2000+	33.13	13.40	2.84
HySpex VNIR-1800	24.78	23.29	6.88

Table 13. L*a*b* values for sample Purple 2.

Purple 2	L*	a*	b*
USB2000+ (Tr)	47.80	18.35	−9.21
HySpex VNIR-1800 (Tr)	49.37	17.02	−7.65
USB2000+	33.74	8.83	−6.24
HySpex VNIR-1800	19.25	17.89	−9.64

Table 14. Summary table of color differences ΔE_{00} .

ΔE_{00}	USB2000+ (Tr) vs. HySpex1800 (Tr)	USB2000+ vs. HySpex1800	USB2000+ (Tr) vs. USB2000+	HySpex1800 (Tr) vs. HySpex1800
Green 1	0.73	0.59	9.70	9.62
Green 2	0.69	1.48	11.10	11.14
Green 3	1.85	1.05	7.89	9.43
Red 1	0.97	14.58	16.47	22.25
Red 2	<u>5.43</u>	17.52	21.75	14.51
Red 3	<u>4.71</u>	17.19	18.90	3.31
Blue 1	<u>3.01</u>	19.99	9.04	22.55
Orange	1.47	7.53	17.71	17.61
Amber				21.90
Amber 1	0.43	6.85	17.92	
Amber 2	1.03	6.22	18.82	
Purple 1	0.96	9.12	17.56	22.89
Purple 2	1.96	12.80	14.42	24.59
Average	<u>1.94</u>	<u>9.58</u>	<u>15.09</u>	<u>16.34</u>

3.2.2. Color Difference ΔE_{00}

The color difference values calculated between the FORS and HSI transmittance and reflectance measurements and between transmittance and reflectance measurements from the same instrument are reported in Table 14. Values above 10 are shown in bold. For the comparison of transmittance between the FORS and HSI, values that are clearly higher than those of most colored pieces are underlined.

4. Discussion

From the point of view of the spectra, the results obtained with HSI are consistent with those produced by the FORS, especially in transmittance mode. Regarding reflectance, a difference in intensity between the FORS and HSI spectra can be noticed in many samples; in general, the spectra obtained by the FORS have a higher intensity than the hyperspectral ones, especially in the case of the darkest samples (Red 2, Red 3, Blue 1). The trend described above is also demonstrated by the ΔE_{00} values calculated between the FORS and HSI in reflectance mode, which are almost always very high. During the experiments, it was observed that the fiber optic seems quite sensitive to the distance from the sample, as also noted in [45], and this fact may have influenced the results. The different geometries and radiance correction procedures of the two instruments could also be other factors that affected the measurements. The fiber optic may be more sensitive to the stray light reflected from the surface of the darkest samples, generating errors during the preprocessing phase.

On the other hand, the FORS and the HSI can generate comparable results when used in transmittance mode. The ΔE_{00} values calculated between the FORS and HSI are relatively low in almost every case, with the darkest samples showing the relatively highest color difference, as shown in Table 14.

The shape of the spectra remains almost always unchanged, regardless of the instrument or modality, except for amber and darker red and blue samples (Red 2, Red 3, Blue 1, Blue 2). Comparing the transmittance and reflectance spectra of amber glass, for example, the absorption bands show a considerable variation in width, which may be related to how the light is reflected, transmitted, and scattered by the glass sample and how the sensor of the instrument collects this light. Regarding the darker glass, the reflectance modality does not perform very well, as most of the light gets absorbed while traveling twice through the glass, so a poor performance can be expected. From a colorimetric point of view, this behavior is shown by higher differences in L^* values between reflectance and transmittance modality for dark-colored glass. In contrast, this difference is less pronounced in the lighter glass. From the spectral point of view, the characteristic peaks of strongly colored glass are entirely lost in reflectance mode, especially in the case of the blue- and red-glass pieces, while visible in transmittance mode. On the other hand, the reflectance modality is very helpful in enhancing the intensity of small peaks in light-colored glass, as previously noted in the work of Rebollo et al. [26]. This can be noticed, for example, in all the green glass, where the weak peaks of iron (Fe^{3+}) and chromium (Cr^{3+}) can be better appreciated in reflectance modality.

5. Conclusions

In this paper, we compared the performance of a fiber-optic spectrometer and a hyperspectral camera in measuring colored glass. The results demonstrated that the two instruments could produce comparable results, especially in transmittance modality. On the other hand, reflectance measurements generated mixed results; in general, there is an apparent disagreement between the reflectance results obtained by the two instruments, especially for very dark glass.

Regardless of the measuring geometries, an advantage of using both instruments lies in the spectral range. In fact, the two devices complement each other, as the FORS and the hyperspectral camera have an extended range in the UV and the IR region, respectively, which allows a more complete characterization of the chromophores used in the colored glass.

Considering future works, a better understanding of the complex interaction between the glass and light would be necessary to explain the differences in the spectral shape, when measuring in different geometries. In this sense, it would be interesting to perform spectral acquisitions from other angles, to understand how much the spectral shape and intensity, and consequently the color, can change within the same sample. In addition, further analysis should be performed to better characterize the chromophores involved in the coloration of the glass pieces.

Future works should also be focused on adjusting the calibration procedure to improve the agreement between the instruments, both in transmittance mode and in reflectance mode.

Supplementary Materials: The following supporting information can be downloaded at: <https://www.mdpi.com/article/10.3390/heritage5030073/s1>, Figures S1–S14: pXRF data of each glass; Figure S15: location of points analyzed with XRF.

Author Contributions: Conceptualization, A.B., P.G., S.G. and J.Y.H.; methodology, A.B. and P.G.; validation, A.B. and P.G.; formal analysis, A.B.; investigation, A.B.; data curation, A.B.; writing—original draft preparation, A.B.; writing—review and editing, A.B., P.G., S.G. and J.Y.H.; visualization, A.B.; supervision, P.G., S.G. and J.Y.H.; project administration, S.G.; funding acquisition, J.Y.H. All authors have read and agreed to the published version of the manuscript.

Funding: This project has received funding from the European Union’s Horizon 2020 research and innovation programme under the Marie Skłodowska–Curie grant no. 813789 (CHANGE-ITN).

Institutional Review Board Statement: Not applicable.

Informed Consent Statement: Not applicable.

Data Availability Statement: Data are available upon request. Please contact the corresponding author.

Acknowledgments: The authors would like to thank Elizabeth Sinnerud at the Nidaros Cathedral Restoration Workshop (Trondheim) for providing the glass pieces used for the experiments; Jan Cutajar at the University of Oslo (UiO) for carrying out the XRF measurements; and Ottar A.B. Anderson at SEDAK for the high-quality pictures of the samples.

Conflicts of Interest: The authors declare no conflict of interest.

References

1. Babini, A.; George, S.; Lombardo, T.; Hardeberg, J.Y. Potential and Challenges of Spectral Imaging for Documentation and Analysis of Stained-Glass Windows. *Lond. Imaging Meet.* **2020**, *2020*, 109–113. [[CrossRef](#)]
2. Fornacelli, C.; Colombari, P.; Memmi, I.T. Toward a Raman/FORS discrimination between Art Nouveau and contemporary stained glasses from CdSxSe1-x nanoparticles signatures. *J. Raman Spectrosc.* **2015**, *46*, 1129–1139. [[CrossRef](#)]
3. Bacci, M.; Corallini, A.; Orlando, A.; Piccolo, M.; Radicati, B. The ancient stained windows by Nicolo di Pietro Gerini in Florence. A novel diagnostic tool for non-invasive in situ diagnosis. *J. Cult. Herit.* **2007**, *8*, 235–241. [[CrossRef](#)]
4. Bracci, S.; Bartolozzi, G.; Burnam, R.K.; Corallini, A. Integration of both non-invasive and micro-invasive techniques for the archaeometric study of the stained-glass window Apparizione degli Angeli in the basilica of Santa Croce in Florence, Italy. *J. Cult. Herit.* **2020**, *44*, 307–316. [[CrossRef](#)]
5. Meulebroeck, W.; Wouters, H.; Nys, K.; Thienpont, H. Authenticity screening of stained glass windows using optical spectroscopy. *Sci. Rep.* **2016**, *6*, 37726. [[CrossRef](#)] [[PubMed](#)]
6. Palomar, T.; Agua, F.; Garcia-Heras, M.; Villegas, M.A. Chemical degradation and chromophores of 18(th) century window glasses. *Glass Technol.-Eur. J. Glass Sci. Technol. Part A* **2011**, *52*, 145–153.
7. Meulebroeck, W.; Baert, K.; Ceglia, A.; Cosyns, P.; Wouters, H.; Nys, K.; Terryn, H.; Thienpont, H. The potential of UV-VIS-NIR absorption spectroscopy in glass studies. In Proceedings of the Integrated Approaches to the Study of Historical Glass—IAS12, Brussels, Belgium, 16–17 April 2012; Volume 8422.
8. Kaplan, Z.; İpekoğlu, B.; Böke, H. Physicochemical properties of glass tesserae in Roman terrace house from ancient Antandros (base glass, opacifiers and colorants). *Mediterr. Archaeol. Archaeom.* **2017**, *17*, 141–157.
9. Rodrigues, A.; Coutinho, M.; Machado, A.; Martinho, B.A.; Cerqueira Alves, L.; Macedo, M.F.; Vilarigues, M. A transparent dialogue between iconography and chemical characterisation: A set of foreign stained glasses in Portugal. *Herit. Sci.* **2021**, *9*, 22. [[CrossRef](#)]
10. Hunault, M.O.J.Y.; Bauchau, F.; Boulanger, K.; Hérold, M.; Calas, G.; Lemasson, Q.; Pichon, L.; Pacheco, C.; Loisel, C. Thirteenth-century stained glass windows of the Sainte-Chapelle in Paris: An insight into medieval glazing work practices. *J. Archaeol. Sci. Rep.* **2021**, *35*, 102753. [[CrossRef](#)]
11. Bidegaray, A.-I.; Godet, S.; Bogaerts, M.; Cosyns, P.; Nys, K.; Terryn, H.; Ceglia, A. To be purple or not to be purple? How different production parameters influence colour and redox in manganese containing glass. *J. Archaeol. Sci. Rep.* **2019**, *27*, 101975. [[CrossRef](#)]
12. Micheletti, F.; Orsilli, J.; Melada, J.; Gargano, M.; Ludwig, N.; Bonizzoni, L. The role of IRT in the archaeometric study of ancient glass through XRF and FORS. *Microchem. J.* **2020**, *153*, 104388. [[CrossRef](#)]
13. Schreurs, J.W.H.; Brill, R.H. Iron and Sulfur Related Colors in Ancient Glasses. *Archaeometry* **1984**, *26*, 199–209. [[CrossRef](#)]
14. Bring, T.; Jonson, B.; Kloof, L.; Rosdahl, J. Colour development in copper ruby alkali silicate glasses: Part 2. The effect of tin (II) oxide and antimony (III) oxide. *Glass Technol.-Eur. J. Glass Sci. Technol. Part A* **2007**, *48*, 142–148.
15. Hunault, M.; Bauchau, F.; Loisel, C.; Hérold, M.; Galois, L.; Newville, M.; Calas, G. Spectroscopic Investigation of the Coloration and Fabrication Conditions of Medieval Blue Glasses. *J. Am. Ceram. Soc.* **2016**, *99*, 89–97. [[CrossRef](#)]
16. Möncke, D.; Papageorgiou, M.; Winterstein-Beckmann, A.; Zacharias, N. Roman glasses coloured by dissolved transition metal ions: Redox-reactions, optical spectroscopy and ligand field theory. *J. Archaeol. Sci.* **2014**, *46*, 23–36. [[CrossRef](#)]
17. Hunault, M.; Lelong, G.; Gauthier, M.; Gelebart, F.; Ismael, S.; Galois, L.; Bauchau, F.; Loisel, C.; Calas, G. Assessment of Transition Element Speciation in Glasses Using a Portable Transmission Ultraviolet-Visible-Near-Infrared (UV-Vis-NIR) Spectrometer. *Appl. Spectrosc.* **2016**, *70*, 778–784. [[CrossRef](#)]
18. Meulebroeck, W.; Wouters, H.; Baert, K.; Ceglia, A.; Terryn, H.; Nys, K.; Thienpont, H. *Optical Spectroscopy Applied to the Analysis of Medieval and Post-Medieval Plain Flat Glass Fragments Excavated in Belgium*; SPIE: Bellingham, WA, USA, 2010; Volume 7726.
19. Hunault, M.O.J.Y.; Loisel, C.; Bauchau, F.; Lemasson, Q.; Pacheco, C.; Pichon, L.; Moignard, B.; Boulanger, K.; Hérold, M.; Calas, G.; et al. Nondestructive Redox Quantification Reveals Glassmaking of Rare French Gothic Stained Glasses. *Anal. Chem.* **2017**, *89*, 6278–6649. [[CrossRef](#)]

20. Capobianco, N.; Hunault, M.O.J.Y.; Balcon-Berry, S.; Galois, L.; Sandron, D.; Calas, G. The Grande Rose of the Reims Cathedral: An eight-century perspective on the colour management of medieval stained glass. *Sci. Rep.* **2019**, *9*, 3287. [[CrossRef](#)]
21. Molina, G.; Murcia, S.; Molera, J.; Roldan, C.; Crespo, D.; Pradell, T. Color and dichroism of silver-stained glasses. *J. Nanopart. Res.* **2013**, *15*, 1932. [[CrossRef](#)]
22. Meulebroeck, W.; Baert, K.; Wouters, H.; Cosyns, P.; Ceglia, A.; Cagno, S.; Janssens, K.; Nys, K.; Terry, H.; Thienpont, H. *The Identification of Chromophores in Ancient Glass by the Use of UV-VIS-NIR Spectroscopy*; SPIE: Bellingham, WA, USA, 2010; Volume 7726.
23. Meulebroeck, W.; Cosyns, P.; Baert, K.; Wouters, H.; Cagno, S.; Janssens, K.; Terry, H.; Nys, K.; Thienpont, H. Optical spectroscopy as a rapid and low-cost tool for the first-line analysis of glass artefacts: A step-by-step plan for Roman green glass. *J. Archaeol. Sci.* **2011**, *38*, 2387–2398. [[CrossRef](#)]
24. Rebollo, E.; Ratti, F.; Cortelazzo, G.M.; Poletto, L.; Bertinello, R. New trends in imaging spectroscopy: The non-invasive study of the Scrovegni Chapel stained glass windows. In Proceedings of the O3A: Optics for Arts, Architecture, and Archaeology III, Munich, Germany, 25–26 May 2011; Volume 8084.
25. Palomar, T.; Grazia, C.; Cardoso, I.P.; Vilarigues, M.; Miliani, C.; Romani, A. Analysis of chromophores in stained-glass windows using Visible Hyperspectral Imaging in-situ. *Spectrochim. Acta Part A-Mol. Biomol. Spectrosc.* **2019**, *223*, 117378. [[CrossRef](#)] [[PubMed](#)]
26. Perri, A.; de Faria, B.E.N.; Ferreira, D.C.T.; Comelli, D.; Valentini, G.; Preda, F.; Polli, D.; de Paula, A.M.; Cerullo, G.; Manzoni, C. Hyperspectral imaging with a TWINS birefringent interferometer. *Opt. Express* **2019**, *27*, 15956–15967. [[CrossRef](#)] [[PubMed](#)]
27. Funatomi, T.; Ogawa, T.; Tanaka, K.; Kubo, H.; Caron, G.; Mouaddib, E.M.; Matsushita, Y.; Mukaigawa, Y. Eliminating Temporal Illumination Variations in Whisk-broom Hyperspectral Imaging. *Int. J. Comput. Vis.* **2022**, *130*, 1310–1324. [[CrossRef](#)]
28. Babini, A.; George, S.; Hardeberg, J.Y. *Hyperspectral Imaging Workflow for the Acquisition and Analysis of Stained-Glass Panels*; SPIE: Bellingham, WA, USA, 2021; Volume 11784.
29. *ISO 5-2; Photography and Graphic Technology—Density Measurements: Part 2: Geometric Conditions for Transmittance Density*. ISO: Geneva, Switzerland, 2009.
30. *CIE 15; Technical Report: Colorimetry 3rd Edition*. International Commission on Illumination: Vienna, Austria, 2004.
31. *ISO 13655; Graphic Technology—Spectral Measurement and Colorimetric Computation for Graphic Arts Images*. ISO: Geneva, Switzerland, 2017.
32. Pillay, R.; Hardeberg, J.Y.; George, S. Hyperspectral imaging of art: Acquisition and calibration workflows. *J. Am. Inst. Conserv.* **2019**, *58*, 3–15. [[CrossRef](#)]
33. Schindelin, J.; Arganda-Carreras, I.; Frise, E.; Kaynig, V.; Longair, M.; Pietzsch, T.; Preibisch, S.; Rueden, C.; Saalfeld, S.; Schmid, B.; et al. Fiji: An open-source platform for biological-image analysis. *Nat. Methods* **2012**, *9*, 676–682. [[CrossRef](#)]
34. IGT Testing Systems. IGT Reference Paper C2846. Available online: <https://www.igt.nl/product/igt-reference-paper/> (accessed on 6 June 2022).
35. *ISO/TS 23031; Graphic Technology—Assessment and Validation of the Performance of Spectrocolorimeters and Spectrodensitometers*. ISO: Geneva, Switzerland, 2020.
36. Ohta, N.; Robertson, A.R. CIE Standard Colorimetric System. In *Colorimetry: Fundamentals and Applications*; John Wiley: Chichester, UK; Hoboken, NJ, USA, 2005.
37. Green, P.; MacDonald, L.W. *Colour Engineering: Achieving Device Independent Colour*; John Wiley and Sons: Chichester, UK, 2002.
38. Luo, M.R.; Cui, G.; Rigg, B. The development of the CIE 2000 colour-difference formula: CIEDE2000. *Color Res. Appl.* **2001**, *26*, 340–350. [[CrossRef](#)]
39. *ISO/CIE 11664-6; Colorimetry—Part 6: CIEDE2000 Colour-Difference Formula*. ISO: Geneva, Switzerland, 2014.
40. Ceglia, A.; Meulebroeck, W.; Wouters, H.; Baert, K.; Nys, K.; Terry, H.; Thienpont, H. Using optical spectroscopy to characterize the material of a 16th c. stained glass window. In Proceedings of the Integrated Approaches to the Study of Historical Glass—Ias12, Brussels, Belgium, 16–17 April 2012; Volume 8422.
41. Ceglia, A.; Meulebroeck, W.; Cosyns, P.; Nys, K.; Terry, H.; Thienpont, H. Colour and Chemistry of the Glass Finds in the Roman Villa of Treignes, Belgium. *Procedia Chem.* **2013**, *8*, 55–64. [[CrossRef](#)]
42. Green, L.R.; Alan Hart, F. Colour and chemical composition in ancient glass: An examination of some roman and wealden glass by means of ultraviolet-visible-infra-red spectrometry and electron microprobe analysis. *J. Archaeol. Sci.* **1987**, *14*, 271–282. [[CrossRef](#)]
43. Ceglia, A.; Meulebroeck, W.; Baert, K.; Wouters, H.; Nys, K.; Thienpont, H.; Terry, H. Cobalt absorption bands for the differentiation of historical Na and Ca/K rich glass. *Surf. Interface Anal.* **2012**, *44*, 219–226. [[CrossRef](#)]
44. Farges, F.; Etcheverry, M.P.; Scheidegger, A.; Grolimund, D. Speciation and weathering of copper in “copper red ruby” medieval flashed glasses from the Tours cathedral (XIII century). *Appl. Geochem.* **2006**, *21*, 1715–1731. [[CrossRef](#)]
45. Colomban, P.; Tournie, A.; Ricciardi, P. Raman spectroscopy of copper nanoparticle-containing glass matrices: Ancient red stained-glass windows. *J. Raman Spectrosc.* **2009**, *40*, 1949–1955. [[CrossRef](#)]
46. Kunicki-Goldfinger, J.J.; Freestone, I.C.; McDonald, I.; Hobot, J.A.; Gilderdale-Scott, H.; Ayers, T. Technology, production and chronology of red window glass in the medieval period—Rediscovery of a lost technology. *J. Archaeol. Sci.* **2014**, *41*, 89–105. [[CrossRef](#)]

47. Manikandan, D.; Mohan, S.; Magudapathy, P.; Nair, K.G.M. Blue shift of plasmon resonance in Cu and Ag ion-exchanged and annealed soda-lime glass: An optical absorption study. *Phys. B Condens. Matter* **2003**, *325*, 86–91. [[CrossRef](#)]
48. Bacon, F.R.; Balluffi, C.J. Color and Spectral Transmittance of Amber Bottle Glass. *J. Am. Ceram. Soc.* **1954**, *37*, 60–66. [[CrossRef](#)]
49. Capobianco, N.; Hunault, M.O.J.Y.; Loisel, C.; Trichereau, B.; Bauchau, F.; Trcera, N.; Galois, L.; Calas, G. The representation of skin colour in medieval stained glasses: The role of manganese. *J. Archaeol. Sci. Rep.* **2021**, *38*, 103082. [[CrossRef](#)]
50. Fernandes, P.; Vilarigues, M.; Alves, L.C.; da Silva, R.C. Stained glasses from Monastery of Batalha: Non-destructive characterisation of glasses and glass paintings. *J. Cult. Herit.* **2008**, *9*, e5–e9. [[CrossRef](#)]

Paper 3

Reprint of:

Agnese Babini, Sony George, & Jon Y. Hardeberg. (2021).
Hyperspectral imaging workflow for the acquisition and analysis
of stained-glass panels. In Proc. SPIE Optics for Arts,
Architecture, and Archaeology VIII (Vol. 11784).

PROCEEDINGS OF SPIE

[SPIDigitalLibrary.org/conference-proceedings-of-spie](https://spiedigitallibrary.org/conference-proceedings-of-spie)

Hyperspectral imaging workflow for the acquisition and analysis of stained-glass panels

Babini, Agnese, George, Sony, Hardeberg, Jon Yngve

Agnese Babini, Sony George, Jon Yngve Hardeberg, "Hyperspectral imaging workflow for the acquisition and analysis of stained-glass panels," Proc. SPIE 11784, Optics for Arts, Architecture, and Archaeology VIII, 117841F (22 June 2021); doi: 10.1117/12.2593735

SPIE.

Event: SPIE Optical Metrology, 2021, Online Only

Hyperspectral imaging workflow for the acquisition and analysis of stained-glass panels

Agnese Babini*, Sony George, Jon Yngve Hardeberg
Department of Computer Science, NTNU – Norwegian University of Science and Technology,
P.O.Box 191, N-2802 Gjøvik, Norway

ABSTRACT

Hyperspectral imaging has become a powerful technique for the non-invasive investigation of works of art. An advantage of this technique is the possibility to obtain spectral information over the entire spatial region of interest, allowing the identification and mapping of the constituent materials of the artefact under study. While hyperspectral imaging has been extensively used for artworks such as paintings and manuscripts, few works have been published on the use of this technique on stained glass. In this paper, a workflow for the imaging and analysis of stained-glass windows is proposed. The acquisition is carried out using a laboratory set-up adapted for transmittance measurement, which can support panels with a maximum size of around 50 x 50 cm. The image processing is carried out with two aims: visualization and chromophore identification. The results of this processing provide a foundation to discuss the potential of hyperspectral imaging for the scientific analysis of stained-glass windows.

Keywords: Hyperspectral imaging, Stained glass, Transmittance imaging, Cultural heritage.

1. INTRODUCTION

Hyperspectral imaging (HSI) has become a powerful technique for the non-invasive investigation of works of art. This technique offers the possibility to obtain spectral information over the entire spatial region of interest, allowing the identification and mapping of the constituent materials of the artefact under study. In the field of cultural heritage, HSI has been extensively used for non-invasive scientific investigation of artworks, especially paintings and manuscripts¹. On the other hand, few works have been published on the use of this technique on stained glass²⁻⁴. The first application of hyperspectral imaging on this kind of artworks dates to 2011 and it was performed on the stained-glass windows of the Scrovegni Chapel (Padua); the panels were taken down and acquired in laboratory under controlled illumination, in transmittance and reflectance (double transmittance) mode. In transmittance mode, the light sources were simply placed at the opposite side of the camera, in a geometry similar to the one proposed in this paper. In double transmittance the camera and the lights were placed at the same side, and a scattering white support was placed below the stained glass to be scanned. The latter solution was exploited for stained-glass panels which could not be acquired vertically and yielded better results for light-colored glass pieces. From the imaging point of view, the paper does not provide any processed images; nonetheless, the authors were able to demonstrate that results from the two methodologies were complementary and able to identify most of the coloring agents (chromophores)². Other two papers were published in 2019. The work of Palomar et al. explored for the first time the application of hyperspectral imaging in situ, exploiting the solar radiation as light source. The Art Nouveau stained glass from the Casa-Museu Dr. Anastácio Gonçalves in Lisbona were used as case study. The analysis showed promising results, especially when comparing and mapping the spectra of glass with same color and composition but with different transparency, despite the changing light conditions and the effect of external background (i.e trees) on the lighter colored glass³. The work of Perri et al. on the other hand, used an artistic stained-glass panel from 1969 as case study to evaluate the performance of a hyperspectral camera based on a Fourier transform approach. As for the previous paper, the acquisition was performed in-situ under natural light. With respect to the other paper the authors were able to demonstrate the ability of HSI in distinguishing and mapping different groups of blue colored glass within the stained-glass⁴.

*agnese.babini@ntnu.no

From this brief review, it is already possible to frame some of the challenges that must be addressed during the acquisition of stained-glass windows. First, to deal with the transparency of the glass, it is necessary to have a set-up that can work for transmittance measurements and can be suitable for the size of the stained-glass under study. For in-situ analysis, solar radiation can represent an easy solution to avoid building complicated support for the light sources. However, as expressed in Palomar et al., the fluctuation of the light condition can affect the quality of the resulting spectra. In addition to this, the high dynamic range of the colored glass, and the complex interaction between light and glass represent other aspects that must be taken into consideration^{5,6}.

Nonetheless, HSI could still represent a valuable technique for the analysis of stained-glass windows. The possibility of documenting large areas non-invasively, could be an advantage with respect to point analysis traditionally used for identification of the coloring agents (chromophores) in the glass, such as such as UV-VIS-IR spectroscopy and X-Ray absorption spectroscopy (XAS/XANES)⁷⁻⁹. The potential contribution of this technique in the field of glass conservation has been discussed thoroughly in a paper recently published by this research group⁵. The aim of this paper is to implement concretely the ideas proposed in the previous paper, by presenting a workflow for the imaging and analysis of stained-glass windows. The acquisition was carried out employing a laboratory set-up adapted for transmittance measurements. In the current configuration, the set-up can support only panels with a maximum size of ca. 50 x 50 cm. Despite the size limitation, it can still be suitable for the investigation of single panels taken down for restorations.

The paper is organized as follows: a detailed description of the acquisition set-up and the pre-processing steps is provided in Section 2, followed by the proposed image processing methodology, which is focused on two aspects of spectral imaging: image visualization and chromophore identification. With regards to chromophore identification, results from X-ray fluorescence spectroscopy (XRF) are shown and used to validate the information obtained with HSI. The results and the challenges related to stained-glass imaging are discussed in Section 3 and used to evaluate the potential of HSI for the analysis of stained-glass windows, before concluding.

2. EXPERIMENTAL

2.1 Case study

The test panel used for the experiment was originally prepared for camera calibration within the Fairford project¹⁰ in 1996. The dimension of the panel is 515 x 405 mm and consist of an array of 10 x 10 rectangular glass tiles, each of size 45 x 35mm, held by 6mm lead calmes. The glass tiles consist of 80 colored and 20 clear glass tiles with grisaille paint and yellow silver stain in various textures. The central area of the rear surface of each tile has been ground away.



Figure 1: Test panel photographed on a light table. *Image credit Dr. Lindsay McDonald*

2.2 The acquisition set-up

The acquisition was carried out using a HySpex VNIR-1800 push-broom hyperspectral camera. The camera acquires 186 images in the visible and near infrared (VNIR) range 400–1000nm, with a spectral sampling of 3.26nm and a spatial

resolution of 1800 pixels across the track. The camera lens has a fixed focusing distance of 30cm from the object, resulting in a linear field of view of around 8cm across the track. The HSI acquisition was performed in transmittance mode. In this configuration, the sample is positioned on a translational stage equipped with a diffusing panel, large enough to cover the field of view of the camera. A halogen lamp is positioned at around 7 cm from the stage, in correspondence with the diffuser panel, so that the light could shine through it and the stained glass (Fig 2). The image is recorded line by line by the line scanner, keeping the camera and the light source fixed, while the translational stage moves.

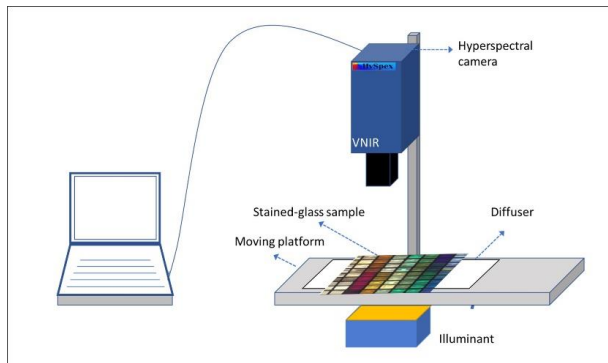


Figure 2: Schematic diagram of the transmittance set-up for the HSI system. The light source is positioned below a diffuser panel on top of which lays the stained-glass sample in direct contact. The transmitted light is collected by the camera.

3. METHODOLOGY

3.1 The image processing workflow

The spectral datacubes were collected in raw format and corrected to radiance through the HySpex-RAD software provided by the manufacturer. Sensor corrections and dark current subtraction was done at this stage. A total of 12 datacubes were recorded to cover the entire panel and later stitched together using the plug-in Pairwise Stitching¹¹ in ImageJ.

After the radiance correction, the datacubes were processed using the open-source software ImageJ. In order to transform the radiance data into transmittance, the image of the stained-glass sample is divided by the image representing a uniform transmitting surface. Usually, this step is performed by acquiring an image of the diffuser alone, under the same illumination condition and with the same size of the image as of the sample². In the present case, only the translating stage moves, while the camera and the light source are kept fixed. Since the camera acquires line by line, it can be assumed that the signal collected and averaged from a few lines can be representative of the light distribution across the whole field of view¹². For this reason, instead of collecting the reference over the entire area covered by the object, a small portion of the diffuser was always included in the image and used to calculate the reference spectrum. A new image can be created by transforming the spectrum extracted from the averaged lines into a single pixel, which size can be adjusted according to the dimension of the image to be corrected. During this step, it is crucial that all the 1800 across track pixel are included when averaging the lines from the reference, to consider the possible variation of the light distribution along the lines. The transmittance is calculated as follows:

$$T = \frac{S_{x,\lambda} - D_{x,\lambda}}{W_{x,\lambda} - D_{x,\lambda}} \quad (1)$$

where $S_{x,\lambda}$ is the signal relative to the light transmitted by the object and $W_{x,\lambda}$ is the signal relative to the light transmitted by the diffuser alone, at pixel location x, λ . Indices x, λ indicate respectively the spatial and the spectral dimension². In this

case the spatial dimension is represented by the 1800 pixel across the track and the spectral dimension is represented by the 186 spectral bands. It must be also specified that the camera acquires and subtract automatically the dark current. In practice, to calculate the transmittance it is only necessary to divide the object image to the reference one.

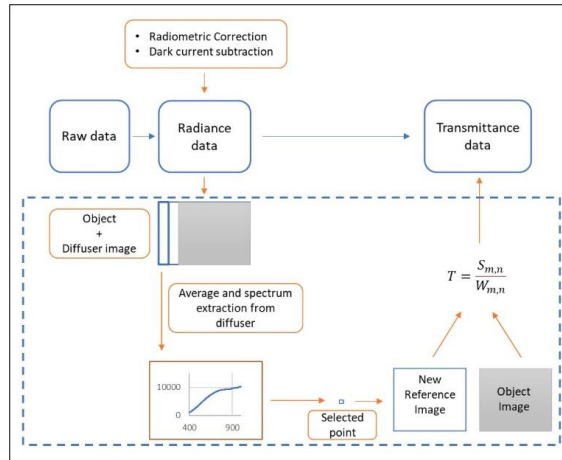


Figure 3: Schematic diagram of the workflow for HSI acquisition and preprocessing of the stained-glass panel.

3.2 Visualization: RGB and false color images

The first step for visualization of HSI is to extract the representative red, green and blue bands to reconstruct the color image. The default bands for red, green, and blue are 642, 549, 463 nm respectively. These bands are specified by the camera manufacturer and are usually stated in the header file of the datacubes. In ImageJ, the RGB image can be built by selecting the three bands and arranging them to create a new image made of three separated channels (red first, green and blue). These selected bands are transformed into a color image.

The false color image can be produced in a similar way. In this case, the two bands related to red (642 nm) and green (549 nm) are kept, and another band can be selected in the near-infrared region. Since there is no standard set for the choice of the infrared band, some trials are performed to understand which bands provide most information. Once the band are selected, they can be rearranged in a new image, putting first the image related to infrared, the red one and lastly the green one. The same procedure used to make the RGB image can be followed to create the false color image.

3.3 Visualization: color rendering

The color rendering of the HSI was performed in MATLAB using and adapting codes made available by Foster and Amano¹³. For the rendering, the CIE 1931-2° standard observer color matching function was used. The values for the daylight series standard illuminants were calculated using formulas retrieved from the Rochester Institute of Technology online repository of useful colorimetric data¹⁴. The values for the color matching function, as well as for the standard illuminant A, were obtained from the same repository. The datacube relative to the top left part of the panel (Fig.3) was used to perform the color rendering under different illuminants, while the entire panel was rendered only with D65, for comparison with the RGB image obtained through band selection (Fig 4a and 4b).

3.4 Complementary analysis

In order to validate the results obtained from hyperspectral imaging, the elemental information on the composition of the glass tiles was studied by means of X-Ray Fluorescence (XRF) spectroscopy. The analysis was performed with a Thermo Scientific Niton XL3t handheld XRF spectrometer, equipped with a silver anode and a GOLDD detector. The analysis was performed in Cu/Zn mining mode, with 40kV voltage. The acquisition time for each measurement was 120s. The Niton

NDT software was used for the spectra interpretation. When possible, the XRF points were collected in the clearest areas of the glass tile.

4. RESULTS AND DISCUSSION

4.1 Visualization

Figures 4a and 4b shows the color images obtained by band selection and color rendering respectively. The rendered image can be considered an improvement with respect to the three bands RGB image as it allows a better visualization of darker glasses; however, it is worthy of mention that the rendering does not take into account other optical properties of glass (such as the refractive index for example), so it may not represent the real appearance of the glass tiles.

With regards to false color images, Figures 4c and 4d shows the results obtained by selecting two different bands in the infrared region, one at 811 nm (Fig. 4c) and one at 996 nm (Fig. 4d). Notice how the selection of the 996 nm band improves a little the visualization of very dark tiles and allows a better distinction of the green colored tiles.

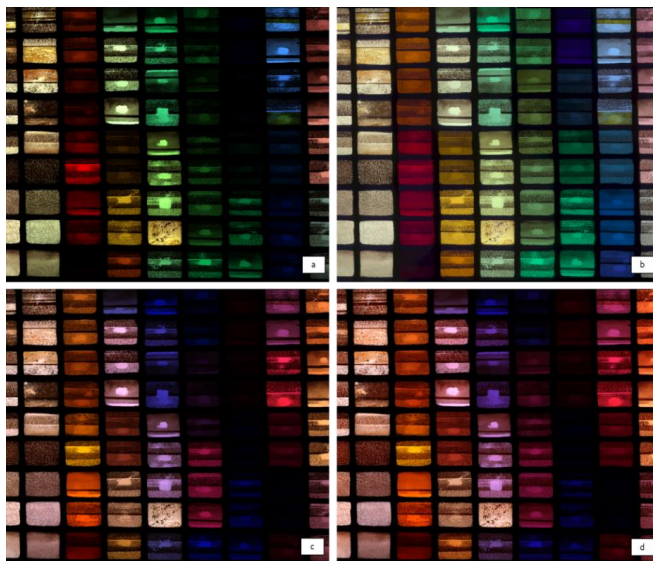


Figure 4: a) RGB color image obtained selecting three bands related to red (642 nm), green (549 nm), and blue (463 nm), from the HSI. Note that the last column and last row are missing as they were not included in the final stitching. b) RGB color image obtained using color matching function. c) false color image obtained selecting a band in the near infrared region at 811 nm d) false color image obtained selecting a band in the near infrared region at 996 nm.

4.2 Spectra interpretation

Looking at the false color image (Fig 4 and 6b), it is already possible to make a preliminary identification of glass made with the same coloring agents. Taking some of the green glass tiles as an example, it is possible to notice how their spectra match their similar color appearance in false color. (Fig. 6).

The second step in chromophore identification is to associate the characteristic peaks to the relative elements responsible for the color of the glass. This task is not easy and requires skills and expertise on glass-making techniques, as well as the mechanism behind the origin of color in glass.

A good starting point is to compare the results with the available literature for reference. It has been already mentioned that few works have been published on HSI applications on glass; nonetheless, one may take advantage of publications regarding the use of UV-VIS-IR spectroscopy, which is commonly used for the study of historical and archaeological glass. However, a simple comparison may not always be enough. While most of the spectral shapes can be easily identified, the variation in chromophore concentration, particle size, and furnace condition^{3,15} can result in small differences between the spectra of the sample and those found in literature. In this case, comparison of the spectra obtained with published references suggests the presence of copper (Cu^{2+}) and chromium (Cr^{3+}) as main chromophores for both groups. The contribution of chromium seems to be higher in Group 2^{2,3,7,15,16} as the two characteristic peaks at become more visible.

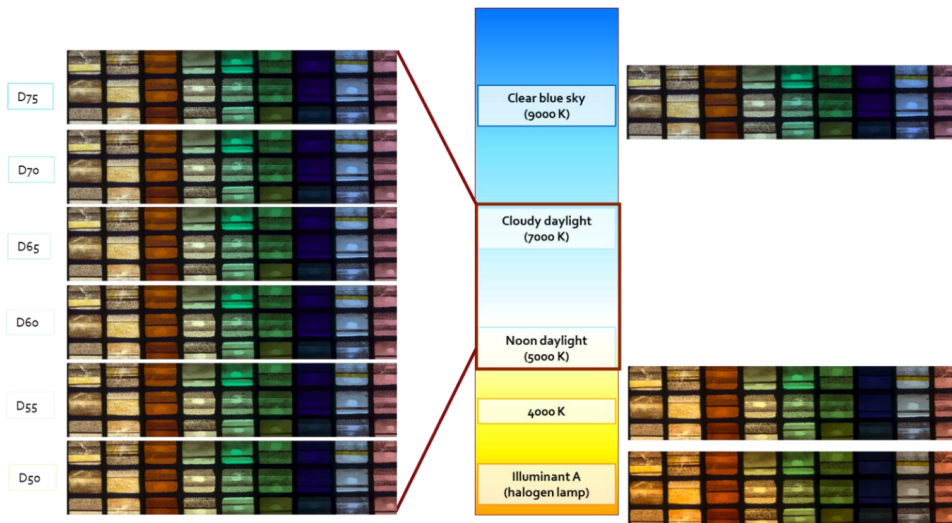


Figure 5: Top part of the stained glass rendered under different standard illuminants. The effect of the color temperature change can be observed best on the light blue and the pink glass on the right side of the rendered images.

In order to have a complete characterization of the glass composition, additional analytical techniques can be applied. Among those, XRF spectroscopy is widely used for the non-invasive characterization of the elemental composition of glass^{5,7}. Presenting the complete results of XRF spectroscopy is beyond the scope of this paper, and a future publication is planned on this part of the research. However, considering the green glass taken as examples, it is already possible to mention that XRF confirmed the presence of copper and chromium as main chromophores in Group 1, with small addition of iron (Fe^{3+}). Regarding Group 2, the copper content seems to be lower in relationship with chromium and iron with respect to the Group 1. In Group 2, it is possible to make another distinction, between tiles 1D/9E and tiles 2, 3 and 4E. The differences between these two subgroups can be explained by the fact that tiles 1D and 1A seems to have a higher content of iron with respect to chromium, while for 2,3 and 4E it is the opposite. This assumption can help in providing a better interpretation of the VIS-NIR spectra: the small shoulder at around 400-450 nm which is present in all the samples, could suggest the presence of the absorption peak of Fe^{3+} (at 380 nm), which falls outside the range of the hyperspectral camera together with that of the Cr^{3+} (at 450 nm). In tiles 1D/9E, this shoulder is more pronounced, and could be correlated to a higher content of iron. On the other hand, the more defined small peak at around 680 nm in tiles 2,3,4E could be associate to the higher content of chromium versus iron^{2,15,16}.

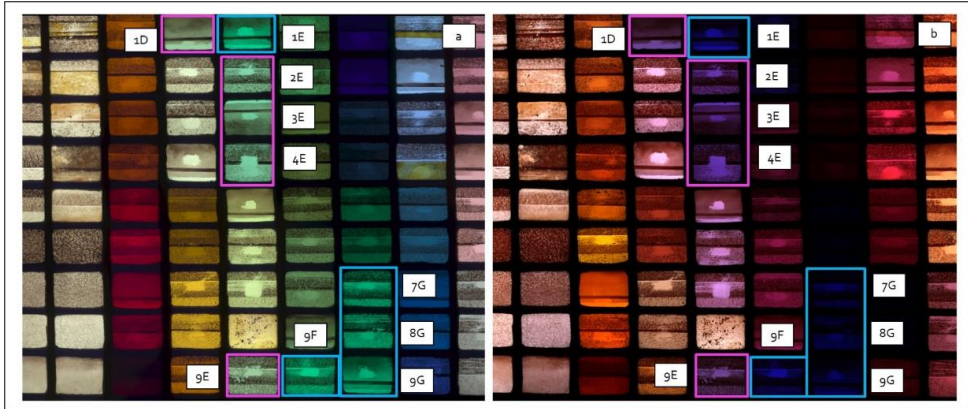


Figure 6: Comparison of color (a) and false color image (b) relative to some green glass.

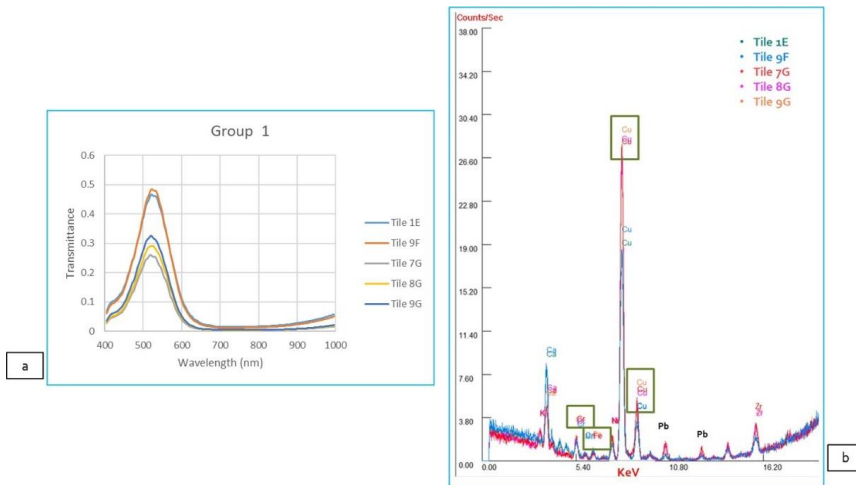


Figure 7: VIS-NIR spectra (a) and XRF spectra (b) of the green glass in group 1. XRF spectra confirm the presence of copper as main chromophore, as well as small quantities of chromium and iron.

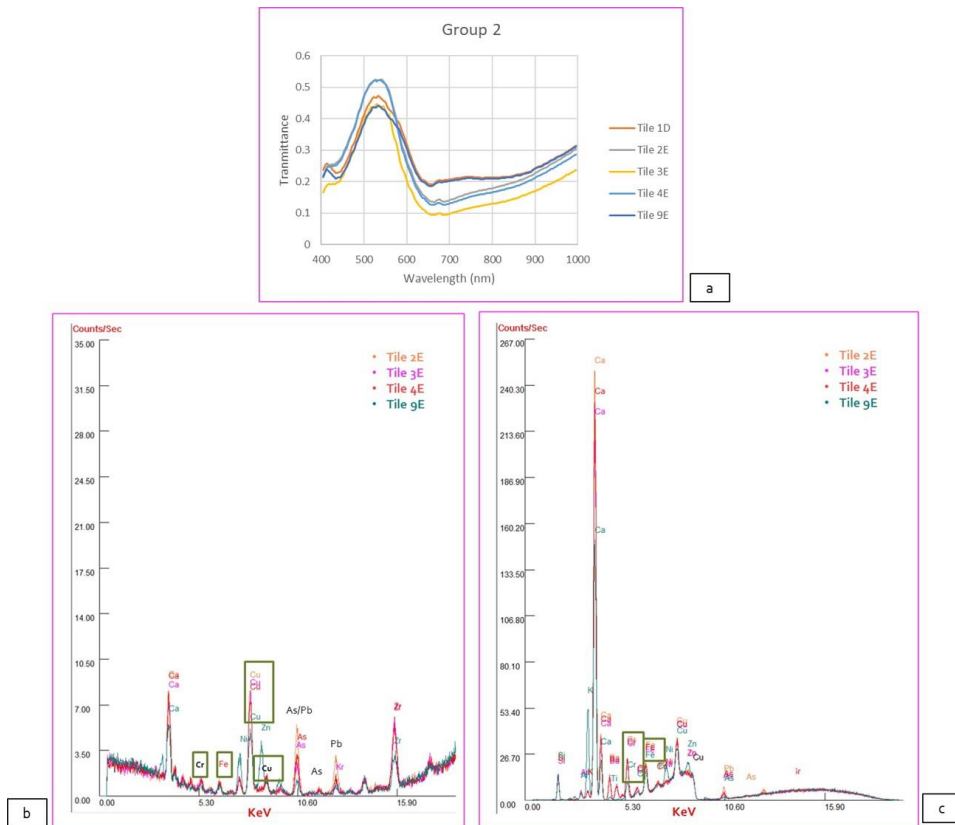


Figure 8: VIS-NIR spectra (a) and XRF spectra of the green glass in group 2 (b,c). XRF results from tile 1D are not available. The XRF spectra on the right (c) refers to the light element mode of the spectrometer, which allows a better distinction of the Cr/Fe ratio among the two sub-groups identified in group 2. It can be noticed that the tile 9E has a lower concentration of chromium with respect to the other three samples in the same group. This confirms that the lighter violet hue observed among the glass in group 2 are due to small difference in composition.

4.3 Challenges

One of the challenges to take into consideration when performing transmittance measurements regards the typology, shape, and positioning of the light source within the set-up. In the current set-up, a powerful halogen lamp is used as the light source, at a close distance to the diffuser. Due to the structure of the halogen lamp, the light distribution is non-uniform on the diffuser, which causes inhomogeneity in the light distribution along the scanned line. Another issue related to the light source is the amount of heat produced by halogen lamps, which can represent a risk for historical objects. A solution that could partially solve both problems would be to keep the light source at a longer distance from the diffuser. It has been noticed during the experiment that the light can be focused into a narrow, homogeneous stripe if the lamp is placed at a distance of around 30 cm from the diffuser. Moreover, the longer distance will also reduce the heat on the surface of the diffuser, and consequently, the stained-glass panel. However, it must be considered that the intensity of the light source could be reduced by this change. Research related to these topics are currently in progress out to better understand the effects of distancing the light from the diffuser on the results.

Another challenging aspect is the transmittance properties of the colored glass and the way these properties influence the result. In many stained-glass panels, it is common to see very dark and very light glass placed close to each other to create striking light effects. This situation may represent an issue when searching for a satisfying exposure time, resulting often in an underexposure of the darker glass. Moreover, in some cases, even glass tiles that appears light colored can show a low transmittance. Increasing the exposure time of the camera may be a solution, but in general it has been observed that it barely improves the results for very dark glass, with the added disadvantages of slowing down the acquisition time and saturating the diffusing panel, as well as the lighter colored glass signals. For this reason, during the experiment the exposure time was set by taking into consideration only the illumination condition of the diffusing plate. Figure 3 shows that in many cases it is possible to obtain a sufficiently good signal even for very dark colored glass.

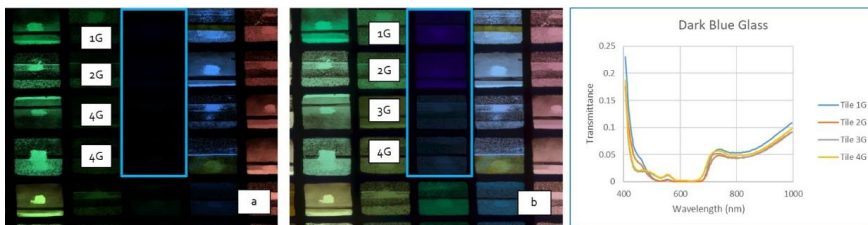


Figure 9: Despite the low transmittance of the very dark glass, the signal obtained provides enough information on the nature of the color in the glass. This can also be noticed by looking at the difference between the three-band RGB image and the spectrally rendered color image, where the blue color can be better appreciated.

5. CONCLUSION

In this paper, a workflow for the hyperspectral image acquisition and analysis of stained-glass windows has been proposed. For the purpose of the research, a test panel has been analyzed using a laboratory set-up adapted for transmittance measurements. Challenges related to the characteristics of the set-up and the optical properties of stained-glass, have been discussed as well. While these challenges can be addressed in different ways, the results obtained showed that hyperspectral imaging technique can be helpful for simultaneous documentation and analysis of stained-glass windows. In addition to the improvement of the current set-up, future works will be focused on two aspects: a better characterization of the coloring agents used in the different tiles of the panels and creation of spectral libraries, and application of classification algorithms for chromophore mapping purposes.

ACKNOWLEDGEMENTS

This research was carried out as part of the CHANGE (Cultural Heritage Analysis for New Generation) Innovative Training Network project funded by the European Union's Horizon 2020 research and innovation programme under the Marie Skłodowska-Curie grant agreement No. 813789. The author would also like to thank Dr. Lindsay McDonald for providing the stained-glass panel for the measurements, Jan Cutajar at the University of Oslo for performing the XRF analysis, and Dr. Tiziana Lombardo for providing valuable insights on glass composition and XRF data interpretation.

REFERENCES

- [1] Picollo, M., Cucci C., Casini A., and Stefani, L., "Hyper-Spectral Imaging Technique in the Cultural Heritage Field: New Possible Scenarios", *Sensors*, 20 (1), 2843 (2020).
- [2] Rebollo, E., Ratti, F., Cortelazzo, G. M., Poletto, L., and Bertonecello, R., "New trends in imaging spectroscopy: the non-invasive study of the Scrovegni Chapel stained glass windows", *Proc. SPIE* 8084, (2011).
- [3] Palomar, T., Grazia, C., Cardoso, I. P., Vilarigues M., Miliani C., and Romani, A., "Analysis of chromophores in stained-glass windows using Visible Hyperspectral Imaging in-situ", *Spectrochim Acta A Mol Biomol Spectrosc*, 223, (2019).
- [4] Perri, A., Nogueira de Faria, B. E., Teles Ferreira, D. C., Comelli, D., Valentini, G., Preda, F., Polli, D., de Paula, A. M., Cerullo, G., and Manzoni, C., "Hyperspectral imaging with a TWINS birefringent interferometer," *Opt. Express* 27, 15956-15967 (2019).
- [5] Babini, A., George, S., Lombardo, T., Hardeberg, J. Y. "Potential and Challenges of Spectral Imaging for Documentation and Analysis of Stained-Glass Windows". *LIM* 2020,109-113, (2020).
- [6] MacDonald, L.W., "A robotic system for digital photography", *Proc. SPIE* 6069. (2006).
- [7] Bracci, S., Bartolozzi, G., Burnam, R. K., and Corallini, A. "Integration of both non-invasive and micro-invasive techniques for the archaeometric study of the stained-glass window Apparizione degli Angeli in the basilica of Santa Croce in Florence", *J. Cult. Herit.*, 44, 307-316 10 (2020).
- [8] Hunault, M.O.J. Y, Lelong, G., Gauthier, M., Gelebart, F., Ismael, S., Galois, L., Bauchau, F., Loisel, C., Calas, G., "Assessment of Transition Element Speciation in Glasses Using a Portable Transmission Ultraviolet-Visible-Near-Infrared (UV-Vis-NIR) Spectrometer", *Appl Spectrosc*, 70 (2016).
- [9] Ceglie, A., Nuyts, G., Meulebroeck W., Cagno, S., Silvestri, A., Zoleo, A., Nys, K., Janssens, K., Thienpont, H., Terry, H., "Iron speciation in soda-lime-silica glass: a comparison of XANES and UV-vis-NIR spectroscopy", *J. Anal. At. Spectrom.*, 30 (2015).
- [10] McDonald, L.W., and Oldfield, J., "Image capture and restoration of medieval stained glass", *CIC* 1996 (1), 44-49, (1996).
- [11] Preibisch, S., Saalfeld, S., and Tomancak, P. "Globally optimal stitching of tiled 3D microscopic image acquisitions", *Bioinformatics*, 25 (11), 1463-1465 (2009)
- [12] Pillay, R., Hardeberg, J.Y., and George, S., "Hyperspectral imaging of art: Acquisition and calibration workflows", *J Am Inst Conserv* (2019).
- [13] Foster, D.H., and Amano, K., "Hyperspectral imaging in color vision research: tutorial.", *J. Opt. Soc. Am. A*, 36, 606-627 (2019).
- [14] Rochester Institute of Technology, "Useful Color Data", https://www.rit.edu/cos/colorscience/rc_useful_data.php (Last visited 25 May 2021).
- [15] Meulebroeck, W., Baert, K., Wouters, H., Cosyns, P., Ceglie, A., Cagno, S., Janssens, K., Nys K., Terry H., Thienpont, H., "The identification of chromophores in ancient glass by the use of UV-VIS-NIR spectroscopy", *Proc. SPIE* 7726, (2010).
- [16] Meulebroeck, W., Wouters, H., Nys K., and Thienpont, H., "Authenticity screening of stained-glass windows using optical spectroscopy", *Sci Rep*, 6 (37726), 2016.

Paper 4

Reprint of:

Agnese Babini, Sony George, Tiziana Lombardo, & Jon Y. Hardeberg. (2022). A Portable Set up for Hyperspectral Imaging of Stained-Glass Panels. In Rocco Furferi, Lapo Governi, Yary Volpe, Kate Seymour, Anna Pelagotti, & Francesco Gherardini (Eds.), *The Future of Heritage Science and Technologies: ICT and Digital Heritage* (Vol. 1645, pp. 57-70). Cham: Springer International Publishing.



A Portable Set up for Hyperspectral Imaging of Stained-Glass Panels

Agnese Babini¹ , Sony George¹ , Tiziana Lombardo² ,
and Jon Yngve Hardeberg¹ 

¹ Norwegian University of Science and Technology, Gjøvik,
Norway

{agnese.babini, sony.george, jon.hardeberg}@ntnu.no

² Collection Centre, Swiss National Museum, Affoltern am Albis, Switzerland
Tiziana.lombardo@nationalmuseum.ch

Abstract. In the past years, hyperspectral imaging has become a popular technique for the non-invasive investigation of works of art and has been extensively used for the analysis of pigments in paintings and manuscripts. The application of spectral imaging on stained glass however is very limited. Due to their transparency, imaging of stained glass presents some challenges, such as the necessity of a proper transmittance setup and the complex interaction between light and glass, which can affect the acquisition.

In this work, we present a portable setup for hyperspectral imaging of stained-glass panels. The setup has been designed for transmittance measurements, and in the current configuration, it can support panels with a maximum size of around 45×45 cm.

The portable setup has been tested at the facilities of the Swiss National Museum on 10 stained-glass panels belonging to the museum's collection, which were selected to be representative of different historical periods and glass-making techniques. Characteristics, advantages, and limitation of the system will be discussed, showing preliminary results on some of the case studies analyzed.

Keywords: Hyperspectral imaging · Stained glass · Transmittance imaging

1 Introduction

In the past years, hyperspectral imaging (HSI) has found many applications in the field of cultural heritage. This technique can be considered a combination of conventional imaging and spectroscopy; by acquiring many images across the electromagnetic spectrum, the spectral information can be obtained at each pixel. By analyzing the spectral data, it is possible to identify and map the materials that constitute the object under study. For this reason, spectral imaging has been successfully used for the non-invasive investigation of artworks, especially paintings and manuscripts [1]. The application of this technique on stained-glass windows however is still limited. The reason may lie in the fact that, due to the transparency/translucency of the glass, imaging of these objects presents some

challenges, such as the necessity of a proper transmittance setup, the complex interaction occurring between light and glass, as well as degradation products present on the glass surface, which affect the image acquisition. At the best of the authors' knowledge, very few works have been published on the use of HSI on stained glass [2–4]. In these reported studies, the acquisition was performed exploiting the solar radiation as light source [3, 4]. Recently, we proposed a methodology for the acquisition of stained-glass panels (maximum size of 50×50 cm) in laboratory condition [5], using a translating stage and an illumination geometry similar to the study presented by Rebollo *et al.* [2].

In this work on the other hand, a *portable* setup for the hyperspectral imaging of stained-glass panels is presented. The setup has been designed for transmittance measurements, and in this current configuration, it can support glass panels with a maximum size of 45×45 cm. The characteristics of the system will be described, discussing design choices, advantages, and limitations.

The practical use of the system has been tested at the facilities of the Swiss National Museum on 10 selected stained-glass panels belonging to the museum's collection. The panels were selected after discussions with the museum conservators for their historical and artistic attributes. Preliminary results on some of the case studies will be shown to highlight some technical aspects regarding the system, as well as the image analysis performed on the acquired HSI data.

2 Materials and Methods

2.1 The Transmittance Setup

The acquisition was carried out using a push-broom hyperspectral camera HySpex VNIR-1800. The camera acquires 186 images in the visible and near infrared (VNIR) range (400–1000 nm), with a spectral sampling of 3.26 nm and a spatial resolution of 1800 pixels across the track. The camera lens has a fixed focus distance of 30 cm from the object, with a field of view of 17° and a pixel resolution of 50 μm .

For the measurements, the camera was mounted on a tripod equipped with a motorized rotating head. Scanning of this rotational stage is controlled from the computer and the movement is synchronized with the HSI acquisition parameters. The datacube is formed recording one line at a time, while the camera moves from left to right. Due to the rotating movement and the focus limit of the camera, it was possible to acquire only 1650 lines for a single acquisition, before significant geometric distortions and blurring occurred. These phenomena are usually visible at the edge of the image going toward the scanning direction (Fig. 1a).

The transmittance system has been designed in the laboratory, and later built using materials easily retrievable in common hardware stores and in conservation laboratories. This system consists of a wooden panel, which acts as support for the artworks, where a square-shaped area (25×25 cm²) has been cut to accommodate a diffuser plate for the transmittance measurement. This diffuser is made of acrylic and has a thickness of 6 mm (Fig. 1c).

Two halogen lamps were used as light source to maximize the light distribution across the field of view. However, this solution had some drawbacks. Halogen lamps are usually the most used light sources for HSI, as they provide a continuous spectrum

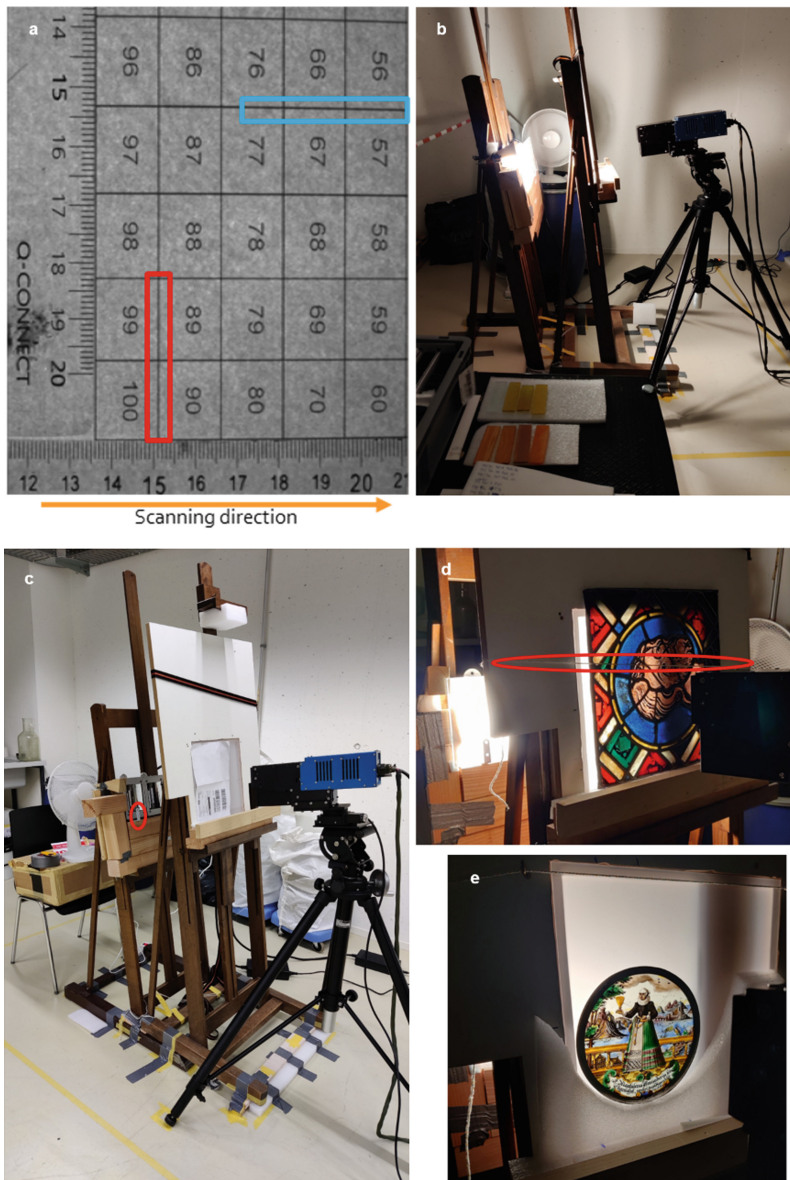


Fig. 1. Horizontal (in blue) and vertical (in red) distortions (a). Setup configuration at the Museum during acquisitions (b). Tentative set up before the beginning of acquisition campaign. The red circle highlights the metal L-shaped piece (a second one is hidden by the easel) that holds the thicker diffuser (c). Safety measures used to prevent the falling of the stained-glass panels during the acquisition: ethafoam sheets were used for the smaller panels (d) while strings were used to hold the bigger ones (e).

from UV up to Mid-IR [6]. However, they also generate a high amount of heat that can be harmful for the stained-glass; indeed, depending on the state of conservation of the object, high temperature could cause expansion of the different materials, as well as

alteration and detachment of painted surfaces [7]. After discussions with the conservators at the museum, it was suggested that the temperature on the surface of the artwork should not exceed 25–30 °C during the acquisitions. To meet this requirement, the lamps were placed at around 30 cm beneath the diffuser area of the wooden panel; a second diffuser was placed between the lamps and the first diffuser. Differently from the first one, the second diffuser has a thickness of 8 mm and is made of glass, with a diffusing sheet applied in both sides. This diffuser is part of the laboratory set-up located at the NTNU Colorlab and was adapted for this acquisition campaign. Two L-shaped metal piece were used to hold the second diffuser. One side of the L-shape was nailed to the wooden pieces used to put the light sources at the necessary height, while the other side held the diffuser plate. This solution not only helped in reducing the exposure of the artwork to thermal radiation, but also improved the light distribution.

Two easels were used as support, one to hold the supporting wooden panel with the diffuser and the other to hold the light sources and the second diffusing plate (Fig. 2a). The safety of the stained-glass panels was ensured by using ethafoam pieces and strings (Fig. 2b, c). The head of the stage was tilted by 8° to account for the inclination of the easels. A cooling fan was also employed as an additional precaution to reduce the temperature. An integration time of 30000 μ s was deemed good enough to obtain a good exposure and reduce the acquisition time and was kept fixed through all the campaign.

2.2 Case Studies

Stained Glass Panels. A total of 10 panels were acquired during the acquisition campaign. These case studies were selected to be representative of different historical periods and glass-making techniques. Information on the panels and acquisition details are reported in Table 1 for the case studies mentioned in the paper.

2.3 Methodology






Image Processing. The HSI datacubes were collected in raw format and corrected to radiance using the HySpex-RAD software provided by the camera manufacturer. Sensor corrections and dark current subtraction was done at this stage. After this step, the datacubes were processed using the open-source software Fiji [8].

In order to transform the radiance data into transmittance, the image of the object has to be divided by the image of a uniform transmitting surface. This task was performed by acquiring a reference image of the diffuser without any object in different moments of the day (morning, midday, afternoon, and evening), to account for any possible fluctuation of the intensity of the light source. A Gaussian blur filter was applied to the spatial dimensions of the reference image to reduce the artifacts caused by the dirt accumulated on the surface of the diffuser. The spectral dimension was not smoothed. This aspect will be discussed in detail in the result section. Lastly, all the spectra have been converted from transmittance to absorbance, to facilitate the observation of the characteristic peaks and an easier comparison with available literature.

Data Visualization. The first step to visualize a HSI datacube is to generate an RGB image, by extracting the representative red, green and blue bands. The default bands

for red, green, and blue (642 nm, 549 nm, and 463 nm) are specified by the camera manufacturer and are usually stated in the header file associated to the datacube. In ImageJ, the RGB image can be built by selecting the three bands and arranging them to create a new image made of three separated channels. These selected bands are transformed into a color image.

Table 1. Information on some of the case studies analyzed during the acquisition campaign. Pictures courtesy of Swiss National Museum

	Panels information	Acquisition details
	ID: LM-12794 Author: N/A Date: 1322 Dimension: 31.2 x 31.6 cm	N. of datacubes: 12 Total data size: 12.4 Gb Total acquisition time: 2 h 20 m
	ID: AG-1170 Author: Karl van Egeri Date: 1551 Dimension: 36.5 x 27.2 cm	N. of datacubes: 12 Total data size: 12.4 Gb Total acquisition time: 1 h 50 m
	ID : LM-19635 Author: Auguste de Pourtales Date: 1633 Dimension: 14.33 cm Ø	N. of datacubes: 4 Total data size: 4.14 Gb Total acquisition time: 30 m
	ID: LM-167914 Author: Louis Halter Date: 1921 Dimension: 37.5 x 26 cm	N. of datacubes: 7 Total data size: 7.25 Gb Total acquisition time: 55 m
	ID: LM-167924 Author: Louis Halter Date: 1948-1950 Dimension: 42.1 x 35.5 cm	N. of datacubes: 15 Total data size: 15.5 Gb Total acquisition time: 2 h 30 m

A similar approach can be used to create false color images. This technique allows to distinguish materials with similar colors, but different spectral property and it is extensively used in the field of cultural heritage for preliminary discrimination of pigments with similar color [9, 10]. False color images are usually created by keeping the two bands related to red and green and selecting another band in the near-infrared region. Since there is no standard set for the choice of the infrared band, some trials were performed to understand which band provides most information. Once the bands were selected, the images were rearranged in a new image, putting the image related to infrared first, followed by images corresponding to red and green. The technique has been tested on a stained-glass panel in a paper we recently published [5], resulting particularly useful for distinction of green and blue glass.

Another form of visualization is color rendering, which converts the spectral data to RGB by means of color matching function and standard illuminants data. This task was performed in MATLAB using and adapting codes made available by Foster and Amano [11]. For the rendering, the CIE 1931–2° standard observer color matching function was used. The values of the D65 standard illuminant used for the color rendering were calculated using formulas retrieved from the Rochester Institute of Technology online repository of useful colorimetric data [12]. The values for the color matching function were obtained from the same repository.

3 Results and Discussion

Figure 2 shows the comparison between the high-resolution pictures provided by the museum (Fig. 2a), color rendered images (Fig. 2b) and band selection RGB images (Fig. 2c) for selected areas of the case studies LM-12794, AG-1170 and LM-167924. First of all, it is worthy of mention that the differences in the aspect ratio between the high-resolution images from the Museum and those created from HSI are due to the geometrical distortion mentioned previously. With respect to the band selection RGB images (Fig. 2c) the rendered images are able to provide a more accurate color representation (Fig. 2b), especially with regards to the visualization of darker glasses. Compared to the high-resolution images (Fig. 2a), the few differences are related to the fact that the rendering is solely based on the transmittance values of the stained-glass, without taking into account other phenomena such as specular reflection occurring on the glass surface. This is visible in areas with red glass, which appear more homogeneously colored in the rendered images from the HSI with respect to the high resolution one obtained with traditional imaging (Fig. 2a and b for the bottom part of case study AG-1170, see blue circle). In this case, the advantage of having a rendered image instead of the band selection images, is the possibility to have a faithful color image (alike the high-resolution images) of the same size of the HSI datacube, that can be exploited for the selection of spectra in regions of interest (Fig. 3). Indeed, due to the evident distortion, spectra selection using the high-resolution images as reference could lead to error.

Figures 3b and 4c represent false color images created by selecting two different bands in the infrared region, one at 811 nm (Fig. 3b) and one at 996 nm (Fig. 3c) compared to rendered images (Fig. 3a). The selection of the last available band in the NIR region in some cases allow a better distinction of green and blue glass. In fact, differently from red,

yellow, and purple glass, most of blue and green glass show a different false color when selecting the 996 nm band, which can be related to the presence of another chromophore absorbing light farther in the NIR range, hinting at a different composition of the colored glass (Fig. 3b and c and Fig. 6). An example of this can be seen in Fig. 3c of AG-1170 (top), where the false color image with the band at 996 nm allow a better discrimination between the green glass employed for the arch (which display a dark blue appearance) and the fragment used in the left corner (purple, see red circled area).

By comparing the appearance in false color images of glass with similar color, as well as their spectral response, it is possible to make some preliminary hypotheses on the coloring agents used by the glassmakers.

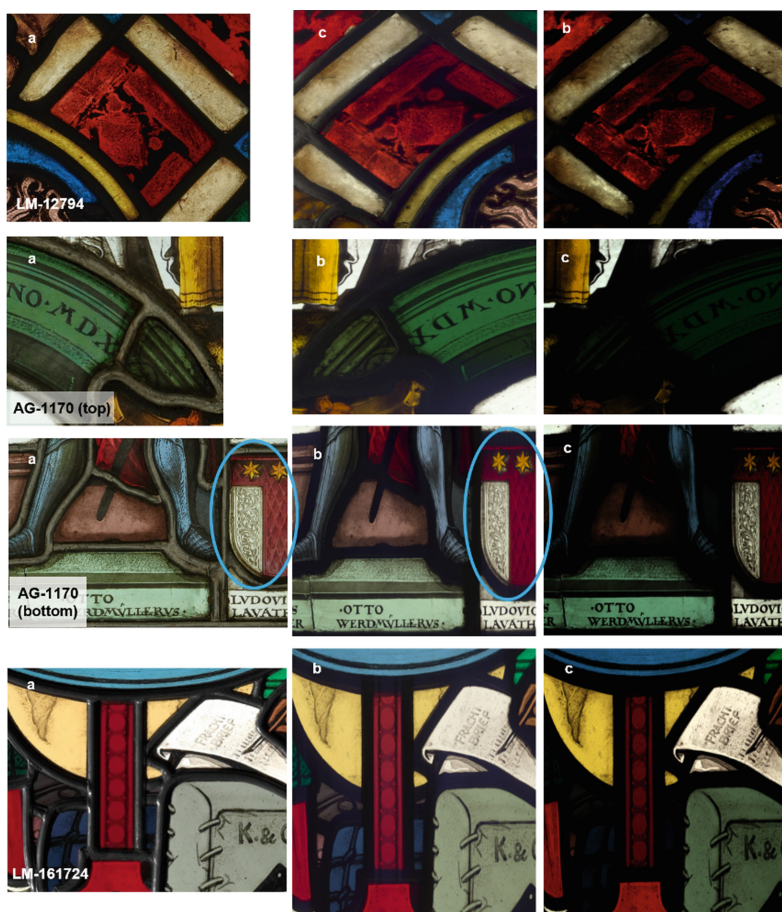


Fig. 2. a) High resolution images (courtesy of Swiss National Museum). b) Color images rendered using color matching function and standard illuminant D65. c) RGB images obtained by band selection. The blue circles show the different appearance of the red glass between the high-resolution image and the rendered one. Note that figure b) and c) for LM-12794 and AG-1170 (on top) are mirrored as those areas of the stained-glass panels were acquired from the back. (Color figure online)

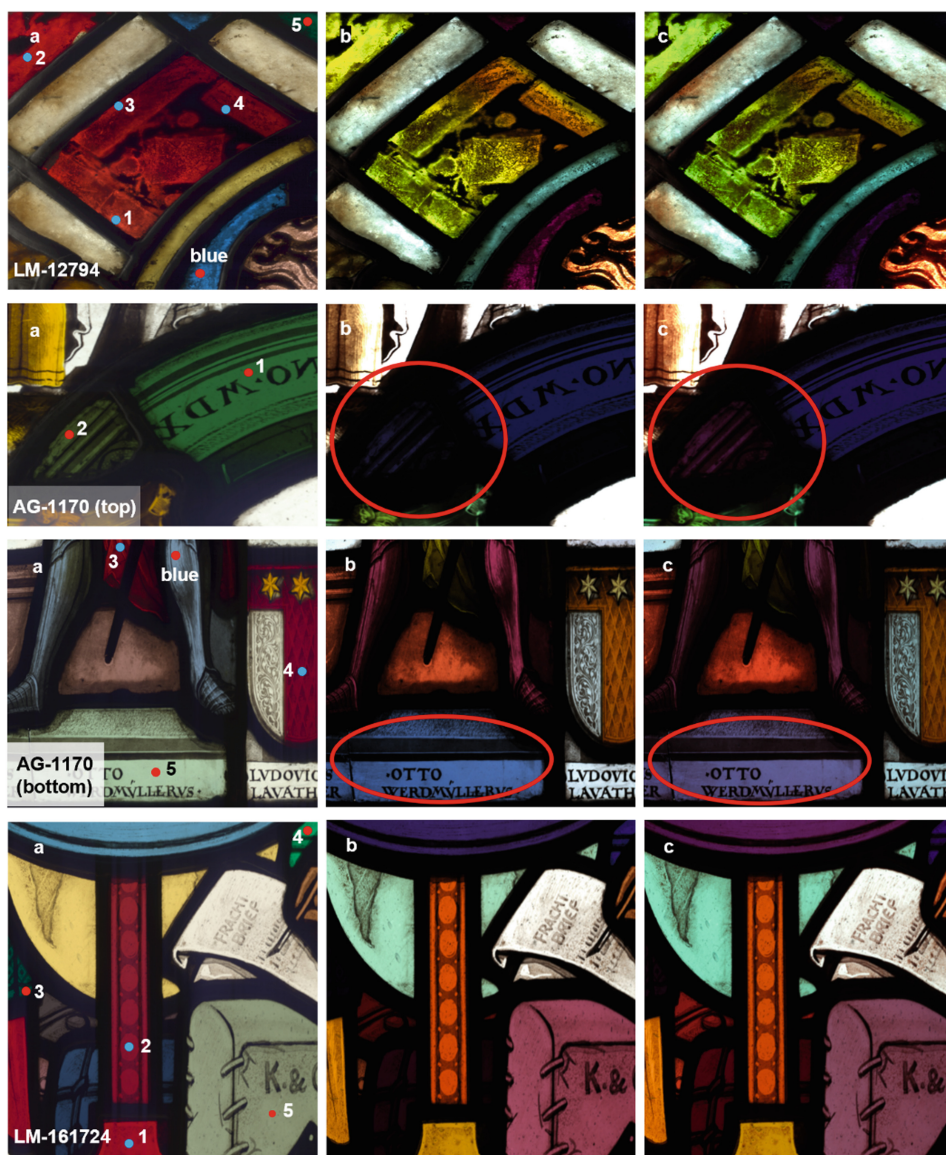


Fig. 3. a) Colored images rendered using color matching function and standard illuminant D65. The points indicate where the spectra were collected in the image for comparison in Fig. 4 and 6. b) False color image obtained by selecting the NIR band at 811 nm c) False color image obtained selecting the NIR band at 996 nm. The red circles show the difference in appearance of some green glass using the two bands. (Color figure online)

Comparing the spectra of red glass in Fig. 4 with the false color images in Fig. 3b, c, it is possible to notice that a lower intensity of the peak at 565 nm (well visible in Fig. 4 for LM-12794 pt. 1, LM-167924 pt. 1 and AG-1170, pt. 3), related to the surface

plasmon resonance of copper nanoparticles (Cu^0) [13–15], generates a shift from a bright greenish yellow to orange (Fig. 3b and c, LM-12794).

Due to the strong absorption of the copper nanoparticle, this kind of red glass were traditionally produced by adding a thin red layer over a transparent one [14]; Bracci *et al.* [13] suggest that the changes in the shape of the spectrum could be related to a different roughness of the red layer, possibly caused by degradation. False color images can thus reveal interesting information on the conditions of the red layer in flashed red glass, even within the same sample, as well as help with the identification of other typology of red glass (Fig. 3 and 4, LM-167924, pt. 2).

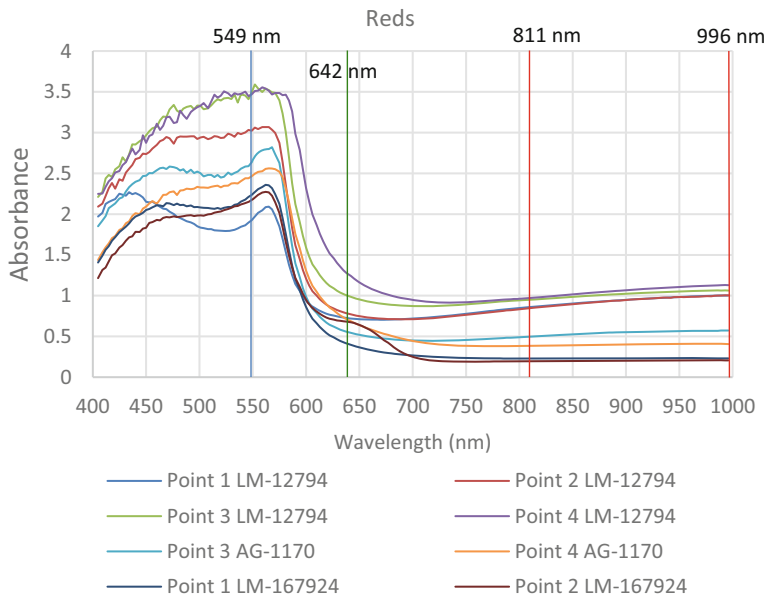


Fig. 4. Spectra of red glass collected on the three case studies. The four lines (one for green and blue and two for red) indicate the bands selected while the color of the lines indicate for which RGB channel are they used. The localization of the points is displayed in Fig. 2a.

The same hypotheses can be made for green glass pieces. By comparing the spectra with the false color images, two different behaviors can be noticed: glass pieces that appear dark blue in false color (Fig. 6a, pt.1 LM-12794, pt.2 AG-1170 top), in general seem to contain copper and iron as main chromophores, with a large absorption band centered at around 770–790 nm (Cu^{2+}) and a smaller one at 410–430 nm (Fe^{3+}) [2, 3, 13, 14]. The small absorption band around 675 nm in the spectrum of pt.4 LM-127924 suggest the presence of Cr^{3+} as well [2, 3]; however, since the absorption of copper seems more dominant, the false color of that green glass does not change significantly. On the other hand, a pinkish/purplish appearance (Fig. 6b), seems to be related to the presence of cobalt, in addition to other coloring agents. The reason behind this phenomenon depends on the fact that the two bands selected for the blue (549 nm) and the green channel (642 nm) fall in regions where characteristic absorbance bands of Co^{2+} [3, 14] can be observed. With regards to the NIR bands used for the red channel, the false color

can shift toward a darker purple depending on the contribution of other chromophores (most probably Fe^{2+} for pt. 5 LM-167924 and Cu^{2+} in case of pt. 2 and 5 AG-1170 and pt. 3 LM-167924). This theory seems to be supported by the comparison of the spectra of cobalt containing green glass (point 2 in AG-1170 and pt. 5 and 3 in LM-167924), with blue glass containing the same chromophore, as well as with available literature [2, 3, 13, 14, 16]. In any case, further investigations, and additional analytical techniques, are needed to confirm these theories.

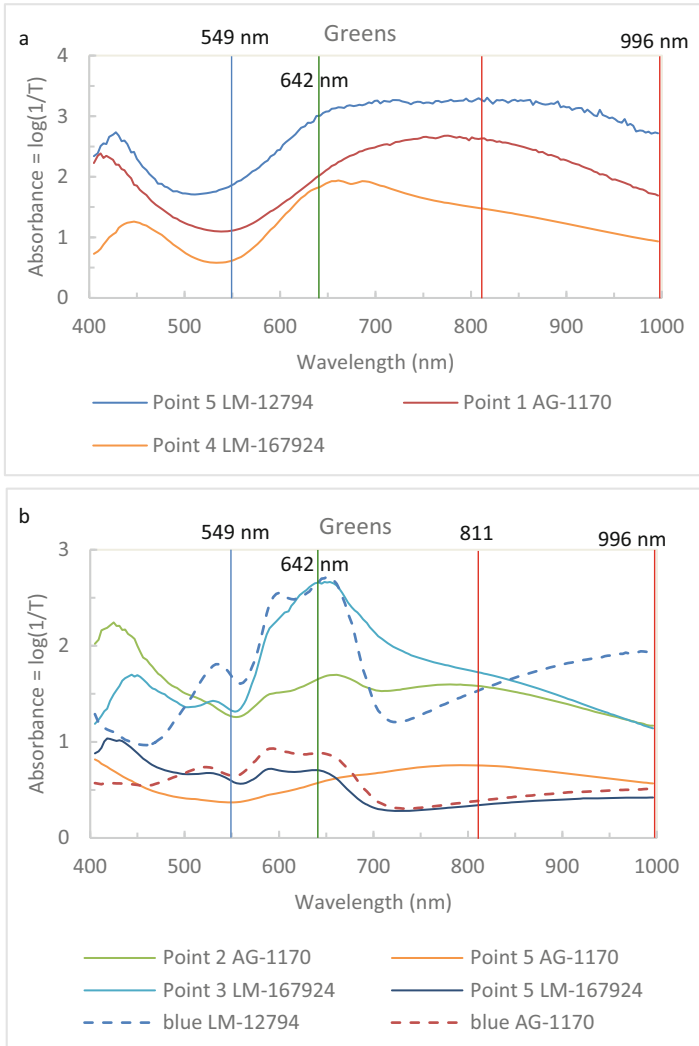


Fig. 5. Spectra of green glass collected on the three case studies. a) glass containing Cu^{2+} as main chromophore. b) glass containing Co^{2+} . Spectra of two blue glass containing cobalt have been added for comparison. The four lines (one for green and blue and two for the red) indicate the bands selected and for which RGB channel are they used. The localization of the points is displayed in Fig. 2a.

3.1 Limitation of the System

The use of a rotating stage instead of a linear translational system represents one of the biggest limitations of the setup. As already mentioned in the experimental section, the use of a rotational stage generates not only vertical distortion, which are related to the camera optics [17], but also horizontal distortion, caused by the rotation of the camera. If the resulting images are considered individually and used for the sole purpose of material identification, this aspect may be left aside. However, it can become an issue when attempting to stitch two images together. As shown in Fig. 1, the side opposite to the scanning direction results more elongated with respect to the other. If the overlapping part have been scanned in two different directions, the two images will not match, as the points taken as reference are shifted. This can be noticed for example by observing the two areas acquired from the panel AG-1170 (Fig. 2) where the two images seem stretched in two different directions. In addition, the movement of the camera causes the out of focus regions at the image edges, that can represent a distortion. From the spectral point of view, the out of focus does not hinder the quality of the spectral data collected (Fig. 7). However, it may become an issue during the stitching process, as the blurring reduces the quality of the final image. (Fig. 7c, d).

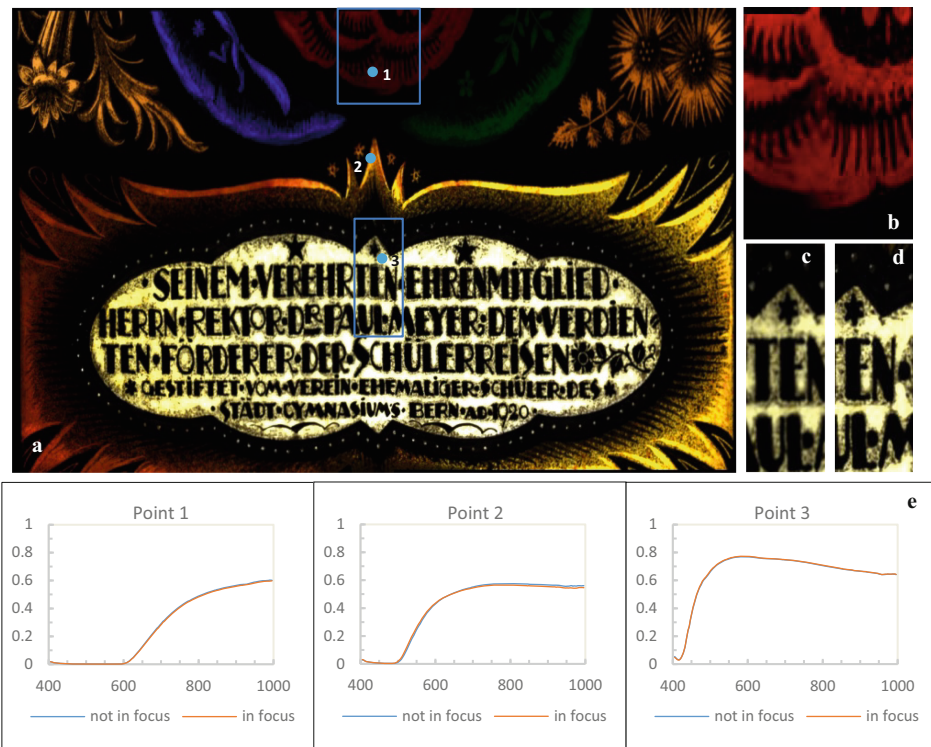


Fig. 6. a) Stitched image (RGB) of the lower part of LM-167914 obtained combining two datacubes. b) Detail of alignment error at the top of the image. c, d) Details of the overlapping areas, showing different focus due to the rotation movement of the camera. e) Comparison of the spectra collected from the overlapping area of the two datacubes.

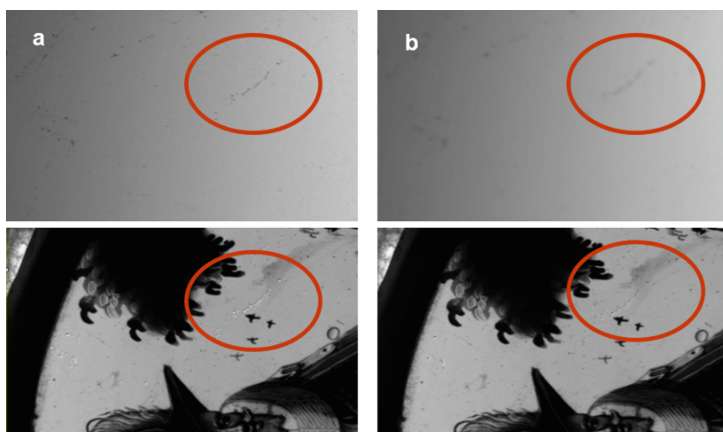


Fig. 7. Details of dirt particles on the diffuser (on top) and their effects on transparent glass (bottom) after flat fielding correction. Fig. b (bottom) show how the application of a Gaussian filter can slightly reduce the visual impact of the artifacts.

The material employed for the diffusing plate also play an important role. In this case, for the diffuser in contact with the artwork, an acrylic panel was preferred to a frosted glass one, as it was able to diffuse the light better. However, the electrostaticity of the acrylic attracts particles of dirt, that can accumulate on the surface despite constant cleaning. The presence of dirt on the diffuser surface can affect the flat fielding process, as the particles of dirt become artifacts in the corrected images.

These artifacts can be visible not only in areas with clean glass, but also in those with colored glass, when they are transparent to certain wavelengths. It was noticed that adding a Gaussian blur filter to the diffuser datacubes helped in reducing those artifacts. A sigma value of 3 was deemed enough for the purpose. The filter was not applied to the case studies datacube, to avoid the loss of details. Moreover, since the filter was applied only on the diffuser datacubes, it was decided to smooth only the spatial dimension, but not the spectral one, in order to avoid differences during the flat fielding process, where the object datacube must be divided by the diffuser one. Figure 8 shows the flat fielding results before and after adding the filter.

4 Conclusion and Perspectives

In this paper, a portable system for the hyperspectral imaging of stained-glass panels is presented, whose feasibility has been tested on selected set of stained-glass panels at the Swiss National Museum. At the moment, the system has some limitations, related to the necessity of using a rotational stage and to some design choices, such as the use of two diffusers, to reduce the heat coming from the light sources.

With regard to the first point, the issue of geometric distortions related to the rotation of the camera has been already discussed in the results section. Future works will be focused on addressing this aspect, by searching for solutions that can correct those distortions, especially in case image stitching is planned.

With regard to the second point, the advantages, or disadvantages of having two diffusers should be investigated more thoroughly. While this solution was helpful in reducing the heat, at the same time it was also limiting the light arriving to the artwork. These aspects can influence the acquisition, as compromises in choosing the right integration time must be done to avoid underexposure of dark glass, as well as a longer exposure time and consequent increase of noise. More efficient light sources should be explored so that the use of double diffuser could be avoided.

Despite these limitations, it was still possible to obtain a sufficiently good signal even for very dark glass and the quality of the data collected were satisfying. Regarding the image processing side, the use of false color images has been proved to be a useful tool for a preliminary identification of colored glass produced with different coloring agents. The comparison of these images with the spectra of the glass under study allowed to formulate some hypothesis, that could be confirmed in the future by complementary analysis.

An important aspect to stress is the constant collaboration with the Museum conservators and staff during the developing phase as well as during the acquisition. This collaboration has been fundamental to design the system in a way it could be possible to scan for a long period of time without damaging the panels. The use of such setup could be encouraged for documentation purposed during conservation treatments; the visualization of the data through rendered and false color imaging could be a fast tool for a first distinction of areas with possible restoration, without the need of complex classification algorithms.

Acknowledgements. This research was carried out as part of the CHANGE (Cultural Heritage Analysis for New Generation) Innovative Training Network project funded by the European Union's Horizon 2020 research and innovation programme under the Marie Skłodowska-Curie grant agreement No. 813789. The author would also like to thank the Swiss National Museum for giving access to the case studies and the Museum staff for the help and support before and during the acquisition campaign; Jan Cutajar and Deepshikha Sharma for helping in building the setup at the Museum; Federico Grillini and Irina Ciortan at NTNU and Silvia Russo for helping with logistic and shipping of the equipment to Switzerland and back.

References

1. Picollo, M., et al.: Hyper-spectral imaging technique in the cultural heritage field: new possible scenarios. *Sensors* **20**(10), 2843 (2020). <https://doi.org/10.3390/s20102843>
2. Rebollo, E., et al.: New trends in imaging spectroscopy: the non-invasive study of the Scrovegni Chapel stained glass windows. In: *Proc. SPIE O3A: Optics for Arts, Architecture, and Archaeology III* 8480 (2011). <https://doi.org/10.1117/12.888839>
3. Palomar, T., et al.: Analysis of chromophores in stained-glass windows using Visible Hyperspectral Imaging in-situ. *Spectrochimica Acta Part A-Molecular and Biomolecular Spectroscopy* **223** (2019). <https://doi.org/10.1016/j.saa.2019.117378>
4. Perri, A., et al.: Hyperspectral imaging with a TWINS birefringent interferometer. *Opt. Express* **27**(11), 15956–15967 (2019). <https://doi.org/10.1364/OE.27.015956>
5. Babini, A., George, S., Hardeberg, J.Y.: Hyperspectral imaging workflow for the acquisition and analysis of stained-glass panels. In: *Proceeding SPIE O3A: Optics for Arts, Architecture, and Archaeology VIII* 11784 (2021). <https://doi.org/10.1117/12.2593735>

6. Mandal, D.J., et al.: Influence of acquisition parameters on pigment classification using hyperspectral imaging. *J. Imaging Sci. Technol.* **65**(5), 50406–1–50406–13 (2021). <https://doi.org/10.2352/J.ImagingSci.Technol.2021.65.5.050406>
7. Palomar, T., Agua, F., Gomez-Heras, M.: Comparative assessment of stained-glass windows materials by infrared thermography. *Int. J. Appl. Glas. Sci.* **9**(4), 530–539 (2018). <https://doi.org/10.1111/ijag.12352>
8. Schindelin, J., et al.: Fiji: an open-source platform for biological-image analysis. *Nat. Methods* **9**(7), 676–682 (2012). <https://doi.org/10.1038/nmeth.2019>
9. Hayem-Ghez, A., Ravaud, E., Boust, C., Bastian, G., Menu, M., Brodie-Linder, N.: Characterizing pigments with hyperspectral imaging variable false-color composites. *Appl. Phys. A* **121**(3), 939–947 (2015). <https://doi.org/10.1007/s00339-015-9458-8>
10. Buoso, M.C., Ceccato, D., Zafirooulos, D.: False-color Infra Red Photography in the Identification of Pigments Used for a late 13th Century Illuminated Manuscript, in LNL Annual Report, Applied and Interdisciplinary Physics Instrumentation (2009)
11. Foster, D.H., Amano, K.: Hyperspectral imaging in color vision research: tutorial. *J. Opt. Soc. Am. A* **36**(4), 606–627 (2019). <https://doi.org/10.1364/JOSAA.36.000606>
12. Rochester Institute of Technology Useful Color Data. <https://www.rit.edu/science/munsell-color-science-lab-educational-resources#useful-color-data>. Accessed 08 Dec 2021
13. Bracci, S., et al.: Integration of both non-invasive and micro-invasive techniques for the archaeometric study of the stained-glass window Apparizione degli Angeli in the basilica of Santa Croce in Florence. Italy. *J. Cult. Heritage* **44**, 307–316 (2020). <https://doi.org/10.1016/j.culher.2020.02.006>
14. Hunault, M.O.J.Y., et al.: Thirteenth-century stained glass windows of the Sainte-Chapelle in Paris: an insight into medieval glazing work practices. *J. Archaeol. Sci. Rep.* **35** (2021). <https://doi.org/10.1016/j.jasrep.2020.102753>
15. Palomar, T., et al.: Chemical degradation and chromophores of 18(th) century window glasses. *Glass Technol. Eur. J. Glass Sci. Technol. Part A* **52**(5), 145–153 (2011)
16. Green, L.R., Alan Hart, F.: Colour and chemical composition in ancient glass: an examination of some roman and wealden glass by means of ultraviolet-visible-infra-red spectrometry and electron microprobe analysis. *J. Archaeol. Sci.* **14**(3), 271–282 (1987). [https://doi.org/10.1016/0305-4403\(87\)90015-X](https://doi.org/10.1016/0305-4403(87)90015-X)
17. Pillay, R., Hardeberg, J.Y., George, S.: Hyperspectral imaging of art: acquisition and calibration workflows. *J. Am. Inst. Conserv.* **58**(1–2), 3–15 (2019). <https://doi.org/10.1080/01971360.2018.1549919>

Paper 5

Reprint of:

Agnese Babini, Tiziana Lombardo, Katharina Schmidt-Ott, Sony George, & Jon Y. Hardeberg. (2023). Acquisition strategies for *in-situ* hyperspectral imaging of stained-glass windows: case studies from the Swiss National Museum. *Heritage Science*, 11(1), 74.

RESEARCH

Open Access



Acquisition strategies for in-situ hyperspectral imaging of stained-glass windows: case studies from the Swiss National Museum

Agnese Babini^{1*}, Tiziana Lombardo², Katharina Schmidt-Ott², Sony George¹ and Jon Yngve Hardeberg¹

Abstract

Over the last decade, hyperspectral imaging has become a popular technique for the non-invasive identification and mapping of painting materials in many typologies of artworks, thanks to the possibility of obtaining spectral information over the spatial region. A few attempts have also been made on stained-glass windows to identify the chromophore elements responsible for glass color. Hyperspectral imaging of stained glass can be complex; in most cases, stained-glass windows are an integral part of buildings, and sunlight represents the natural light source for illuminating these artifacts. While it may be considered an advantage, sunlight is not homogeneous throughout the day, and different weather conditions can affect the quality of the hyperspectral images. In addition, the presence of buildings and vegetation in the background could also modify the colors of the stained-glass windows and consequently alter the characteristic peaks of the chromophores in the spectra. This work aims to solve some of these issues and proposes different strategies to improve the results obtainable in situ. The methodology was tested on stained-glass panels displayed in the windows of the Swiss National Museum. Stained-glass panels located in windows of an internal wall were also analyzed, developing a lighting setup to account for the lack of natural light. Hyperspectral images of the selected stained glass were acquired multiple times, choosing different transmittance references for the preprocessing and exposure time to evaluate differences in the collected spectral images. The use of a diffuser sheet to mitigate the effect of external factors was also tested on some panels exposed to sunlight. Results from representative case studies will be presented to discuss the feasibility and limitations of in-situ hyperspectral imaging applications on stained glass and provide some general recommendations to consider during the acquisitions.

Keywords Stained-glass, Hyperspectral imaging, Transmittance, In-situ measurement

Introduction

Since its first application in the cultural heritage field, over the years, hyperspectral imaging (HSI) has become a versatile technique for the non-invasive investigation of works of art [1]. This technique is based on the acquisition of many images finely sampled across a portion of the electromagnetic spectrum; as a result, a three-dimensional image is created (often referred to as a datacube) consisting of two spatial and one spectral dimension. In this way, a full spectrum can be obtained in each pixel of the image, providing information on the materials used

*Correspondence:

Agnese Babini
agnesebabini3@gmail.com

¹ Department of Computer Science, NTNU - Norwegian University of Science and Technology, Teknologivegen 22, 2815 Gjøvik, Norway

² Collection Centre, Swiss National Museum, Lindenmoosstrasse 1, 8910 Affoltern Am Albis, Switzerland



© The Author(s) 2023. **Open Access** This article is licensed under a Creative Commons Attribution 4.0 International License, which permits use, sharing, adaptation, distribution and reproduction in any medium or format, as long as you give appropriate credit to the original author(s) and the source, provide a link to the Creative Commons licence, and indicate if changes were made. The images or other third party material in this article are included in the article's Creative Commons licence, unless indicated otherwise in a credit line to the material. If material is not included in the article's Creative Commons licence and your intended use is not permitted by statutory regulation or exceeds the permitted use, you will need to obtain permission directly from the copyright holder. To view a copy of this licence, visit <http://creativecommons.org/licenses/by/4.0/>. The Creative Commons Public Domain Dedication waiver (<http://creativecommons.org/publicdomain/zero/1.0/>) applies to the data made available in this article, unless otherwise stated in a credit line to the data.

as well as their distribution across the artwork under study [2]. Various HSI systems have been developed to analyze and document paintings on different supports, manuscripts, and photographic materials [1–9]. A few papers have also been published recently regarding the application of HSI on stained-glass windows to identify the chromophore elements responsible for glass color [10–15]. However, research on this topic is still limited; imaging stained glass can be complex, and many factors must be considered. If the stained glass panels are removed from their original location (e.g., for restoration treatments), or in the case of separately stored panels, it is possible to use acquisition systems based on standard transmittance geometry and stable light sources, such as halogen lamps [13, 15]. Thanks to these characteristics, such setups allow for comparable results to UV–VIS–IR spectroscopy, a widely used technique to analyze historical and archaeological glass [14].

However, in most cases, stained-glass windows are an integral part of buildings, and due to their transparency, solar radiation represents the natural light source for the illumination of these artifacts. Palomar et al. [12], were the first to explore the potential of this technique to identify the chromophore elements of an Art Nouveau stained-glass window, exploiting solar radiation as a light source. The work showed promising results, and the authors were able to distinguish and map glass with the same color and composition but different transparency, despite the changing light conditions. Nonetheless, the paper stressed how the vegetation in the background could affect the spectra of light-colored glass and the difficulties in identifying the chromophores in the spectra of dark-colored glass. Funatomi et al. [10], explored the possibility of reconstructing a spectral datacube from raster scanning fiber optic to solve the issue of illumination variation during the acquisition. However, the proposed methodology is still in the experimental stage and is not publicly available.

The aim of this research is to propose acquisition strategies to tackle those challenges and improve results from *in-situ* hyperspectral imaging of stained-glass windows using a commercially available camera. The proposed methodology was tested on eight stained-glass panels displayed in windows at the Swiss National Museum, chosen after discussion with the museum conservators considering various factors related to the environment and the artwork characteristics. In order to evaluate the quality of the HSI datacubes obtained in different contexts, all the case studies were captured multiple times, selecting various transmittance references for the pre-processing. Some panels exposed to sunlight were captured before and after placing a diffusing sheet behind the windows and, in a few cases, acquired at different

moments of the day. To the best of the authors' knowledge, this is the first time HSI has been applied to analyze stained glass in such a systematic way.

Stained-glass panels located in windows of an internal wall were also chosen; since they are not directly exposed to the sun, the analysis of these case studies allowed studying a different solution to make the acquisition possible. A lighting setup consisting of a photography light diffuser and a halogen lamp was developed and tested for the purpose.

Results from five representative case studies, four exposed to natural sunlight and one from the internal wall, will be presented to compare the different acquisition scenarios (natural vs. artificial illumination) and discuss the proposed methodology's contributions and limitations.

Experimental

Case studies

Eight stained-glass panels were chosen for the experiments; the selection was based on the panels' location, sun exposure, homogeneity of the background behind the windows, and artistic attributes. The influence of these parameters will be discussed in detail in "Results" section. Six of those panels are displayed within the external windows of the Swiss National Museum, while two are located in windows of an internal wall. After a preliminary data interpretation of all eight case studies, five of them were chosen as the most representative to discuss the main findings of the research and answer specific research questions. Technical information, the number of acquisitions performed, and the research questions addressed by each case study are summarized in Table 1.

Regarding the discarded case studies, one of them was made of very dark-colored pieces of glass, and it was impossible to obtain satisfying results. The other two case studies, one exposed to sunlight and one located in the inner window, have very similar palettes to the case studies discussed in this paper. For this reason, it was decided not to include them in the manuscript; however, results from these two panels are available in Additional file 3.

Setup

A portable push-broom hyperspectral camera (Specim IQ, Specim, Spectral Imaging Ltd.) was employed for the experiments. The camera acquires 204 bands between 400 and 1000 nm in visible and near-infrared (VNIR region) and has a spatial sampling of 512 pixels per line. Since the number of imaged lines is fixed to 512, the result is a square image with a resolution of 512×512 pixels. The field of view is $31^\circ \times 31^\circ$. The image's actual resolution depends on the distance the camera was

Table 1 Summary table containing technical information, the number of acquisitions taken, and the research questions for each case study analyzed in the paper

Case studies	Information	Number of acquisitions	Research questions
IN-64.11	Author: Hans Caspar Lang Date: 1609 Dimension: Ø 19,6 cm Location: Lochmannsaal Description: Allianzscheibe. Ornamental rim with scroll-work motifs and putti heads. Content: Alliance coat of arms Hans and Barbara Im Thurn-Peyer. Lion head motif (coat of arms)	13	Effects of background Effects of selection of different areas as reference for Radiometric correction evaluation of differences in acquisitions taken at different times of the day
AG-1177	Author: N/A Date: 1574 Dimension: Ø 21,5 cm Location: Lochmannsaal Description: Allianzscheibe. The two coats of arms stand between two strong columns in front of a colorless background. Content: Alliance coat of arms of Marx and Margaretha Escher-Blarer von Wartensee	12	Effects of background and vegetation Effects of selection of different areas as reference for radiometric correction
LM-8368	Author: N/A Date: 1599 Dimension: 31,8 × 22,2 × 0,6 cm Location: Roseburgsaal Description: Bauernscheibe. Man as halberdier in a blue robe, his wife in a red skirt. Content: Married couple Jos Abderhalden. Dairy farming (upper image)	4	Effects of background and vegetation Effects of selection of different areas as reference for radiometric correction
LM-749	Author: N/A Date: 1627 Dimension: 30,2 × 19,6 cm Location: Seidenhof (internal wall) Description: Wappenscheibe. Queen of Sheba at King Solomon, giving him the flower riddle. Content: personal coat of arms Christoph Werdmüller	8	Development of a setup for stained glass not exposed to sunlight Material identification and distinction
LM-660.1	Author: N/A Date: 1567 Provenance: Entlebuch Dimension: 46,1 × 33,5 × 0,7 cm Location: Rosenburgsaal Description: Bannerträgerscheibe from Entlebuch. Content: horseman	6	Effects of background and vegetation Material identification and distinction

positioned during the measurement. Details are given in Additional file 1: Tables s1–s5).

Further technical details regarding the camera are described in [16, 17]. Compared to other line scanner cameras, which are relatively heavy and must be mounted on translating or rotating stages, this camera has the advantage of being smaller, lighter, and more compact and offers easy mobility within the museum's spaces. The museum environment was an important aspect to consider since the rooms have historical walls and floors, and fragile artworks are exposed in the proximity of the area required for the scanning. For this reason, portable cameras like the Specim IQ were preferred for the experiment.

The camera was mounted on a tripod that could reach a maximum height of around 220 cm (Fig. 1). A table was used in specific cases to achieve an optimal height. Since

the camera offers the flexibility to adjust focus distance, it was possible to place it in a way that allowed acquiring the entire panels in a single acquisition. Sunlight was used as the light source for all the panels except for LM-794, which is installed in the window of the internal wall. In this case, a temporary transmittance setup was developed using a photography light diffuser and a halogen lamp (Fig. 2).

All the configurations were previously evaluated in the laboratory using mock-up glass. Those tests were crucial to optimize the acquisition process since the time allocated for the imaging campaign was constrained by the museum's opening hours, and only 2 days were available on site.

In order to evaluate the best imaging conditions and parameters, the panels were acquired multiple times. With regard to the panels exposed to sunlight, a novel

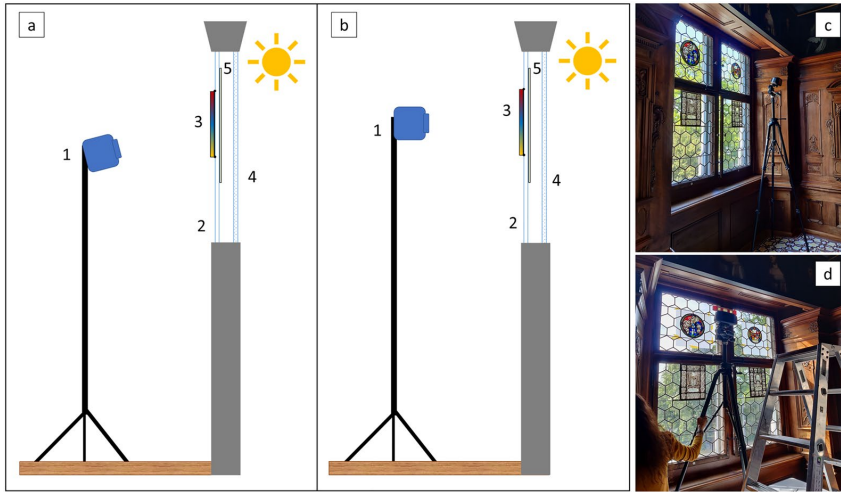


Fig. 1 a, b Schematics of the set-up for the stained-glass panels exposed to sunlight: 1) hyperspectral camera; 2) historical glass; 3) stained-glass panel; 4) modern glass. 5) Baking paper (diffusing sheet). c, d Pictures of the setup in use during the campaign

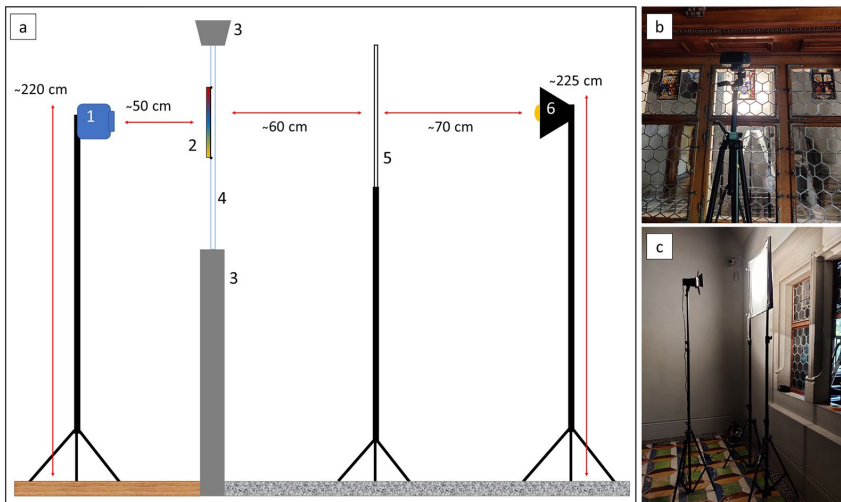


Fig. 2 a, b Schematics of the set-up for the stained-glass panels exhibited in the inner wall: 1) hyperspectral camera; 2) stained-glass panel; 3) wall; 4) historical glass; 5) diffusing fabric; 6) light source. c, d Pictures of the setup in use during the campaign

approach was tested to limit the interference of the environment behind the windows on the color of the glass. This approach involves placing a baking paper sheet behind the stained glass to be analyzed. The baking paper represented an affordable yet efficient solution to diffuse the light since it is thin, lightweight, and easy to attach to glass surfaces using simple masking tape. This method

could be implemented because the stained-glass panels are encased in historical windows, which were moved and integrated into the museum spaces together with the stained-glass panels. These historical windows are, in turn, protected by additional modern windows (Fig. 3).

After discussing with the museum conservators, it was possible to open the historical windows partially and



Fig. 3 Examples from the acquisitions of case studies IN-64.11; the diffusing sheet is placed on the glazing (historical window) behind the stained glass panel, so that it is not in touch with the artwork. In case of IN-64.11 the historical window was kept open to avoid having the tower (on the left side) within the field of view during the acquisition. For the other case studies the historical windows were closed after placing the diffusing sheet

attach the diffusing sheet behind the stained-glass panel (Fig. 3).

Figure 4 shows the rooms' orientation and the stained-glass panels' location within the room. Additional file 1: Tables s1–s5 reports the conditions and parameters of the acquisitions of the five stained glass panels discussed in this paper. Figures showing the sun's position during the acquisitions of IN-64.11, AG-1177, and LM-8368 are available in Additional file 1: Figs. s1–s3).

Image preprocessing

The image preprocessing is performed by the camera software directly during the acquisition. The default recording mode of the camera was used for almost all the recordings; in this mode, there are two options to perform the radiometric correction from raw data to reflectance (transmittance in this case). The first option ("simultaneous mode") is to select an area representing the white reference from the scene itself. The stored signal is then used to process the image before saving it (Fig. 5). The second option ("custom mode") allows the user to record and store the entire background as a reference. This reference can then be used for all the subsequent measurements. Since it was not possible to completely open the windows to capture the background,

"simultaneous mode" was used for almost all the acquisitions. An attempt to use custom mode was performed only on case study LM-660.1 since it is located in a window that can be fully opened, but it was decided that presenting the results from this mode was beyond the scope of this paper. A detailed workflow of the camera acquisition process is described by Behmann et al. [16].

Once the acquisition is finished, the obtained output is a dataset made of separate folders containing the raw datacube (together with the dark current and the white reference data), the processed datacube, and the meta-data file. The processed datacubes were analyzed through the Fiji implementation of the open-access software ImageJ [18].

Results

Panels exposed to solar radiation

In order to understand the main contribution of in situ hyperspectral imaging of stained-glass windows, it is important first to address the most common challenges that must be taken into consideration during the imaging process. With regards to the stained-glass windows exposed to sunlight, these challenges can be distinguished into three groups:

- Camera-related: transmittance reference acquisition, storage, and use during the radiometric correction process.
- Imaging environment-related: changes in lighting conditions while utilizing solar radiation as the source of light due to the variation of sun position; changes in atmospheric condition; the presence of buildings, vegetation, or other such obstacles behind the stained glass; noise from atmospheric water (H_2O) absorption band in NIR region (925–970 nm) [16].
- Object-related: transparency, translucency, and thickness of the colored glass; possibility to select a suitable transmittance reference (transparent glass) within the field of view; chemical composition of the reference transparent glass.

Despite this categorization, it is important to stress that those challenges are closely intertwined and should not be considered separately. In this section, results from the selected case studies will be shown to provide practical examples of the effects of these factors and the solutions adopted to limit them.

Reference selection: consequences of a non-homogeneous background and light variation

The selection of a suitable reference for radiometric calibration is a fundamental aspect to take into consideration

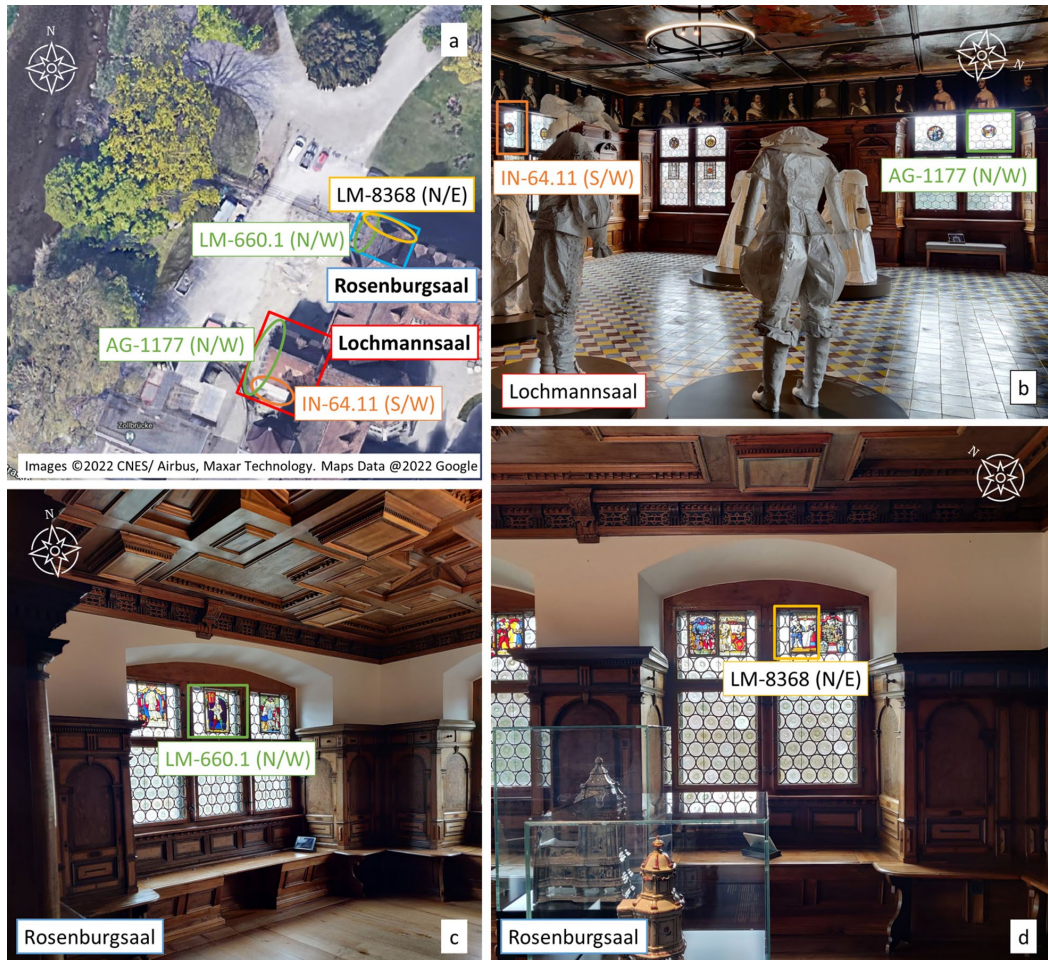


Fig. 4 a Aerial view of the Swiss National Museum, showing the overall orientation of the rooms and the selected panels. b–d Figures showing the specific location of each panel within the room where they are exhibited

during HSI acquisition and processing. The best option would be to acquire an image of the background without the stained glass, representing the light distribution of the entire field of view, ideally as homogeneous as possible. In most in-situ scenarios, however, the stained glass occupies the whole window space, and often the reference must be selected from transparent pieces within the stained glass itself.

Referring to the case studies presented in this paper, two distinct scenarios can be noticed. In the first case, the panels are installed in a historical window consisting of flat hexagonal glass panes (Fig. 6).

In this case, the reference can be picked in one of the panes closer to the panel, and since they are relatively large, the signal obtained can be considered representative of at least a portion of the stained glass. In the second scenario (see section "Stained glass within crown-glass windows", Fig. 12a), the stained-glass panels are located within a crown glass window; in this case, only the tiny glass triangles between the crown glass can be used for image processing since they are flat and uncolored. The availability of such a small area as a reference represents a disadvantage, as it can be considered representative of only a minimal part of the field of view. In the following



Fig. 5 Reference region selection step during the acquisition process of the case study LM-660.1 (a) and LM-789 (b). The camera shows areas with the same intensity (in white) from where the most suitable reference can be chosen (in green)

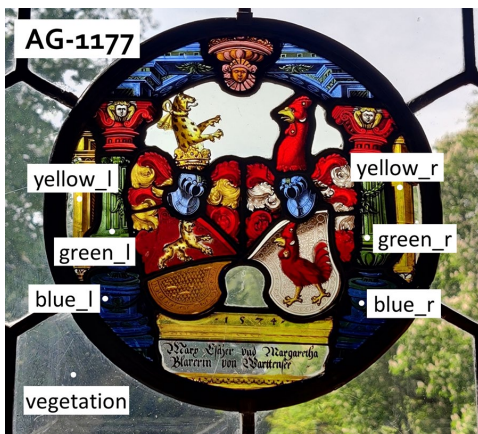


Fig. 6 Close-up picture of case-study AG-1177, showing the points selected for the spectra comparison. The vegetation in background is very visible from the transparent glass surrounding the stained-glass

sections, examples from the two scenarios will be shown to demonstrate how these situations affect the quality of the results.

Stained glass within windows with hexagonal panes Figure 6 shows the example of case study AG-1177; the panel is oriented North/West, which means it receives most of the sunlight in the afternoon from the left side. At the moment of the acquisition, the sky was cloudy; in addition, trees can be observed in the background.

The first step to exclude the presence of the trees inside the camera field of view was to tilt the camera to a certain degree (see Table 1s in Additional file 1 for details). Since

the tilting angle is relatively small (15° on average), the geometric distortions are negligible and do not affect the data interpretation. Despite this solution, however, it can be noticed that the trees are still visible on the left side in acquisitions #1 and #2 (Fig. 7a and e).

Figure 7b–d and f–h show how the spectra of glass sections with the same color appear entirely different, whether collected from the left or right side of the panel. In fact, it can be noticed that the characteristic peaks of chromophores are covered by the signal of vegetation in all the spectra obtained on the left side. In this case, the possibility of placing a diffusing sheet behind the stained glass, covering the entire field of view, represented a good solution to improve the quality of the spectra taken from the left side, as the peaks associated with the vegetation are eliminated (Fig. 7j–l).

Nonetheless, despite the use of a diffusing sheet, variations of spectra intensity and shape can still occur. Figure 8 shows six acquisitions carried out in different configurations: the first group (acquisitions #4, #6, and #7) was acquired between 4:40 pm and 4:45 pm, with the camera tilted at around 15°. The second group of images (#9, #10, and #12) was recorded between 5:30 and 5:40 pm with the camera facing the panel straight. In addition, for each group, the transparent reference was selected in three different areas: on the right (acquisitions #4 and #9), inside the panel (acquisition #6 and #12), and on the left (acquisition #7 and #10) (Fig. 8).

Figure 9 shows the spectra plots obtained from yellow, green, and blue glass selected on the left and right sides of the panel. For each colored glass, the comparison is also made between the pair of datacubes acquired with the same hexagonal glass pane as reference but taken at different camera inclinations. In most cases, the spectra from the two sides are more comparable, sometimes even overlapping, when taken from the second group of images (orange, red, and yellow lines). Having the camera facing straight may have contributed to improving the results for the second group of datacubes; however, the main reason behind this behavior is most probably related to the sun's position during the acquisitions.

The six acquisitions were made within one hour, from around 4.40 pm to 5.40 pm. Since the panel is exposed North/West and the datacubes were collected in mid-late afternoon, the sunlight hit the stained-glass panel from the left side. It can be noticed from Fig. 8c–f how acquisitions #7 and #10, where the reference was selected on the left side, are less affected by the light changing during the imaging session, as the two images show a similar light distribution. On the other hand, acquisitions #4 and #9 show some differences, especially in the lower part of the image, which appears less illuminated in acquisition #9. This may also explain why the spectra of acquisitions #7

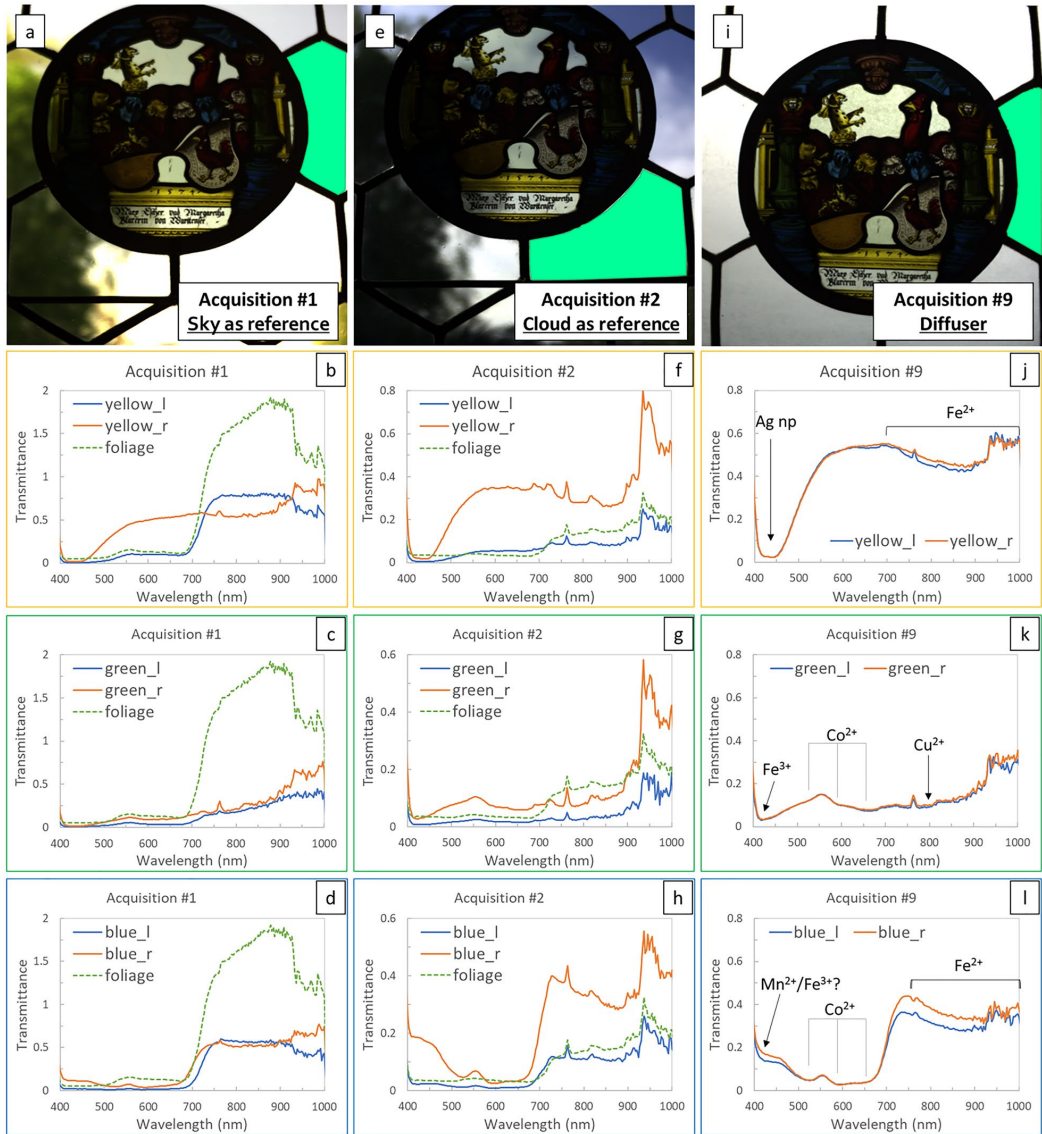


Fig. 7 a, e, i Pictures showing the areas chosen as transmittance reference (in green). b–l) spectra comparison for the three selected colors (yellow, green, and blue) from acquisition #1 (b–d), acquisition #2 (f–h) and acquisition #9 (j–l). The bands’ position of the main chromophores (np = nanoparticles) are indicated with arrows, except for Fe^{2+} . Since the maximum of the Fe^{2+} band falls outside the camera spectral range (1100 nm), and the NIR region is quite noisy, it was preferred to indicate the band width for this chromophore. The peak at 750 nm is an artifact probably due to the sunlight spectrum or interference from the atmosphere. Postfixes in curve labeling: l = left; r = right. Figure 6 shows the points where the spectra were taken



Fig. 8 Pictures showing the areas chosen as transmittance reference (in green) for the acquisitions #4 to #12 of the case study AG-1177. The differences between the pictures in the first row and the ones in the second row are due to the inclination of the camera during the recording of the first set of images. Acquisitions #4 and #9 (a, d), #6 and #12 (b, e) and #7 and #10 (c, f) were processed using the same glass pane. Some paper sheets were also placed on the sides of the panel during acquisition #12 to decrease the contrast between the dark colored glass and the transparent ones

and #10 are more comparable in terms of intensity than the other two couples of datacubes.

Different spectral shapes are clearly visible, especially in the NIR region for the spectra obtained from the datacubes processed with the stained glass and those processed with the transparent glass from the historical window. These differences influence the identification of the signature band of ferrous iron (Fe^{2+}), characterized by a broad absorption with a maximum at around 1100 nm [19, 20] (outside of the Specim IQ camera sensitivity), and it is related to the chemical composition of the glass selected as the reference. This aspect will be explained further in the "Discussion" section.

Another example of the influence of light variation is given by case study IN-64.11 (Fig. 10); this panel is oriented South/West and, differently from AG-1177, has a clear background. A tower outside can be seen on the left side, but the possibility of partially opening the window

(Fig. 3) allowed for excluding its presence in the image during the HSI acquisition.

The HSI of this stained glass was performed at two specific moments of the day. The first set of images (acquisitions #7 and #9) was recorded in the late morning (11.20–11.25 am); the sun was high in the sky but covered by the tower outside on the left. The second set was recorded mid-afternoon, between 15.46 and 16.17 (acquisition #10 and #13), with the sun well visible on the right side of the field of view.

As for the case study AG-1177, three pairs of colored glass present specularly on the left and right sides were chosen for comparison. It can be noticed how the spectra taken from the datacubes recorded in the morning (#7 and #9) are separated into two distinct groups. The first group (Fig. 11, light-colored lines) represents the spectra taken from the right side of the two datacubes, while the second one (Fig. 11, dark-colored lines) represents the ones taken from the left side. In general, the spectra collected on the right side seem to have a lower intensity

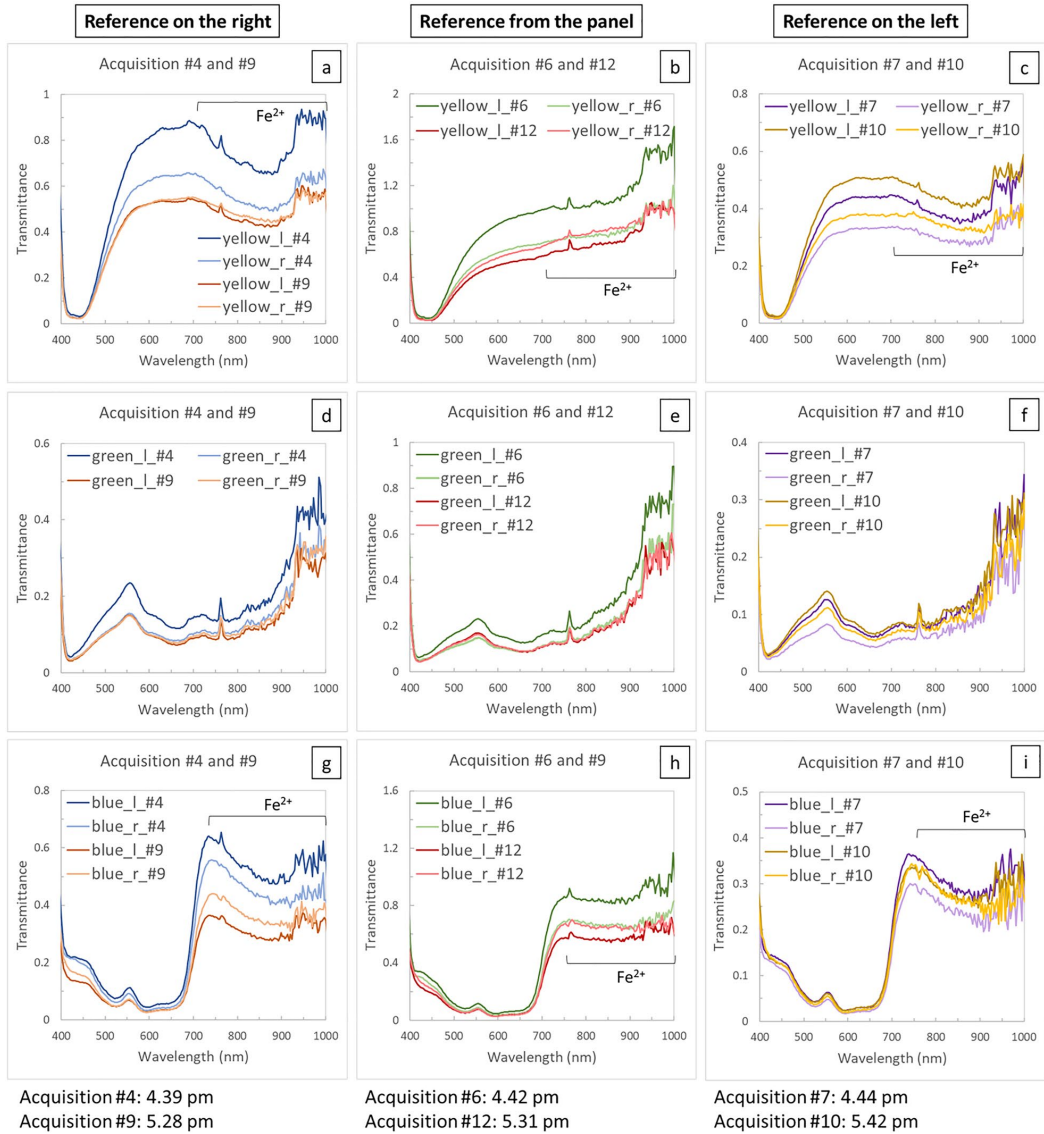


Fig. 9 Comparison of spectra obtained on the left and right side from the pair of datacubes processed using the same glass pane as reference for the three selected colors (yellow, green, and blue). The width of the band in the NIR region associated to Fe²⁺ is indicated. The peak at 750 nm is an artifact probably due to the sunlight spectrum or interference from atmosphere. Notice how the band of Fe²⁺ tends to disappear when the radiometric correction is performed using a transparent area inside the stained-glass panel as reference. Figure 6 shows the points where the spectra were taken

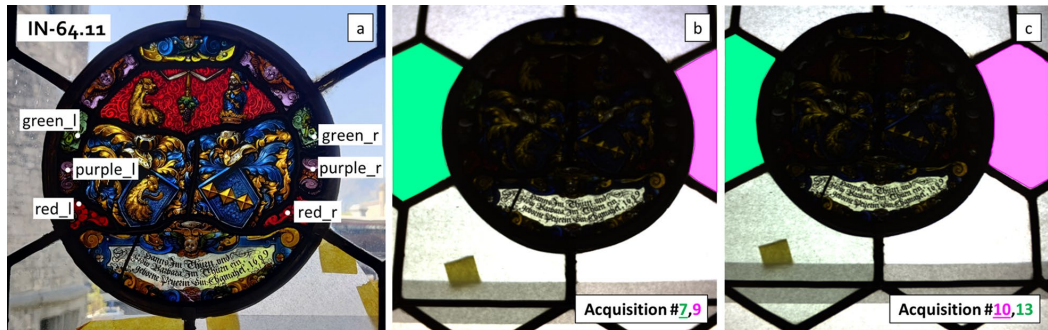


Fig. 10 **a** Close-up picture of case-study IN-64.11, showing the points selected for the spectra comparison. **b** Picture showing the areas chosen as transmittance reference for two of the acquisitions taken in the morning (#7, in green, and #9, in pink). **c** Picture showing the areas chosen as transmittance reference for two of the acquisition taken in the afternoon (#10, in green, and #13, in pink). The underlined number indicates the database from which the RGB image was taken

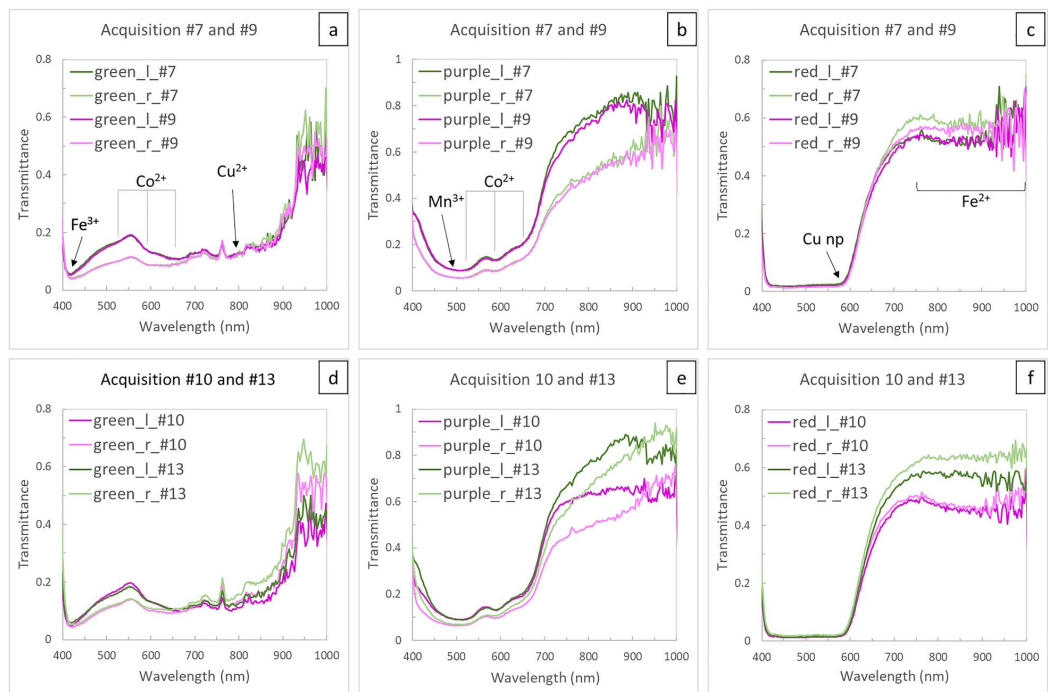


Fig. 11 **a–c** Comparison of spectra obtained on the left and right side from the pair of databases recorded in the morning, for three selected colors (green, purple, and red). **d–f** Comparison of spectra obtained on the left and right side from the pair of databases recorded in the afternoon, for the three selected colors (green, purple, and red). The bands' position of the main chromophores (np = nanoparticles) are indicated with arrows, except for Fe^{2+} . Since the maximum of the Fe^{2+} band falls outside the camera spectral range (1100 nm), and the NIR region is quite noisy, it was preferred to indicate the band width for this chromophore. The small peak at 750 nm in **a** and **d** is an artifact probably due to the sunlight spectrum or interference from atmosphere. Postfixes in curve labelling: l = left; r = right. Figure 10 shows the points where the spectra were taken

than those taken from the left side, except for the red-colored glass. It is also worthy of mention that the spectra in the two groups seem to overlap almost perfectly regardless of where the transmittance reference region was selected.

On the other hand, the spectra from the datacubes collected in the afternoon (#10 and #13) show an opposite trend. In this case, the spectra taken from the two sides of the same image are more similar in intensity and shape. At the same time, a difference in the NIR region can be observed between the two datacubes, especially in the red and purple glass. These variations may be explained as follows:

- Morning acquisitions: the stained glass does not receive any direct light in the morning, and the window is open towards the inside from right to left. Thus, the spectral differences may depend on the fact that the left side is less exposed to the light, resulting in spectra with lower intensity.
- Afternoon acquisition: in this case, the sunlight hit from the right side almost directly on the stained glass. This situation probably reduced the variations related to the differences in sunlight exposure of the two sides and enhanced those associated with the selection of the glass pane for transmittance reference. As for the case study AG-1177, a slight difference in the red—NIR region (750–1100 nm) can be noticed, whether the radiometric correction has been performed using a glass panel or another reference. This aspect will be commented on further in "Discussion" section by comparing the results from other case studies presenting a similar situation.

Stained glass within crown-glass windows As mentioned at the beginning of the section, the HSI of stained-glass panels within a crown glass window (Fig. 12) represents a more challenging task than those in windows made of hexagonal panels. The case study LM-8368 was chosen as a representative example to show the consequences of this scenario. The panel is oriented North/East and does not receive direct sunlight at any time of the day. It also faces an urban green area, and many trees are visible in the background, even after applying the diffusing sheet. The strong impact of the vegetation signal is demonstrated by visualizing the false color image of the panel (Fig. 12b, d, f). The false-color image was created with the Fiji software by selecting three images from the datacube corresponding to the green (549 nm), the red (643 nm), and the NIR (811 nm) bands. Those single images were rearranged into a new RGB image, putting the infrared image first, then the red and the green. The result is an image that

enhances the difference between similar colors but with different spectral features [21, 22]. In this case, for example, three different situations can be observed depending on which transparent area has been used to perform the radiometric calibration.

The bright pink color visible in most of the transparent areas of the window not covered by the diffuser can be correlated to the vegetation signal, as the images selected for the blue and the green bands fall in regions where the characteristic bands of leaf pigments can be observed (Fig. 13) [23, 24]. The pink color, in different tones, can also be observed in the transparent areas covered by the diffuser in acquisitions #1 and #2, while it is almost absent in acquisition #3. Spectral variations presented in Fig. 13 show the change in intensity of the transmittance band, starting at 700 nm. This is more or less proportional to the intensity of the leaf pigments' bands (500–700 nm) in acquisitions #1 and #2. In acquisition #3, on the other hand, the band's intensity is reduced, but the signal of the leaf pigments is still relatively high. The lower intensity of the band in the NIR might be the reason for the bluish color. This difference in the false color appearance may be correlated to the fact that the three areas where the reference has been taken show a variable amount of vegetation. It might be possible that the signal of vegetation (or the lack of it, as in the case of acquisition #1—see Figs. 12a and 14a) has impacted the radiometric correction in different ways.

The disadvantage of using a tiny area for the radiometric calibration, with such an inhomogeneous background, is well demonstrated by looking at the spectra of red and yellow colored glass. It can be observed from Fig. 14 that the shape of these spectra is distorted depending on the position of the reference glass in relation to the colored glass. Practically, if the reference glass is selected from the upper part of the window (Fig. 14, turquoise area), all the spectra taken from that part until half of the stained glass appear perfectly smooth. On the other hand, the spectra taken from different locations will show an absorbance band starting abruptly at around 700 nm, which may be related to the signal of the vegetation present in the lower part of the stained glass (Fig. 14b, c). The same reasoning can be done if the reference is selected from the lower portion of the window; in this case, the vegetation signal will appear as a bump starting at around 700 nm (Fig. 14d, e). In both cases, these distortions are generated because the area selected as a reference is too small to be considered representative, especially when two highly different areas are in the background. In this case, performing two distinct acquisitions is a good solution to obtain the best results for both halves of the stained glass.



Fig. 12 **a, c, e** RGB images created by the camera after the acquisition, showing the area where the reference was collected (turquoise triangle for acquisition #1, magenta area for acquisition #2 and green triangle for acquisition #3); **b, d, f** false color images for each of the acquisitions. The band used to create the false color are stated in Fig. 13. The yellow circle indicates the area where the signal of vegetation (see Fig. 13) was taken. The black pixels visible in the small triangular glass pane and partially in the crown glass on the top left are saturated pixels

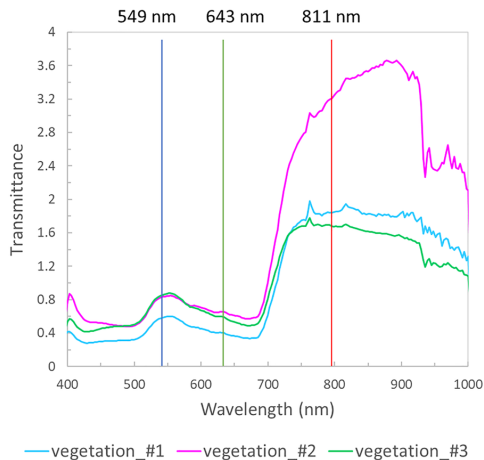


Fig. 13 Spectra of vegetation taken from the small triangle on the bottom-left corner (yellow circle) in Fig. 12. The three lines indicate the wavelengths related to the images selected to reconstruct the false-color image, while the colors of the lines indicate which RGB channel each image substitutes

Internal wall

One of the most significant advantages of analyzing panels within a window of an internal wall is the

possibility of using a stable light source instead of solar radiation. This way, the issues related to light variation and noise from the atmosphere signal could be eliminated; however, developing a proper setup to diffuse the light can still be challenging.

As shown in Fig. 2, the lighting setup used in this work consisted of a single halogen studio light positioned in the center of the object under study. The light is diffused by a diffusing textile material commonly used in photography studios, held by a makeshift stretcher and two poles. The studio light and the diffusing fabric were placed at a long distance from each other and from the object to improve the light distribution across the field of view (Fig. 2). However, this was not sufficient to obtain a perfectly diffused illumination. It can be observed from Fig. 15 that the light distribution is characterized by an intensely illuminated area that gradually loses intensity at the edges. The difficulties in keeping the diffusing textile well stretched also contributed to the sub-optimal lighting conditions. The folds generated by the lack of rigidity of the fabric contributed to generating additional shadows within the field of view.

Figure 16 shows the comparison between acquisitions #7 and #6. Acquisition #7 was performed by using a glass pane from the right, and acquisition #6 by using a transparent glass piece inside the stained glass. It can

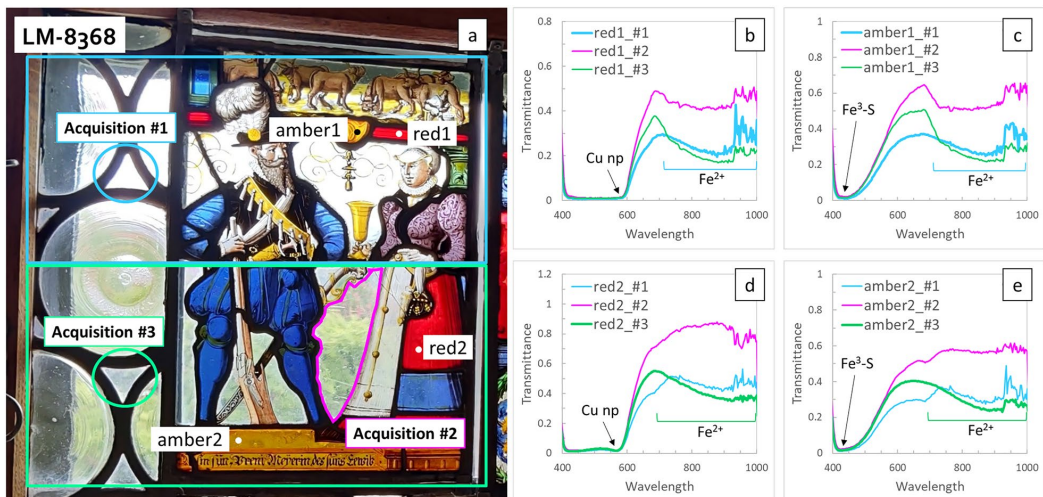


Fig. 14 **a** Close-up picture of case study LM-8368. The green and blue triangle and the magenta border indicates where the references were taken for the three acquisitions. The blue and green rectangular areas delimits the area where the associated reference performs well. **b–e** Spectra comparison for amber and red colored glass from three acquisitions performed using three different Fe transparent areas as reference. The bands’ position of the Cu nanoparticles (np) and the Fe^{3+} -S complex are indicated with arrows. Regarding Fe^{2+} , it was preferred to indicate the band width for this chromophore, since the maximum of its band falls outside the camera spectral range (1100 nm), and the red-NIR region is distorted by noise and artifacts from the radiometric correction

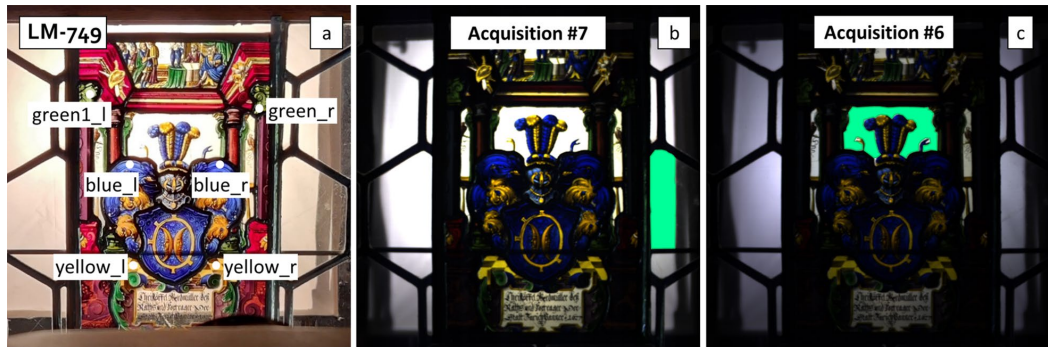


Fig. 15 a Close-up picture of case-study LM-749, showing the points selected for the spectra comparison. b, c Pictures showing the areas chosen as transmittance reference (in green)

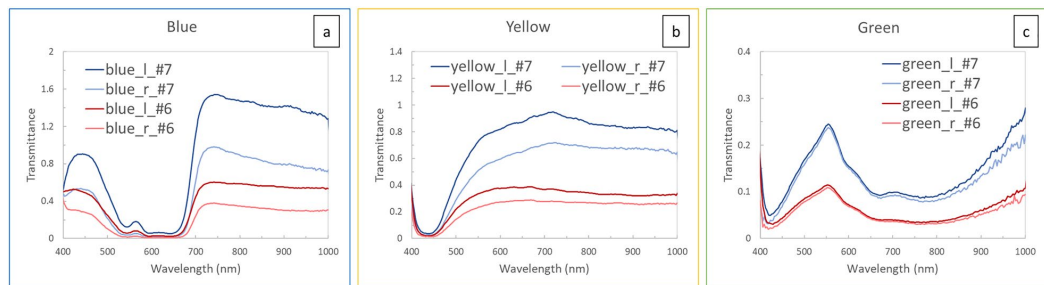


Fig. 16 Comparison of spectra obtained on the left and right side from acquisitions #7 and #6 for three selected colors (blue, yellow, and green). Figure 14 shows the points where the spectra were taken

be noticed that the spectra from acquisition #6 are flatter and smoother in the region after 700 nm, a situation similar to the case study AG-1177. The explanation behind this phenomenon will be discussed in detail in the following section.

Discussion

Importance of reference selection: considerations on chemical composition and background influence

As mentioned in "Results" section, in some case studies (AG-1177, IN-64.11, and LM-749), the spectra present a different shape, whether the radiometric correction is performed using a transparent glass from the stained glass or one of the window panes as reference. Two specific variations can be observed: in the first scenario, such as in the case of AG-1177, the large absorbance band in the NIR region, usually associated with ferrous iron (Fe^{2+}), disappears (Fig. 17, green and red lines) when the transmittance reference is chosen from inside the stained

glass. This phenomenon is especially visible in yellow and blue glass (Fig. 17b, c).

By observing the spectra obtained from the datacubes corrected with one of the window's panes (Fig. 17a, blue, orange, gray, and yellow line), the transparent glass of the stained glass likely contains a certain amount of iron as well. Unfortunately, it was impossible to perform XRF analysis on the transparent section of the stained glass, as the area was too small to fit the head of the instrument. However, the spectra seem comparable with results published in the literature regarding the analysis of historical windows [20, 25].

From these considerations, it is possible to hypothesize that, during the image processing, the Fe^{2+} bands are subtracted from the rest of the colored glass, disappearing. If Fe^{2+} is not present in the colored glass in the first place, the distortion appears as an increase of the signal in the NIR region, as shown in the example of the green glass (Fig. 17d).

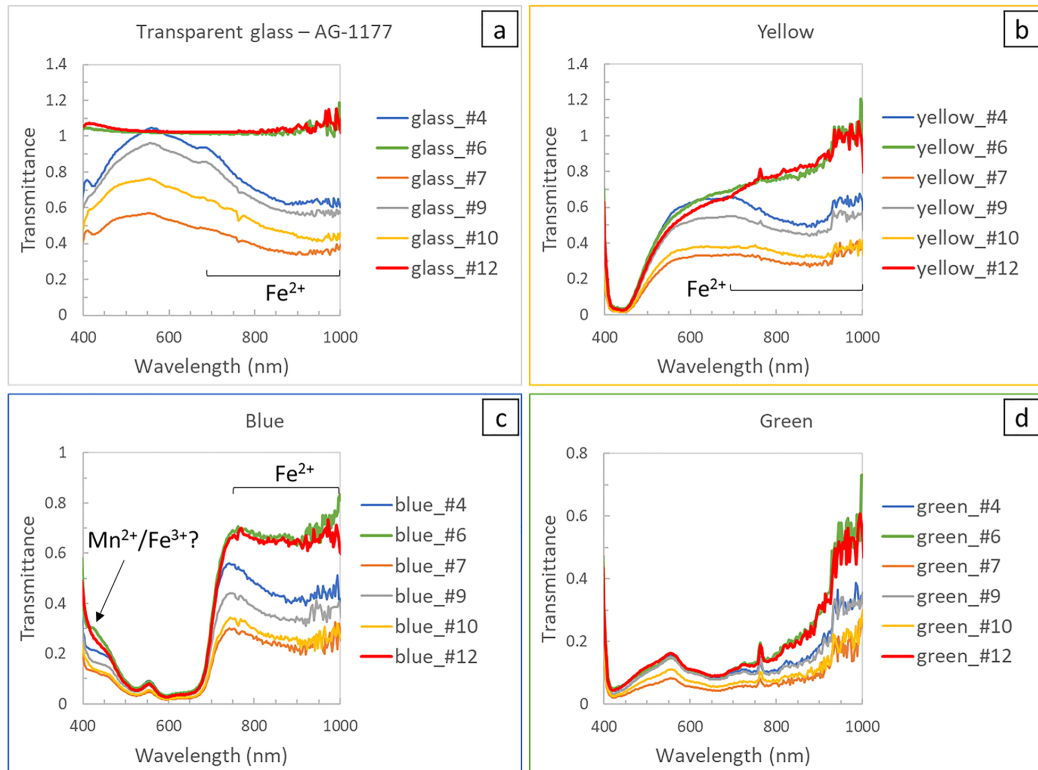


Fig. 17 **a** Comparison of spectra of the transparent area inside the stained glass, taken from all the acquisitions of AG-1177. Each spectrum is an average signal obtained by selecting the entire transparent area (Fig. 8b and e). The red and green lines refer to the spectra obtained when the transmittance reference is taken inside the stained glass, which appear flat due to the division occurring during the image processing phase. The characteristic bands of the transparent glass can be observed when the reference is taken from the windows' panes. **b–d** Comparison of spectra of yellow, blue, and green glass on the right side of the panel, taken from all the acquisitions. The red and green lines refer to the spectra obtained when the transmittance reference is taken inside the stained glass and appear slightly different from the others due to effects related to the radiometric correction. Figure 6 shows the points where the spectra of colored glass were taken

The same phenomenon has also been partially observed in the case study IN-64.11, especially in red and purple glass (Fig. 11e and f). In the case of purple glass, as for the green glass, the distortion appears as a signal increase in the NIR region. Unlike the other examples, however, this panel has no original transparent area sufficiently large to be used as a reference. It is worth reminding that the windows where the panels are placed were produced with historical recipes and are not as pure as contemporary glass would be. In addition, the various glass panes composing the windows may have been substituted through time for reparation before being installed in the museum or even afterward. In this case, qualitative XRF analysis (see Additional file 2, Fig. s5) revealed that the hexagonal glass panes on the right side contain a lower amount of

iron and manganese than the one on the left side, which may explain this difference.

In the second scenario, the spectra of stained-yellow glass from datacubes processed using a glass pane from the historical window show three additional bands (at around 530, 590, and 660–680 nm). This behavior can be observed in two very different situations: in the first case (LM-8368), vegetation is present in the background; at first look, these additional bands may be related to the signal of the vegetation in the background of the stained glass (Fig. 18a, b), which signal should have been limited by the diffusing sheet. A strong transmittance band starting abruptly at around 700 nm can also be observed.

In the second case (LM-749), when vegetation is absent, the reason behind the additional bands (at around

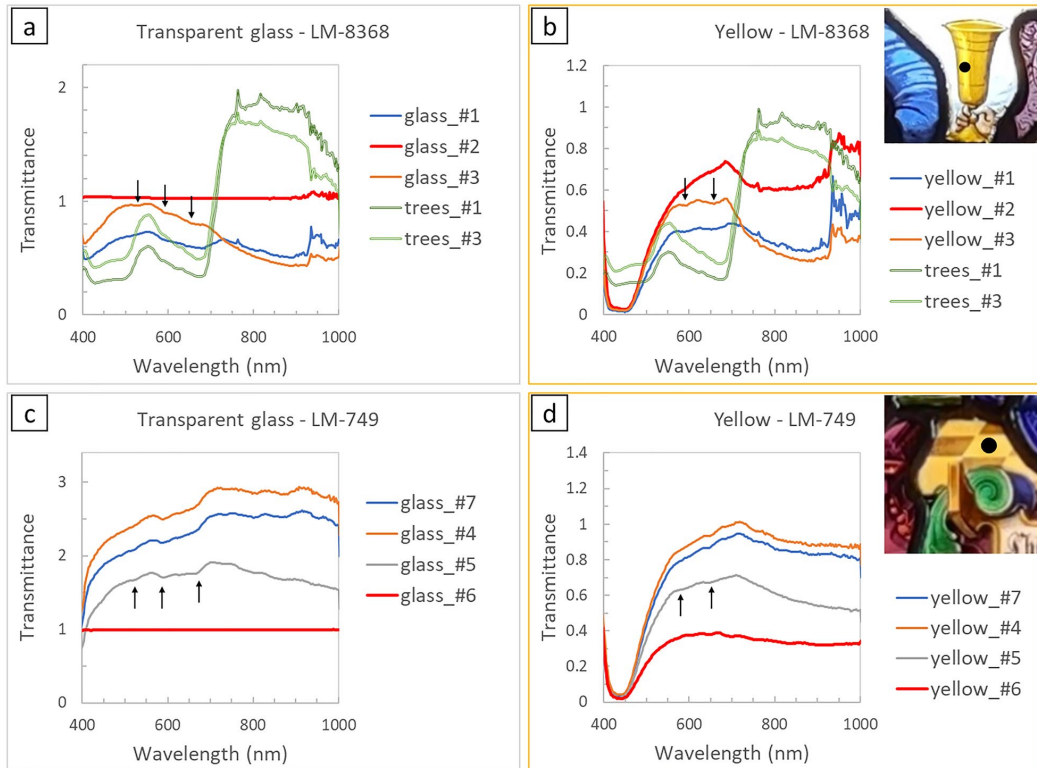


Fig. 18 **a** Comparison between spectra from the transparent area inside the stained glass and the vegetation. The spectra are taken from all the acquisitions of LM-8368. Each spectrum is an average signal obtained by selecting the entire transparent area (Fig. 14a). The red line refers to the spectra obtained when the transmittance reference is taken inside the stained glass, which appears flat due to the division occurring during the image processing phase. The characteristic bands of the transparent glass can be observed when the reference is taken from the windows' panes. **b** Comparison between spectra of an area painted with stained yellow and vegetation, taken from all the acquisitions of LM-8368. The red line refers to the spectra obtained when the transmittance reference is taken inside the stained glass and appears slightly different from the others due to effects related to the radiometric correction. **c** Comparison of spectra of the transparent area inside the stained glass (Fig. 15c), taken from all the acquisitions of LM-749. **d** Comparison between spectra from an area painted with stained yellow, taken from all the acquisitions of LM-749

530–540, 590–600, and 660 nm) may be associated with cobalt (Co^{2+}) impurities. The fact that these bands are also visible in the yellow-colored glass may be related to the thinness of the stained yellow layer. The similarity of the spectral shapes in the two scenarios depends on the fact that the leaf pigments and the cobalt ions absorb light almost in the same region [20, 23–25]. However, when radiometric calibration is performed using the transparent area inside the stained glass, the three bands tend to disappear entirely in both cases (red lines, Fig. 18b, d). For this reason, in the case of LM-8368, those bands cannot be related to vegetation but most probably to the composition of the transparent glass used as reference. Following the same reasoning formulated

previously regarding Fe^{2+} , it might be possible that the three bands of Co^{2+} are eliminated during the image processing phase. This means that even when vegetation is present, it is still possible to infer the presence of cobalt impurities if a diffusing sheet is applied.

XRF analysis was performed on the transparent area of LM-8368 to characterize the glass composition and verify this hypothesis. However, it was not possible to detect cobalt in the glass, as its concentration was probably under the instrument's detection limit.

Between the two situations, a slight difference can still be observed: if vegetation is present in the background, the strong absorbance band between 700 and 1000 nm is still visible, even if the reference is selected from a

transparent area inside the stained glass (Fig. 18b, red line). This fact means that, in the presence of vegetation, the selection of the transmitting reference inside or outside the stained-glass panel does not entirely eliminate the influence of the background from the final results.

In light of these considerations, it is clear that the transmittance reference selection can significantly impact the quality of the results. Repeating the acquisition multiple times using different transparent areas as a reference, together with a good knowledge of the fingerprint absorbance bands of the main chromophores, can help identify any anomalies in the results obtained and avoid erroneous interpretation.

Effectiveness of in-situ hyperspectral imaging for chromophore identification

Despite the numerous challenges discussed in the previous sections, in-situ HSI can still represent a valuable tool for the preliminary characterization of chromophores in stained glass. In light of the results obtained from the case studies, it is possible to draw some conclusions about the effectiveness of the in-situ application of hyperspectral imaging.

In general, the spectral range between 450 and 700 nm is not affected by the background unless vegetation is present. Nonetheless, using a diffusing sheet can help eliminate the vegetation's signal, as shown in the case of AG-1177. The following bands are almost always recognizable, regardless of the reference selection:

- The surface plasmonic resonance (SPR) of the copper nanoparticles in red glass (Cu^0) at around 565 nm (Figs. 11c, f, 14b, d) [12, 13, 26, 27].
- The broad band of Mn^{3+} in purple glass, at about 490–500 nm (Fig. 11b, e) [12, 13, 26, 28].
- The three bands of Co^{2+} in blue (Figs. 7l, 9g–i, 16a), green (Figs. 7k, 9d–f, 11a, d, 16c), and purple glass (Fig. 11b, e), at around 530–540, 590–600, and 650–670 nm [12, 13, 26, 27]. However, the band at about 590–600 nm may disappear if the glass used as a reference contains cobalt impurities (Fig. 16a).
- The band associated with silver nanoparticles (Ag^0) in glass painted with stained yellow (Figs. 7j, 9a–c, 16b). The position of this band may vary between 420 and 450 nm. The shift is usually influenced by the dimension and shape of the silver nanoparticles, as well as the possible presence of copper nanoparticles and the proportions in the Ag–Cu mixture. [29–31].
- The band associated with the ferric-sulfide ($\text{Fe}^{3+}\text{-S}$) complex in amber glass at around 410–420 nm (Fig. 14c, e) [26, 27].

On the other hand, the characteristic bands of Fe^{2+} , Fe^{3+} , Mn^{2+} , and partially Cu^{2+} are more prone to be altered for the following reasons:

- The intensity of the Fe^{2+} band is very susceptible to the amount of this oxide contained in the transparent glass used as a reference.
- The Fe^{3+} , Mn^{2+} , and the iron-manganese complex absorption bands, located at the end of the camera's spectral range in the UV region [19, 20, 28], can be masked or altered by a noise peak present in almost all the spectrum at around 400 nm, more or less intense depending on the imaging conditions.
- The region between 650 and 1000 nm is generally noisier on green glass pieces (probably due to their dark color and low transmittance), resulting in alterations of the absorbance band of Cu^{2+} , located at around 780–800 nm [12, 26, 27].
- If the acquisition is performed using sunlight as the light source, part of the Fe^{2+} and Cu^{2+} bands in the NIR region can be altered by the noise generated by the atmospheric water.

The alterations described above can considerably impact the data interpretation, especially when they hinder the identification of iron oxides (Fe^{3+} and Fe^{2+}) and manganese (as Mn^{2+}) since they can be used to determine the provenance of raw materials, furnace conditions, and the age of the glass under study [20]. The general color appearance of the stained glass can also be affected. For example, in Fig. 8, it is possible to notice that when the reference is selected from within the panel, the glass pieces appear less yellow. It is possible that the slight coloration of the transparent glass, given by iron impurities or wanted addition, is eliminated during the image processing step. In this case, repeating the measurements using different transparent glass sections can help verify any change in the spectral shape of both colored and uncolored glass and identify eventual anomalies.

In the previous sections, the identified chromophores were briefly indicated in the plots of all the studied panels. Here, on the other hand, the case studies LM-749 and LM-660.1 (Figs. 19 and 20) are shown as examples to highlight the potential of HSI in distinguishing glass of similar colors made with different chromophores. LM-749, as stated in section "Internal wall", has been acquired using a stable light source and homogeneous background. On the other hand, LM-660.1, as LM-8368, is located within a crown glass window facing an urban green space with trees. Despite the two different situations, it was possible to successfully identify the main chromophores for both stained glass (Figs. 19 and 20).

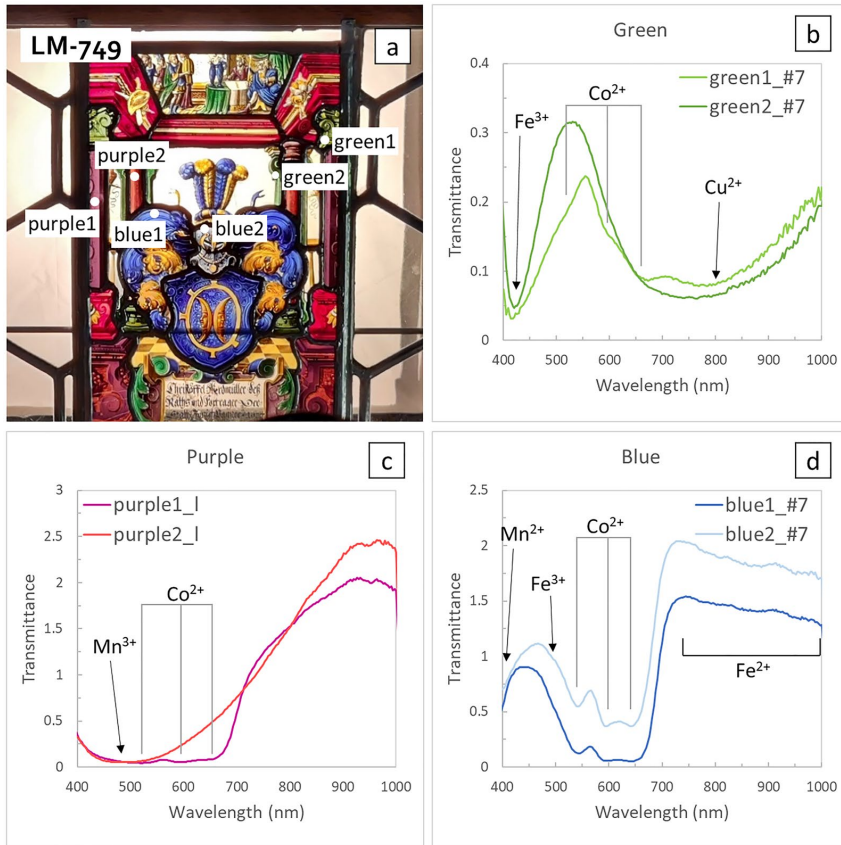


Fig. 19 **a** Close-up picture of case-study LM-794, showing the points selected for the spectra comparison. **b** Comparison of two green glass. **c** Comparison of two purple glass; **d** Comparison of two blue glass. The bands' position of the main chromophores are indicated



Fig. 20 **a** Close-up picture of case-study LM-660.1, showing the points selected for the spectra comparison. **b** Close-up picture of case-study LM-660.1, after the application of the diffusing sheet. **c** False-color image obtained from acquisition #6

In LM-749, for example, it is possible to identify two types of green and purple glass (Fig. 19). Regarding the green glass, the darker one was obtained using only Cu^{2+} (the broad band with an absorbance maximum at 780 nm), and Fe^{3+} (band at around 420 nm), while the lighter green shows the addition of Co^{2+} (three bands at 540, 590, and 660 nm). Concerning the purple glass, the reddish-purple one seems to contain only Mn^{3+} as the main chromophore (490 nm), while the other purple glass has a more bluish hue due to the additional presence of Co^{2+} .

On the other hand, the pale and the darker blue seem to have been colored using the same chromophores (mainly cobalt) but in different concentrations. The slight difference in the region between 450 and 500 nm could be related to a different amount of Fe^{3+} in the two areas (additional weak band at 480–490 nm)[19], but further analyses should be performed to confirm this hypothesis.

The case study LM-660.1 (Fig. 20) is particularly interesting from the conservation-restoration point of view. For instance, a few purple glass pieces have probably been

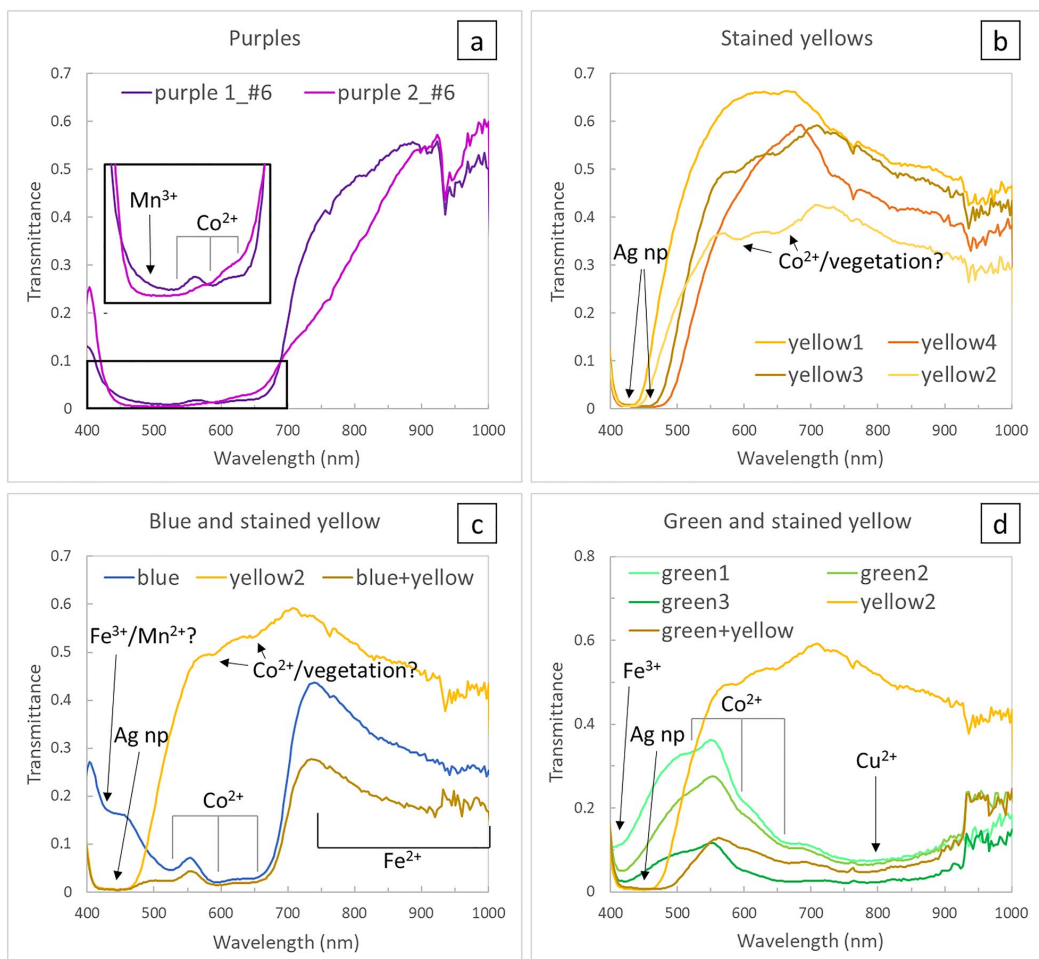


Fig. 21 **a** Comparison of the original purple glass with a probable later addition. **b** Comparison of four stained yellows, characterized by a shift of the silver nanoparticles band from 420 (light yellow) to 450 nm (intense yellow); **c** Comparison of blue glass, stained yellow and the combined layers. **d** Comparison of green glass, stained yellow and the combined layers. The band's position of the main chromophores are indicated. Figure 20a shows the points where the spectra were taken

substituted using purple glass with a different composition. This theory seems to be confirmed by comparing the spectra from the original purple glass and the possible addition (Fig. 21a), which shows how the replacement glass contains a lower amount of cobalt.

Thanks to HSI, it was also possible to understand the application of the stained yellow layer across the stained-glass panel. Figure 21b shows the spectra of possibly four typologies of stained yellow, characterized by a shift of the silver nanoparticle band from 420 (light yellow) to 450 nm (intense yellow). According to the literature, this shift may be related to the size and dimension of the silver nanoparticles or the addition of copper nanoparticles, which provided an orange color to the stained yellow [29–31].

Stained yellow has also been applied over blue and green glass to depict details like the capitals' decorations and the pavement's border. Figure 21c and d show how it is possible to distinguish the contributions of the two layers by comparing the spectrum of the mixed layer with those of the pure colors. The spectra of the blue and green glass, covered by stained yellow, are both characterized by the painted layer's contribution in the region between 420 and 460 nm, while the rest of the spectrum shows the characteristic bands of the chromophores of the layer below. This is especially noticeable in the blue glass (Fig. 21c).

Conclusion

This paper presented the results from an extensive *in-situ* hyperspectral imaging campaign on stained glass windows exhibited at the Swiss National Museum. Hyperspectral imaging was applied both on stained glass exposed to sunlight and on stained glass displayed in a window of an inner wall to evaluate the challenges related to these two different environments and identify the advantages and limitations of the technique.

Regarding stained glass exposed to sunlight, the results' quality depends significantly on the size and chemical composition of the transparent area chosen as reference and external factors such as the presence of vegetation and changing illumination throughout the day. In this specific case, the possibility of applying a diffusing sheet behind the panels allowed for minimizing the influence of these external factors and obtaining successful results in most cases. However, the authors are aware of this situation's exceptionality and that it may not always be possible to apply this methodology everywhere (for example, in large windows of religious or secular buildings that cannot be opened). It is also worth mentioning that the collaboration with the museum's staff and conservators was essential to test this approach to ensure that opening

the window and applying the diffusing sheet was not damaging the artworks.

Factors such as the weather, and the sun's position in relation to the object during the acquisitions, must also be taken into consideration since they determine the amount of light reaching the stained glass and its distribution. During the preliminary tests and the imaging *in-situ*, it has been observed that a foggy day or a clear sky (with the sun far away from the field of view) provides the most homogeneous background and, consequently, the best imaging conditions. On the other hand, the light intensity may be too low to allow the identification of the darkest-colored glass, especially the green ones. In this case, having direct sunlight in the field of view can improve the visualization of the deep-colored glass. However, the contrast between the more illuminated areas with the rest of the scene can become an issue during the radiometric correction. The risk of overexposing the light-colored glass is also very high due to the intensity of the solar radiation reaching the stained glass, even with a minimal camera exposure time. The best moment for the acquisition should then be judged case-by-case, making compromises according to the research questions that need to be answered. If budget and time allow, it would be advisable to perform multiple acquisitions, not only on the same day but also in different seasons and weather conditions.

Concerning the panels displayed on internal walls' windows, a lighting setup was developed to perform the HSI acquisition. The makeshift system allowed encouraging results; however, it still necessitates improvements. In this sense, further work should be focused on implementing a rigid diffuser to avoid the formation of rippling shadows due to the folds of the fabric. Using multiple light sources instead of a single one is advised to improve light distribution.

In both situations, nonetheless, it was possible to acquire sufficiently good results to have a qualitative understanding of the chromophores involved in the coloration of the glass pieces in a completely non-invasive way. While some characteristic bands could be altered due to external or camera-related issues, a good knowledge of the absorption behavior of chromophores can help formulate initial hypotheses, which can then be validated by complementary analysis.

Supplementary Information

The online version contains supplementary material available at <https://doi.org/10.1186/s40494-023-00923-6>.

Additional file 1: Table s1. Acquisitions parameters of case study IN-11.64. **Table s2.** Acquisitions parameters of case study AG-1177. **Table s3.** Acquisitions parameters of case study LM-8368. **Table s4.** Acquisitions parameters for case study LM-749. **Table s5.** Acquisition

parameters for case study LM-749. **Figure s1.** sun position during HSI acquisitions for case study AG-1177, calculated through the website SunCalc.org. **Figure s2.** Sun position during HSI acquisitions for case study IN-64.11, calculated through the website SunCalc.org. **Figure s3.** sun position during HSI acquisitions for case study LM-8368, calculated through the website SunCalc.org.

Additional file 2: Figure s4. a) close-up picture of case-study AG-1177, showing the point selected for the XRF analysis. b) XRF spectra of the two glass panes used as reference for radiometric correction. c) zoom of the spectra showing the differences in concentration of iron and manganese in the two glass panes. **Figure s5.** a) close-up picture of case-study LM-8368, showing the point selected for the XRF analysis. b) XRF spectra of the two glass panes used as reference for radiometric correction. c) zoom of the spectra showing the differences in concentration of iron and manganese in the two glass panes.

Additional file 3: Table s6. Technical information and number of acquisitions taken for the case studies LM-2632.c and AG-1183. **Table s7.** Acquisitions parameters of case study LM-2632. **Table s8.** Acquisitions parameters of case study AG-1183. **Figure s6.** a) close-up picture of case-study LM-2632.c, showing the points selected for the spectra comparison. b) pictures showing the areas chosen as transmittance reference (in green). c) spectra comparison of two purple glass. d) spectra comparison of two blue glass, one light and one dark. The dark blue is enamel glass characterized by areas with different thickness. Notice how the band of Co^{2+} at 590 nm disappears in thicker areas. e) spectra comparison of two green glass with different composition. D) Spectra comparison of stained-yellow and amber glass. Stained-yellow glass shows two peaks at around 590–600 and 660 nm which may be related to cobalt impurities from the transparent glass. **Figure s7.** a) close-up picture of case-study AG-1183, showing the points selected for the spectra comparison. b) pictures showing the areas chosen as transmittance reference (in green). c) spectra comparison of two purple glass; one containing cobalt as additional chromophore d) spectra comparison of three blue glass, obtained from different concentration of iron and cobalt. Manganese (as uncolored Mn^{2+}) may be present in higher concentration in the lighter glass. e) spectra comparison of three flashed red glass. The different position and shape of the band at 565 nm could be related to variations in size and dimension of the copper nanoparticles (np). d) Spectra comparison of stained-yellow and amber glass. Besides visual examination, from the spectral point of view the two colored glass can be distinguished from the shape of the slope in the region between 400–550.

Acknowledgements

The authors would like to thank Tino Zagermann, conservator-restorer, for his help during the acquisitions at the Swiss National Museum and Dr. Mylène Rouss, curator at the SNM, for the permission to analyze the stained-glass windows.

Author contributions

Conceptualization, AB, TL, KS, SG, and JYH; methodology, AB; resources, AB, TL, KS; investigation (HSI), AB, TL (supporting); investigation (XRF), TL; formal analysis, AB; visualization, AB; writing—original draft preparation, AB; writing—review and editing, AB, TL, KS, SG, and JYH; supervision, TL, KS, SG, and JYH; project administration, SG, JYH; funding acquisition, JYH. All authors read and approved the final manuscript.

Funding

Open access funding provided by Norwegian University of Science and Technology. This research has been carried out as part of a PhD program within the CHANGE Innovative Training Network. The CHANGE-ITN project has received funding from the European Union's Horizon 2020 research and innovation program under the Marie Skłodowska-Curie grant agreement No. 813789.

Availability of data and materials

The most relevant data generated or analyzed during this study are included in this published article (and its supplementary information files). Additional datasets used and analyzed during the current study are available from the corresponding author upon reasonable request.

Declarations

Competing interests

The authors declare that they have no competing interests.

Received: 28 December 2022 Accepted: 2 April 2023

Published online: 14 April 2023

References

- Piccolo M, Cucci C, Casini A, Stefani L. Hyper-spectral imaging technique in the cultural heritage field: new possible scenarios. *Sensors* (Basel). 2020;20(10):2843.
- Radpour R, Delaney JK, Kakoulli I. Acquisition of high spectral resolution diffuse reflectance image cubes (350–2500 nm) from archaeological wall paintings and other immovable heritage using a field-deployable spatial scanning reflectance spectrometry hyperspectral system. *Sensors*. 2022;22(5):1915.
- Cutajar JD, Babini A, Deborah H, Hardeberg JY, Joseph E, Frøysaker T. Hyperspectral imaging analyses of cleaning tests on Edvard Munch's monumental Aula paintings. *Stud Conserv*. 2022;67(sup1):59–68.
- Gabrieli F, Delaney JK, Erdmann RG, Gonzalez V, van Loon A, Smulders P, et al. Reflectance Imaging Spectroscopy (RIS) for operation night watch: challenges and achievements of imaging Rembrandt's masterpiece in the glass chamber at the Rijksmuseum. *Sensors*. 2021;21(20):6855.
- Cucci C, Piccolo M, Chiarantini L, Uda G, Fiori L, De Nigris B, et al. Remote-sensing hyperspectral imaging for applications in archaeological areas: non-invasive investigations on wall paintings and on mural inscriptions in the Pompeii site. *Microchem J*. 2020;158: 105082.
- Balas C, Epitropou G, Tsapas A, Hadjinicolaou N. Hyperspectral imaging and spectral classification for pigment identification and mapping in paintings by El Greco and his workshop. *Multimedia Tools Appl*. 2018;77(8):9737–51.
- Cucci C, Bracci S, Casini A, Innocenti S, Marcello P, Stefani L, et al. The illuminated manuscript Corale 43 and its attribution to Beato Angelico: non-invasive analysis by FORS, XRF and hyperspectral imaging techniques. *Microchem J*. 2017;138:45–57.
- Cucci C, Delaney JK, Piccolo M. Reflectance hyperspectral imaging for investigation of works of art: old master paintings and illuminated manuscripts. *Acc Chem Res*. 2016;49(10):2070–9.
- Daniel F, Mounier A. Mobile hyperspectral imaging for the non-invasive study of a mural painting in the Belves Castle (France, 15th C). *Sci Technol Archaeol Res*. 2015;1(2):81–8.
- Funatomi T, Ogawa T, Tanaka K, Kubo H, Caron G, Mouaddib EM, et al. Eliminating temporal illumination variations in whisk-broom hyperspectral imaging. *Int J Comput Vision*. 2022;130:1310–24.
- Perri A, Nogueira de Faria BE, Ferreira DCT, Comelli D, Valentini G, Preda F, et al. Hyperspectral imaging with a TWINS birefringent interferometer. *Opt Express*. 2019;27(11):15956–67.
- Palomar T, Grazia C, Cardoso IP, Vilariques M, Miliani C, Romani A. Analysis of chromophores in stained-glass windows using Visible Hyperspectral Imaging in-situ. *Spectrochimica Acta Part a-Mol Biomol Spectrosc*. 2019;223: 117378.
- Rebollo E, Ratti F, Cortelazzo GM, Poletto L, Bertonecello R. New trends in imaging spectroscopy: the non-invasive study of the Scrovegni Chapel stained glass windows. *Proc SPIE, O3A: Optics for Arts, Architecture, and Archaeology III*. 80842011. p. 808407.
- Babini A, Green P, George S, Hardeberg JY. Comparison of hyperspectral imaging and fiber-optic reflectance spectroscopy for reflectance and transmittance measurements of colored glass. *Heritage*. 2022;5(3):1401–18.
- Babini A, George S, Hardeberg JY. Hyperspectral imaging workflow for the acquisition and analysis of stained-glass panels. *Proc SPIE Optics for Arts, Architecture, and Archaeology VIII*. 11784 2021. p. 117841F
- Behmann J, Acebron K, Emin D, Bennertz S, Matsubara S, Thomas S, et al. Specim IQ: evaluation of a new, miniaturized handheld hyperspectral camera and its application for plant phenotyping and disease detection. *Sensors*. 2018;18(2):441.

17. Piccolo M, Casini A, Cucci C, Jussila J, Poggesi M, Stefani L. A New Compact VNIR Hyperspectral Imaging System for Non-Invasive Analysis in the Fine Art and Architecture Fields. *Proceedings e report: Firenze University Press*; 2018. p. 69–74.
18. Schindelin J, Arganda-Carreras I, Frise E, Kaynig V, Longair M, Pietzsch T, et al. Fiji: an open-source platform for biological-image analysis. *Nat Methods*. 2012;9(7):676–82.
19. Micheletti F, Orsilli J, Melada J, Gargano M, Ludwig N, Bonizzoni L. The role of IRT in the archaeometric study of ancient glass through XRF and FORS. *Microchem J*. 2020;153: 104388.
20. Meulebroeck W, Nys K, Patin M, Thienpont H. The interaction between daylight and fifteenth and sixteenth century glass windows from the low countries. *Sci Rep*. 2021;11(1):21338.
21. Hayem-Ghez A, Ravaud E, Boust C, Bastian G, Menu M, Brodie-Linder N. Characterizing pigments with hyperspectral imaging variable false-color composites. *Appl Phys A*. 2015;121:939–47.
22. Buoso MC, Ceccato D, Zafiropoulos D. False-color Infra Red Photography in the Identification of Pigments Used for a late 13th Century Illuminated Manuscript. LNL Annual Report, Applied and Interdisciplinary Physics Instrumentation 2009:153–4.
23. Thenkabail P, Mariotto I, Gumma M, Middleton E, Landis D, Huemmrich K. Selection of hyperspectral narrowbands (HNBS) and composition of hyperspectral twoband vegetation indices (HVIs) for biophysical characterization and discrimination of crop types using field reflectance and hyperion/EO-1 Data. *IEEE J Sel Top Appl Earth Obs Remote Sensing*. 2013;6:427–39.
24. Jiang J, Comar A, Burger P, Bancal P, Weiss M, Baret F. Estimation of leaf traits from reflectance measurements: comparison between methods based on vegetation indices and several versions of the PROSPECT model. *Plant Methods*. 2018;14(1):23.
25. Cagno S, Van der Snickt G, Legrand S, Caen J, Patin M, Meulebroeck W, et al. Comparison of four mobile, non-invasive diagnostic techniques for differentiating glass types in historical leaded windows: MA-XRF, UV-Vis-NIR, Raman Spectrosc IRT X-Ray Spectrom. 2021;50(4):293–309.
26. Bracci S, Bartolozzi G, Burnam RK, Corallini A. Integration of both non-invasive and micro-invasive techniques for the archaeometric study of the stained-glass window Apparizione degli Angeli in the basilica of Santa Croce in Florence. Italy. *J Cult Heritage*. 2020;44:307–16.
27. Hunault MOJY, Bauchau F, Boulanger K, Hérold M, Calas G, Lemasson Q, et al. Thirteenth-century stained glass windows of the Sainte-Chapelle in Paris: an insight into medieval glazing work practices. *J Archaeol Sci Rep*. 2021;35: 102753.
28. Bidegaray A-I, Godet S, Bogaerts M, Cosyns P, Nys K, Terryn H, et al. To be purple or not to be purple? How different production parameters influence colour and redox in manganese containing glass. *J Archaeol Sci Rep*. 2019;27: 101975.
29. Patin M, Nys K, Thienpont H, Meulebroeck W. Prestige markers in art: subtle stratagems in material selection for fifteenth-century stained-glass windows. *Heritage Sci*. 2022;10(1):106.
30. Delgado J, Vilarigues M, Ruivo A, Corregidor V, da Silva RC, Alves LC. Characterisation of medieval yellow silver stained glass from Convento de Cristo in Tomar, Portugal. *Nucl Instrum Methods Phys Res, Sect B*. 2011;269(20):2383–8.
31. Molina G, Murcia S, Molera J, Roldan C, Crespo D, Pradell T. Color and dichroism of silver-stained glasses. *J Nanopart Res*. 2013;15(9):1932.

Publisher's Note

Springer Nature remains neutral with regard to jurisdictional claims in published maps and institutional affiliations.

Submit your manuscript to a SpringerOpen® journal and benefit from:

- Convenient online submission
- Rigorous peer review
- Open access: articles freely available online
- High visibility within the field
- Retaining the copyright to your article

Submit your next manuscript at ► [springeropen.com](https://www.springeropen.com)

Paper 6

Agnese Babini, Tiziana Lombardo, Sony George, Jon Y. Hardeberg. (2023). Blind unmixing of hyperspectral images of stained glass: adapting the LUMoS algorithm for chromophores mapping.

Draft paper.

This paper will be submitted for publication and is therefore not included.

ISBN 978-82-326-7294-3 (printed ver.)
ISBN 978-82-326-7293-6 (electronic ver.)
ISSN 1503-8181 (printed ver.)
ISSN 2703-8084 (online ver.)



NTNU

Norwegian University of
Science and Technology